ISM S-BAND CUBESAT RADIO DESIGNED FOR THE POLYSAT SYSTEM BOARD

A Thesis

presented to

the Faculty of California Polytechnic State University,

San Luis Obispo

In Partial Fulfillment

of the Requirements for the Degree

Master of Science in Electrical Engineering

by

Craig Lee Francis

June 2016

COMMITTEE MEMBERSHIP

TITLE:	ISM S-Band CubeSat Radio designed for the PolySat System Board
AUTHOR:	Craig Lee Francis
DATE SUBMITTED:	June 2016
COMMITTEE CHAIR:	Dr. Dennis Derickson, Ph.D. Department Chair of Electrical Engineering
COMMITTEE MEMBER:	Dr. Jordi Puig-Suari, Ph.D. Professor of Aerospace Engineering
COMMITTEE MEMBER:	Dr. John Bellardo, Ph.D. Associate Professor of Computer Science

ABSTRACT

ISM S-Band CubeSat Radio designed for the PolySat System Board

Craig Lee Francis

Cal Poly's PolySat CubeSat satellites have begun to conduct more complex and scientifically significant experiments. The large data products generated by these missions demonstrate the necessity for higher data rate communication than currently provided by the PolySat UHF radio. This thesis leverages the proliferation of consumer wireless monolithic transceivers to develop a 250kbps to 2000kbps, 2W CubeSat radio operating within the 2.45GHz Industrial, Scientific, and Medical (ISM) radio band.

Estimating a link budget for a realistic CubeSat leads to the conclusion that this system will require a large deployable CubeSat antenna, large earth station satellite dish, and a fine-pointing attitude control system. Noise floor measurements of a CubeSat ground station demonstrate that terrestrial ISM interference can be minimized to below the thermal noise floor by carefully choosing the operating frequency.

The radio is specifically designed as a daughter board for the PolySat System Board with a direct interface to the embedded Linux microprocessor. A state-of-the-art ZigBee transceiver evaluation board is measured to confirm its suitability for a CubeSat radio. A schematic is developed, which integrates the transceiver, power amplifier, low noise amplifier, amplifier protection circuitry, switching regulators, and RF power measurement into a single printed circuit board assembly (PCBA). The circuitry is then squeezed into a high-density, 1.4" x 3.3" layout. The PCBA is then manufactured, troubleshot, tuned, and characterized.

TABLE OF CONTENTS

LIST OF TABLES

Table Page

LIST OF FIGURES

Figure Page

1 Introduction

1.1 PolySat/CubeSat Laboratory Background

PolySat is a multi-disciplinary graduate and undergraduate engineering team that focuses on custom CubeSat satellite development. The PolySat lab currently resides in Building 192, room 101 and within the Advanced Technology Laboratory on the campus of California Polytechnic State University, San Luis Obispo. Instead of purchasing off-the-shelf CubeSat kits, the PolySat team designs custom electronics, structures, and software. Within a span of approximately three years, a PolySat member will typically design, build, test, and operate a full CubeSat satellite mission on a multidisciplinary team of mechanical, electrical, computer, aerospace, and software engineering students.

Within the same lab as the PolySat team, the CubeSat team maintains the worldwide CubeSat standard cofounded by CubeSat's principal investigator, Dr. Jordi Puig-Suari. CubeSat performs integration and testing services for the launch of CubeSat missions. CubeSats "piggyback" on launch vehicles for conventional satellites already being launched by other organizations, such as NASA or the NRO. The CubeSat team maintains the design for the Poly Picosatellite Orbital Deployer (P-POD) which is a spring-loaded box that deploys CubeSats from the launch vehicle after reaching orbit.

Since its founding in 2000, PolySat has launched eight CubeSat missions. PolySat's missions are generally scientific or experimental pursuits funded by outside entities. The recently launched IPEX satellite is a great example of a PolySat mission. The IPEX mission was a joint effort between PolySat and the NASA Jet Propulsion Laboratory (JPL) and was funded by NASA's Earth Science Technology Office (ESTO). IPEX is a 1U CubeSat, the smallest size in the CubeSat standard, corresponding to dimensions of 10x10x10cm in volume and 1kg in weight. A picture of IPEX is shown in Figure 1. IPEX houses five cell phone cameras on five different faces of the CubeSat for

capturing pictures of Earth; the low-resolution cameras are placeholders for actual science instruments on future NASA missions. A secondary payload processor is loaded with specialized onboard planning software developed by JPL to validate autonomous payload operations for the NASA HYperSPectral Infra-Red Instrument (HyspIRI) mission. [1] IPEX was launched in December 2013 and successfully completed all mission objectives within its six month mission life span before becoming unresponsive after one year of operation. Not shown in the picture is IPEX's deployable monopole antenna tuned for 437MHz; this antenna is deployed automatically after ejection into space. All communication and data downlink for the mission was through this simple antenna at a data rate of 9.6kbps.

Figure 1: IPEX, PolySat 1U CubeSat (10x10x11cm) [1]

CubeSats are low earth orbit (LEO) satellites generally between 300km and 1000km in altitude and travel at approximately 8 km/s. The satellites circle the Earth approximately every 90 minutes and are within line-of-sight of a single point on Earth approximately 5 times a day for less than 15 minutes as they fly horizon to horizon. As the satellites fly overhead, they are communicated with by actively pointing a high-gain antenna across the sky following the satellite's path. All data is transmitted between the

satellite and earth station during these short passes. Figure 2 is a picture of the PolySat “Friis” 437MHz earth station antenna, which is an array of four Yagi-Uda antennas combined as a phased array to behave as a single antenna with high gain. This antenna is located on the roof of Building 192 on the Cal Poly campus.

Figure 2: PolySat Earth Station, 437MHz Yagi Antenna Array

1.2 CubeSat Communication Frequencies

Cal Poly and PolySat alumnus Bryan Klofas maintains a table of CubeSat communication systems along with his published papers and presentations on his website: klofas.com. [2] According to the website, as of March 2015, 256 CubeSats have deployed into space; the communication details of each CubeSat are published in his

table including: satellite size, radio, frequency, satellite service, protocol, data rate, funding source, and life time. A snippet of the chart is shown in Figure 3. [3]

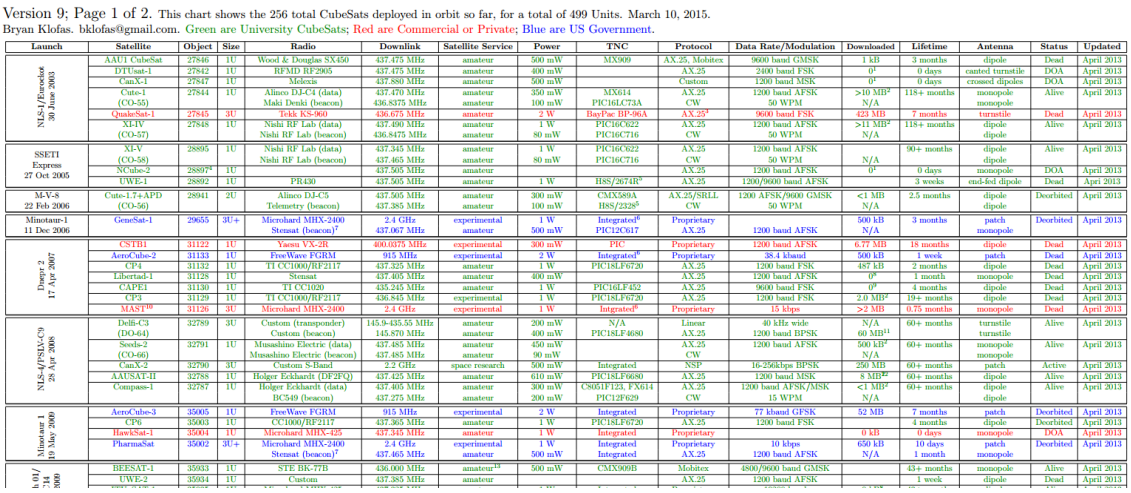

Version 9; Page 1 of 2. This chart shows the 256 total CubeSats deployed in orbit so far, for a total of 499 Units. March 10, 2015.
Bryan Klofas. bklofas@gmail.com. Green are University CubeSats; Red are Commercial or Private; Blue are US Government.

Launch	Satellite	Object	Size	Radio	Downlink	Satellite Service	Power	TNC	Protocol	Data Rate/Modulation	Downloaded	Lifetime	Antenna	Status	Updated
NLS-1/Eurockot 30 June 2003	AAU1 CubeSat	27846	1U	Wood & Douglas SX450	437.475 MHz	amateur	500 mW	MX909	AX.25, Mobitex	9600 baud GMSK	1 kB	3 months	dipole	Dead	April 2013
	DTUsat-1	27842	1U	RFMD RF2905	437.475 MHz	amateur	400 mW		AX.25	2400 baud FSK	0[1]	0 days	canted turnstile	DOA	April 2013
	CanX-1	27847	1U	Motorola	437.880 MHz	amateur	500 mW		Custom	1200 baud MSK	0[1]	0 days	crossed dipoles	DOA	April 2013
	Cute-1	27844	1U	Alinco DJ-C4 (data)	437.470 MHz	amateur	350 mW	MX614	AX.25	1200 baud AFSK	>10 MB[2]	118+ months	monopole	Alive	April 2013
	(CO-55)			Maki Denki (beacon)	436.8375 MHz	amateur	100 mW	PIC16LC73A	CW	50 WPM	N/A		monopole		
	QuakeSat-1	27845	3U	Tekk KS-960	436.675 MHz	amateur	2 W	BayPac BP-96A	AX.25[4]	9600 baud FSK	423 MB	7 months	turnstile	Dead	April 2013
	XI-IV	27848	1U	Nishi RF Lab (data)	437.490 MHz	amateur	1 W	PIC16C622	AX.25	1200 baud AFSK	>11 MB[2]	118+ months	dipole	Alive	April 2013
	(CO-57)			Nishi RF Lab (beacon)	436.8475 MHz	amateur	80 mW	PIC16C716	CW	50 WPM	N/A		dipole		
SSETI Express 27 Oct 2005	XI-V	28895	1U	Nishi RF Lab (data)	437.345 MHz	amateur	1 W	PIC16C622	AX.25	1200 baud AFSK		90+ months	dipole	Alive	April 2013
	(CO-58)			Nishi RF Lab (beacon)	437.465 MHz	amateur	80 mW	PIC16C716	CW	50 WPM	N/A		dipole		
	NCube-2	28897[4]	1U		437.505 MHz	amateur			AX.25	1200 baud AFSK	0[1]	0 days	monopole	DOA	April 2013
	UWE-1	28892	1U	PR430	437.505 MHz	amateur	1 W	H8S/2674R[3]	AX.25	1200/9600 baud AFSK		3 weeks	end-fed dipole	Dead	Apri 2013
M-V-8 22 Feb 2006	Cute-1.7+APD	28941	2U	Alinco DJ-C5	437.505 MHz	amateur	300 mW	CMX589A	AX.25/SRLL	1200 AFSK/9600 GMSK	<1 MB	2.5 months	dipole	Deorbited	April 2013
	(CO-56)			Telemetry (beacon)	437.385 MHz	amateur	100 mW	H8S/2323[5]	CW	50 WPM	N/A		dipole		
Minotaur-1 11 Dec 2006	GeneSat-1	29655	3U+	Microhard MHX-2400	2.4 GHz	experimental	1 W	Integrated[6]	Proprietary		500 kB	3 months	patch	Deorbited	April 2013
				Stensat (beacon)[7]	437.067 MHz	amateur	500 mW	PIC12C617	AX.25	1200 baud AFSK	N/A		monopole		
Dnepr 2 17 Apr 2007	CSTB1	31122	1U	Yaesu VX-2R	400.0375 MHz	experimental	300 mW	PIC	Proprietary	1200 baud AFSK	6.77 MB	18 months	dipole	Dead	April 2013
	AeroCube-2	31133	1U	FreeWave FGRM	915 MHz	experimental	2 W	Integrated[6]	Proprietary	38.4 kbaud	500 kB	1 week	patch	Dead	April 2013
	CP4	31132	1U	TI CC1000/RF2117	437.325 MHz	amateur	1 W	PIC18LF6720	AX.25	1200 baud FSK	487 kB	2 months	dipole	Dead	April 2013
	Libertad-1	31128	1U	Stensat	437.405 MHz	amateur	400 mW		AX.25	1200 baud AFSK	0[8]	1 month	monopole	Dead	April 2013
	CAPE1	31130	1U	TI CC1020	435.245 MHz	amateur	1 W	PIC16LF452	AX.25	9600 baud FSK	0[8]	4 months	dipole	Dead	April 2013
	CP3	31129	1U	TI CC1000/RF2117	436.845 MHz	experimental	1 W	PIC18LF6720	AX.25	1200 baud FSK	2.0 MB[2]	19+ months	dipole	Dead	April 2013
	MAST[10]	31126	3U	Microhard MHX-2400	2.4 GHz	experimental	1 W	Integrated[6]	Proprietary	15 kbps	>2 MB	0.75 months	monopole	Dead	April 2013
NLS-4/PSLV-C9 28 Apr 2008	Delfi-C3	32789	3U	Custom (transponder)	145.9-435.55 MHz	amateur	200 mW	N/A	Linear	40 kHz wide	N/A	60+ months	turnstile	Alive	April 2013
	(DO-64)			Custom (beacon)	145.870 MHz	amateur	400 mW	PIC18LF4680	AX.25	1200 baud BPSK	60 MB[11]		turnstile		
	Seeds-2	32791	1U	Musashino Electric (data)	437.485 MHz	amateur	450 mW		AX.25	1200 baud AFSK	500 kB[2]	60+ months	monopole	Alive	April 2013
	(CO-66)			Musashino Electric (beacon)	437.485 MHz	amateur	90 mW		CW		N/A		monopole		
	CanX-2	32790	3U	Custom S-Band	2.2 GHz	space research	500 mW	Integrated	NSP	16-256kbps BPSK	250 MB	60+ months	patch	Active	April 2013
	AAUSAT-II	32788	1U	Holger Eckhardt (DF2FQ)	437.425 MHz	amateur	610 mW	PIC18LF6680	AX.25	1200 baud MSK	8 MB[12]	60+ months	dipole	Alive	April 2013
	Compass-1	32787	1U	Holger Eckhardt (data)	437.405 MHz	amateur	300 mW	CS051F123, FX614	AX.25	1200 baud AFSK/MSK	<1 MB[2]	60+ months	dipole	Alive	April 2013
				BC549 (beacon)	437.275 MHz	amateur	200 mW	PIC12F629	CW	15 WPM	N/A		dipole		
Minotaur 1 19 May 2009	AeroCube-3	35005	1U	FreeWave FGRM	915 MHz	experimental	2 W	Integrated	Proprietary	77 kbaud GFSK	52 MB	7 months	patch	Deorbited	April 2013
	CP6	35003	1U	CC1000/RF2117	437.365 MHz	amateur	1 W	PIC18LF6720	AX.25	1200 baud FSK		4 months	dipole	Deorbited	April 2013
	HawkSat-1	35004	1U	Microhard MHX-425	437.345 MHz	amateur	1 W	Integrated	Proprietary		0 kB	0 days	monopole	DOA	April 2013
	PharmaSat	35002	3U+	Microhard MHX-2400	2.4 GHz	experimental	1 W	Integrated	Proprietary	10 kbps	650 kB	10 days	patch	Deorbited	April 2013
				Stensat (beacon)[7]	437.465 MHz	amateur	500 mW	Integrated	AX.25	1200 baud AFSK	N/A	1 month	monopole		
4-01/ 714 000	BEESAT-1	35933	1U	STE BK-77B	436.000 MHz	amateur[13]	500 mW	CMX909B	Mobitex	4800/9600 baud GMSK		43+ months	monopole	Alive	April 2013
	UWE-2	35934	1U	Custom	437.385 MHz	amateur			AX.25	1200 baud AFSK		1 week	dipole	Dead	April 2013

Figure 3: CubeSat Communication Systems Table Snippet, Bryan Klofas [3]

In February 2014, Klofas presented a presentation titled *"CubeSat Radios: From kilobits to Megabits,"* in which he totaled the CubeSat transmit frequencies, satellite service, and maximum data rates in the diagrams shown in Figure 4, Figure 5, and Figure 6.

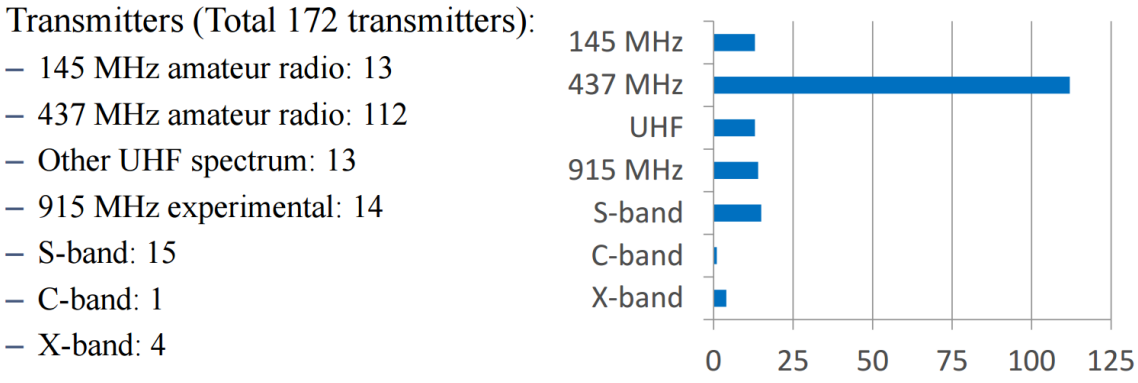

Figure 4: CubeSat Transmit Frequencies (2003 to 2014), Bryan Klofas [4]

Satellite Service (Total 196 transmitters):

- Amateur: 100
- Experimental: 53
- Government: 29
- Other:
  - Earth exploration: 2
  - Meteorological: 2
  - Space research: 4
  - Unlicensed/unknown: 6

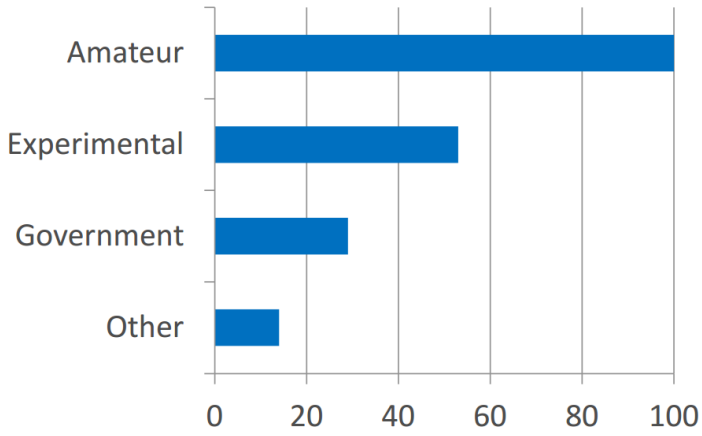

Figure 5: CubeSat Satellite Service Licenses, (2003 to 2014), Bryan Klofas [4]

Max data rates (Total 144 transmitters):

- < 9600 baud or CW: 85
- 9600 baud: 36
- 9600 baud to < 1 Mbps: 16
- 1 Mbps or greater: 7
  - Hayato, DICE, CINEMA, Dove+

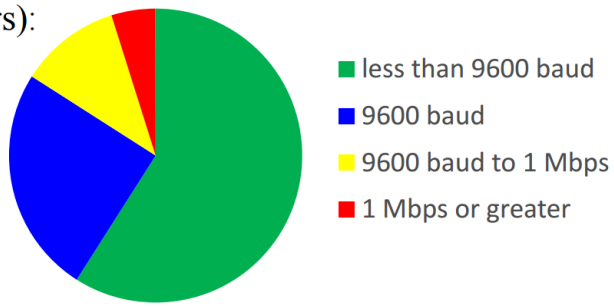

Figure 6: CubeSat Data Rates, (2003 to 2014), Bryan Klofas [4]

As of March 2015, 31 of 256 CubeSats have data rates greater than 9.6kbps and 11 CubeSats have been capable of data rates greater than 1000kbps. The first CubeSat capable of communication above 1000kbps launched in 2010. The majority of CubeSats have operated in the Amateur 70cm satellite band of 435MHz to 438MHz at data rates of 1.2kbps or 9.6kbps, including the latest Cal Poly PolySat satellites which communicate at a data rate of 9.6kbps at 437MHz. After one year of operation, the PolySat IPEX mission downlinked greater than 20MBs of data and imagery; this is the current data record for the PolySat lab and is roughly equivalent to the size of five mp3 song files.

1.3 Motivation and Objectives of the S-Band Radio

The motivation of an S-Band radio is simply to increase the data downlink capability for future PolySat missions requiring high data throughput. The radio will be designed to consume minimal power and volume within the spacecraft. The radio will be designed to fit within the current PolySat HyperCube bus architecture as a daughter board for the System Board at a PCBA size of 1.4” x 3.3”. Another desired feature described in “*5.5 Amplifier Protection and RF Power Measurement*,” is to protect the radio amplifiers from open/short load conditions and excessive power input during satellite development. The general high-level objectives of the S-Band radio are listed below.

S-Band radio high level objectives:

- Increase satellite downlink and uplink data rate
    - Data Rate > 100kbps
- Conform to PolySat System Board, daughter board B dimensions
    - Size < 1.4” x 3.3”
- Minimize power consumption
    - Receive mode power consumption <200mW
- Power and low noise amplifier protection
    - Protection from excessive VSWR and excessive input power

2 Summary of UHF Communication System

The primary radio for PolySat's CP8 (IPEX), CP9, and CP10 (ExoCube) spacecraft is the UHF radio board designed by Austin Williams in his thesis*: A Compact, Reconfigurable UHF Communication System Design for use with PolySat's Embedded Linux Platform.* [5] The UHF board is tuned for the 70cm band, specifically for the amateur satellite band 435-438 MHz; most CubeSat UHF communications are allocated within this 3MHz bandwidth. The UHF board supports FSK, GFSK, MSK, GMSK, BPSK, and OQPSK modulation, data rates from 1.2kbps to 600kbps, and 1W of transmit power. [5]

Although the UHF board can technically support up to a 600kbps data rate, the actual data rate is limited by satellite and earth station antenna gains, noise floor, sensitivity, and transmit power. The UHF radio is used as the primary beacon and command radio, therefore it is desirable to have a low-gain, omnidirectional antenna. Low-gain, omnidirectional antennas ideally transmit and receive radiation equally in all directions, which allow communication regardless of the satellite's orientation with regard to the ground station. This is desirable for the satellite's primary command and control radio link, because a robust link is required for mission critical commands and data gathering. However, the low gain UHF antenna limits the data rate of the satellite. In PolySat's current missions, the UHF board is being utilized at a 9.6kbps data rate, but further experimentation and optimization with the satellite and earth station may bring that data rate higher in the future.

The highest practical data rate for the UHF link can be estimated by assuming a low-gain satellite antenna and a high-gain ground station, such as the PolySat "Friis" ground station. As described on the PolySat website, "*The antennas consist of four phased 436CP42UG yagi antennas built by M2 Antenna Systems Inc. mounted on a*

AlfaSpid rotor system. A LNA 435 MKII low noise amplifier as attached on the mast." [6] According to the 436CP42UG antenna datasheet, the gain for each circularly-polarized antenna is 18.9dBi equating to a beam width of 21 degrees. [7] Four 436CP42UG antennas optimally phased together would theoretically result in a gain increase of 3dB per doubling of antenna [8]; with four antennas, this equates to 18.9dBi + 3dB + 3dB = 24.9dBi. In practice, the gain of the antenna array would be less, but for this estimate we will assume optimal phasing. David Adamy's "*EW101, A First Course in Electronic Warfare*," is a great reference for calculating link budgets and general overview of RF. Page 14 presents the link equation:

$$\boldsymbol{P_R = P_T + G_T - L + G_R}$$

Where P_R= received power in dBm; P_T = transmitter output power in dBm; G_T = transmitting antenna gain; L = link losses including path loss, pointing loss, and atmospheric loss; G_R= receiving antenna gain in dB. [9]

The link loss L can be broken down into four major components:

$$\boldsymbol{L = L_s + L_a + L_{point} + L_{pol}}$$

Where L_s = spreading loss dependent on distance and frequency; L_a= atmospheric loss dependent on frequency and angle which varies the distance traveled through earth's atmosphere; L_{point} = pointing loss due to misalignment of maximum gain boresights of the antennas; L_{pol} = polarization mismatch loss due to differences in polarization between antennas. For the UHF ground station, spreading loss is the most significant loss equal to $L_s = 32.4 + 20\log(f) + 20\log(d)$. Where f = transmitted frequency in MHz and d = transmission distance in km. For UHF, the atmospheric loss is insignificant with worst-case loss of approximately 0.1dB at an elevation angle of 5 degrees from the horizon. [10] To keep our estimate as optimistic as possible, we will assume no misalignment between the ground station maximum gain boresight and the satellite with

L_{point} = 0. The satellite antenna is linearly polarized and the ground station is circularly polarized resulting in a polarization loss approximately equal to 3dB according to *EW101*. [9]

Generally, the satellite transmit power is less than the ground station transmit power; this is true for the PolySat UHF link. The satellite transmits 1W (30dBm), whereas the ground station transmits up to 1kW (60dBm); therefore, assuming the ground station and satellite receive sensitivity are equal, the weakest period of the radio link is when the satellite is transmitting and ground station receiving. The Friis Cal Poly ground station uses the UHF radio developed in Austin Williams' thesis for both the satellite and ground station radio. Williams measured the receive sensitivity of the radio at various data rates, reproduced in the figure below. [2]

Table 1: Sensitivity of PolySat UHF Radio, Williams [5]

DataRate (kbps)	Modulaton Type	Packet Length (Bytes)	# Packets Transmitted	Packet Error Rate (%)	Signal Strength (dBm)
1.2	FSK	8	613	0	-119
			519	0.2	-120
			508	0.8	-121
			545	6.3	-121
2.4	FSK	8	555	0	-118
			541	0	-119
			543	0	-119
			509	0.4	-120
			524	1	-121
			594	5	-121
4.6	FSK	256	222	0	-115
			206	0	-117
			313	0.6	-118
			315	9.2	-119
		8	585	0.2	-118
			509	0.8	-119
			524	3.2	-120
			371	14.5	-121
9.6	FSK	256	534	0	-97
			506	0	-107
			553	0	-111
			510	0	-114
			502	0	-116
			503	4	-117
		8	508	0.2	-117
			510	1.5	-118
19.2	FSK	256	511	0	-108
			557	0	-111
			747	0	-112
			561	0.2	-114
			514	0.4	-115
			516	3.1	-116
38.4	FSK	256	575	0	-109
			527	0	-112
			550	0.5	-113
			522	5.5	-114
	PSK	256	592	0	-112
			596	0	-114
			542	0	-114
			532	0	-116
			534	1.1	-116
			517	7	-117
100	FSK	256	1023	0	-101
			1147	0	-104
			1037	0.4	-106
			1236	1.2	-107
	PSK	256	1115	0.7	-107
			1028	1	-108
			1102	1.5	-109
			1058	1.2	-110
			1029	0.9	-111
			1022	1.9	-112
			1080	4.4	-113

For the link distance, we will use PolySat's IPEX satellite's maximum altitude of 800km at an elevation angle of 15 degrees from the horizon. This is a real-world and typical scenario for a low-earth orbit satellite. Using the "*AMSAT/IARU Annotated Link Model System"* excel calculator, the 800km, 15 degree, link distance equates to 2033km. [11]

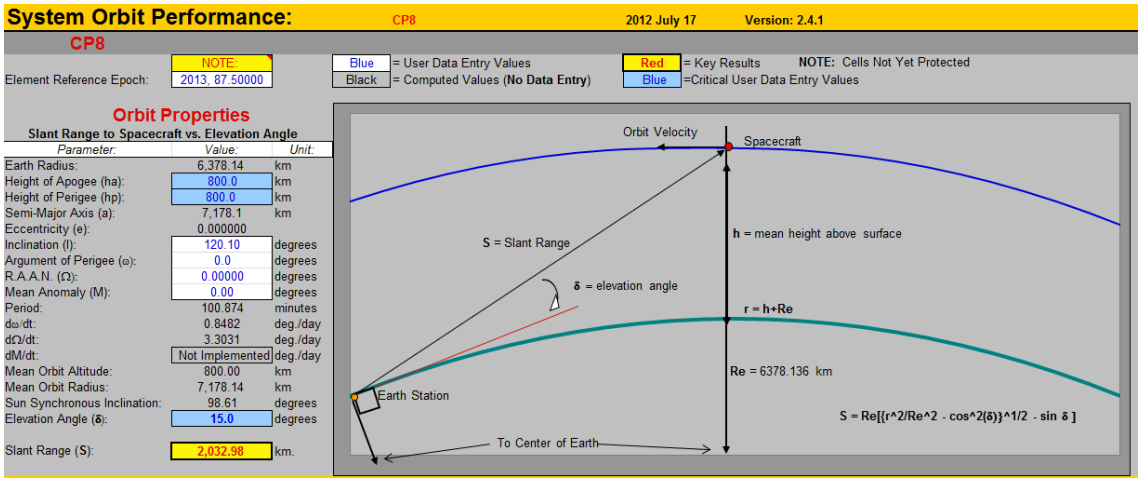

Figure 7: IPEX (CP8) Link Distance Calculation

For this calculation, an optimistic (theoretical maximum) gain of 2.15dBi will be assumed for the satellite dipole antenna. With the distance, frequency, losses, and antenna gains defined, the best-case receive power at the ground station can be calculated by inputting the numbers into the link equation.

$$\boldsymbol{P_R = P_T + G_T - \left(32.4 + 20log(d) + 20log(f)\right) - L_a - L_{point} - L_{pol} + G_R}$$

$$\boldsymbol{P_R = 30dBm + 2.15dB - \left(32.4 + 20log(2033) + 20log(437)\right)dB - 0 - 0 - 3dB + 24.9dB}$$

$$\boldsymbol{P_R = -97.3dBm}$$

Looking at the receive sensitivity measurements from William's thesis, it is theoretically possible to achieve a 100kbps link with a margin of -97.3dBm – (-108dBm) = 10.7dB in the absolute best case scenario. The UHF board's Axsem AX5042 transceiver can actually be configured up to a 600kbps data rate with a sensitivity of -102dBm using PSK modulation according to the datasheet. [12] From Williams' measurements, the UHF radio LNA increases the sensitivity by about 2dB; therefore a 600kbps link is theoretically possible with a margin of 6.7dBm.

In reality, satellite line losses, satellite antenna imperfections, pointing losses, elevated noise floor from spacecraft electronics, and ground station imperfections will reduce this receive downlink power. Even though the antenna would ideally be isotropic, the spacecraft dipole has a point of minimum gain called the null. If the spacecraft is tumbling or the ground station is not perfectly pointed at the satellite, the received power will be further reduced in the form of pointing loss; this is the largest source of additional loss. Williams' thesis calculated the loss of a 5 degree pointing error, 10 degrees from the antenna null as -8.2dB. Williams also estimated additional losses from line loss and antenna imperfections to be -4dB. [2] In practice, the combination of these imperfections equates to between 10 and 20dB of signal strength decrease from the optimistic downlink power calculated before. Therefore, as a rule of thumb, the link budget should have more than 15dB of margin than the best case, no-loss, perfectly aligned scenario. It is simpler to calculate link budgets with idealized numbers and add margin than attempting to model unpredictable pointing and implementation losses. PolySat's IPEX and Exocube (CP8 and CP10) satellites utilize the UHF radio at 9.6kbps. At 9.6kbps, the UHF radio has a receive sensitivity margin of -97.3 – (-117) = 19.7dB. The realistic receive power, including a 15dB margin is shown below:

$$P_R = P_T + G_T - \left(32.4 + 20log(d) + 20log(f)\right) - L_a - L_{point} - L_{pol} + G_R - Margin$$

$$P_R = 30dBm + 2.15dB - \left(32.4 + 20log(2033) + 20log(437)\right)dB - 0 - 0 - 3dB + 24.9dB - 15dB$$

$$P_R = -112dBm$$

Even accounting for pointing and unexpected losses with this 15dB margin, the IPEX mission still experienced spotty uplink at 9.6kbps. The receive sensitivity of IPEX was measured to be -105dBm in an idle state and -99dBm during high activity. This 12 to 18dB reduction in spacecraft receive sensitivity was caused by spacecraft EMI radiated by the close-proximity, poorly-shielded electronics near the UHF antenna, which was mitigated but difficult to eliminate entirely due to the small form factor of CubeSats. However, IPEX's reduced receive sensitivity was compensated by a 100W ground station amplifier which should have overcame the spacecraft noise floor with a total uplink margin of around 20dB. Unfortunately, the issue was confounded by aging ground station hardware and the bring-up and troubleshooting of the new ground station hardware and software, so the true cause of the poor uplink is unknown. Regardless, IPEX completed its mission successfully and the ground station successfully decoded more data than any other PolySat satellite to date (>20MBs).

3 Increasing Receive Signal Strength

In order to investigate methods to increase downlink signal strength and thus higher data rate of future satellites, the link equation will be investigated:

$$\boldsymbol{P_R = P_T + G_T - \left(32.4 + 20log(d) + 20log(f)\right) - L_a - L_{point} - L_{pol} + G_R}$$

The antenna gain equation for a typical 55% efficient parabolic dish, according to EW101 [9]:

$$\boldsymbol{G = -42.2 + 20log(D) + 20log(f)}$$

Where D = reflector diameter in meters and f = frequency in MHz.

Plugging the antenna gain equation into the link equation reveals:

$$\boldsymbol{P_R = P_T - 42.2 + 20log(D_{sat}) + 20log(f) - \left(32.4 + 20log(d) + 20log(f)\right) - L_a - L_{point}}$$

$$\boldsymbol{- L_{pol} - 42.2 + 20log\left(D_{ground}\right) + 20log(f)}$$

Reducing and simplifying gives:

$$\boldsymbol{P_R = P_T + 20log(D_{sat}) + 20log(f) - 20log(d) - L_a - L_{point} - L_{pol} + 20log\left(D_{ground}\right) - 116.8}$$

As tertiary payloads, CubeSats do not usually get to choose their orbit; therefore losses from distance and atmosphere are not in control of CubeSat engineers.

The equation can be reduced to parameters controllable by CubeSat developers:

$$\boldsymbol{P_R = P_T + 20log(D_{sat}) + 20log(f) + 20log\left(D_{ground}\right) - L}$$

Where L = link loss dependent on orbit, pointing accuracy, and additional losses not easily controlled by CubeSat hardware developers.

Looking at the equation shows that doubling transmit power will increase receive signal strength by 3dB, however, due to the small size of a cubesat (3U cubesat = 10cm x 300cm), increasing the transmit power will quickly reach a limit due to thermal dissipation limits and limited solar input power. A maximum practical cubesat transmit power is about 4W. Doubling satellite antenna size will increase receive signal strength by 6dB, but the small size of a CubeSat also limits the practical maximum size that can

be folded into its volume. Deployable dish antennas have been implemented by several CubeSat developers, for example the Aeneas 3U nanosatellite built by University of Southern California featured a 0.5m deployable dish. [13]

Receive power increases with $20log(f)$ and $20log(D_{ground})$, therefore receive signal strength increases by +6dB for each doubling of frequency or doubling of ground station antenna size. After a certain point, doubling the ground station dish size is no longer practical. After about 12m (~40ft), the antenna cost due to size becomes impractical for non-government entities.

Therefore, several changes can be employed to increase data rates for PolySat satellites: transmit power from the satellite should be at least doubled to 2W for an additional 3dB, the radio frequency should be increased, satellite antenna size should be increased, and ground station antenna size should be increased. A large change in any one of these parameters is impractical, but a combination of increasing each parameter by a practical amount will result in a higher data rate system.

Increased data rate is the primary motivation behind an S-Band communication system. The method of increasing the data rate is by changing the parameters of the link equation until economic or practical limits are reached, these changes are listed below:

1. Increase the frequency from 400MHz to 2400MHz, resulting in increased antenna gain compared to physical size. Consumer-off-the-shelf (COTS) components and design literature are available for 2400MHz designs due to the proliferation of ISM communication devices. The next highest frequency with COTS component support would be 5.8GHz. However, at 5.8GHz more specialized design techniques are required due to the increased significance of PCB trace length, the requirement to move from lumped elements (surface mount inductors and capacitors) to distributed microstrip elements, and required

simulation software packages. Features longer than 1/20th of a wavelength are significant in RF design, at 2.4GHz this is 6.25mm and at 5.8GHz this is 3mm. Designing a 5.8GHz radio would require more time, money, and effort than designing a 2.4GHz radio, but moving to a higher frequency is unavoidable in the future.

2. Adding a 4.5m dish to the PolySat ground station network. A 4.5m dish, under $15,000, seems practical and manageable for the PolySat lab. At 2.4GHz, a 4.5m dish kit with a gain of 39.4dB can be purchased online from rfhamdesign.com. [14]
3. Increase satellite transmit power to 2W (33dBm), resulting in a 3dB increase compared to 1W. 2.4GHz COTS amplifiers above 2W are not easily available and require more complex thermal management.
4. Requiring a higher gain antenna on the satellite, either a patch or deployable dish. Realistically a deployable dish would be required to meet the link budget margin at the higher data rates. A high gain dish would also require more complex attitude control systems, such as the system designed for PolySat's ExoCube mission, to steer and point the satellite at the ground station. A 0.5m dish would provide around 17dBi of gain.

The S-Band radio could also provide redundancy in the event of an UHF communications system failure, but with a high gain antenna, communication would be less robust.

4 ISM S-Band Radio System Requirements and Overview

The derived requirements for the Intrepid S-Band ISM Radio (ISIR) are as follows:

Table 2: Intrepid S-Band ISM Radio Derived Requirements

ISIR Target Specifications	
Frequency Range	2400 – 2483.5 MHz (ISM Band)
Maximum Transmit Power	2W (33dBm)
Receive Mode Power Consumption	200mW
Transmit Mode Power Consumption	8W
Digital Interface	SPI or UART
Doppler Tolerance or Correction Capability	+/- 70kHz
Physical Dimensions	Intrepid Daughter Board B, 1.4” x 3.3”
Minimum Link Distance	2100 km
Amplifier Protection	PA and LNA

The receive power draw was derived from the 130mW consumption of the UHF radio in receive mode with added margin. [2] The transmit power draw is derived from 2W power amplifier operating at a saturated efficiency of 30% and powered from a 90% efficient power regulator with an added margin of 0.5W. The radio must be able to correct or tolerate a Doppler shift of approximately 50 kHz as described later in *4.5.2 Evaluation Board Doppler Tolerance Measurement*; a 20 kHz margin was added. The minimum link distance was taken from the IPEX orbit of 800km at an elevation angle of 15 degrees, which seems like a typical CubeSat low-earth-orbit (LEO). The link distance will not only depend on the radio receive sensitivity, but also the ground station specifications such as antenna gain, transmit power, and noise floor.

Figure 8 shows a conceptual diagram of the Intrepid S-Band ISM Radio (ISIR). The transceiver interfaces to the command and data handling (C&DH) processor through either SPI or UART. The RF output of the transceiver is switched between an external power amplifier (PA) and low noise amplifier (LNA) for transmit and receive. Circuits for amplifier protection are desirable to prevent damage during lab testing.

Transmit power measurement is desired for closed loop control of the power amplifier output power by the C&DH. The radio will interface to one or two directional antennas mounted on the satellite through coaxial connectors. Not shown in the picture are the power regulators, power sensors, temperature sensors, and additional glue circuitry.

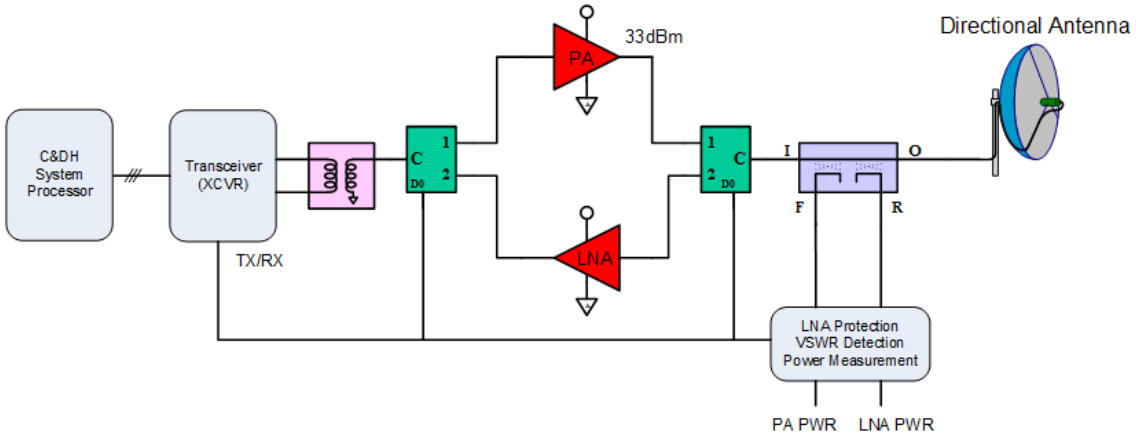

Figure 8: Intrepid S-Band ISM Radio (ISIR) Diagram

4.1 Component Trade Studies

Every RF component for the Intrepid S-Band ISM Radio was carefully selected by comparing commercially available components and choosing the component with the best figure of merits; this process is referred to as a component trade study. The most critical component in the radio design is the transceiver IC, which is the transducer between the satellite processor's data interface and the RF signal. The transceiver is an RFIC microcontroller that filters, demodulates, decodes, and converts the RF signal onto a data bus interface supported by the satellite microprocessor, usually SPI or UART. The transceiver was selected based on the following criteria from most significant to least significant: temperature range, receive sensitivity, frequency range, power consumption, data rates, evaluation board availability, software availability, transmit power, modulation types, buffer size, forward error correction, and antenna interface.

Over 20 transceivers were researched online and compiled into an Excel table for easy comparison. The excel table is too large for this document, but a snap shot of a portion of the table is shown in Figure 9.

Manufacturer	Part Number	Supply Voltage	Standby Current	Frequency Range	Data Rate	Interface	Antenna Interface	Protoc
Texas Instruments	CC2530	2-3.6V	24mA	2.394-2.507GHz	250kbs	SPI, I2C	Differential	802.15.4, 2
Texas Instruments	CC2500	1.8-3.6V	18.8mA	2.4-2.4835GHz	1.2-500kBaud	SPI	Differential	None?
Atmel	ATR2406	2.9-3.6V	57mA	2.4-2.4835GHz	72/144/288/576/1152kbps	SPI	Single (Tx) and Diff (Rx)	
Analog Devices	ADF7242	1.8-3.6V	19mA	2.4-2.4835GHz	50-2000kbps (variable)	SPI	Dual Differential (Rx & Tx), or Diff with diversity	802.15.4, 8
Analog Devices	ADF7241				250kbps			
Austrian Microsystems	AS3940	2.2-3.6V	20.9mA	2.405 to 2.48GHz	250, 1000, 2000 kbps	SPI	Differential	None?
Cypress Semiconductor	CYRF7936	1.8-3.6V	21.2mA	2.4 to 2.483GHz	250 with DSSS, 1mbps at GFSK	Proprietary	Differential	
CEL	ZIC2410	1.5V and 3V	33.2mA	2.4 to 2.483GHz	250, 500, and 1000kbps	SPI	Differential	802.15.4, 2
Ember	EM260	2.1-3.6V	36mA	2.4 to 2.485GHz	250kbps	uart, SPI	Single (optional dual)	802.15.4, 2
Freescale Semiconductor	MC1323x	1.8 to 3.6V	34.2mA	2.405 to 2.48 GHz	250kbps	SPI, I2C, UART	Differential	802.15.4, 2
Freescale Semiconductor	MC13202	2-3.4V	37mA	2.405 to 2.48 GHz	250kbps	SPI	Dual Differential	802.15.4, 2
Atmel	AT86RF230	1.8 to 3.6V	16mA	2.405 to 2.48 GHz	250kbps	SPI	Differential	802.15.4, 2
Atmel	AT86RF231		12.3mA		250, 500kbps, 1, 2mbps		Diff, with antenna diversity	
MicroChip	MRF24J40	2.4-3.6V	19mA	2.405 to 2.48 GHz	250, 625 kbps	SPI	Differential	802.15.4
RFMD	ML2724	2.7-3.3V	55mA	2.4 to 2.485GHz	1.536Mbps	3 Wire Serial	Singe and Dual?	N/A
RFMD	ML2730	3-3.6V	63mA	2.4 to 2.485GHz	576, 1152, 1536, 1755, 2048kbps	3 Wire Serial	Separate: Single Rx, Diff Tx	N/A
Texas Instruments	CC2520	1.8-3.8V	22.3mA	2.394 to 2.507GHz	250kbps	SPI	Differential	802.15.4, 2
MicroHard	MHX2400	5V	212mA	2.4 to 2.4835GHz	2.4 to 115.2kbps	UART (RS232)	Single	N/A
Atmel	AT86RF233	1.8-3.6V	11.8mA	2.322 to 2.527GHz	250kbps, 500kbps, 1000kbps, 2000kbps	SPI	Differential	802.15.4, 2
Nordic	nRF24L01+	1.9 - 3.6	13.5mA	2.4GHz	250kbps, 1Mbps, 2Mbps	SPI		

Figure 9: Portion of Transceiver Trade Study Excel Sheet

The Atmel AT86RF233 ZigBee transceiver was selected due to its high receive sensitivity, low power draw, variable frequencies and data rates, evaluation board availability, and sufficient software support. The Atmel AT86RF233 transceiver specifications are summarized in the bulleted list below:

- **Frequency**: 2.322 to 2.527 GHz, 500kHz channel spacing
- **Channel Size:** 2.3MHz (Spread-spectrum)
- **Modulation**: O-QPSK
- **Protocol**: ZigBee IEEE 802.15.4, supports FEC
- **Processor Interface:** SPI bus, 128 FIFO SRAM buffer size.
- **Data Rates**: 250kbps, 500kbps, 1000kbps, or 2000kbps.
- **Receive Sensitivity**: varies with data rate
    - 250kbps: -101dBm
    - 500kbps: -96dBm
    - 1000kbps: -94dBm
    - 200kbps: -88dBm
- **Programmable Transmit Power**: -17dBm to 4dBm
- **Power Consumption**: 20mW RX, 46mW TX.
- **Antenna Interface**: Differential
- **Temperature Range**: -40C to +125C
- **Noise Figure**: 6dB
- **Additional Features**:
    - Antenna diversity algorithm
    - External amplifier control
    - RSSI and LQI measurement
    - AES 128-bit hardware encryption
    - Time and phase measurement support (ranging)

As the schematic was developed, trade studies were performed for each critical component in the design including the: transceiver, low noise amplifier, high power amplifier, bandpass filter, low pass filter, high power RF switch, low power RF switch, directional couplers, balun, oscillator, RF detectors, and power regulators. The power draw of the radio must be minimized, so power consumption is a significant specification when searching for components. The peak power generation of a 1U CubeSat with 2 solar cells per side is approximately 2W while illuminated, but the average power depends on the orbit parameters and the resulting duty cycle of sunlight and eclipse. IPEX had periods of 1.2W average solar power due to the amount of time spent in the sunlight compared to the time spent in the shadow of the Earth. The radio is an important, but small part of the satellite mission. The radio power draw must be minimized so that the solar power can be utilized by the mission payload to meet mission objectives.

Table 3 lists the figures of merit and power draw for the five most important components in the radio design: the transceiver, power amplifier, low noise amplifier, oscillator, and power regulator.

Table 3: Important Components and Figures of Merit

Description	Manufacturer	Part Number	Important Figures of Merit	Power Draw
Transceiver (XCVR)	Atmel	AT86RF233	TX Power: -17dBm to 4dBm Noise Figure: 6dB Receive Sensitivity: -101dBm at 250kbps Data Rates (kbps): 250, 500, 1000, 2000 Interface: SPI Modulation: O-QPSK	20mW RX 46mW TX
Power Amplfiier (PA)	RFMD	RFPA2026	Maximum TX Power: 34.5dBm Efficiency: 30% Gain: 37dB Noise Figure: 5.6dB	6.8W TX
Low Noise Amplifier (LNA)	Maxim	MAX2692	NF: 1.1dB Gain: 18dB P1dB: -16dBm	13.2mW
Temperature Controlled Crystal Oscillator (TCXO)	ECS	ECS-2532HS-160-3-G	Frequency Stability: +/-10ppm	30mW
Power Regulator	Texas Instruments	TPS63020	Efficiency: 90% Max Current: 3A	-

4.2 ISM Noise Floor

The radio operates in the unlicensed 2.400 to 2.4835 GHz industrial, scientific, and medical (ISM) radio band. Twelve portions of the radio spectrum are allocated for the ISM band by the FCC with frequencies ranging from 6.78MHz up to 245.00 GHz. [15] ISM is reserved for non-communication applications such as heating, cooking, ultrasonics, cleaners, particle accelerators, radio astronomy, space research, and mechanical vibration. [15] ISM equipment is permitted to radiate unlimited energy within the ISM bands but the field strength level at specified distances is regulated by the FCC. [15] These non-communication applications of RF radiation are segregated into these ISM “junk” bands in order to isolate the high power noise generated by these applications from the sensitive communication services utilizing the remainder of the radio spectrum.

In 1985, the FCC approved unlicensed spread spectrum radio communication within the 915, 2450, and 5800 MHz ISM bands. [16] Allowing unlicensed devices to share these ISM bands for communication purposes facilitated the proliferation of consumer wireless devices such as cordless phones, wireless networking, garage door openers, and other low power, short distance communication standards such as Bluetooth, ZigBee, and WiFi. In order to share the unlicensed bands most effectively, the FCC limits the types of modulation and output power radiated in these ISM bands. The goal of these FCC limits is to maximize the number of devices successfully sharing the ISM band by reducing interface. Radio communication within the ISM bands must employ spread spectrum modulation techniques and are limited to a maximum of 1W output power. These spread spectrum techniques deliberately increase the bandwidth of a signal in order to reduce its susceptibility and contribution to interference to other devices sharing the band.

The consumer ISM industry provides a vast supply of consumer-off-the-shelf components (COTS) for use in a 2.4GHz satellite radio design. ISM COTs components greatly reduce the cost, reduce design time, increase performance, and increase reliability of 2.4GHz transceivers by leveraging the billions of dollars and man hours already spent by companies to design, test, and improve ISM consumer devices. However, the popularity of unlicensed ISM devices is also a weakness for satellite communications due to the high interference levels produced by the ever-growing number of ISM devices transmitting in-band. The earth station must be capable of receiving a weak signal from an orbiting satellite greater than 1800km away through the sea of interference caused by unpredictable, high power, in-band ISM devices transmitting nearby. There are several potential fixes to this ISM interference issue: the earth station can be located in a remote area devoid of ISM transmitters, the earth station can employ filtering, shielding, or antenna design techniques to reduce terrestrial

ISM interference, the satellite frequency can be carefully chosen to occupy a “quieter” portion of the ISM band, the modulation of the signal can be modified to increase resistance to common ISM interference, and so forth.

Traditional, government satellites utilize expensive, specialty designed radios for communicating in the quieter satellite S-Band spectrum: 2200 to 2300 MHz. However, CubeSats cannot afford the same luxuries as traditional satellites: low budgets and short schedules prevent CubeSat teams from obtaining government licenses in these satellite bands and acquiring cost effective radios for these frequencies. Also, this S-Band spectrum is reserved only for government-funded projects. The tradeoff of using a cheap, efficient, reliable COTS ISM transceiver for a satellite S-Band radio is that it must operate at lower data rates due to less specialized hardware and more in-band interference.

In order to characterize the 2.4GHz noise floor of the earth station, the typical transmitters must be identified in terms of frequency and power. Typical 2.4GHz consumer communication devices in an urban environment include cordless phones, Bluetooth devices, 802.11b Wi-Fi wireless routers, wireless USB devices, phones, video game controllers, and ZigBee devices. The typical non-communication 2.4GHz device is the microwave oven. A man-made noise floor study in the S and L bands by NASA was conducted utilizing a feed horn antenna, spectrum analyzer, power supply, and computer called the L and S band Spectrum Measurement (LSSM) system shown in Figure 10. [17] Figure 11 shows the LSSM power spectrum measurement in the 2.4GHZ ISM band in downtown San Jose at ground level; the noise floor in the AT86RF233’s 2.3MHz bandwidth would be around -78dBm which is 32dB higher than the thermal noise floor of -110dBm. Interference strength of -78dBm is unacceptable for a satellite earth station and the station would not be able to receive data from the satellite with this

amount of ISM interference; the satellite would have to increase its transmit power by three orders of magnitude to overcome this level of interference.

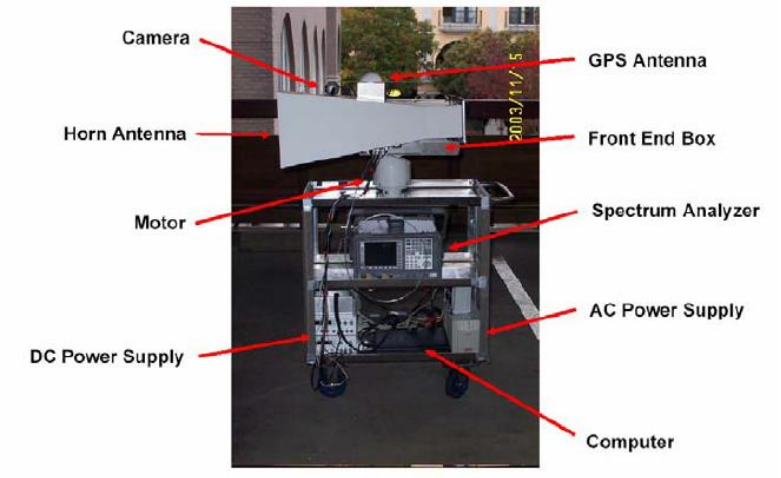

Figure 10: NASA Measurements of Man-Made Noise Floor, L and S bands Spectrum Measurement System (LSSM) [17]

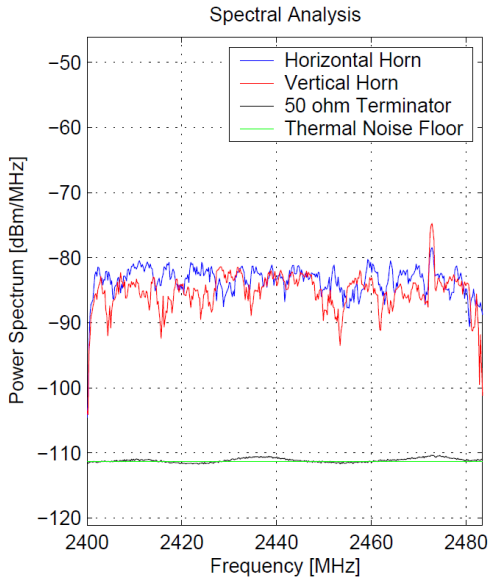

Figure 11: LSSM 2.4GHz Noise Floor Measurements, Downtown San Jose, 0 Degree Elevation [17]

However, the measurements made in this NASA study are taken from a 16dBi horn antenna rotated at 0 degree elevation at street level. This means the high gain antenna was pointed directly at the interfering transmitters, which maximizes the measured interference. These measurements are not directly applicable for high gain earth station antennas pointed into the sky and away from consumer ISM interference. Figure 12 shows measured interference power from the same study at a nature preserve as the antenna is held at 0 elevation ground level and azimuthally rotated. A -85dBm interference spike is shown at 120 degrees when the horn is directly pointed at an ISM transmitter. However, when horn is pointed away from the interference the power level drops to the thermal noise floor of -110dBm; this demonstrates that pointing a high gain antenna away from interference sources greatly reduces the interference. Average power measurements of a high gain antenna pointed into the sky at varying elevation angles would be more useful for aerospace application, but such a study could not be found. It is surprising that NASA would only study the noise level at 0 degrees of elevation, when most of their applications are pointed toward the sky.

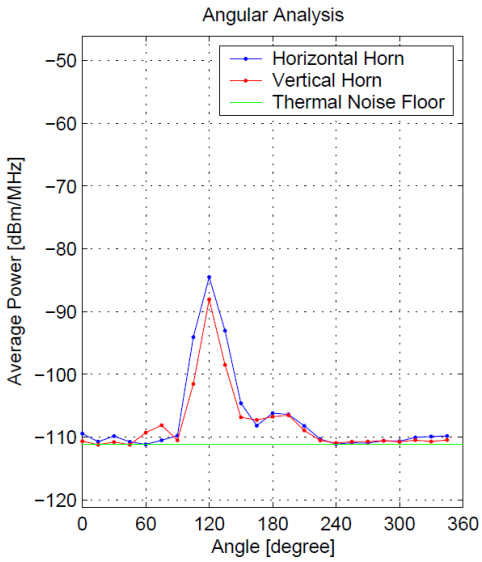

Figure 12: LSSM 2.4GHz Noise Floor Measurements, Jasper Ridge Preserve, 0 Degree Elevation, Azimuth Angle Varied

The Atmel AT86RF233 not only supports the standard 16 ZigBee channels defined in IEEE 802.15.4 but also any frequency from 2322MHz to 2527MHz with 500 kHz spacing. Because the satellite is not required to follow the ZigBee standard, this frequency selection flexibility allows the designer to select a frequency with the least interference within the 2.400 to 2.4835 GHz ISM range. Interference can be minimized by selecting a frequency outside or in between standard ISM channels.

The FCC requires that ISM communication be spread spectrum, this is generally performed in two ways: frequency hop spread spectrum (FHSS) or direct sequence spread spectrum (DSSS). For example, Bluetooth is a FHSS standard that changes frequency 1600 times per seconds across pre-defined channels across the entire 2.4GHz ISM band. On the other hand, Wi-Fi is a DSSS standard that directly modulates the carrier signal using a pseudo-random chipping code sequence which increases the bandwidth of the signal but minimizes the effect of narrow-band interference sources within the bandwidth while also rejecting signals with different pseudo random sequences. ZigBee is a DSSS standard, so interference from FHSS sources are less detrimental than interference from other DSSS sources; narrow band FHSS interference will be reduced after de-spreading and the interference will only be temporary.

Figure 13 is a plot from an Atmel application note of ZigBee channels and the most commonly used 2.4GHz Wi-Fi channels: Channel 1, Channel 6, and Channel 11. [18] This figure shows that the satellite frequency can be chosen carefully by surveying the ISM channels in use around the ground station site and choosing a frequency with minimal overlap with those interference sources.

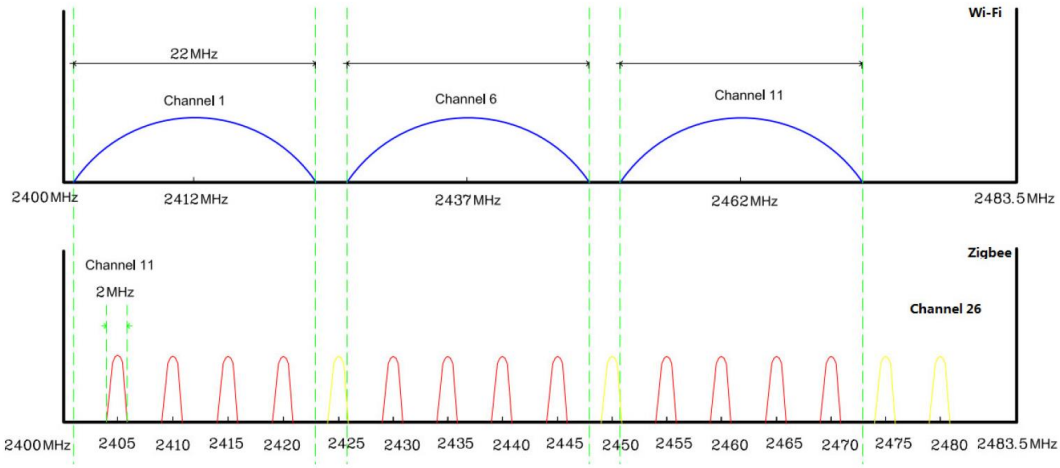

Figure 13: Wi-Fi and ZigBee Channel Frequencies and Spacing [18]

To better understand the ISM interference problem, a rooftop interference survey was performed on a commercial building rooftop in Irvine, California. A 24dBi parabolic mesh antenna was purchased online for $45 and mounted on the pre-existing CubeSat antenna rotor system as shown in Figure 14.

Figure 14: 2.4GHz, 24dBi Parabolic Antenna Mounted on Rotor System

A Mini-Circuits ZX60-272LN+ low-noise amplifier, with 14dB gain and 0.75 noise figure, was connected directly after the antenna as close to the antenna as possible to minimize the effects of cable loss and to increase the sensitivity of the spectrum analyzer; this mast-mounted low noise amplifier is typical for high-frequency antennas systems. Figure 15 shows the low-noise amplifier connected as close to the parabolic antenna as possible.

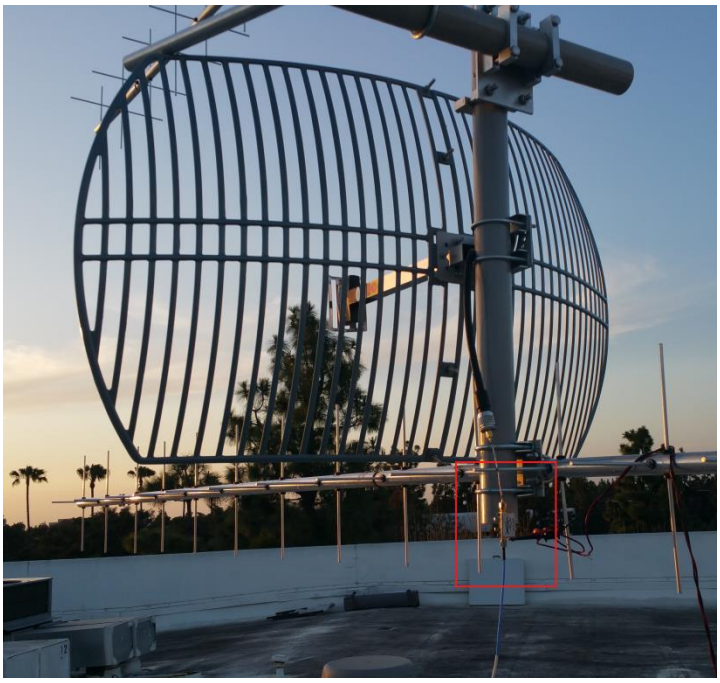

Figure 15: Low Noise Amplifier Connected to Antenna as Close as Possible

Figure 16 shows a diagram of the interference measurement setup. The antenna was pointed at various directions and elevations while taking measurements of 2.4GHz ISM activity.

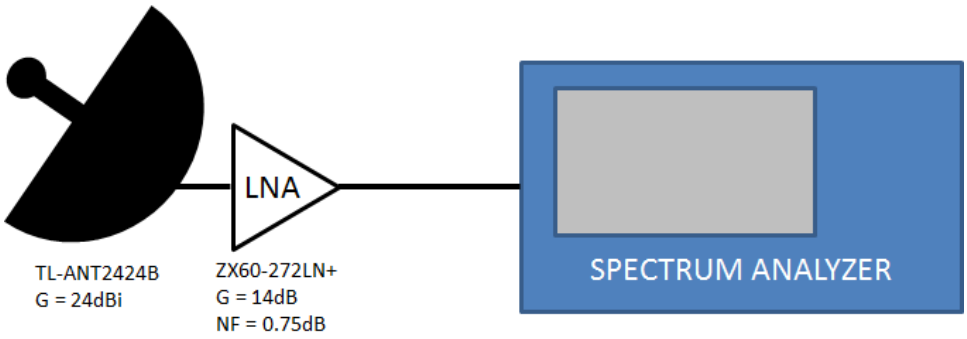

Figure 16: Rooftop Interference Survey Diagram

The antenna was pointed at the azimuth angle of 285° toward the most buildings and maximum ISM interference. Figure 17 and Figure 18 show the primary antenna azimuth pointing direction during the interference survey. The antenna was kept at this azimuth direction and the elevation of the antenna was varied between 0° and 90° while taking spectrum measurements.

Figure 17: Antenna Side View

Figure 18: Antenna Pointing at 285 Degrees Azimuth, 15° Elevation, Toward Buildings, Interference Survey Direction

Figure 20 shows a one minute max hold measurement of the ISM band at an elevation angle of 0 degrees. An elevation of 0 degrees produces that maximum terrestrial interference. Note that the ISM band is 2.400 GHz and 2.4835 GHz, which explains the low noise floor after 2.4835 GHz to the right of the measurement; this 2.4835 to 2.500 GHz portion of the frequency spectrum is purchased and reserved for Globalstar satellite phone service. On the other side of the ISM band, 2.3325 to 2.345 GHz is reserved for XM and Sirius satellite radio and 2.300 to 2.390 GHz is reserved for aeronautical mobile service telemetry.

Figure 19 shows an average power measurement of a 50 Ohm load input to the low noise amplifier to characterize the measurement noise floor. Note that the spectrum analyzer figure numbers do not take into account the 14dB of gain from the mast-mounted low noise amplifier, so 14dB needs to be subtracted from the numbers in the figures. Figure 21 shows the ISM band measured with a 50 point average to identify the most persistent ISM interference. The three humps are Channel 1, Channel 6, and

Channel 11 WiFi communication, which could be local or from the buildings on the horizon. Figure 22 and Figure 23 show the same measurements with the antenna pointed skyward at an elevation angle of 45 degrees; the ISM interference is reduced by 7 to 15 dB compared to 0 degree elevation.

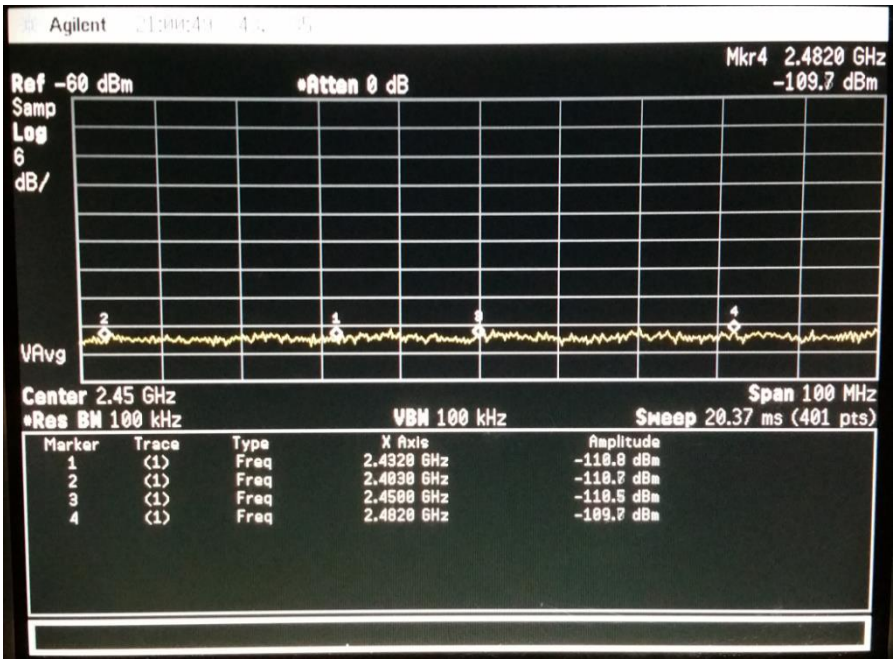

Figure 19: 50 Ohm Load, 50 Point Average, Instrument Noise

(Subtract 14dB for External LNA)

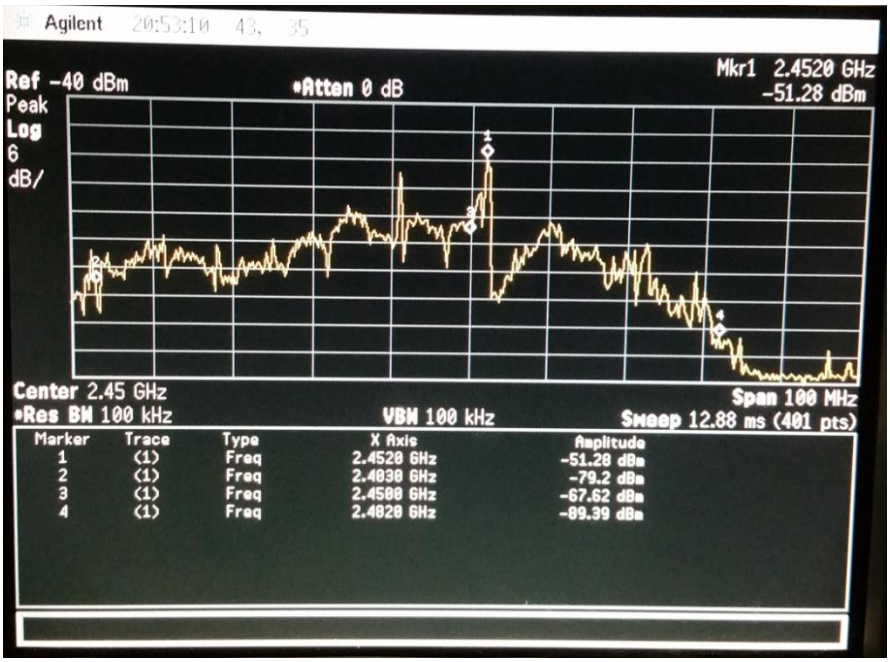

Figure 20: ISM Interference Max Hold 1 Minute, Azimuth: 285°, Elevation 0°

(Subtract 14dB for External LNA)

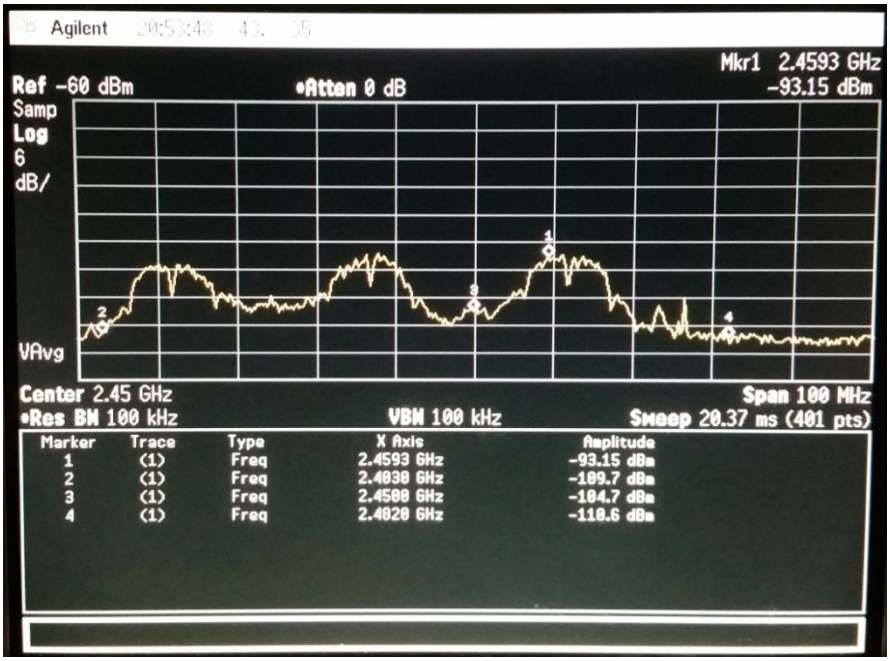

Figure 21: ISM Interference 50 Point Average, Azimuth: 285°, Elevation 0°

(Subtract 14dB for External LNA)

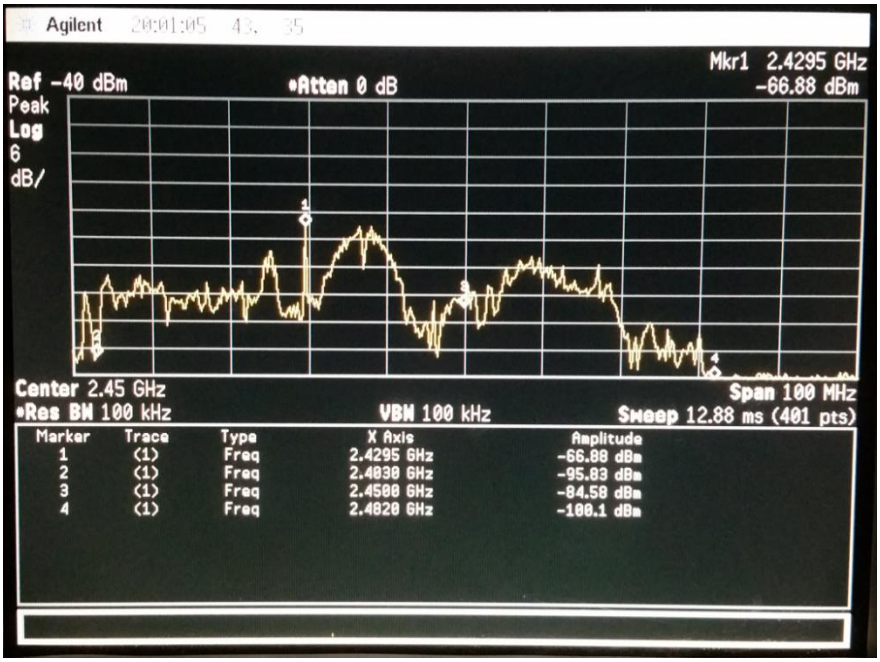

Figure 22: ISM Interference Max Hold 1 Minute, Azimuth: 285°, Elevation 45°

(Subtract 14dB for External LNA)

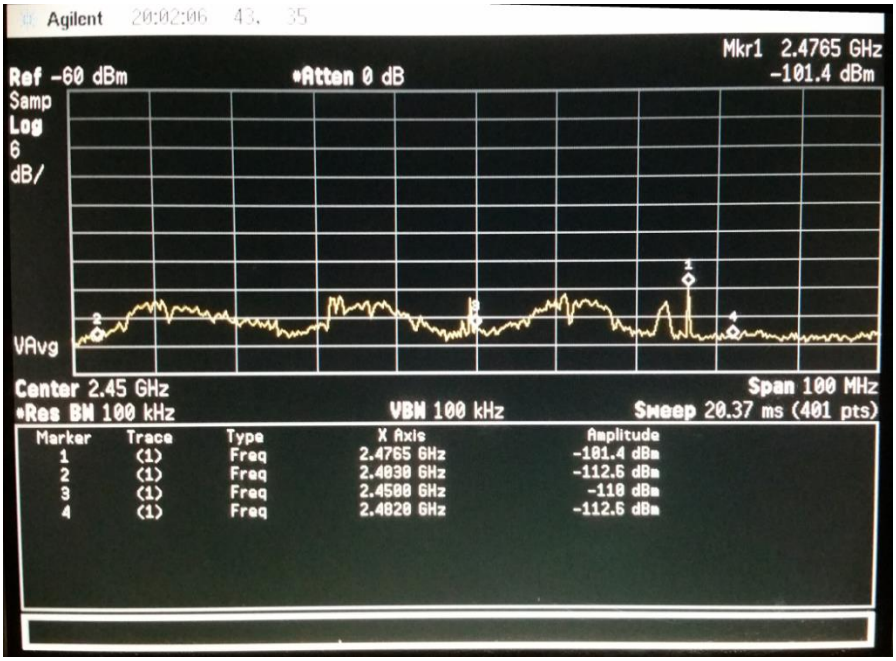

Figure 23: ISM Interference 50 Point Average, Azimuth: 285°, Elevation 45°

(Subtract 14dB for External LNA)

The Wi-Fi interference is present at every elevation and azimuth angle which indicates that the interference is likely from Wi-Fi hot spots nearby and most likely within the building the antenna is mounted. In this sea of interference, points of little activity can still be located. Marker 4 in these figures is the measurement at 2.4820 GHz; this frequency is at the very edge of the ISM band and the edge of WiFi channel 11. The peak interference at 45 degrees is -114dBm at 100kHz bandwidth and the average level of interference at 2.4820GHz is below the noise floor of the measurement.

The interference sources at 2.4820 GHz were observed to be frequency hopping FHSS signals that would minimally interfere with the DSSS radio receiver for short bursts causing minimal packet drops. Figure 24 shows a 1 minute max hold zoomed in at 2.482 GHz at an elevation of 0 degrees, which captured the peaks of the frequency hopping transmissions. Figure 25 shows the same measurement at 45 degree elevation showing that the interference sources are completely eliminated below the measurement noise floor by pointing the antenna toward the sky. Based on these max hold and average power measurements, 2.482 GHz would be the best choice for the ISM satellite radio frequency at this ground station.

Figure 26 and Figure 27 show channel power measurements at 2.482 GHz and also at 2.440 GHz for comparison. The AT86RF233 transceiver bandwidth is 2.3MHz, so interference power within a 2.3MHz bandwidth was measured with a 50 point average. The average interference at 2.482 GHz is more than 18dB less than the interference present at 2.440 GHz; any possible interference at 2.482 GHz is below the measurement noise floor at -109 dBm measured with a 50 Ohm load in Figure 28. Max Hold and average measurements of the ISM band were made at different azimuth angles as well, which confirmed low noise at 2.482 GHz in all directions; Figure 29 shows the max hold measurement made at an azimuth of 180 degrees.

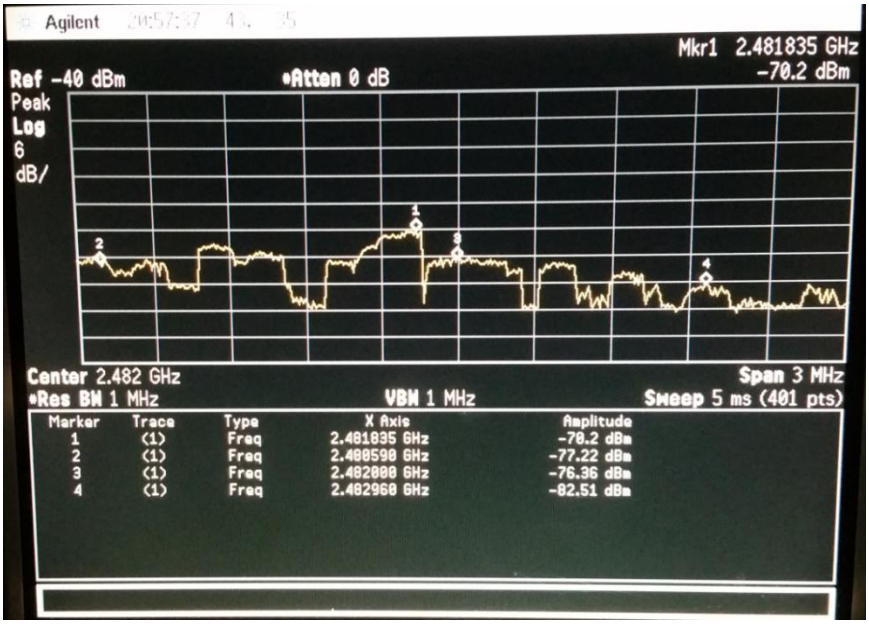

Figure 24: 1 Minute Max Hold 2.482 GHz, Azimuth: 285°, Elevation 0°, FHSS Interference (Subtract 14dB for External LNA)

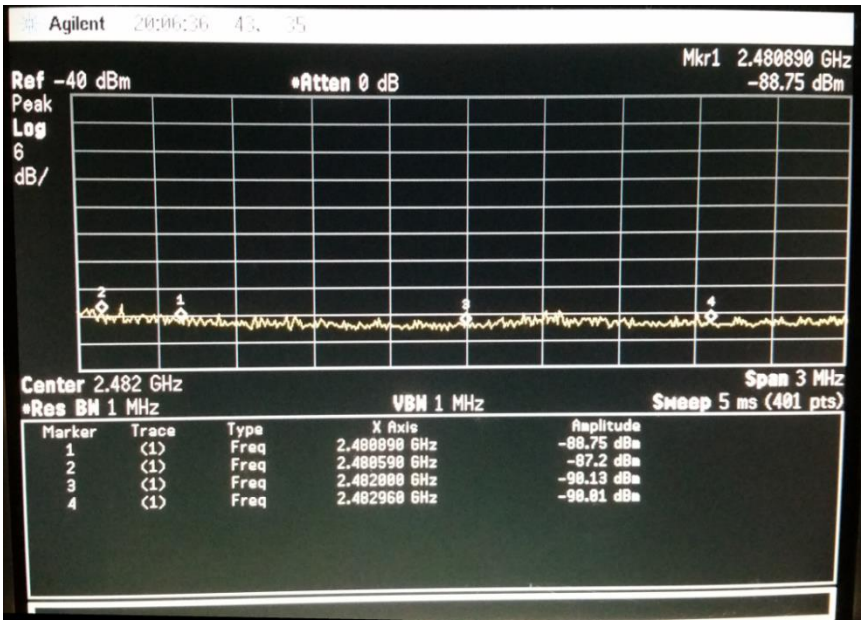

Figure 25: 1 Minute Max Hold 2.482 GHz, Azimuth: 285°, Elevation 45°, FHSS Interference Reduced (Subtract 14dB for External LNA)

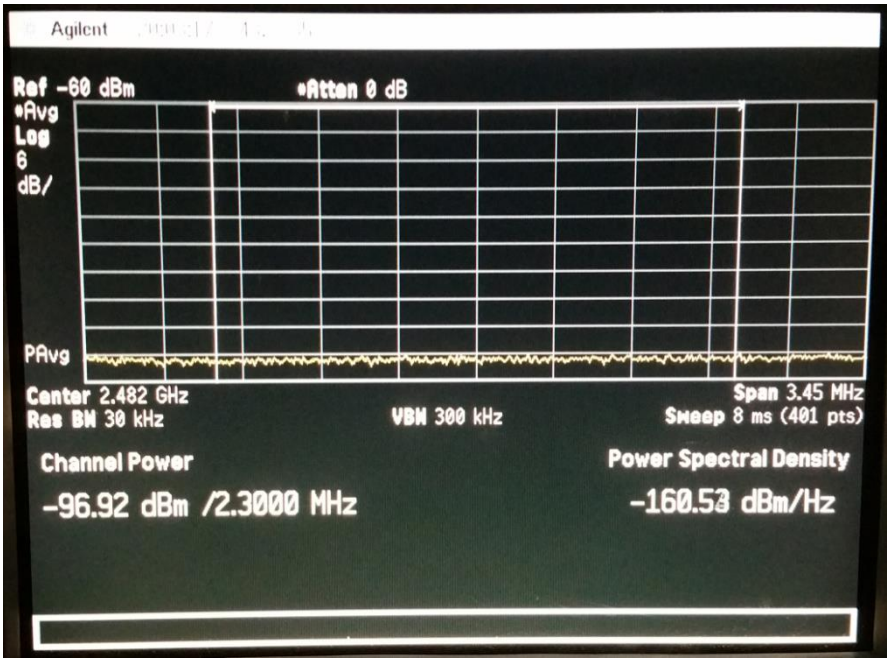

Figure 26: Interference Channel Power 2.482 GHz, Azimuth: 285°, Elevation 45°

(Subtract 14dB for External LNA)

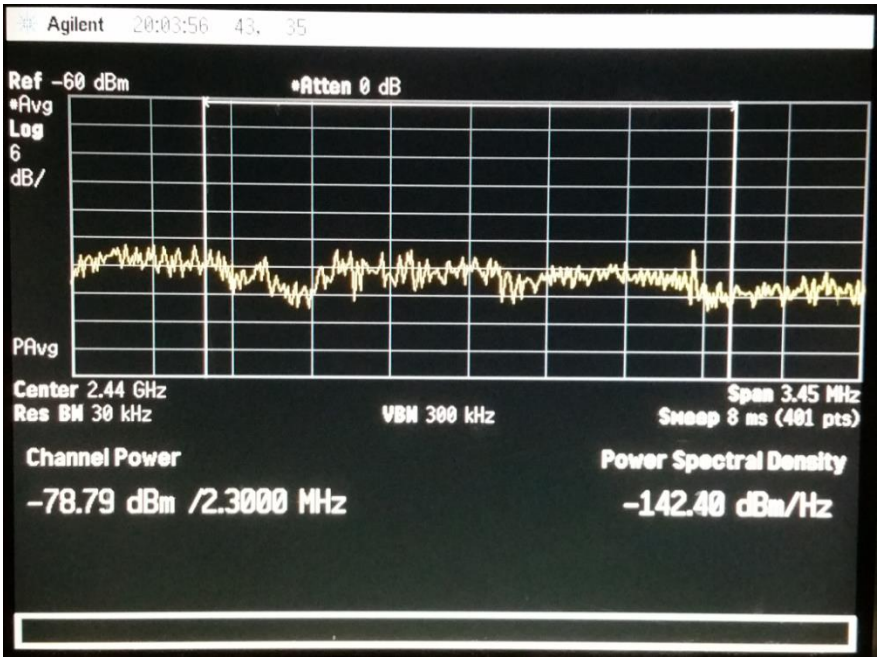

Figure 27: Interference Channel Power 2.440 GHz, Azimuth: 285°, Elevation 45°

(Subtract 14dB for External LNA)

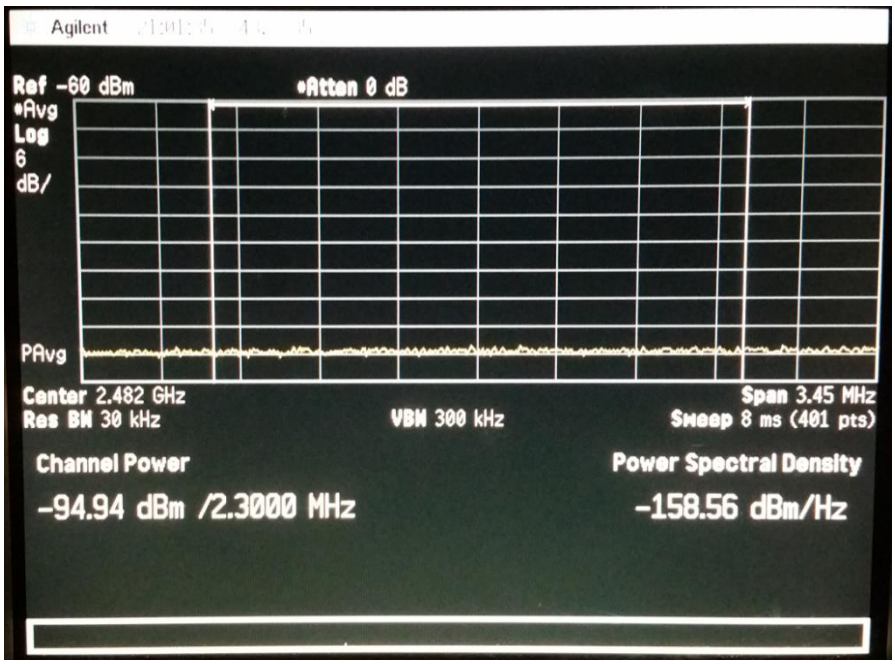

Figure 28: 50 Ohm Load Channel Power, Measurement Noise Floor

(Subtract 14dB for External LNA)

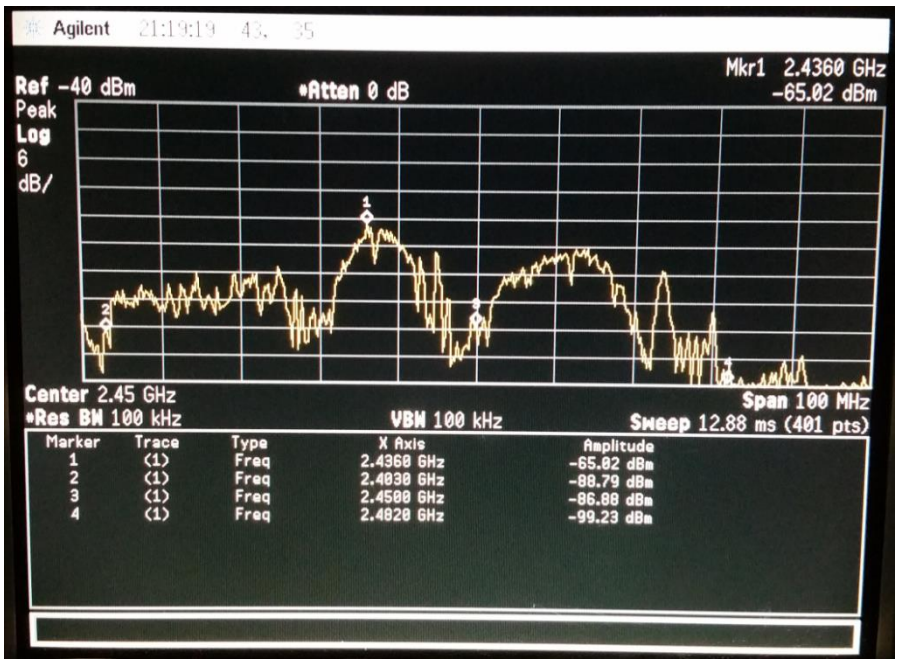

Figure 29: ISM Interference Max Hold 1 Minute, Azimuth: 180°, Elevation 15°

(Subtract 14dB for External LNA)

Figure 30 shows a plot of the average noise within a 2.3MHz bandwidth at three frequencies in the ISM band as a function of antenna elevation angle. As discussed earlier, 2.482 GHz had the least interference while 2.440 GHz was located in a more active region of the band. The 2.440 GHz interference only decreases by 7dB when the antenna is pointed toward the sky, indicating the noise is most likely local to the ground station. The 2.450 GHz interference decreases by 16 dB at an elevation angles above 45 degrees, which probably indicates the transmitter was miles away.

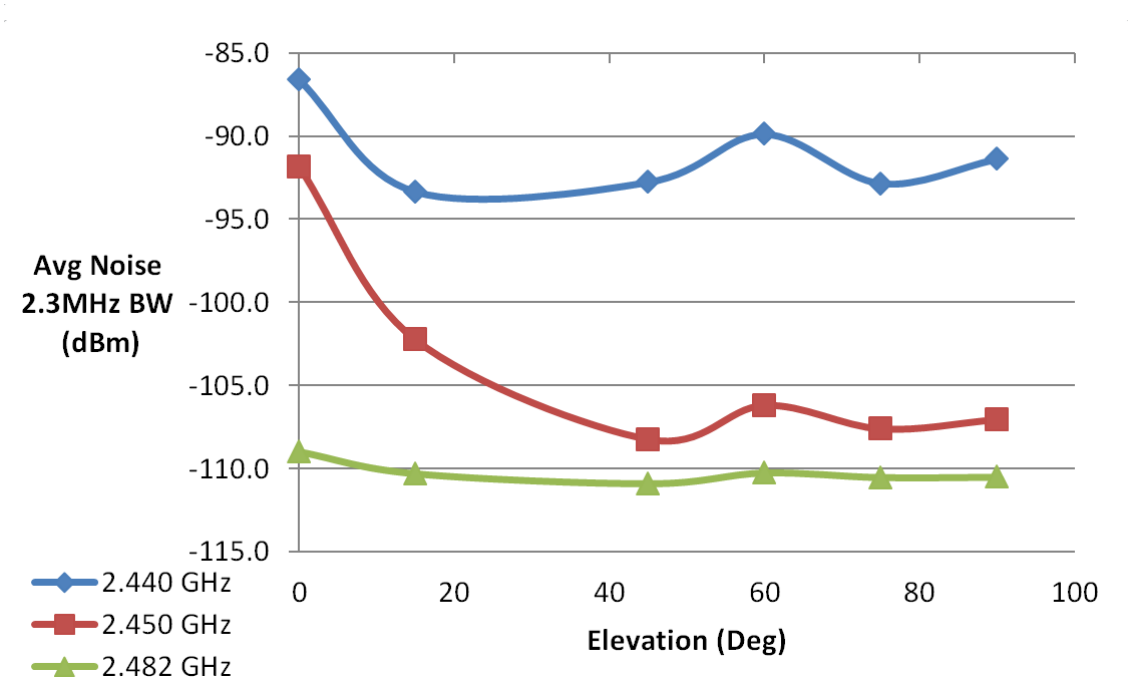

Figure 30: Interference vs Antenna Angle Measurements

The parabolic antenna used in this noise survey has 16dB less gain than the 5.8 meter dish proposed for the final ISM S-Band ground station. The interference is expected to be reduced even further for the 4.5m dish while pointed skyward. These measurements demonstrate the importance of surveying the ground station location and carefully choosing the spacecraft communication frequency. However, even if unexpected noise does appear within the chosen frequency, the spacecraft could be

commanded to another ISM frequency over the UHF link. The process of determining and selecting a clear channel could be automated and coordinated between the satellite and ground station computer during a pass, providing additional interference mitigation. Also, if the satellite is communicating with a network of ground stations, each ground station could indicate its local clear channel.

If pointing the dish toward the sky and carefully picking the satellite frequency is not enough to reduce ground ISM interference, another approach is to locate the ground station in a remote area with minimal ISM interference sources. For instance, a Cal Poly ISM earth station could be located in a field near the agricultural areas on campus and away from the library, dormitories, offices, labs, and class rooms.

4.3 Frequency Licensing

Even though the radio will operate in the internationally unlicensed ISM radio band, satellite transmitters are still required to obtain a license from the federal government. Non-federal missions are licensed with the FCC and federally-funded missions are licensed through the NTIA. If the CubeSat is utilizing the amateur bands, it must also coordinate with the International Amateur Radio Union (IARU). In 2013, the FCC released a public notice titled *“Guidance on Obtaining Licenses for Small Satellites,”* which recommends that CubeSats obtain a special license called an “experimental license,” for missions that involve experimental (scientific and research) operations. [19]

Experimental licenses typically last for a few years and can be renewed regularly. Experimental licenses do not have explicit frequency restrictions and an application can be submitted for any frequency at any power. However, the acceptance of an application is entirely at the discretion of the FCC. The FCC reviews each application on a case-by-case basis and will reject any applications that they believe infringes or interferes with

existing licenses and services. Additionally, the license can be canceled at any time and transmission must be immediately halted if operations cause interference to licensed users.

The FCC posts all experimental licenses, correspondence, and supporting documents online with an accompanying search system. [20] By reviewing the accepted and rejected experimental licenses, one can determine the de-facto frequency bands allowed for CubeSat communication. Although the AT86RF233 transceiver is capable of communicating in the quiet areas outside the ISM band 2.322 to 2.400 GHz and 2.4835 to 2.527 GHz, it is unlikely the FCC will approve a license utilizing those frequencies. Searching the experimental license database demonstrates that historically no CubeSat licenses have been approved for these frequencies. Applications that incorrectly requested the ISM band of 2.4 to 2.5 GHz were rejected because the ISM band technically ends at 2.483 GHz; this demonstrates that the FCC is deliberately limiting CubeSat S-Band communication to the ISM band. Many CubeSat licenses in the database are for the frequency range of 2400-2483.5 MHz, which does not restrict the mission to an exact frequency and allows the mission to change its frequency within the ISM band at will.

Experimental licenses allow CubeSats to transmit at power levels greater than the general ISM 1W ERIP restriction. For example, Texas A&M was granted a CubeSat license for 2400-2483.5 MHz at a transmit power of 8W ERP. [21] This precedent is what allows the Intrepid ISM S-Band Radio to transmit above the ISM limit.

4.4 Link Budget Estimates

4.4.1 Noise Floor Calculations

EW 102, Chapter 7 is referenced for estimating the link budget of the ISM system. [22] The noise floor of the satellite and ground station will be estimated using the thermal noise equation:

$$\boldsymbol{P_{Noise} = kTB}$$

The equation in decibel form:

$$\boldsymbol{P_{Noise}(dBm) = k + 10LOG(T) + 10LOG(B)}$$

Where P_{Noise}= Noise Power in dBm, k = Boltzmann's Constant = -198.6dBm/HzK, T = system temperature in Kelvin, and B = Bandwidth in Hz.

The system noise temperature is the sum of the equivalent receiver temperature and the equivalent temperatures of other noise sources in the system. The equation for system noise temperature is as follows:

$$\boldsymbol{T_s = T_{ANT} + T_{RCVR} + T_{OTHER}}$$

Where T_s = system noise temperature, T_{ANT} = antenna noise temperature, T_{RCVR} = receiver noise temperature including line loss to antenna, and T_{OTHER} = equivalent temperature of in-band interference, such as overlapping ISM channels.

The antenna noise temperature depends on what falls within the beam of the antenna. The earth is approximately 290K, the sky is 10K or lower, and the sun temperature is so high that the system is useless until the antenna is pointed away from the sun. If the antenna pattern partially includes the earth and the sky, then the weighted average of the temperatures estimates the antenna temperature. In the case of this CubeSat, a high gain antenna will be pointed at a ground station on earth, so the antenna noise temperature is 290K.

The receiver noise temperature is the fixed amount of noise the receiver adds to the signal which can be calculated from the receiver noise figure using the equation:

$$\boldsymbol{T_{RCVR} = \left(10^{\frac{NF}{10}} - 1\right) T_0}$$

Where F = noise figure in dB and T_0 is the standard reference room temperature of 290K. The AT86RF233 transceiver has a noise figure of 6dB, but the addition of an LNA will reduce the system noise figure to approximately 4dB including the component and line losses before the LNA. The satellite will not have additional noise due to ISM interference due to its distance from ISM transmitters, so the additional temperature is 0. The satellite noise floor is calculated to be approximately -106dBm as shown in Table 4.

Table 4: Estimated Satellite Noise Floor

Description	Value
Antenna Temp, Pointed at Earth (K)	290
Sat ReceiverTemp, NF = 4 (K)	438.4
Other Noise (K)	0
Total Temperature (K)	728.4
Total Temperature (dBK)	28.6
2.3MHz Channel Bandwidth (dBHz)	63.6
Boltzman Constant	-198.6
Satellite Noise Floor (dBm)	**-106.4**

The ground station antenna beam will be pointed into the sky toward the satellite, so its antenna temperature will be approximately 30K. It is assumed that the ground station will have an additional LNA on its mast to decrease noise due to cable loss from the antenna to the receiver. The mast LNA will reduce the noise figure of the system; the ground station noise figure is approximated as 2dB. The ground station will have an increased noise floor due to nearby terrestrial ISM interference. Noise floor measurements shown earlier in Figure 30 demonstrates the importance of choosing a frequency with minimal terrestrial ISM interference. At the Irvine ground station surveyed, 2.482 GHz was completely free of any interference above elevations of 15 degrees; the

interference power within the channel was below the -110dBm, 2.3MHz thermal noise floor. A margin of 3dB will be added for the ISM noise floor at the ground station to be an equivalent temperature of 631K which is an interfering signal level of -107dBm. Table 5 shows the calculation of the ground station noise floor of -105.5dBm.

Table 5: Estimated Ground Station Noise Floor

Description	Value
Antenna Temp, 15 degrees elevation (K)	30
GS ReceiverTemp, NF = 2.5 (K)	225.7
ISM Interference, -107dBm (K)	631.0
Total Temperature (K)	886.7
Total Temperature (dBK)	29.5
2.3MHz Channel Bandwidth (dBHz)	63.6
Boltzman Constant	-198.6
Ground Noise Floor (dBm)	**-105.5**

Table 4 and Table 5 show that the satellite's noise floor is dominated by its receiver noise figure, whereas the ground station noise floor will be dominated by terrestrial ISM interference. In this estimate, the ground station noise floor is increased by 4.5dB from ISM interference, which will reduce the total signal to noise ratio by 4.5dB.

The signal to noise ratio of a received signal determines whether a receiver will successfully decode a signal. Higher signal to noise ratio links can support higher data rates. The required signal to noise ratio for the AT86RF233 receiver to decode a packet can be calculated from its datasheet values for "receive sensitivity", noise figure, and signal bandwidth of 2.3MHz.

It is important to note that the datasheet's "receive sensitivity" measurement assumes a certain level of noise added to the signal. The receive sensitivity in the datasheet is measured in a laboratory setting with a transmitter transmitting directly to the receiver through a coaxial connection and attenuator. Therefore, the noise input into the receiver the thermal noise level at room temperature, which is 290K. The noise

figure of the transceiver indicates that the transceiver adds a fixed amount of additional noise to the signal before decoding it equal to the noise figure. The noise added to the signal is calculated by adding the thermal noise level to the noise figure noise:

$$\boldsymbol{P_{Noise}(dBm) = -\frac{198.6\text{dBm}}{\text{HzK}} + 10LOG(290K) + 10LOG(2.3MHz) + 6 = -104.4dBm}$$

This -104.4dBm noise level will be subtracted from the receive sensitivity to calculate the corresponding signal to noise ratio. An external LNA is added in front of the transceiver, which reduces the overall noise figure so it is important to use the required signal to noise ratio instead of the datasheet receive sensitivity for link budgets. Table 6 shows the required signal to noise ratio for the transceiver's four data rates.

Table 6: AT86RF233 Data Rate versus Required SNR

Data Rate (kbps)	Datasheet RX Sensitivity (dBm)	Calc SNR (dB), NF = 6
250	-101	3.4
500	-96	8.4
1000	-94	10.4
2000	-88	16.4

4.4.2 Satellite with Patch Antenna

A simple antenna for a CubeSat would be patch antenna mounted on one of its faces. Figure 31 shows a 3U CubeSat developed by Tyvak Nano-Satellite Systems with an S-Band patch antenna mounted in between solar cells. The practical gain of a patch antenna this size at 2.4GHz is approximately 6dBi, which is the number that will be used for this link budget.

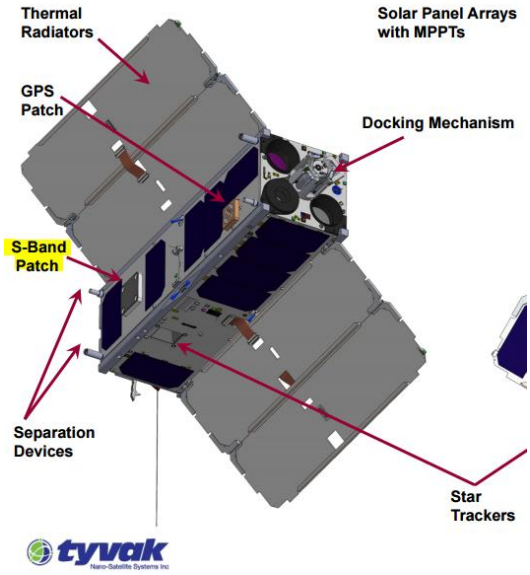

Figure 31: CubeSat with S-Band Patch Antenna, CPOD [23]

The link equation is rewritten below:

$$\boldsymbol{P_R = P_T + G_T - L + G_R}$$

A link distance of 2100km corresponds to a satellite at an elevation of 800km with an elevation angle of 15 degrees to the ground station as shown in Figure 7. The ground station antenna gain of 39.4dBi was extrapolated from the specifications of a 4.5m mesh dish kit available for purchase from RF HAMDesign's website. [14] A picture of the RF HAMDesign 4.5m dish with rotator and feed horn is shown in Figure 32. The rotor shown in the figure is single axis, but a two axis rotator would be required for the CubeSat

ground station. The ground station is assumed to have an external amplifier with transmit power of 10W, which is the power level of several Wi-Fi boosters that can be purchased online.

Figure 32: RF HAMDesign 4.5m RF Mesh Dish Kit [14]

Table 7 shows the uplink budget (ground station transmit to satellite) for a satellite with a patch antenna. The signal to noise ratio is 24dB, which corresponds to a 19.3dB margin for the 250kbps data rate, 14.3dB for 500kbps, 12.3dB for 1000kbps, and 6.3dB for 2000kbps. The margins greater than 15dB are colored green to indicate high possibility of successful link, yellow indicates lower than 15dB margin, and red indicates negative margin and no possible link. This table shows that a satellite with a patch antenna and a ground station with a 4.5 meter dish would most likely support uplink at 250kbps and might sometimes work at 500kbps, 1000kbps and 2000kbps.

Table 7: Patch Antenna: Uplink Budget

GS TX, 10W (dBm)	40
GS Gain, 4.5m dish (dB)	39.4
Total Loss, 2100km (dB)	-169.1
Sat Gain, patch (dB)	6
Sat RX (dBm)	-83.7
Sat Noise (dBm)	-106.4
Satellite SNR (dB)	**22.7**
250kpbs Margin	19.3
500kbps Margin	14.3
1000kbps Margin	12.3
2000kbps Margin	6.3

Table 8: Patch Antenna: Downlink Budget

Sat TX, 2W (dBm)	33
Sat Gain, patch (dB)	6
Total Loss, 2100km (dB)	-169.1
GS Gain, 4.5m dish (dB)	39.4
Sat RX (dBm)	-90.7
GS Noise (dBm)	-105.5
GS SNR (dB)	**14.8**
250kpbs Margin	11.4
500kbps Margin	6.4
1000kbps Margin	4.4
2000kbps Margin	-1.6

Table 8 shows the downlink budget for a satellite with patch antenna where the satellite is transmitting and the ground station is receiving. The downlink is 7.9dB weaker than uplink at a signal to noise ratio of 14.8dB, which does not provide a 15dB margin for any data rate and definitely will not work for 2000kbps. The downlink is much weaker due to the low satellite transmit power and the elevated ISM terrestrial noise floor. The link might work intermittently at 250kbps with a margin of 11.4dB, but this shows that a satellite with patch antenna will not be sufficient for this mission and this ground station.

This link budget demonstrates that uplink to the satellite is the easier than downlink from the satellite due to higher ground station transmit power and absence of terrestrial ISM noise in space.

4.4.3 Satellite with Deployable Dish

A more complex CubeSat could incorporate a deployable satellite dish similar to the 0.5 meter dish shown in Figure 33. There are several CubeSat teams who have worked on or are working on deployable dishes for future missions.

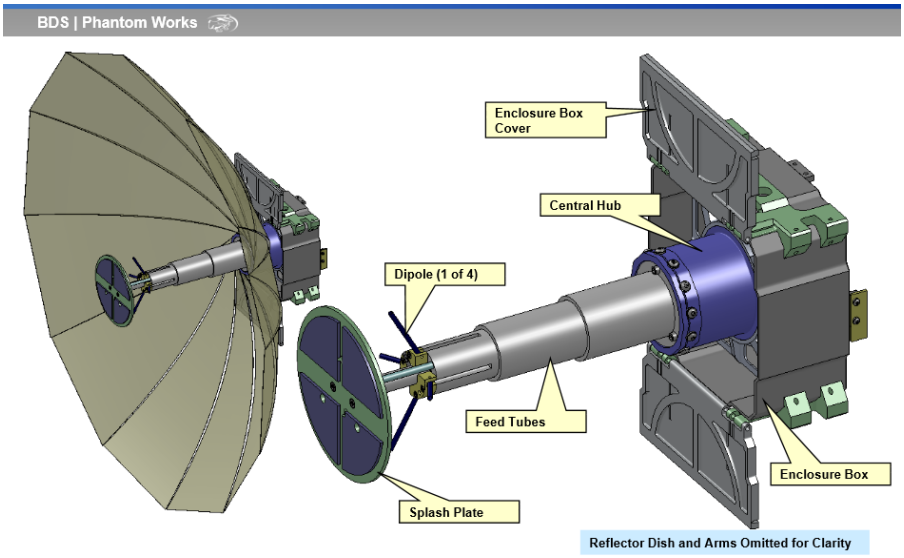

Figure 33: Deployable 0.5m Dish, Boeing Phantom Works [24]

The directivity of the dish shown in Figure 33 was approximated as 18.6dBi, so a value of 17dBi will be used in the link budget estimates. [24] Table 9 shows the uplink budget for a CubeSat with dish and Table 10 shows the downlink budget. Once again, the uplink budget is strong with greater than 15dB margin up to 2000kbps, and the downlink budget shows sufficient margin up to 1000kbps. 2000kbps downlink could be possible, but would most likely be intermittent with a margin of 10.7dB. Note that these link budgets do not attempt to estimate pointing or implementation losses, so a margin of 15dB is estimated as required for a successful link.

Table 9: Dish Antenna: Uplink Budget

GS TX, 10W (dBm)	40
GS Gain, 4.5m dish (dB)	39.4
Total Loss, 2100km (dB)	-169.1
Sat Gain, Dish 0.5m (dB)	17.0
Sat RX (dBm)	-72.7
Sat Noise (dBm)	-106.4
Satellite SNR (dB)	**33.7**
250kpbs Margin	30.3
500kbps Margin	25.3
1000kbps Margin	23.3
2000kbps Margin	17.3

Table 10: Dish Antenna: Downlink Budget

Sat TX, 2W (dBm)	33
Sat Gain, Dish 0.5m (dB)	17.0
Total Loss, 2100km (dB)	-169.1
GS Gain, 4.5m dish (dB)	39.4
Sat RX (dBm)	-79.7
GS Noise (dBm)	-105.5
GS SNR (dB)	**25.8**
250kpbs Margin	22.4
500kbps Margin	17.4
1000kbps Margin	15.4
2000kbps Margin	9.4

These link budgets demonstrate that a sizable antenna will be required on the CubeSat for data rates above 250kbps. With a 0.5m CubeSat dish, the link has sufficient margin up to 1000kbps and 2000kbps would be marginal.

4.5 Evaluation Board Testing

The Atmel AT86RF233 transceiver REB233SMAD-EK evaluation kit was purchased to confirm the transceiver specifications by measuring the receive sensitivity and Doppler sensitivity of the transceiver. The evaluation kit consists of two AT86RF233 (REB233SMAD) transceiver PCBs, interfaced to two microcontroller boards (REB-CBB)

which provide battery power and interface to a microcontroller pre-loaded with evaluation software. A computer interfaces to the microcontroller through a terminal program such as Putty through a USB to serial converter. The evaluation software contains a packet error rate measurement program which transmits from one board to the other while measuring the number of packets successfully decoded. The frequency, transmit power, data rate, and various register settings can be changed through the terminal, allowing measurement of the radio link quality (receive sensitivity) while varying other factors. Each board has two SMA RF connectors for demonstrating the AT86RF233 antenna diversity feature. Hardware diagrams from the *REB233SMAD-EK User Guide* are shown in Figure 34 and Figure 35. [25]

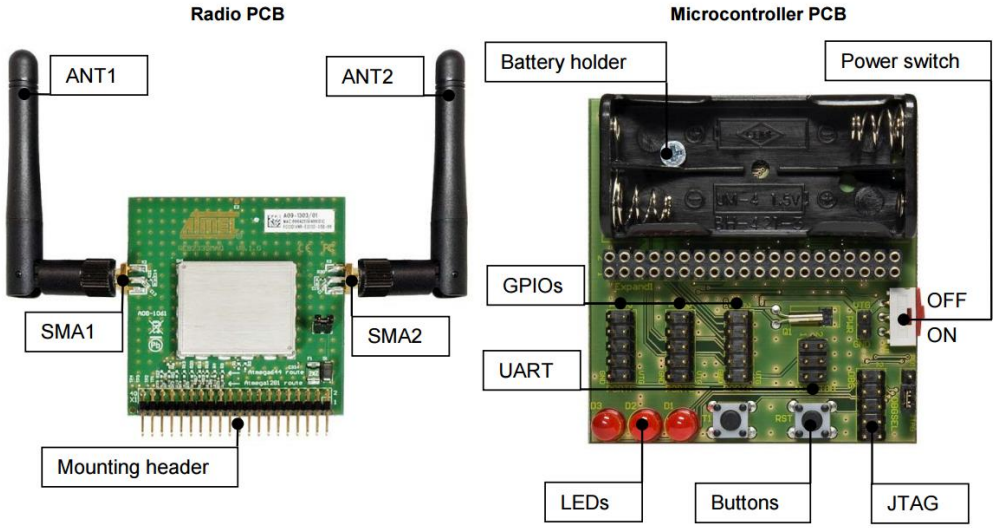

Figure 34: Atmel REB233SMAD-EK Evaluation Kit Hardware, 1 of 2 Modules [13]

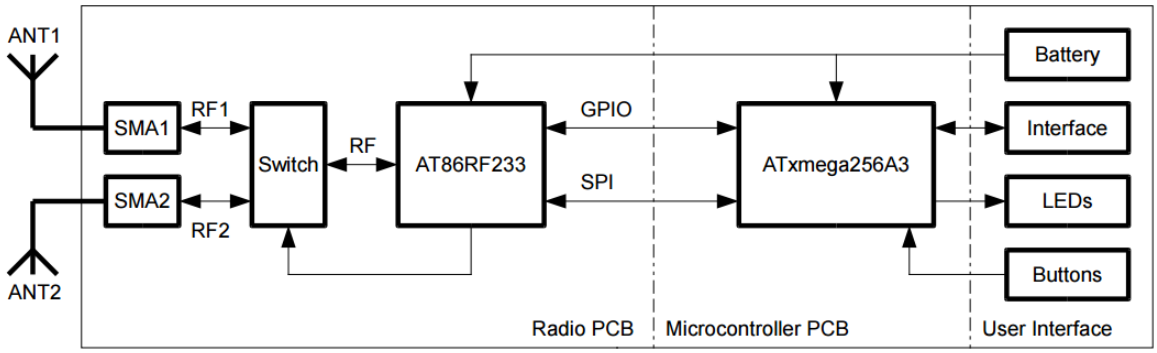

Figure 35: Atmel REB233SMAD-EK Evaluation Kit Hardware Block Diagram [13]

4.5.1 Evaluation Board Receive Sensitivity Measurements

Measuring a receiver's sensitivity seems simple in theory: a variable attenuator is inserted between a transmitter and receiver and the attenuation is varied until exceeding a certain error rate, then the power into the receiver is measured. The measured power is the receive sensitivity of the receiver. However, in practice, the measurement is complicated by RF leakage between the two units as described in Ivan Bland's thesis *"Receive Sensitivity Characterization of the PolySat Satellite Communication System"* [26] If the transmitter and receiver are simply placed on a benchtop with their output and input ports terminated with 50 ohm loads or with a variable attenuator at maximum attenuation, successful communication would still be achieved at 0% packet loss; this successful communication is due to RF leakage.

The transmitter PCB radiates a miniscule amount of the RF signal from the components and copper on the PCB before the RF connector; this tiny amount of RF energy can be decoded by the receiver which will pick up the energy by the components and copper on its PCB. The AT86RF233 has a receive sensitivity of -101dBm at 250kbps which equates to 79pW of power indicating it is a very sensitive receiver. The problem of RF leakage was confirmed and demonstrated to be the case for these

evaluation boards. Therefore, the transmitter and receiver must be further isolated (shielded) from one another during receive sensitivity testing. RF leakage must be eliminated to obtain an accurate receive sensitivity measurement; a lot of time was spent attempting to eliminate RF leakage from spoiling the measurements.

The faraday cage constructed in Bland's thesis was utilized to shield RF leakage between the transmitter and receiver. The faraday cage must provide enough shielding to reduce the leakage RF below the noise floor of the receiver so the leakage RF does not falsely improve the measured receiver sensitivity. The faraday cage was found to be adequate by setting the variable attenuator between the two units to its maximum attenuation and then confirming no packets were received by the receiver during a packet error rate test.

The evaluation board receive sensitivity test setup is shown in Figure 36 through Figure 41. The transmitter board resides in the faraday cage with 30dB attenuation in series; the receiver is connected to a variable attenuator which is then connected to the faraday cage output through direct coax. The test frequency of 2.330GHz was selected because low interference was measured at this frequency in the laboratory. The packet error rate program is repeated on the laptop while increasing the variable attenuator. Receive sensitivity was arbitrarily defined as a packet error rate of 5%, meaning 95% of the packets transmitted by the transmitter were successfully decoded by the receiver. Once the packet drop rate consistently reaches 5% or less, the receiver is disconnected from the variable attenuator and the spectrum analyzer is connected in its place.

The evaluation software settings are listed below:

- **ACK Request = FALSE**
- **TX Power = -17dBm**
- **CSMA = FALSE**
- **Number of Frames = 1000**
- **Frame Length = 127**
- **Frequency = 2330 MHz**

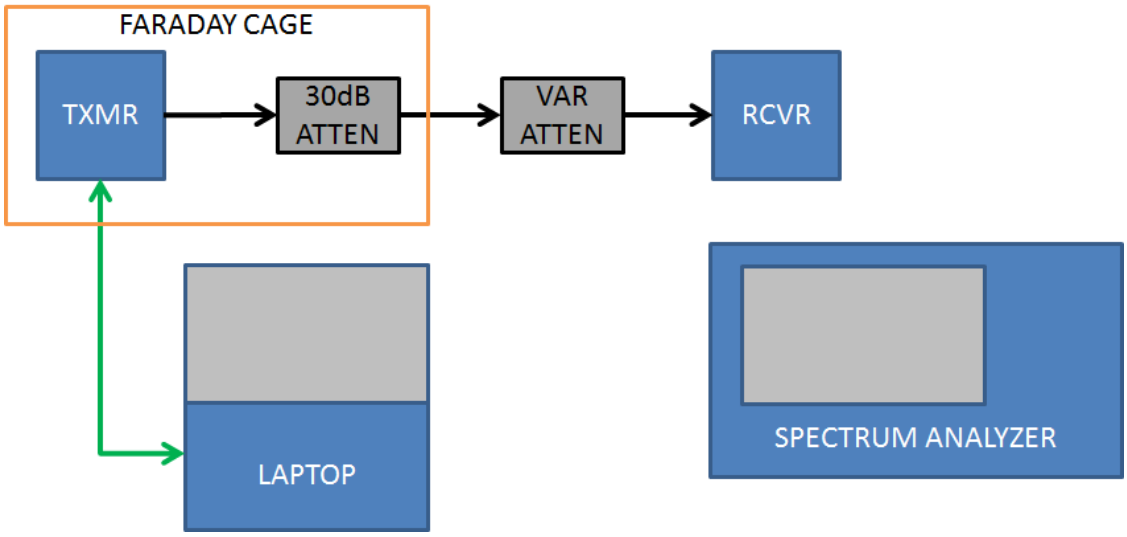

Figure 36: Evaluation Board Receive Sensitivity Diagram, Packet Error Rate Threshold

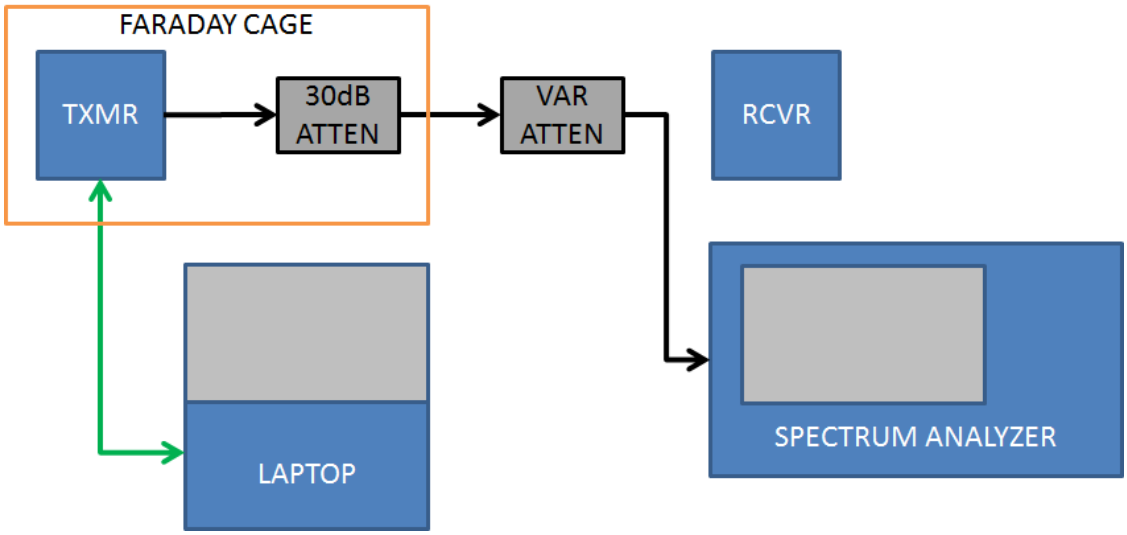

Figure 37: Evaluation Board Receive Sensitivity Diagram, Measurement

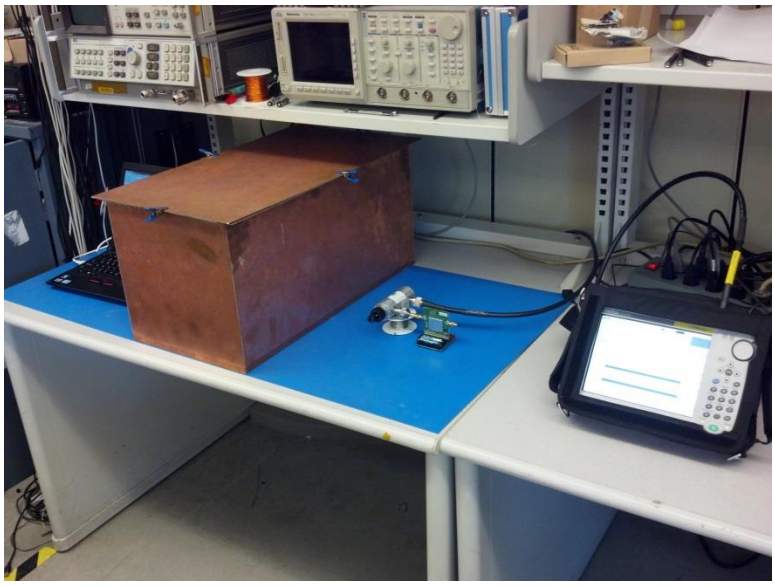

Figure 38: Evaluation Board Receive Sensitivity Test Setup, Packet Error Rate Threshold

Figure 39: Evaluation Board Receive Sensitivity Test Setup, Measurement

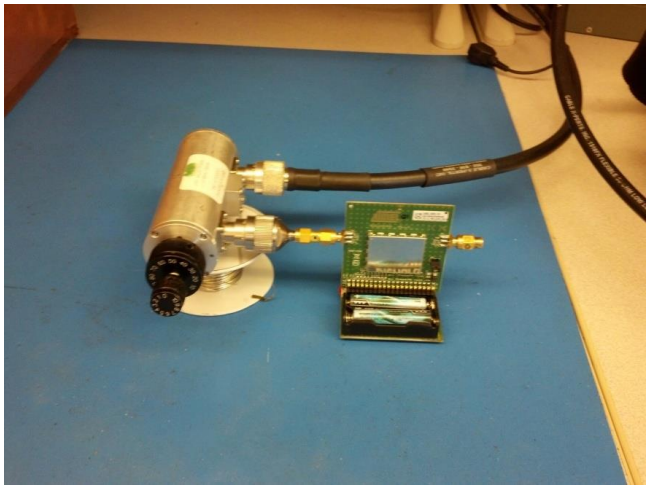

Figure 40: Evaluation Board Receive Sensitivity Test Setup, Receiver

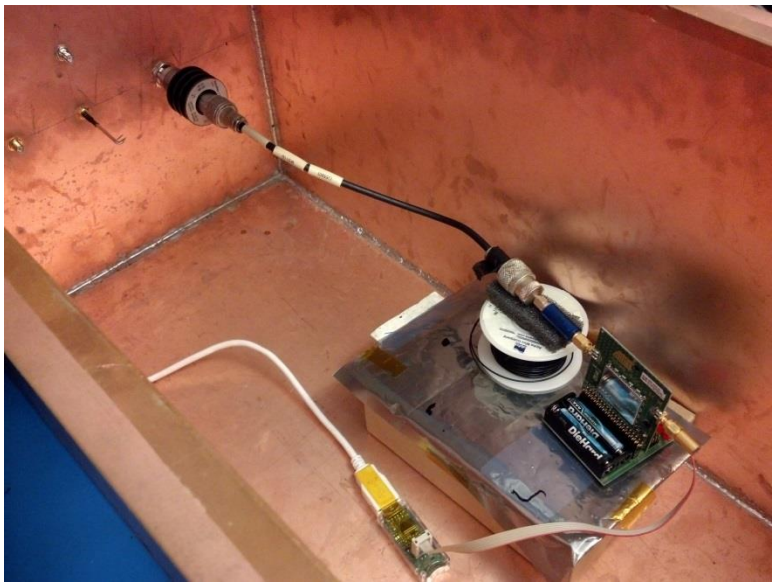

Figure 41: Evaluation Board Receive Sensitivity Test Setup, Transmitter

In this test, the faraday cage was only used for receiver and transmitter RF leakage isolation only. The transmitter, instead of the receiver, was placed inside the faraday cage so the leakage path between the transmitter and spectrum analyzer would be reduced; if the transmitter were not shielded during the measurement, the signal leaking between from the transmitter, bypassing the attenuation, and into the spectrum

analyzer would increase the measured signal power, falsely increasing the receive sensitivity measurement. Ideally, the receiver would be shielded as well to reduce any laboratory in-band interference from raising its noise floor and thus decreasing its receive sensitivity; however, one shield on the transmitter and using the non-ISM 2.330GHz frequency proved adequate for this test.

The channel power measurement feature of the spectrum analyzer was utilized to measure the signal power within the 2.3MHz bandwidth of the signal; this measurement feature performs the integration necessary to calculate the power within the channel bandwidth and the measurement does not vary with change in resolution or visual bandwidth settings. Therefore, the resolution bandwidth was set to 100kHz to minimize the spectrum analyzer noise floor but still have an acceptable sweep rate. The spectrum analyzer was configured to display the average of 100 traces for both the signal and noise floor measurements. The preamplifier was enabled on the spectrum analyzer to decrease the noise floor further, however the 250kbps signal was still near the magnitude of the noise floor which introduced error to the measurement. To reduce this error, the measured noise power was subtracted from the measured signal power to calculate the actual signal power and eliminate error due to the addition of the spectrum analyzer's noise power in the measurement.

The spectrum analyzer settings are listed below:

- **Reference Level:** -95dBm
- **Center Frequency:** 2.330GHz
- **Span:** 10MHz
- **Detection:** RMS/AVG (log)
- **RBW:** 100kHz, VBW: 100kHz
- **Averaging:** 100
- **Input Attenuation:** 0dB
- **Preamp:** On

The noise floor power of the spectrum analyzer within the 2.3MHz bandwidth measured at -101.5dBm as shown in Figure 42. The receive sensitivity measurement at

250kbps is shown in Figure 43. The measurements for 500kbps, 1000kbps, and 2000kbps are tabulated in Table 11. The spectrum analyzer noise was subtracted from the signal power by converting from dBm to watts, then subtracting, and then converting back to dBm. The formula for this operation is $\boldsymbol{sig = 10\log\left(10^{\frac{meas}{10}} - 10^{\frac{noise}{10}}\right)}$, where sig = signal strength in dBm, meas = signal strength in dBm, and noise = spectrum analyzer noise floor in dBm. As the signal power becomes larger in magnitude compared to the spectrum analyzer noise floor (>8dB), the error introduced by the noise floor becomes negligible as illustrated by the 1000kbps and 2000kbps calculations.

The variable attenuator switches in steps of 1dB and the differences in insertion loss between the receiver and spectrum analyzer are on the order of 0.2 to 0.5dB. Therefore, this test setup is assumed to be accurate to about 1dB and thus the final calculations are rounded to the nearest 1dBm.

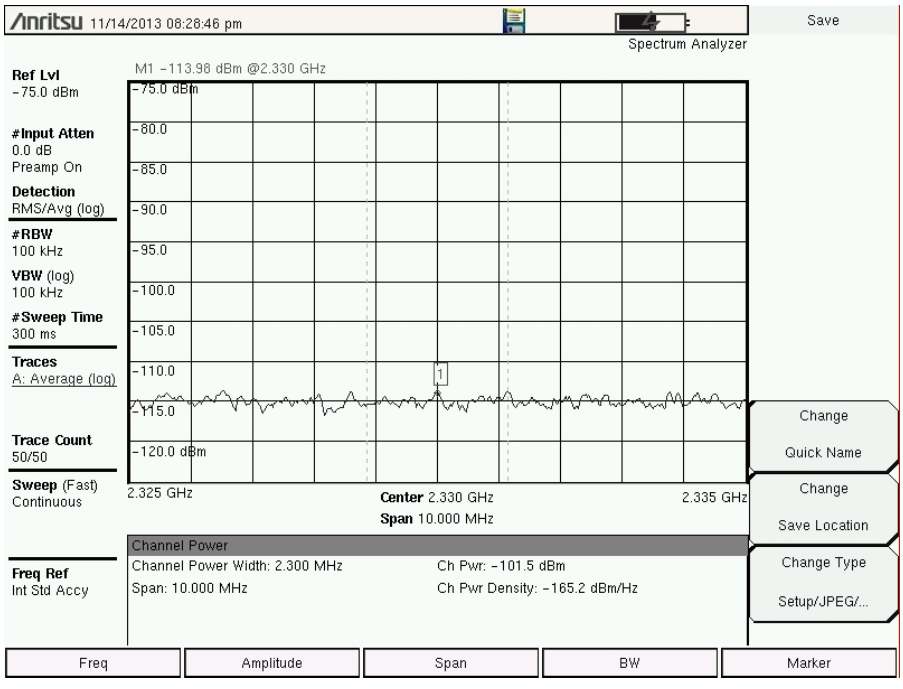

Figure 42: Evaluation Board Receive Sensitivity Test, Spectrum Analyzer Noise Floor (-101.5 dBm noise floor)

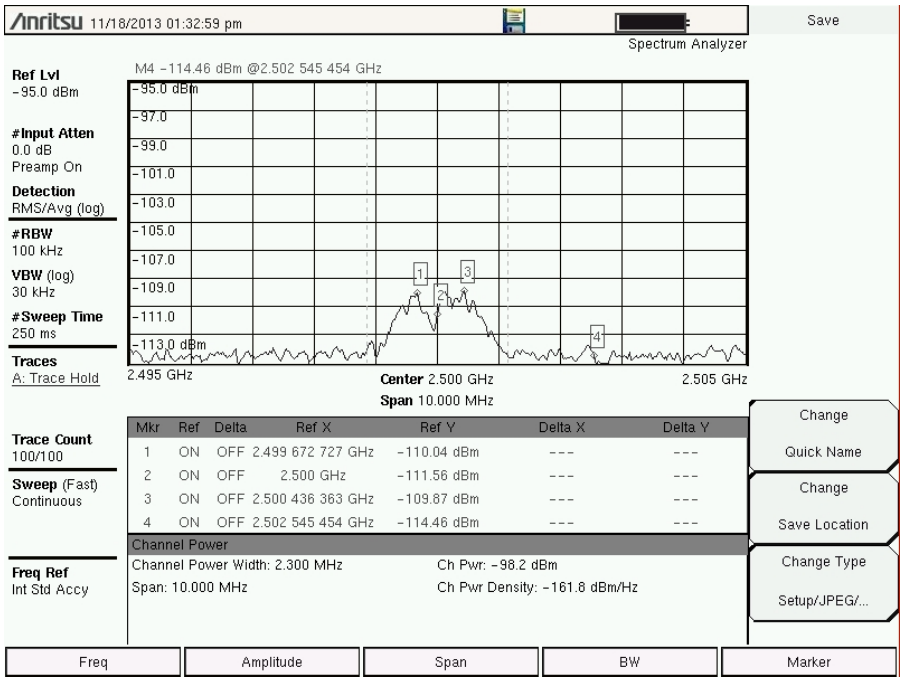

Figure 43: Evaluation Board Receive Sensitivity Test, 250kbps Receive Sensitivity

Table 11: Evaluation Board Receive Sensitivity Test Results

Data Rate (kbps)	PER (%)	Meas. Signal Power (dBm)	Meas. SA Noise(dBm)	Calc. RX Sens. (dBm)	Datasheet RX Sens. (dBm)
250	1%	-98.2	-101.5	-101	-101
500	6%	-95.4	-101.5	-97	-96
1000	4%	-92.8	-101.5	-93	-94
2000	5%	-86.6	-101.5	-87	-88

The evaluation board receive sensitivity measurements matched the datasheet specifications within 1dB, which was the assumed accuracy of the test setup.

4.5.2 Evaluation Board Doppler Tolerance Measurement

As a high velocity satellite travels above an earth station, its relative velocity toward the station changes during the duration of the pass. The satellite travels in an arc across the sky while the ground station actively points its antenna at the satellite in a

circular motion during the duration of the pass. At the beginning and end of the pass, while the satellite rises and falls at the horizon, the satellite's relative velocity toward the ground station is at its maximum magnitude. During the middle of the pass, at the apex of the arc, the relative velocity component between the ground station and satellite is zero.

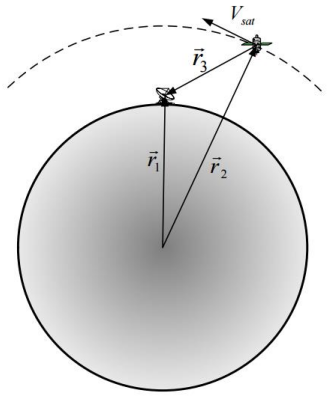

Figure 44: Position and Velocity Vectors of Satellite and Earth Station [15]

The change in relative velocity between the satellite and ground station during a pass causes a change in the observed communication frequency between the satellite and ground station due to the Doppler Effect. The Doppler Shift equation is:

$$\Delta \boldsymbol{f} = \frac{\Delta \boldsymbol{v}}{\boldsymbol{c}} \boldsymbol{f_0}$$

Where Δf = the observed change in frequency relative to the transmitted frequency, Δv = the relative velocity between transmitter and receiver, c = speed of light, and f_0 = transmitted frequency.

A LEO satellite travels at a typical speed of 7.5 km/s, which equates a maximum Doppler shift of +/- 60kHz if the satellite's velocity vector is pointing directly toward the ground station, which is never the case. If one were to calculate the practical Doppler shift using orbital mechanics, the satellites orbit, and the visible elevation angles when communication occurs, the actual maximum Doppler shift during the usable portion of

the pass is around 10kHz. [27] However, to keep things conservative, a Doppler shift of +/-60kHz will be assumed for this project.

For a successful satellite link, the earth station must either dynamically correct for Doppler shift or must tolerate the Doppler shift during the pass. If the same AT86RF233 transceiver is utilized for both the satellite and ground, as is the case with the PolySat Friis UHF earth station, the AT86RF233 must be able to compensate for the Doppler shift. However, unlike the AX5042 (UHF transceiver), the AT86RF233 can only change its frequency in discrete steps of 500kHz, which is too large to be useful for Doppler shift compensation. Therefore, the AT86RF233 must be able to tolerate the Doppler shift without any compensation. Unlike the AX5042 (UHF transceiver) with a signal bandwidth of 10kHz at 9.6kbps, the AT86RF233 transceiver transmits a spread spectrum signal of 2.3MHz bandwidth; therefore the 60kHz Doppler shift is only 2.6% of the signal bandwidth. Therefore, intuitively, there is a good chance the receiver can tolerate this 2.6% Doppler shift.

The AT86RF233 datasheet states that the maximum “TX/RX carrier frequency offset (Sensitivity loss $\leq$ 2dB)” = +/- 300kHz (+/- 120 ppm). [28] Therefore, the transceiver most likely can tolerate Doppler shift of 60kHz without any dynamic correction on the ground. However, the maximum carrier frequency offset of +/-300kHz also includes the mismatch of the transmitter and receiver frequency sources; therefore the maximum Doppler shift tolerance is less than 300kHz and must be measured to confirm that if it is above 60kHz.

The Doppler shift tolerance of the AT86RF233 evaluation boards can be measured using a Doppler shift simulator circuit described in a paper summarizing Stanford’s NarcisSat communication system [16]. A diagram of the Doppler shifter is shown in Figure 45. The Doppler shifter consists of two RF synthesizers with an output frequency difference equal to the desired frequency shift. First, the input signal is mixed down to an

intermediate frequency of 1.5GHz with the first synthesizer, mixer, and low-pass filter. The 1.5GHz intermediate signal is then mixed up with the second synthesizer to a center frequency equal to the sum of the input frequency and the Doppler shift. Finally, a band-pass filter was added for additional filtering of the higher frequency output of the mixer as well as attenuating any leakage intermediate signals.

The hardware to implement the Doppler shift circuit was purchased from Mini-Circuits [29] and is listed in Table 12.

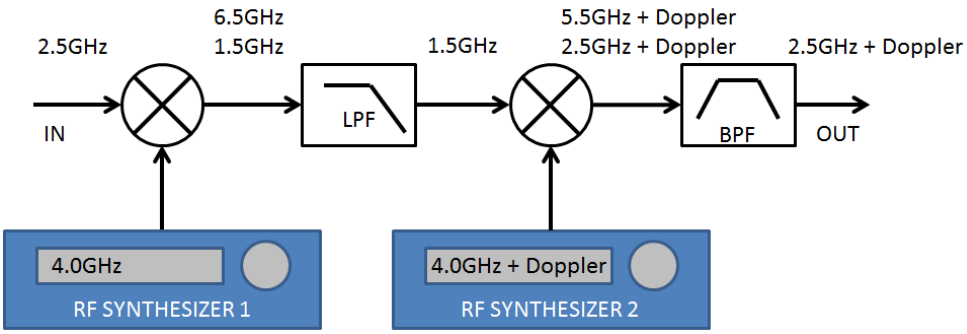

Figure 45: Doppler Shifter Diagram

Table 12: Doppler Shifter Circuit Components

Mini-Circuits Part Number	Description
SLP-2400+	Low Pass Filter, DC – 2220MHz
ZX05-83-S+	Frequency Mixer 1, 2300 – 8000 MHz
ZX05-83-S+	Frequency Mixer 2, 2300 – 8000 MHz
VBFZ-2340-S+	Band Pass Filter, 2020 – 2660 MHz

The common synthesizer frequency of 4.0GHz was chosen to provide a large enough frequency difference between the output signals of the first mixer to be filtered out by the low pass filter. If the 6.5GHz signal were not adequately filtered by the low-pass filter, it would simply be mixed back down to 2.5GHz in the second mixer,

introducing no Doppler shift and corrupting the test. Due to the small 60 kHz Doppler shift compared to the synthesizers' common frequency of 4.0GHz, the test required synthesizers capable of matched frequencies to 15ppm (60kHz/4.0GHz). The synthesizers located in the PolySat lab had too large of a frequency drift; instead two synthesizers from the Cal Poly, Electrical Engineering RF Microwave Lab were borrowed for this test. However, the synthesizers still produced a maximum Doppler shift drift difference of 10kHz between the beginning and end of the receive sensitivity testing; this means the Doppler shift at the end of the test was measured to be 10kHz different than the Doppler shift at the beginning of the test due to the frequency drift between the two synthesizers over the duration of the test.

The functionality of the Doppler shifter was verified by outputting an attenuated continuous wave (CW) signal from the AT86RF233 transmitter at 2.5GHz and measuring both the input and output of the Doppler shifter. A Doppler shift of 175.5kHz is shown in Figure 46.

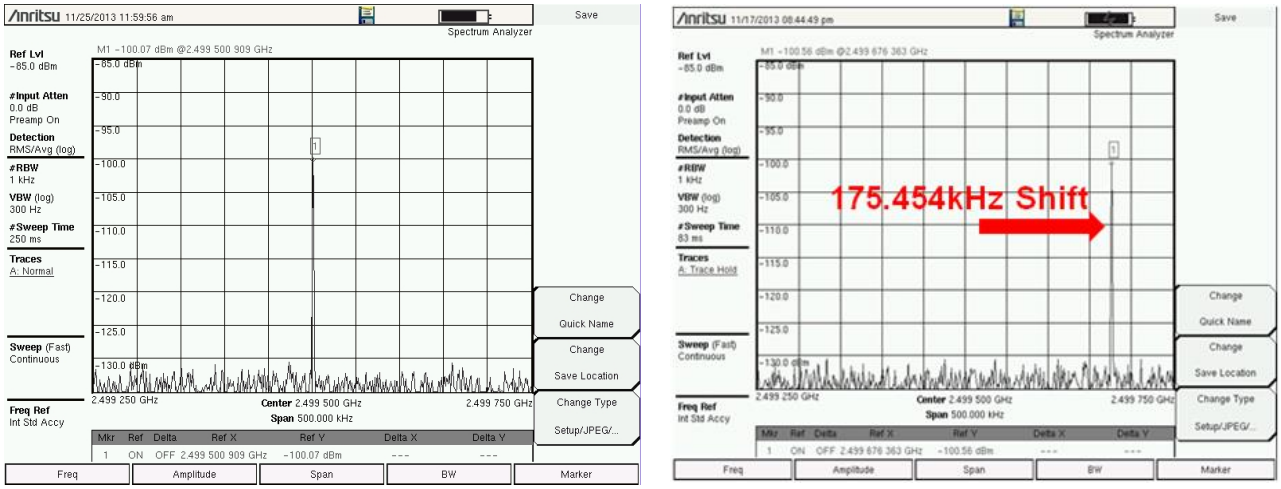

Figure 46: Doppler Tolerance Test Circuitry Input and Output Measurements

After verifying functionality of the Doppler shifter, the Doppler shifter circuitry was simply added in line to the receive sensitivity test setup as shown in Figure 47 and Figure 48.

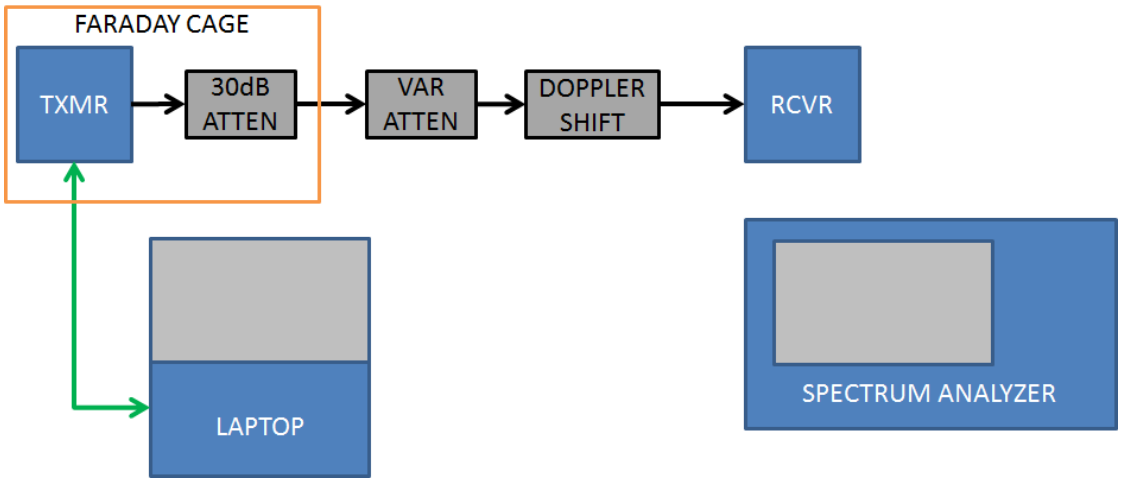

Figure 47: Receive Sensitivity Doppler Shift Tolerance Diagram, Packet Error Rate Threshold

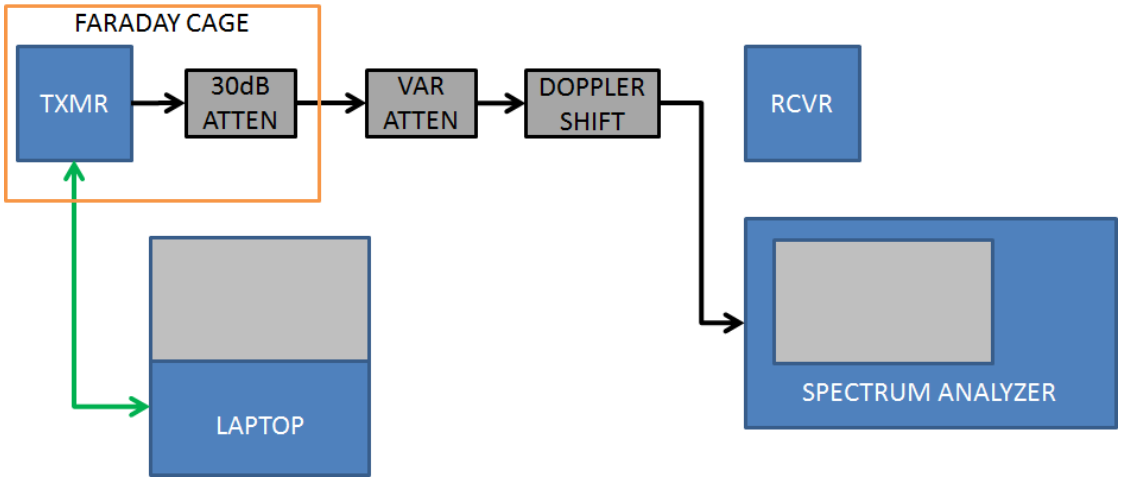

Figure 48: Receive Sensitivity Doppler Shift Tolerance Diagram, Measurement

The receive sensitivity of the receiver was measured without the Doppler shift and then with the Doppler shift, the difference in receive sensitivity at a certain Doppler shift is used as a figure of merit. The receive sensitivity was measured for the four data rates: 250kbps, 500kbps, 1000kbps, and 2000kbps. The simplified procedure was as follows:

1. Measure the receive sensitivity without the Doppler shift circuitry (Figure 36 and Figure 37)

2. Add the Doppler shift circuitry in between the transmitter and spectrum analyzer (Figure 48)
    a. Configure the transmitter to transmit a continuous wave
    b. Set the desired Doppler shift
    c. Capture a screen shot of the initial Doppler shift frequency
3. Disconnect the spectrum analyzer, place the receiver at the output (Figure 47)
    a. Vary the variable attenuator until a packet drop rate of 5% is consistently reached
    b. Remove the receiver, place the spectrum analyzer at the output
    c. Capture a screen shot of the Doppler receive sensitivity
4. Configure the transmitter to transmit a continuous wave
    a. Capture a screen shot of the final Doppler shift frequency (frequency change due to synthesizer drift)

The change in receive sensitivity with respect to Doppler shift was drastic after reaching a certain cutoff value. Similar to receive sensitivity, the packet error rate declined rapidly after the 5% cutoff; for instance at 250kbps, a Doppler shift of -188kHz produced a drop rate of 5%, whereas a shift of 267kHz produced a drop rate of 67%. The test setup is shown in Figure 49 and Figure 50 and test results in Table 13.

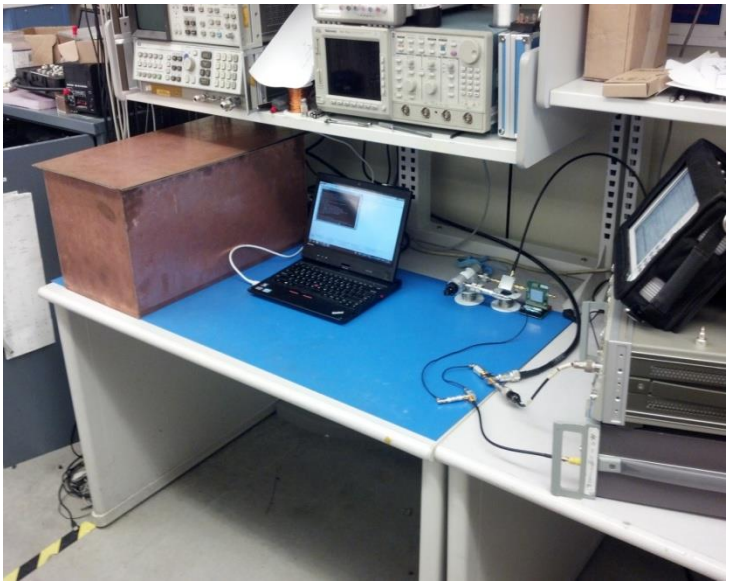

Figure 49: Doppler Tolerance Test Setup, Full View

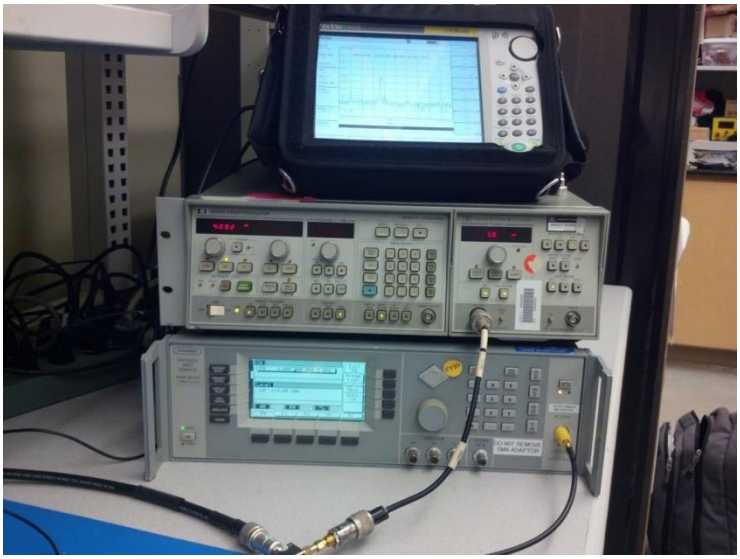

Figure 50: Doppler Tolerance Test Setup, Synthesizers and Spectrum Analyzer

Table 13: Doppler Tolerance, Receive Sensitivity Test Results

Data Rate (kbps)	Doppler Shift (kHz)	PER (%)	Receiver Desensitization (dB)
250	145	5	3.6
250	-188	5	2.4
250	-38	3	0.0
500	166	6	2.1
500	-215	5	6.4
1000	103	2	0.4
1000	-93	2	0.3
2000	108	7	0.8
2000	-87	4	1.0

The results demonstrate that the AT86RF233 can tolerate Doppler Shift below 100 kHz with a receiver desensitization of 2dB or less.

5 Schematic Development

After testing the AT86RF233 transceiver evaluation board, the schematic for the Intrepid S-Band ISM Radio (ISIR) was developed. The schematic was developed using OrCAD Capture 16.6. The PCBA is designed to interface primarily as a daughter board for the PolySat “Intrepid” System Board shown in Figure 51, but it also has a connector to interface as a daughter board to the AT86RF233 evaluation processor board for testing. The PCBA interfaces the AT86RF233 transceiver to an external RF front-end for improved transmit power and receive sensitivity. There are two switching regulators that provide power to the circuitry from an unregulated 3.7V lithium ion supply. Amplifier protection circuitry was designed to protect the power amplifier from no load conditions and the low noise amplifier from high input power conditions. Additional logic was added for temperature sensing, power isolation, transmitted and reflected power measurements, and an EEPROM for board configuration values.

The full schematic is provided in *Appendix A: Intrepid S-Band ISM Radio R1 Schematic.* Sections of the schematic are explained in detail in the following sections.

The ISIR conforms to the Intrepid System Board Daughter Board B specification in order to fit within the Intrepid CubeSat satellite bus shown in Figure 52.

Figure 51: Intrepid System Board [30]

The satellite bus consists of a “top hat” which is a sandwich of five PCBAs mounted to the mechanical top hat shown in Figure 52. The System Board is at the center of the stackup which contains the primary command and data handling microprocessor of the satellite as well as the electrical power system, hardware watchdogs, and additional sensors and peripherals. Four connectors with spring contacts break out signals from the system board to Daughter Board A and Daughter Board B. The daughter boards simply have pads that press against the spring contacts on the System Board, minimizing stack height.

Daughter Board A is utilized for the UHF Radio, so Daughter Board B was selected for the S-Band radio allowing both low data rate UHF and high data rate S-Band radio communication on the same satellite. The system board has four additional high-density connectors on the bottom and top of the PCBA which break out the signals for the satellite payload interface board and the external –Z side panel. The Intrepid top hat occupies less than 1/4th of a 1U (10 cm x 10 cm x 13cm) CubeSat, providing use of the remainder of the volume for mission specific payloads. An example of a PolySat mission specific payload is shown in a preliminary CAD of IPEX in Figure 53 and Figure 54.

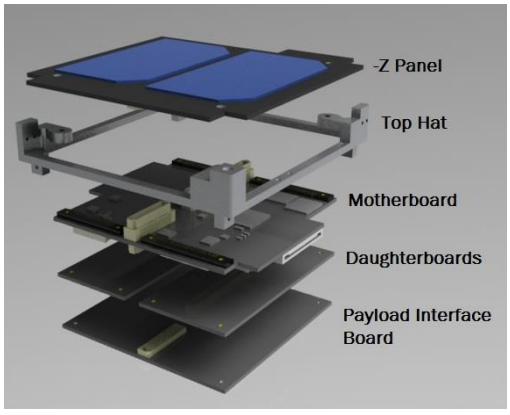

Figure 52: Intrepid Top Hat Stackup CAD

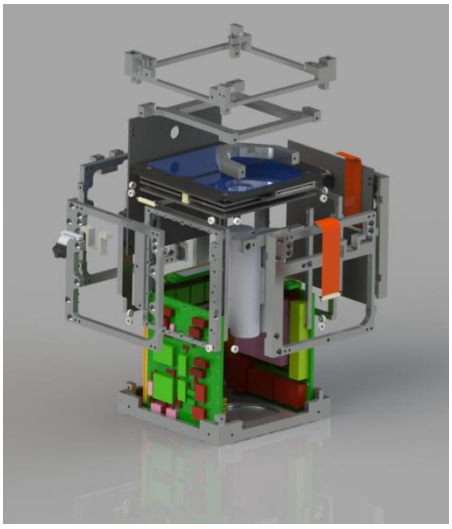

Figure 53: IPEX Preliminary CAD Model

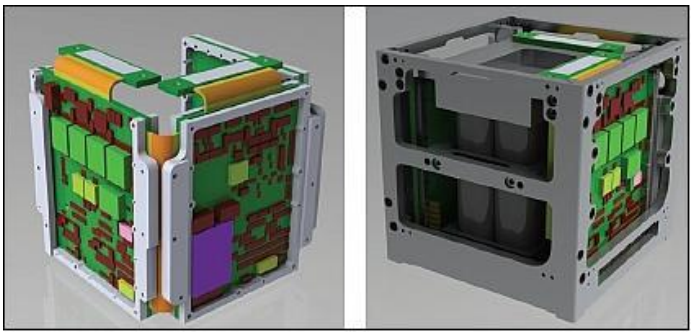

Figure 54: IPEX Preliminary Payload CAD Model without Top Hat

5.1 Intrepid System Board Interface

Figure 55 shows the schematic for the system board interface between the PolySat Intrepid System Board and the ISIR. J7 and J8 are simply pads on the PCBA that press against the System Board's daughter board B spring contacts: Samtec SEI-125-02-G-S-E-AT, shown in Figure 56. [31] FL1 and FL2 are low pass filters added in line with the SPI bus to reduce potential in-band interference from SPI bus activity. The resistors are simply pull-downs and pull-ups to define a signal's logic state if the system

board is de-energized or the pins are placed in a high impedance mode.

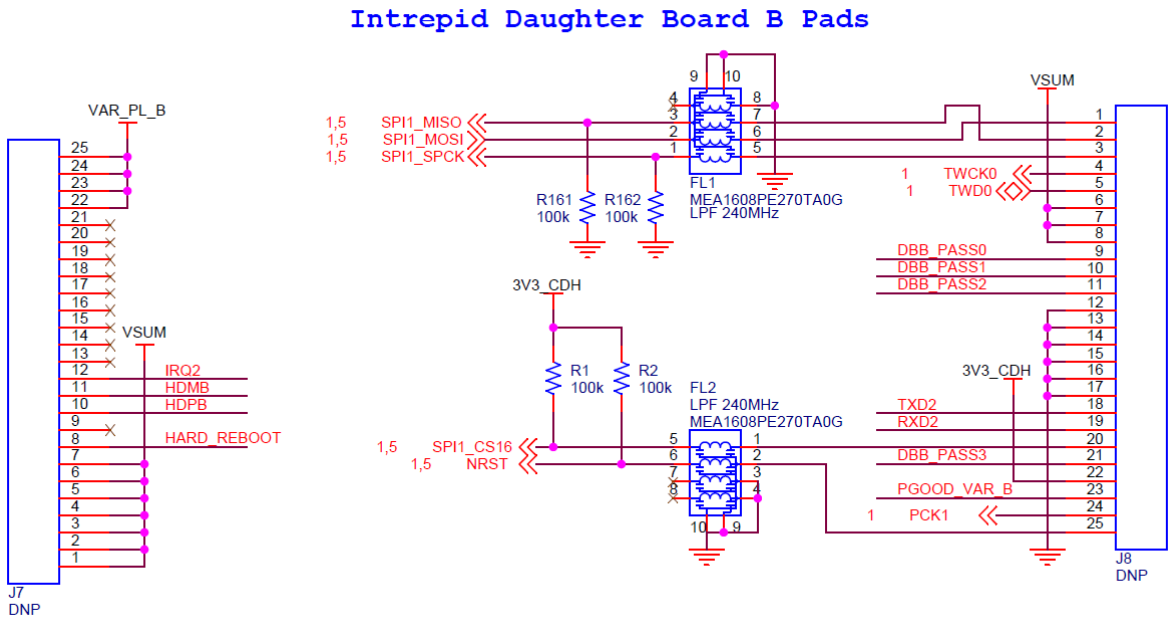

Figure 55: System Board Daughter Board B Interface

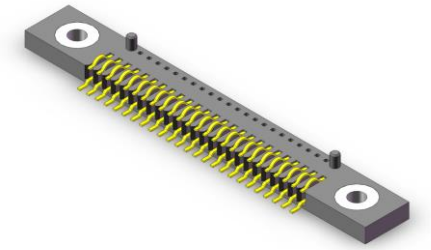

Figure 56: Samtec SEI-125-02-G-S-E-AT, System Board's Daughterboard Spring Contacts

The Daughter Board B connectors break out several interfaces from the Atmel AT91SAM9G20 microprocessor: one SPI bus, one I2C bus, one serial bus, unregulated battery power, the daughter board B regulator, and several GPIOs. The pinout and signal information was extracted from the Intrepid System Board User Guide [30] is

shown in Table 14. Only the SPI, I2C, unregulated power, and a few GPIOS are utilized by the ISIR.

Table 14: System Board Daughterboard B Connectors Pinout Information [30]

Daughterboard B Connectors								
J7 (25 Pins)				J8 (25 Pins)				
Signal	Pin#	Atmel PIO		Atmel PIO	Pin#	Peripheral A	Peripheral B	GPIO
UNREG	1	--		PB1	1	SPI1_MOSI		
UNREG	2	--		PB0	2	SPI1_MISO		
UNREG	3	--		PB2	3	SPI1_SPCK		
UNREG	4	--		PA24	4	I2C_TWCK [0]		
UNREG	5	--		PA23	5	I2C_TWD [0]		
UNREG	6	--		--	6	UNREG		
UNREG	7	--		--	7	UNREG		
HARD_REBOOT	8	--		--	8	UNREG		
GND_SOLAR	9	--		--	9	DBB_PASS [0]		
HDP [B]	10	*		--	10	DBB_PASS [1]		
HDM [B]	11	*		--	11	DBB_PASS [2]		
IRQ [2]	12	PC14		--	12	GND_POWER		
GND_BATTERY	13	--		--	13	GND_POWER		
GND_BATTERY	14	--		--	14	GND_POWER		
GND_BATTERY	15	--		--	15	GND_POWER		
GND_BATTERY	16	--		--	16	GND_POWER		
GND_BATTERY	17	--		--	17	GND_POWER		
GND_BATTERY	18	--		PB8	18	TXD [2]	--	GPIO [32]
GND_BATTERY	19	--		PB9	19	RXD [2]	--	GPIO [33]
GND_BATTERY	20	--		PC1	20	SPI_CS [16]		
GND_BATTERY	21	--		--	21	DBB_PASS [3]		
DBB_REG	22	--		--	22	3V3_LOWPOW		
DBB_REG	23	--		GPIO-EXP	23	PGOOD_DBB_REG		
DBB_REG	24	--		PC2	24	--	PCK [1]	GPIO [34]
DBB_REG	25	--		*	25	NRST		

Figure 57 shows the mechanical details of the Intrepid bus top hat. As recommended in the Intrepid user guide, the ISIR is a single-sided board (components only on one side) to allow clearance for the System Board's components residing within the 1.65mm daughter board gap. The components on the daughterboard must fit within the remaining 5.75mm clearance on the side facing the Plus Z Payload Breakout Board.

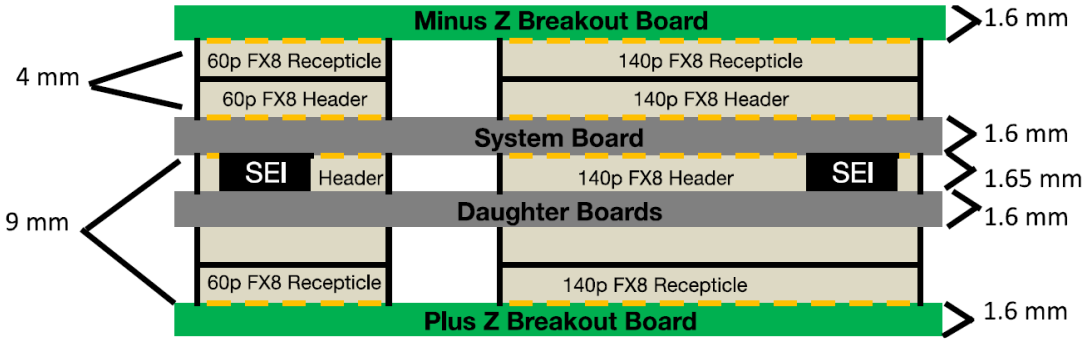

Figure 57: Intrepid Stackup Details [30]

A board level shield for the RF portion of the ISIR was added to reduce potential interference emitted from other PCBAs within the top hat including oscillators, the microprocessor, RAM, switching regulators, and circuitry on other PCBAs. The board level shield must fit within the 5.75mm clearance allocated between the daughter board and the Plus Z Payload Breakout Board. The 3mm high Laird BMI-S-210-F shield was chosen based on this height restriction as well as the specified Daughter Board B dimensions. The schematic snippet for the board level shield is shown in Figure 58. The 3mm height provides 2.75mm clearance for the components on the Plus Z Payload Breakout Board toward the ISIR.

A rule of thumb for faraday shields is that the largest aperture in the shield shall be less than 1/20th of a wavelength at the frequency of interest; 1/20th of a wavelength at 2.4GHz is 6.25mm. The largest gap size in the BMI-S-210-F shield is 2.2mm indicating that it will be effective at 2.4GHz. The 0.2mm shield thickness is well above the skin

depth at 2.4GHz. The board level shield will be solidly connected to the PCBA's ground plan with vias at every pad; it is important to minimize the size of the gaps in the Faraday shield comprised by the PCBA's ground plane and the board level shield.

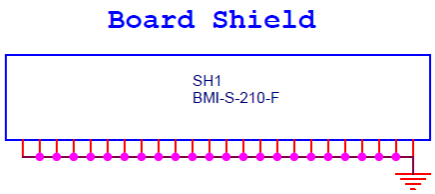

Figure 58: Board Level Shield

Figure 59 and Figure 60 show the signal power isolation circuitry between the signals from the system board and the circuitry on the ISIR. These components are level translators with support for partial power down conditions.

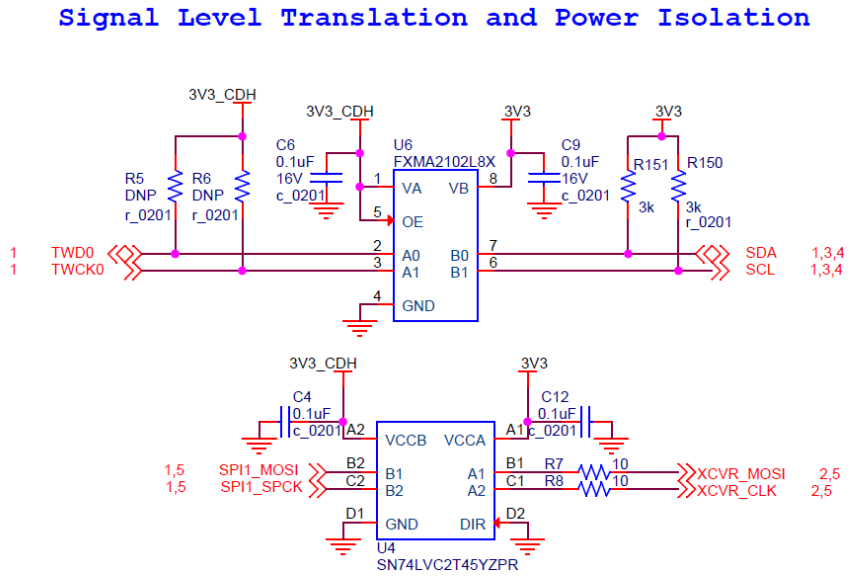

Figure 59: Signal Power Isolation 1

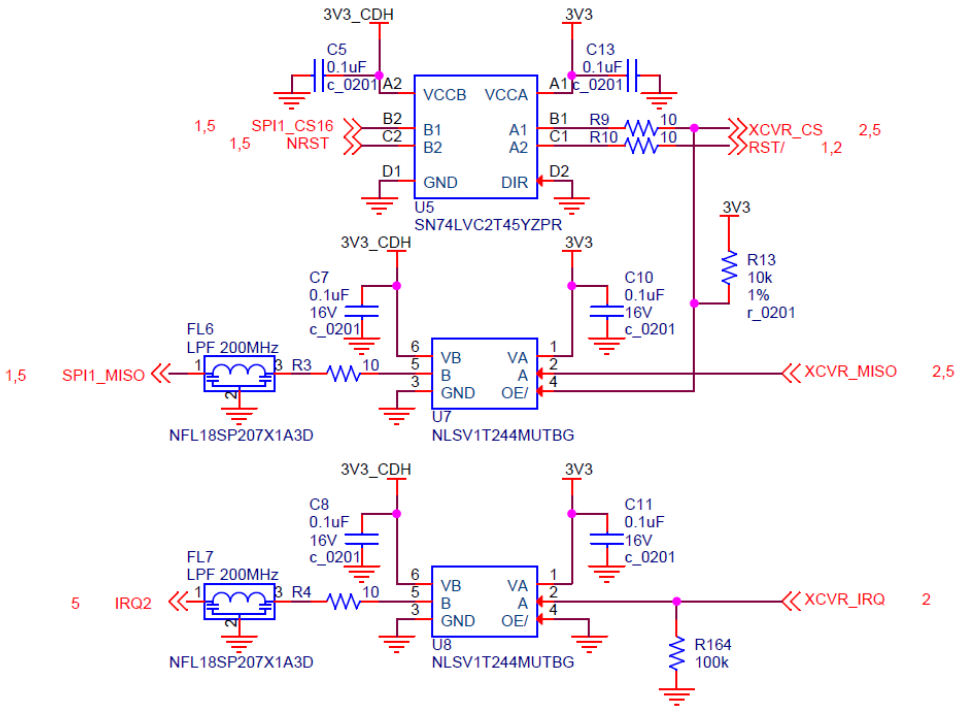

Figure 60: Signal Power Isolation 2

A system with multiple power rails that can be enabled and disabled to conserve power is called a system with partial power down states. The ISIR allows partial power down by allowing the system board to control the enable signal to the regulators powering its circuitry. This introduces the situation where the System Board is powered and the ISIR is unpowered and therefore the System Board can drive signals (SPI, I2C, GPIOS) into the unpowered ICs on the ISIR.

Typically, ICs cannot tolerate voltages on its input pins if the IC is unpowered due to the ESD and clamping structures on the device's pins. For example, the AT86RF233 transceiver cannot tolerate 3.3V logic on its SPI bus input pins when it is powered down; this is evident from the "Absolute Maximum Ratings" stated on the device's datasheet highlighted in Figure 61. The AT86RF233 cannot tolerate voltages 0.3V above its power rail Vdd including when the device is powered down. This indicates that normal System Board 3.3V SPI bus activity present on an unpowered AT86RF233's inputs will cause

excessive current draw that can damage the transceiver. This scenario would occur if the System Board powered down the ISIR to conserve power, but still communicated with other devices on the SPI bus. Further information about partial power down can be found in Texas Instruments Application Note: *"Using High-Speed CMOS and Advanced CMOS Logic in Systems With Multiple Vcc Supplies or Partial Power Down."* [32]

12.1 Absolute Maximum Ratings

Note: Stresses beyond those listed under "Absolute Maximum Ratings" may cause permanent damage to the device. This is a stress rating only and functional operation of the device at these or any other conditions beyond those indicated in the operational sections of this specification are not implied. Exposure to absolute maximum rating conditions for extended periods may affect device reliability.

Symbol	Parameter	Condition	Min.	Typ.	Max.	Unit
T_{STOR}	Storage temperature		-50		150	°C
T_{LEAD}	Lead temperature	T = 10s (soldering profile compliant with IPC/JEDEC J STD 020B)			260	°C
V_{ESD}	ESD robustness	Human Body Model (HBM) [4], Charged Device Model (CDM) [5]	4 750			kV V
P_{RF}	Input RF level				+10	dBm
V_{DIG}	Voltage on all pins (except pins 4, 5, 13, 14, 29)		-0.3		V_{DD}+0.3	V
V_{ANA}	Voltage on pins 4, 5, 13, 14, 29		-0.3		2.0	V

Figure 61: AT86RF233 Absolute Maximum Ratings [28]

The FXMA2102L8X, SN74LVC2T45YZPR, and NLSV1T244MUTBG level translators all support partial power-down as highlighted in their respective datasheets. A snippet from the SN74LVC2T45YZPR datasheet [33] is shown in Figure 62. When either supply pin to the level translator is unpowered, the ports of the level translator are put into a high impedance state, preventing damage to the interfaced unpowered device. The level translators also buffer signals by providing additional drive strength and protects against possible logic failures if the System Board 3.3V supply changes voltage relative to the ISIR's 3.3V supply due to a failure condition; however the primary motivation for these level translators is to allow partial power down of the system so the satellite can conserve energy when the ISIR is not in use.

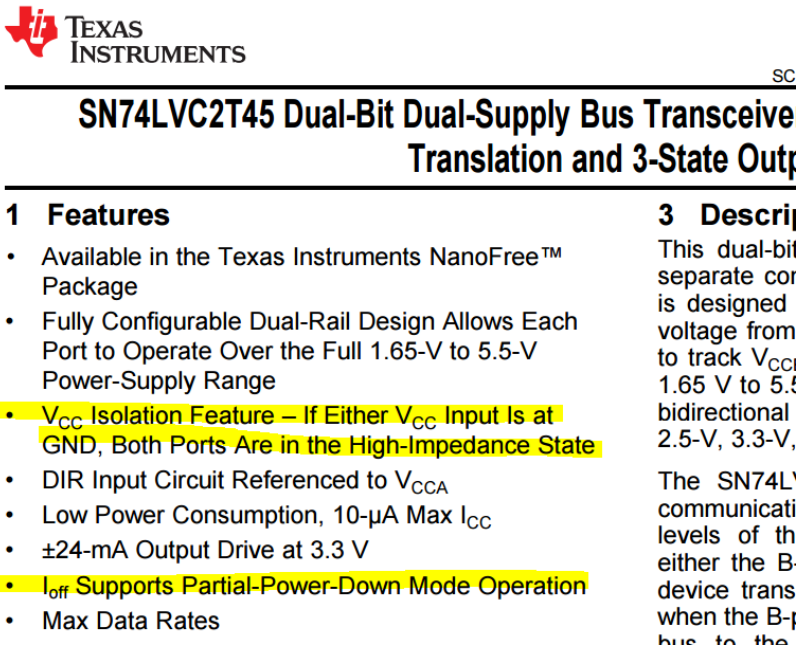

TEXAS INSTRUMENTS

SC

SN74LVC2T45 Dual-Bit Dual-Supply Bus Transceive
Translation and 3-State Outp

1 Features

- Available in the Texas Instruments NanoFree™ Package
- Fully Configurable Dual-Rail Design Allows Each Port to Operate Over the Full 1.65-V to 5.5-V Power-Supply Range
- V_{CC} Isolation Feature – If Either V_{CC} Input Is at GND, Both Ports Are in the High-Impedance State
- DIR Input Circuit Referenced to V_{CCA}
- Low Power Consumption, 10-µA Max I_{CC}
- ±24-mA Output Drive at 3.3 V
- I_{off} Supports Partial-Power-Down Mode Operation
- Max Data Rates

3 Descri

This dual-bit
separate cor
is designed
voltage from
to track V_{CC}
1.65 V to 5.5
bidirectional
2.5-V, 3.3-V,

The SN74LV
communicati
levels of th
either the B
device trans
when the B-p
bus to the

Figure 62: TI SN74LVC2T45YZPR 2-Bit Transceiver, Partial Power Down Information [33]

Series termination resistors are placed on the outputs of the level translators in an attempt to impedance match the driver to the micro strip transmission line; these resistors reduce signal ringing due to the mismatch between the drive impedance of the IC and the high impedance CMOS inputs the level translators are driving. The series termination resistors for U4 are shown in Figure 63. The theory behind a source-series termination is covered in most signal integrity books, such as *Signal and Power Integrity* authored by Dr. Eric Bogatin. [34] The sum of the IC's drive impedance and the series termination value should equal to characteristic impedance of the copper trace in order to completely terminate and absorb the reflected signal from receiver's CMOS high impedance input.

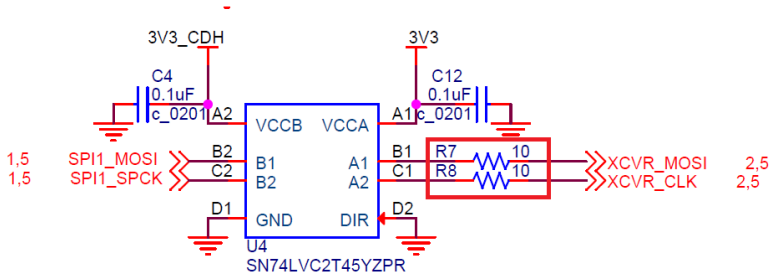

Figure 63: Series Termination Resistors on IC Outputs

Figure 64 is an excerpt from Bogatin's section on source-series termination. [34] Without the series termination, an underdamped waveform is observed on the receiver's input due to the digital step waveform reflecting between the high impedance receiver input and the mismatched driver output. If the driver is matched to the transmission line, the signal is transmitted from the driver, reflects once from the receiver input, travels back down the transmission line, and then is completely absorbed by the matched termination on the driver side; this results in the clean (no-ringing) waveform shown in Figure 64.

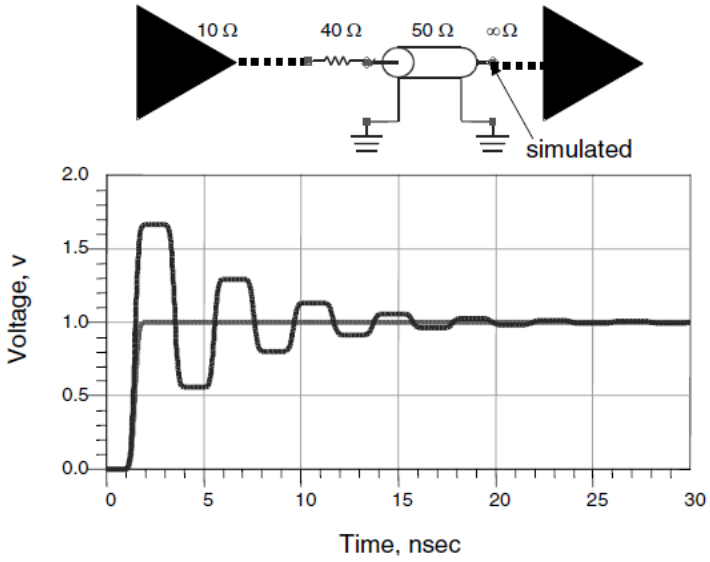

Figure 64: Voltage Signal of a Fast Edge, at the Far End of the Transmission Line with and without the Source Series Terminating Resistor [34]

There are two reasons for reducing the ringing on this SPI bus:

1. Higher SPI Data Rate
    a. SPI does not have a formal standard and no maximum data rate. The maximum data rate is limited by the hardware; an unterminated trace limits the data rate of the bus by degrading the signal received at the receiver.
2. Reduction of Potential EMI
    a. Ringing introduces higher frequency content on the trace, which may radiate and interfere with other circuitry or jam radios in-band with the EMI
    b. According to Bogatin, ringing can increase the magnitude of radiated emissions by a factor of 10. [34]

Another question is whether we need the series termination at all for the relatively slow clock rate of the SPI bus (1 to 10MHz) and the short copper trace length on the PCBA; this question is also answered in signal integrity texts. First, the clock rate of the SPI bus is irrelevant to whether the line should be terminated; the important characteristic is the rise and fall time (slew rate) of the signal. The slew rate of the signal determines its frequency bandwidth, not the clock rate. The SPI bus clock may run at 1MHz, but the signal slew rate is dependent on the drive strength of the IC which depends on how the IC was fabricated.

According to Bogatin, IC fabricators use the same chip size and wafer process for all ICs regardless if the chip is to be used in a high or low speed application to save costs; therefore even though the chip may not need the faster rise time, the rise time will increase as IC fabricators upgrade their processes for the fastest ASICs being developed. [34] The switching characteristics from the SN74LVC2T45 datasheet are

shown in Figure 65; the highlighted numbers are the slew rates for the application at 3.3V. The rise time of the level translator can be as fast as 0.7ns, which equates to a frequency bandwidth of approximately 500MHz using the rule of thumb from Bogatin: $BW = \frac{0.35}{RT}$, where BW is the highest "significant" frequency of the signal and RT is the rise time of the signal; here significant is defined as the 3dB bandwidth (half-power point) of the signal. [34] The signal still has higher harmonics than this 3dB bandwidth that can still radiate or cause EMI problems which are further amplified by ringing.

The result is that the slew rate of the level translator is overkill for this application which may degrade functionality if not properly terminated or filtered. The rule of thumb from Bogatin for the maximum length of an unterminated line is *1 inch per nanosecond rise time*. [34] For example, a 1ns rise time signal requires termination if the trace is longer than one inch and a 0.5ns rise time signal requires termination if the trace is longer than half an inch; as rise times become faster, the minimum trace length before signal integrity problems occur becomes shorter. On this PCBA, the trace length may be longer than 0.7 inches indicating a need for the series termination resistor.

6.8 Switching Characteristics: V_{CCA} = 3.3 V ± 0.3 V

over recommended operating free-air temperature range, V_{CCA} = 3.3 V ± 0.3 V (unless otherwise noted) (see Figure 17)

PARAMETER	FROM (INPUT)	TO (OUTPUT)	V_{CCB} = 1.8 V ±0.15 V		V_{CCB} = 2.5 V ±0.2 V		V_{CCB} = 3.3 V ±0.3 V		V_{CCB} = 5 V ±0.5 V		UNIT
			MIN	MAX	MIN	MAX	MIN	MAX	MIN	MAX	
t_{PLH}	A	B	2.1	15.5	1.4	8	0.7	5.6	0.7	4.4	ns
t_{PHL}			2	12.6	1.3	7	0.8	5	0.7	4	
t_{PLH}	B	A	1.7	8.3	1.3	6.4	0.7	5.8	0.6	5.4	ns
t_{PHL}			1.8	7.1	1.3	5.4	0.8	5	0.7	4.5	
t_{PHZ}	DIR	A	5	10.9	5.1	10.8	5	10.8	5	10.4	ns
t_{PLZ}			3.4	8.4	3.7	8.4	3.9	8.1	3.3	7.8	
t_{PHZ}	DIR	B	11.2	27.3	8	13.7	5.8	10.4	2.9	7.4	ns
t_{PLZ}			9.4	17.7	5.6	11.3	4.3	8.3	1	5.6	
t_{PZH} (1)	DIR	A		26		17.7		14.1		11	ns
t_{PZL} (1)				34.4		19.1		15.4		11.9	

Figure 65: SN74LVC2T45 Switching Characteristics, Datasheet Excerpt

The value of 10 Ohms was chosen arbitrarily without any analytical calculations; values between 10 to 40 Ohms are typically chosen because they have been found to resolve ringing issues in the past. No calculations were performed because the characteristic impedance of the digital signal lines are not tightly controlled on this PCBA and the trace width is the smallest allowed by the PCB fabricator, whereas future revisions of the board may have different stack ups or thinner traces. Also, test points, harnesses, IC pads, differences in trace impedance across boards, and other practical considerations will influence the ideal value of the series termination which reduces the value of an analytical calculation. However, the value can be fine-tuned with an oscilloscope and resistor kit during testing if problems occur due to imperfect termination on the line; the important thing is that the series resistor is there to be tuned if a problem occurs without requiring invasive cutting of traces on the PCB.

In addition to the series terminations, long trace length lines have capacitive filters to reduce the frequency content of the signal. As a trace becomes longer, its potential to radiate does as well. The low pass filter on the SPI MISO signal is shown in Figure 66. The purpose of these filters is to reduce potential high frequency EMI by limiting signal bandwidth. In this application, the SPI bus will run at a maximum clock rate of 10MHz; this digital square wave signal requires a minimum bandwidth up to its 5^{th} harmonic of 50MHz for acceptable distortion. The lowest frequency of concern on the spacecraft is the UHF receiver tuned to 437MHz, so the filter needs to attenuate potential in-band EMI at 437MHz. The low pass frequency of 200MHz was chosen to attenuate components in-band with UHF at 437MHz but the low pass filter could be lowered to the minimum of 50MHz for more attenuation if necessary.

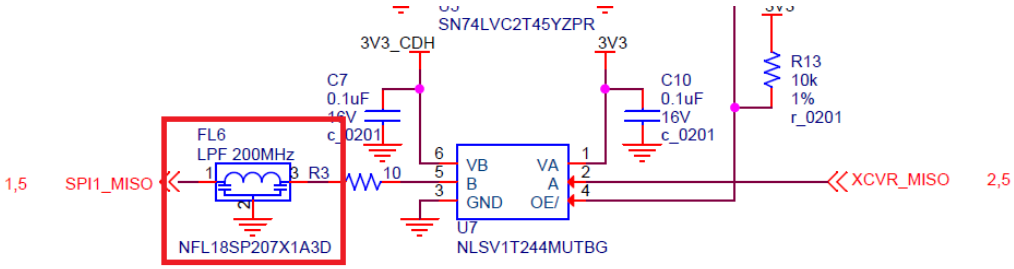

Figure 66: Low Pas Filter on SPI MISO Signal

Figure 67 is the schematic of the GPIO expander on the ISIR. The purpose of a GPIO expander is to reduce the required number of signals broken out from the satellite microprocessor. The GPIO expander interfaces to the microprocessor through its I2C bus. The microprocessor commands the GPIO expander to configure its pins as an input or output and can read and set values on the pins as fast as the I2C bus allows. I2C is a low speed (100 kHz) interface for connecting many ICs to a microprocessor using only two signals, SDA (data) and SCL (clock), each device on the bus is required to have a unique 7-bit address. I2C GPIO expanders are only used for low speed applications, because the speed of the GPIOs is limited by the speed of the I2C transactions; for instance, the GPIO expander pin toggling speed would be inadequate to drive another bus or high speed interrupt line.

Most I2C devices have configurable addresses so multiple of the same device can be utilized on the same bus without conflict. The TCA9539 GPIO expander has configurable address pins and the hex address 0x75 was chosen by referencing the devices datasheet and pulling the A1 and A0 pins to the corresponding nets. The GPIO expander active low reset “/RST” pin is interfaced to the microprocessor’s “NRST” signal which goes low when the processor resets; this ensures that the GPIO expander is in a known default state when the microprocessor boots avoiding issues caused by undefined states. The transceiver is also interfaced to the NRST signal.

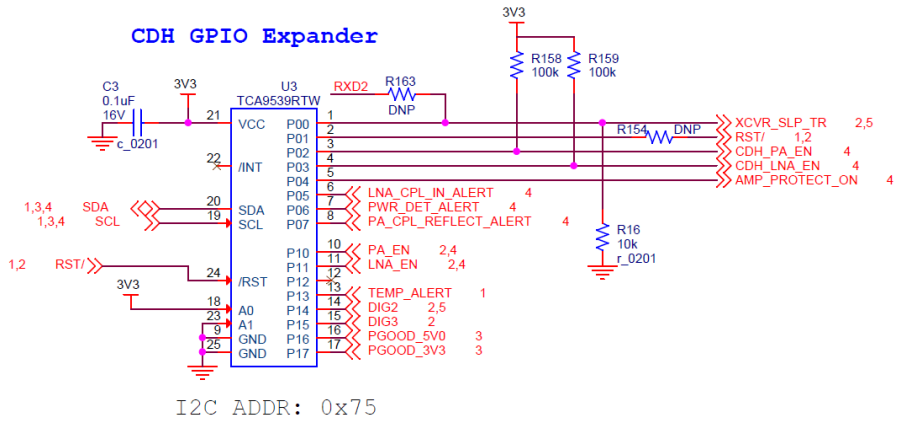

Figure 67: I2C GPIO Expander

Figure 68 shows the board's I2C temperature sensor with alert pin. The temperature sensor is located as close as possible to the board's RF amplifier, which will be the highest temperature component on the board. The microprocessor can retrieve the temperature from this sensor and can cut transmission before the RF amplifier exceeds its absolute maximum ratings. The temperature sensor can be configured to issue an alert after exceeding a certain temperature value. The temperature alert signal is interfaced to the GPIO expander for monitoring by the microprocessor.

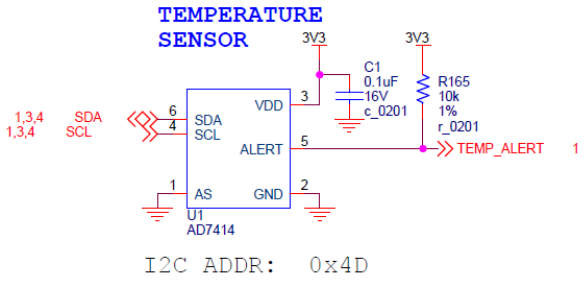

Figure 68: I2C Temperature Sensor

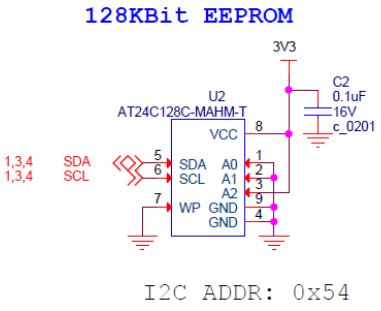

Figure 69: I2C EEPROM

Figure 69 shows the board's 128kbit EEPROM for use by the microprocessor for storing ISIR board calibration and identification information.

5.2 Transceiver and RF Front End

Figure 70 shows the schematic for the AT86RF233 transceiver, balun, in-line test points, and low power RF TX/RX switch. U13 is simply a level translator which translates the transceiver's antenna selection signals from 3.3V to the required 5.0V signal levels required by the antenna selection switch elsewhere on the schematic.

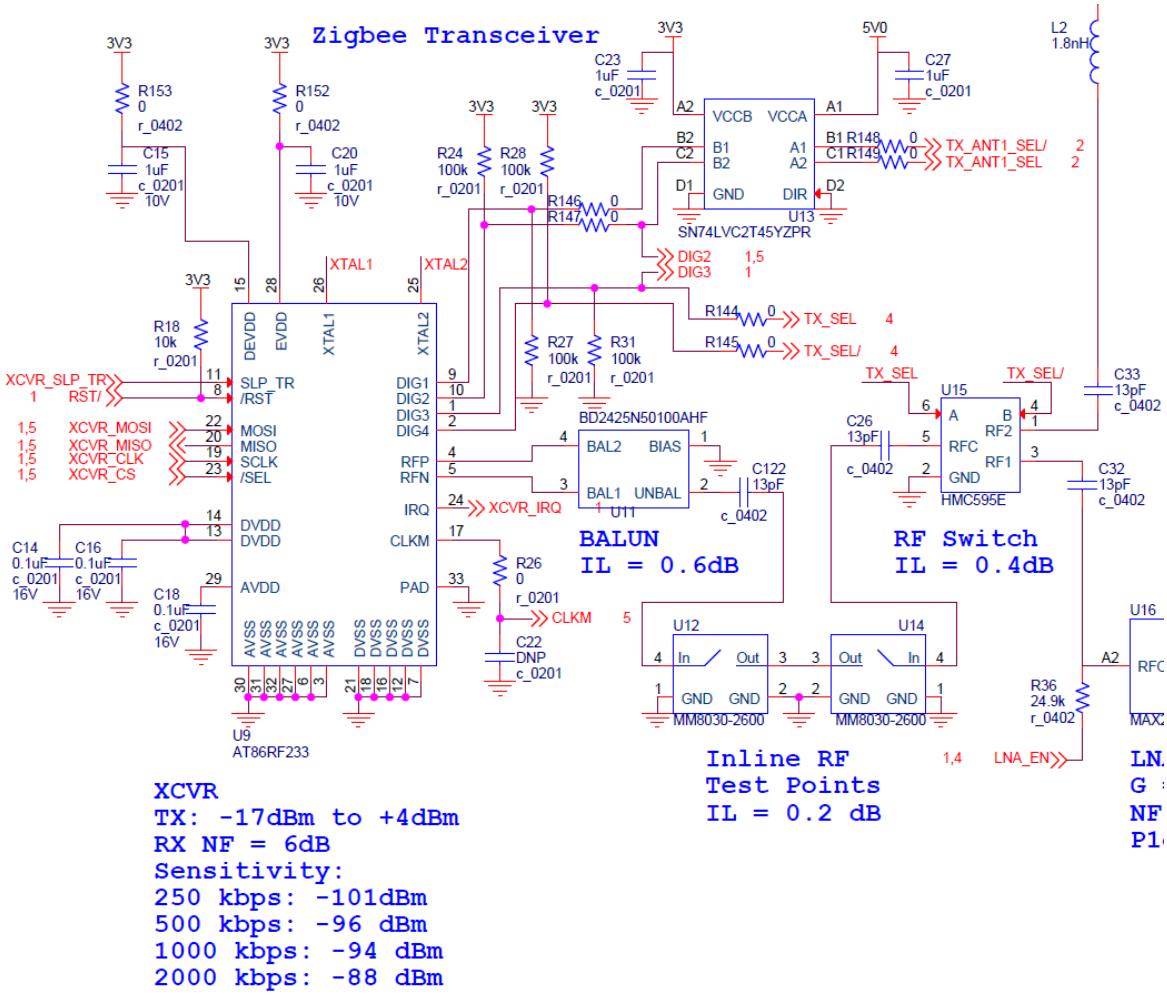

Figure 70: AT86RF233 Transceiver, Test Points, and Low Power RF Switch

The Anaren, BD2425N50100AHF balun, U11, transforms the transceiver's balanced differential RF signal into a single-ended unbalanced signal. According to the AT86RF233 datasheet, the transceiver's differential RF routing suppresses the switching noise of its internal digital signal processing blocks. [28] However, the spacecraft

antenna will connect to the PCBA through a typical single-ended coaxial cable, so the signal must be converted from differential to single ended at some point in the circuit. Most commercial RFICs are single-ended, so the decision was made to convert from differential to single-ended immediately after the transceiver. Following Atmel's recommendation in its application note "Atmel AT02865: RF Layout with Microstrip," the balun was chosen based on its pin pitch to match the pin spacing of the transceiver for better alignment and minimize impedance mismatch. [35] After selecting baluns with pin spacing matching the transceiver's QFN package, the balun with the lowest insertion loss (0.6dB) was chosen to maximize transmitted signal strength and maximize received signal to noise ratio.

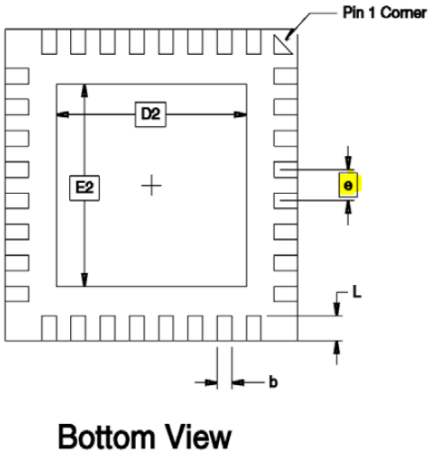

COMMON DIMENSIONS
(Unit of Measure = mm)

SYMBOL	MIN.	NOM.	MAX.	NOTE
D		5.00 BSC		
E		5.00 BSC		
D2	3.20	3.30	3.40	
E2	3.20	3.30	3.40	
A	0.80	0.90	1.00	
A1	0.0	0.02	0.05	
A2	0.0	0.65	1.00	
A3		0.20 REF		
L	0.30	0.40	0.50	
e		0.50 BSC		
b	0.18	0.23	0.30	2

Figure 71: Transceiver AT86RF233 QFN Package, 0.5mm Pin Pitch [28]

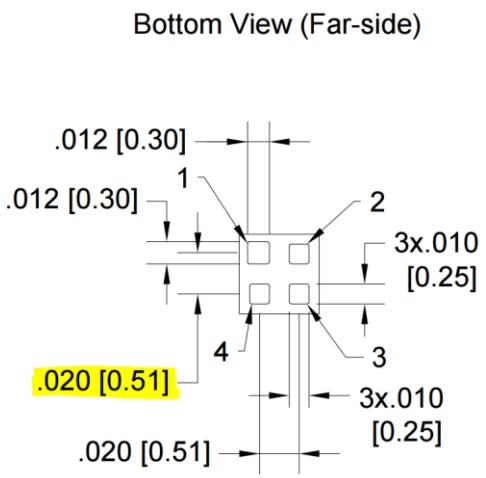

Figure 72: Balun BD2425N50100AHF Package, 0.51mm Pin Pitch [36]

The HMC595E TX/RX switch, U15, switches the transceiver's RF signal to the external transmit chain when the transceiver transmits and switches to the receive chain when the transceiver receives. The TX_SEL and TX_SEL/ signals controlling the low power TX/RX switch are automatically outputted by the transceiver during transmit and receive with appropriate delays between switching and transmitting. The HMC595E introduces a 0.4dB insertion loss to the RF chain.

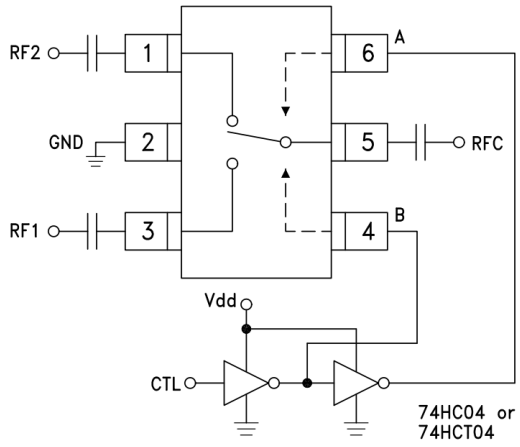

Figure 73: HMC595E, RF Switch Application Circuit [37]

Two Murata, MM8030-2600, coaxial test points were inserted between the balun and the switch to be utilized during testing, characterization, and tuning of the board. The MM8030-2600 connectors mate to a specialized probe that converts to a standard female SMA connector for use with external test equipment such as a spectrum analyzer or VNA. When the probe is inserted into the connector, the input signal is switched to the probe. When the probe is absent, the connector passes through the signal from input to output introducing a small 0.1dB insertion loss. By arranging two MM8030-2600 test points as shown in the schematic, external equipment can be added in series between the transceiver and RF switch. These test points allow measurement of the transmit chain's gain, the receive chain's gain and noise figure, and general troubleshooting.

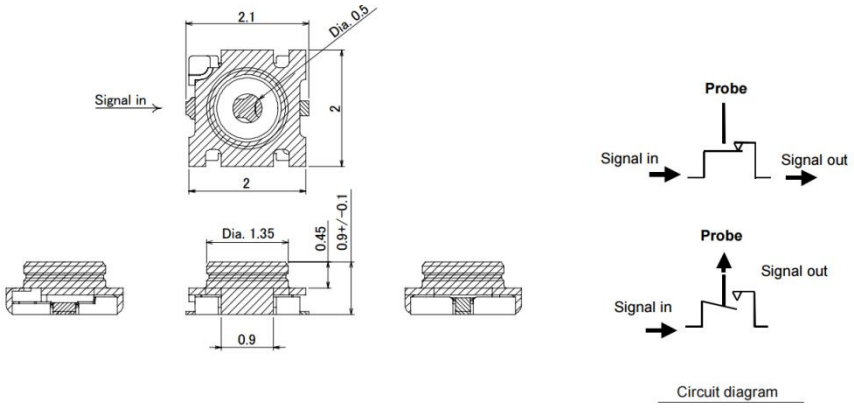

Figure 74: Murata MM8030-2600, RF Coaxial Connector / Test Point [38]

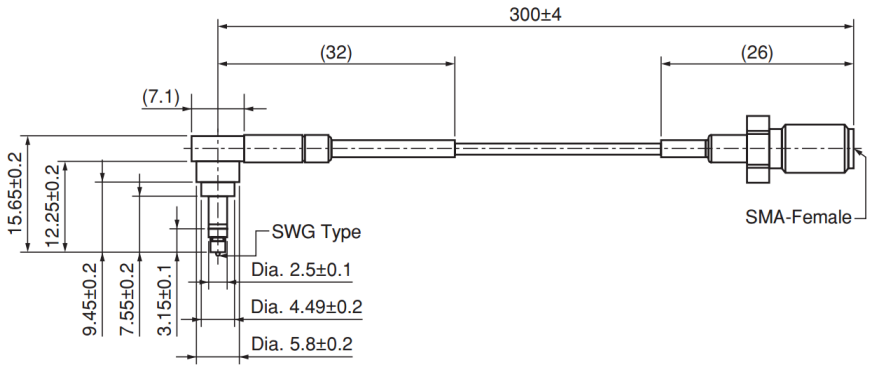

Figure 75: Murata Measurement Probe for MM8030-2600 [39]

Coupling capacitors are required throughout the RF chain before and after switches and amplifiers to block DC currents while passing RF signals; the value, size, dielectric, and model of the coupling capacitor was chosen carefully. The size of the capacitor was chosen so that its width was closest to the width of the PCB micro-strip transmission line in order to best match characteristic impedance of the trace; a surface mount 0402 capacitor most closely matched the trace width. A high-Q, low-loss, NP0 temperature coefficient ceramic capacitor with a tolerance of 2% was chosen so its behavior would remain consistent over frequency and temperature.

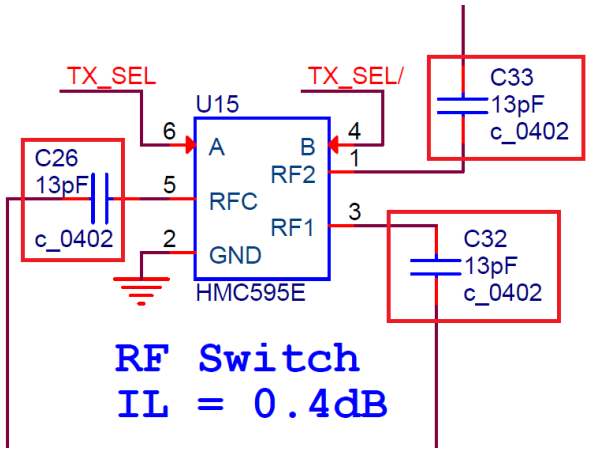

Figure 76: 13pF AC Coupling Capacitors throughout the Schematic

The goal of the ac coupling capacitor is to block DC currents and pass the frequencies of interest with minimal insertion loss. All capacitors block DC currents, but all capacitors do not provide the same insertion loss at the same frequency. A practical capacitor does not behave as an ideal capacitor at all frequencies; the first-order equivalent electrical model of a practical capacitor is a series RLC circuit as shown in Figure 77; the capacitor model is comprised of the capacitor's capacitance, equivalent series inductance (ESL) , and equivalent series resistance (ESR).

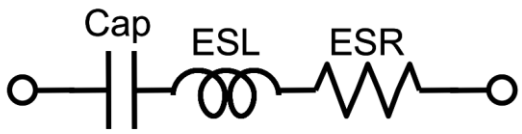

Figure 77: Capacitor Equivalent Circuit [40]

Equivalent series inductance and resistance does not only include the inductance inherent to the physical component stand-alone, but also the inductance and resistance introduced by the way the capacitor is mounted and its pads connected to other components on the PCBA. Figure 78 shows the frequency characteristics of the first order model of a practical capacitor. At low frequencies the highest impedance component of the circuit is the capacitance and the capacitor behaves as an ideal capacitor. As frequency increases, the positive reactance contributed by inductance increases while the negative reactance contributed by the capacitance decreases until at a certain frequency they become equal in magnitude and cancel each other out. This point is called self-resonance and the impedance of the capacitor is at its minimum value equal to its equivalent series resistance (ESR). After the self-resonant point, as frequency increases, the inductive reactance continues to increase while capacitive reactance continues to decrease which causes capacitor's impedance to increase. Therefore, after self-resonance, a capacitor behaves as an ideal inductor with impedance that increases with frequency.

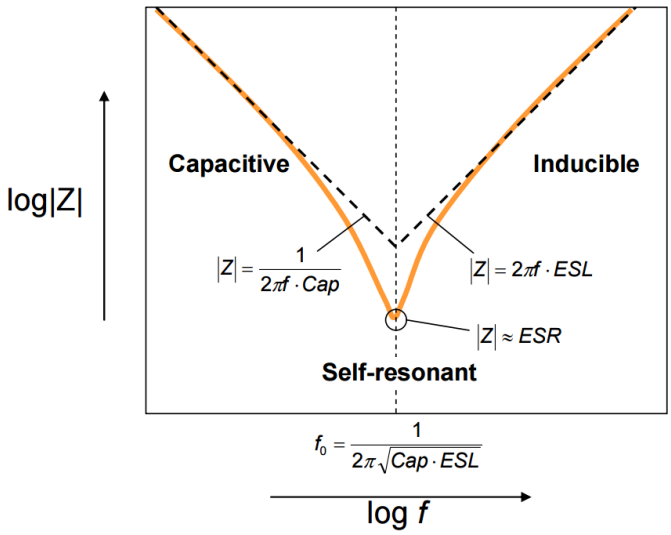

Figure 78: Capacitor Frequency Characteristics [40]

The region with minimal insertion loss is the frequency range at which the capacitor is at self-resonance, therefore this is the optimal point to operate an AC coupling capacitor. However, because the ESL and ESR are dependent on layout of the PCBA, most application notes recommend using coupling capacitors below their series resonance so that the impedance can be accurately modeled and predicted and proceed with the assurance that the capacitor continues to "act as a capacitor." However, in the pursuit for minimal insertion loss, the capacitor was chosen at its series resonance utilizing Murata's online "SimSurfing" tool which simulates the characteristics of Murata passive components. [41] One Ohm was defined as the preferred impedance for the capacitor in the frequency band of interest, which is 2400 MHz to 2500MHz. The Murata, GJM1555C1H130GB01, 13pF capacitor shown in Figure 79 met the desired behavior and was chosen as the AC coupling capacitor used throughout the RF circuit.

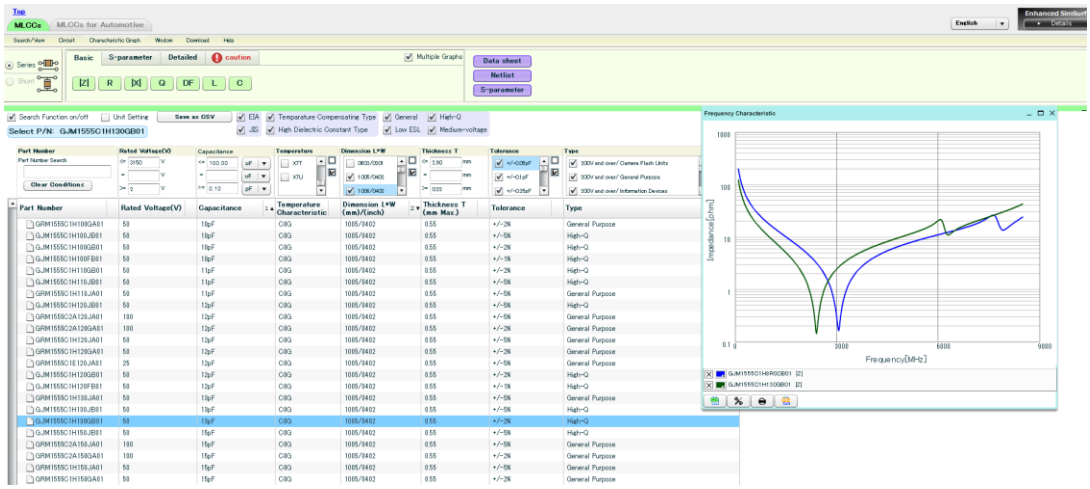

Figure 79: Murata SimSurfing Capacitor Simulation Tool [41]

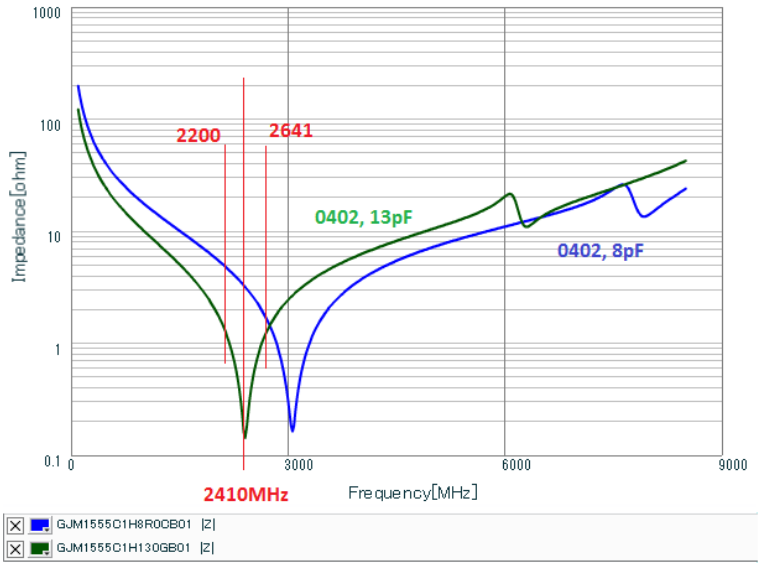

Figure 80: 13pF Coupling Capacitor, Murata GJM1555C1H130GB01 Frequency Characteristics

The transmit chain is shown in Figure 81. When the transceiver transmits, the signal passes through the external RF power amplifier (PA) U17 followed by the low pass filter (LPF) FL5 and then the directional coupler U19.

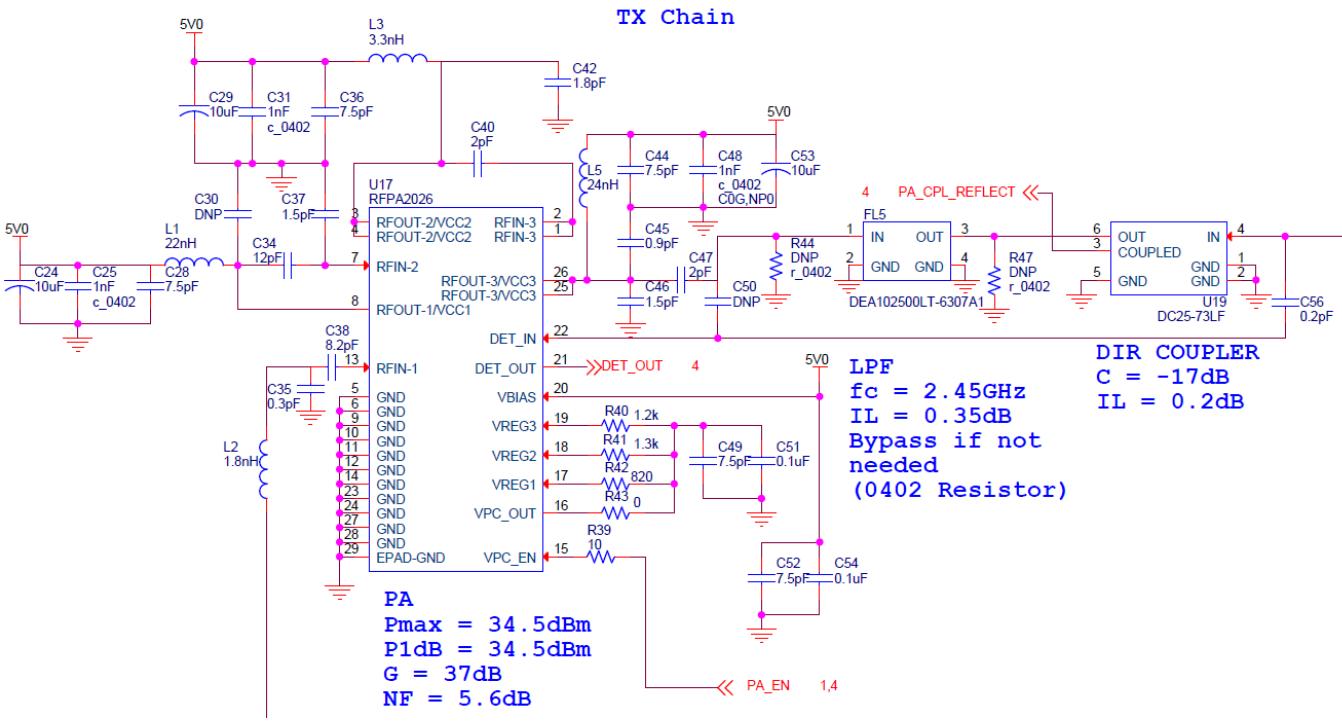

Figure 81: ISIR Transmit Chain: External Power Amplifier, Low Pass Filter, Directional Coupler

The RFMD RFPA2026 power amplifier is a 3-stage, 2W amplifier within a 6.0 mm x 6.0 mm package for use in the 700MHz to 2700MHz frequency range. The datasheet for the RFPA2026 provides application schematics for 728MHz to 768MHz, 2.11GHz to 2.17 GHz, and 2.58GHz to 2.69GHz, however none of these frequency ranges are the desired ISM 2.4GHz to 2.5GHz range. However, after contacting an RFMD application engineer, a circuit for the 2.3GHz to 2.7GHz range was provided as a modification to the datasheet's 2.58GHz to 2.69GHz evaluation board as shown in Figure 82. Additionally, measurements were provided for gain, output power, OIP3, ACPR, and S parameters.

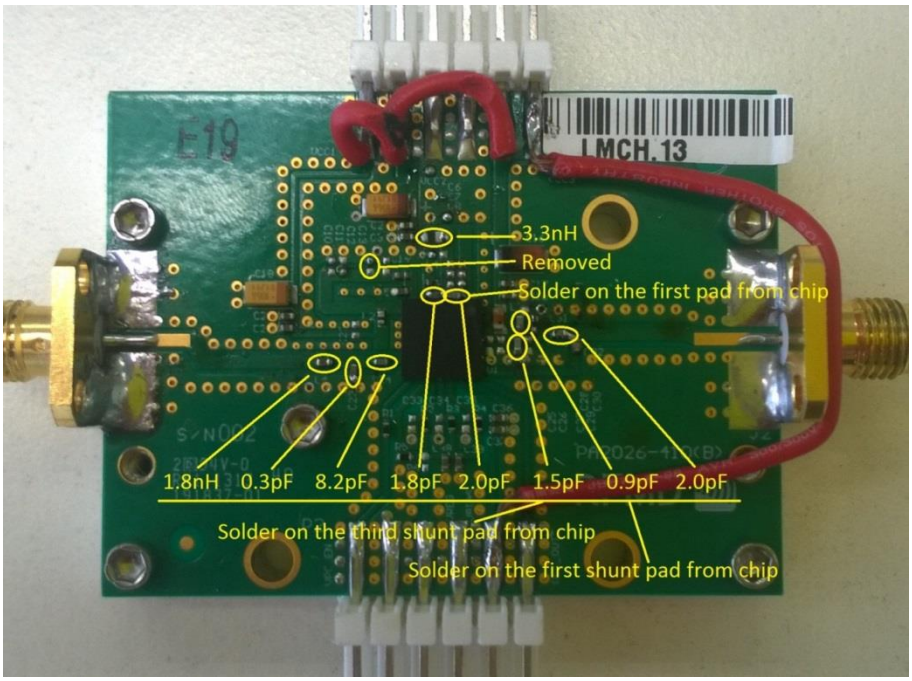

Figure 82: RFMD RFPA2026, 2.58GHz to 2.69GHz Evaluation Board Modified for 2.3GHz to 2.7GHz [42]

The modified evaluation board picture and evaluation board design files were used to back out the values used by the RFMD application engineer and incorporated into the schematic. However, at 2.4GHz, the values of the components are extremely dependent on the PCBA layout, trace lengths, and component parasitics; therefore the intention was to use this evaluation board schematic as a starting point before fine-tuning the circuit component values.

Figure 83 and Figure 84 show the gain and input power compared to the output power of the modified RFPA2026 evaluation board. These graphs show that the P1dB compression point occurs at 34dBm at 2400MHz with a gain of 37dB. The RF signal is modulated using OQPSK which allows use of a power amplifier at its compression point without significant degradation. According to the graphs, the RFPA2026 consumes a total 1.175A at 5V which equates to 5.9W while outputting 2.5W (34dBm); therefore the

amplifier is 42% efficient. This also indicates that 3.4W of the input power is converted into heat at the amplifier which indicates that heat sinking is required at the RFPA2026 component.

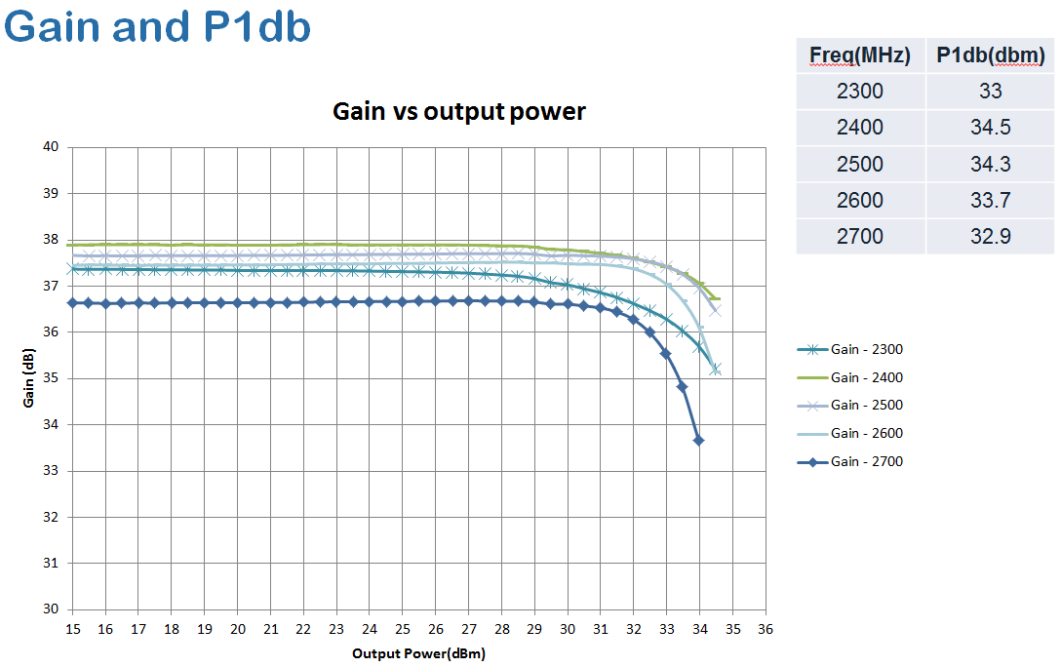

Figure 83: Gain vs Output Power of Modified RFPA2026 Evaluation Board [43]

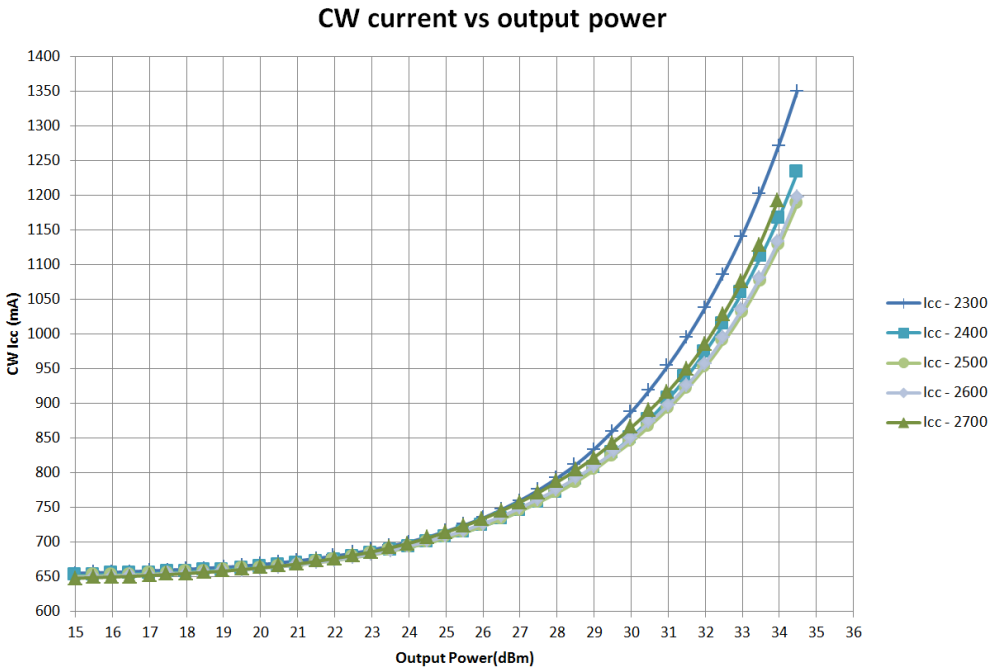

Figure 84: Input Power vs Output Power of Modified RFPA2026 Evaluation Board [43]

FL5 is the DEA102500LT-6307A1 2.45GHz low pass filter for the 2.4GHz ISM band. The purpose of the low pass filter is to suppress out of band spurs outputted by the power amplifier in order to reduce possible interference from the transmitter into higher frequency bands. FL5 reduces the 2nd and 3rd harmonics at 4800MHz and 7200MHz by 25dB, as shown in Figure 85. Depending on the launch vehicle, mission, and program requirements the transmission profile of the satellite must attenuate out of band noise and satisfy radiated emission requirements. If the low pass filter is not required for the mission, it may be removed and bypassed with a 0 Ohm 0402 resistor.

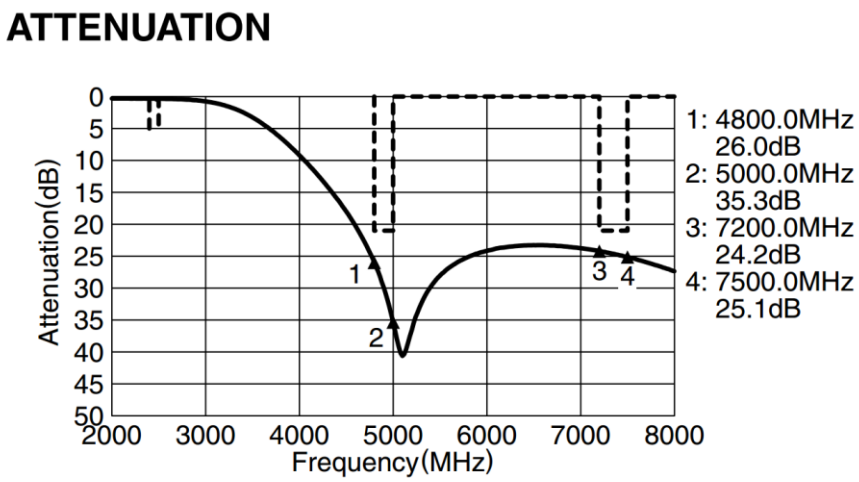

Figure 85: TDK DEA102500LT-6307A1 Low Pass Filter, Attenuation Plot [44]

The Skyworks DC25-73LF -17dB directional coupler, U19, is placed at the end of the transmit chain to sample the signal reflected back toward the power amplifier and provide this measurement to the amplifier protection circuitry and the C&DH. The DC25-73LF is a directional coupler for 2.3GHz to 2.6GHz, the block diagram is shown in Figure 86.

Measuring the reflected power provides a way to estimate the VSWR of the antenna which can be utilized to protect of the power amplifier if the reflected power exceeds the amplifier's rating. Typically, if an amplifier is operated into an open or short load (no antenna, or shorted antenna) the amplifier will become permanently damaged. Forgetting to install an antenna, accidently disconnecting an antenna, or forgetting to deploy a stowed antenna and transmitting was the most prevalent failure of the PolySat UHF radio, which resulted in excessive reworking and replacing of amplifier IC. Therefore, protection circuitry was added to the ISIR in order to prevent accidental damage to the power amplifier from transmitting into a mismatch load.

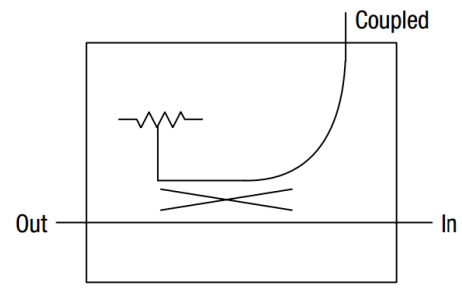

Figure 86: Skyworks DC25-73LF Directional Coupler, Block Diagram

The receive chain for the ISIR is shown in Figure 87; it is comprised of a low noise amplifier (LNA), band pass filter (BPF), and directional coupler.

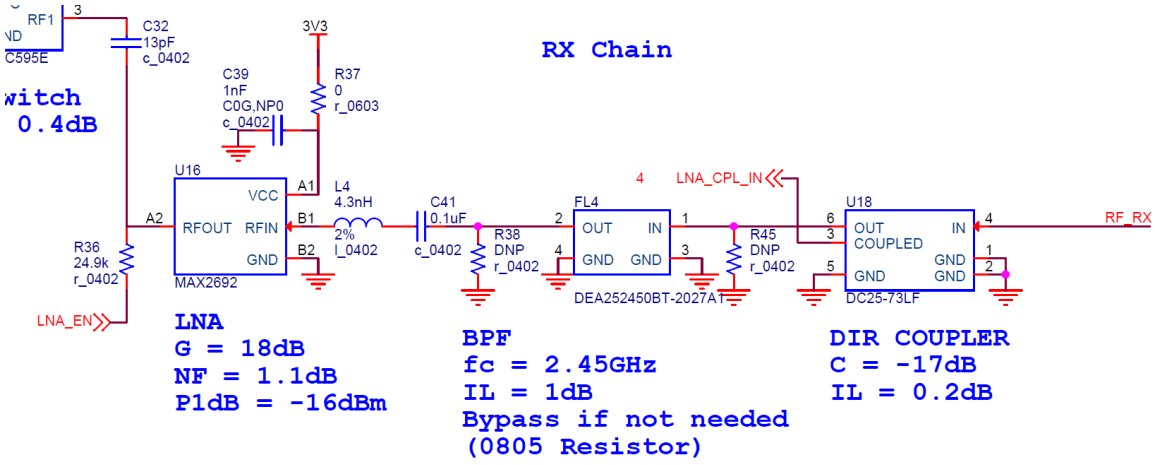

Figure 87: ISIR Receive Chain: Low Noise Amplifier, Band Pass Filter, and Directional Coupler

The received signal first enters the directional coupler which samples the receive signal so its signal strength can be measured. This sampled signal is fed into additional protection circuitry that disables the LNA if the signal strength is above the LNA's maximum value so permanent damage does not occur. Excessive signal strength commonly occurs during benchtop testing when two radios are connected to each other

through coaxial cable without adequate attenuation. The absolute maximum input power into the LNA is 5dBm; therefore if a 2W (33dBm) radio directly transmitted into the LNA without protection circuitry, permanent damage would occur. The directional coupler is the same model as the one used within the transmit chain.

The TDK DEA252450BT-2027A1 2.45GHz bandpass filter, FL4, is placed before the LNA in order to prevent saturation of the LNA from out of band sources; this situation could occur if another radio on the satellite such as the UHF radio were transmitting at the same time the ISIR is receiving; the LNA could conceivably become saturated and the 2.45GHz signal would be distorted. However, the ISIR LNA is tuned to the 2.45GHz band with low gain and high return loss in out of band frequencies. If the band pass filter is not needed, FL4 can be removed and bypassed with a 0805 resistor. The bandpass filter was chosen based on lowest insertion loss; however it still introduces a 1dB loss before the LNA which equates to 1dB degradation in signal to noise ratio of the received signal if the noise floor is limited by thermal noise.

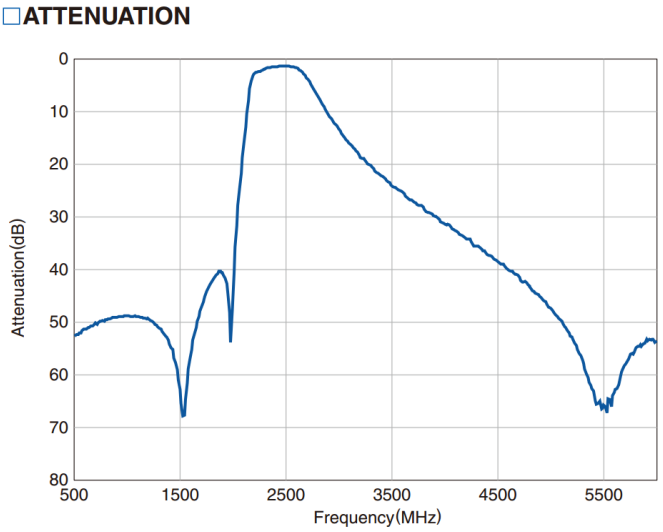

Figure 88: TDK DEA252450BT-2027A1, 2.45GHz Bandpass Filter Attenuation Profile [45]

U16 is the Maxim MAX2692 low noise amplifier for the 2.45GHz ISM band, the typical application circuit is shown in Figure 89. The MAX2692 was selected because it is low power and had the lowest noise figure and acceptable gain compared to competing options. The MAX2692 has an excellent noise figure of 1.1dB and gain of 18dB. The purpose of the LNA is to increase the receive sensitivity of the radio by decreasing the overall noise figure of the radio.

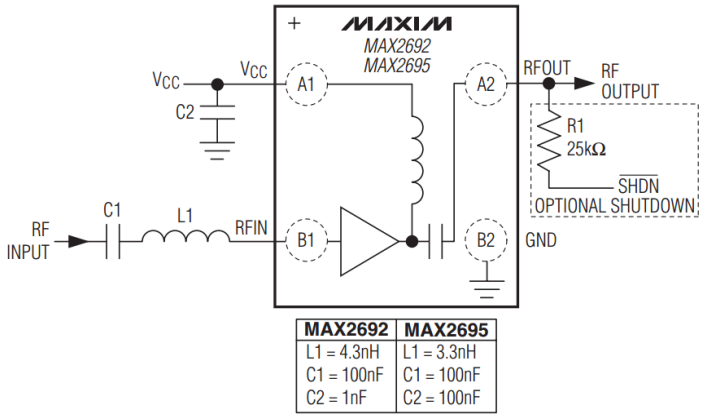

Figure 89: Maxim MAX2692 Low Noise Amplifier, Typical Operation Circuit [46]

Let use the transceiver and its specifications to explore the concept of noise figure and the application of the LNA to improve receive sensitivity. The datasheet for the AT86RF233 transceiver states a receive sensitivity of -101dBm at 250kbps with a noise figure of 6dB. This means that in a thermal noise floor limited scenario (no external interference) at 290K, the AT86RF233 increases the noise floor by 6dB, which decreases the signal to noise ratio by 6dB and degrades the receive sensitivity by 6dB. The AT86RF233 always adds a fixed amount of noise into the signal which can be calculated the relation:

$$\boldsymbol{F = 1 + \frac{N_{added}}{kT_0B}}$$

Where **F** = the Noise Factor (noise figure is noise factor in dB), $\boldsymbol{N_{added}}$ = the noise added by the component, and is $\boldsymbol{kT_0B}$ the thermal noise power within the specified bandwidth **B** at the standard temperature of $\boldsymbol{T_0}$ = 25C using the Boltzmann constant **k**.

Using the relation, the AT86RF233 with a noise figure of 6dB always adds a fixed 27.3pW of noise to the signal which equates to -105.6dBm. The bandwidth of the transceiver is 2.3MHz, which contains inherent thermal noise of -110.4dBm (kTB). Adding the thermal noise with the noise from the AT86RF233 results in a noise floor of -104.4dBm is 6 dB higher than the thermal noise, which is the noise figure. These numbers suggest that a standalone AT86RF233 can decode a 250kbps signal with a signal to noise ratio of 3.4dB (-101dm - (-104.4dBm)), whether that noise is thermal or from external interference, and the AT86RF233 always adds -105.6dBm (27.3pW) of its own noise on top of the input noise. If the AT86RF233 did not contribute additional noise, then the transceiver could theoretically receive signals as low as -107dBm at 250kbps.

The LNA improves the receive sensitivity by amplifying both the signal and noise while introducing little noise itself. The LNA amplifies the input noise to the point that the AT86RF233's 27.3pW of additional noise makes little to no difference to the overall signal to noise ratio. Suppose we receive a signal at -105dBm which is then combined with the PCB's inherent thermal noise floor of -110.4dBm. The MAX2692 LNA amplifies the signal and noise by 18dB while adding 1.1dB of its own noise (-110.4 + 1.1 +18). The signal is now at -87dBm and the noise is at -91.3dBm which equates to a signal to noise ratio (SNR) of 4.3dB. The AT86RF233 transceiver then receives the signal and adds -105.6dBm of noise to the input noise, equating to -91.1dBm of total noise (only a 0.2dB increase in noise). The SNR received by the AT86RF233 is still high at 4.1dB which exceeds the 3.4dB limit and is decodable by the AT86RF233. Without the LNA, the AT86RF233 would have only been able to decode a -101dBm signal, but with the LNA the radio could theoretically decode a -105.7dBm signal.

However, the components before the LNA appreciably degrade the SNR. To find the noise figure and gain for the complete receive chain, the equation for the noise figure of cascaded networks is used:

$$\boldsymbol{F = F_1 + \frac{F_2 - 1}{G_1} + \frac{F_3 - 1}{G_1 G_2} + \cdots}$$

Where $\boldsymbol{F_1}$= the noise figure of the 1st stage, $\boldsymbol{G_1}$ = the gain of the first stage, $\boldsymbol{F_2}$= the noise figure of the 2nd stage, $\boldsymbol{G_2}$ **=** the gain of the 2nd stage, etc.

Assuming a 0.1dB loss for each AC coupling cap and the insertion losses stated in the schematic, the calculation results in a total F = 3.64dB and G=14.2dB for the receive chain. This means the radio has a 2.36dB improvement of receive sensitivity compared to the standalone transceiver with a theoretical receive sensitivity of -103dBm.
The receive sensitivity of the radio will also decrease when exposed to additional noise such as internally generated electromagnetic interference (EMI) from nearby electronics, in-band noise from external transmitters, or the antenna pattern intersecting with a hot object such as the sun.

5.3 Power Regulation

The Switching mode power supply circuits shown in Figure 90 and Figure 91 provide efficient regulated power to the board. The 3.3V net provides power for the transceiver, digital logic, and the LNA. The 5.0V net provides power for the antenna RF switch, RF power detectors, and the power amplifier. The Texas Instruments TPS63020 high efficiency buck-boost regulator IC was utilized for both power rails. The input to the regulators is the unregulated battery voltage from the satellite's battery pack, which is typically multiple single lithium ion battery cells connected in parallel. The typical voltage range of a single lithium ion battery is 3.0V to 4.2V; therefore a buck/boost regulator was required for the 3.3V voltage rail because the input voltage can be below or above 3.3V.

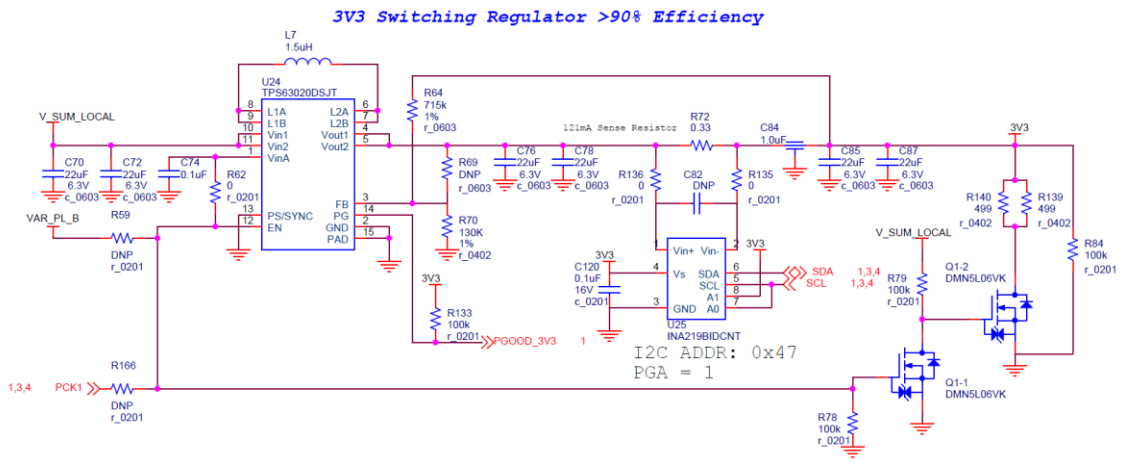

Figure 90: 3.3V Switching Regulator Provides Power for Transceiver, Digital Logic, and LNA

To keep things simple, the same regulator was used for both 3.3V and 5.0V; however, different regulators could have been chosen to reduce space on the PCBA. For instance, the 3.3V regulator only required an output current of 200mA whereas the 5.0V regulator required a maximum output current of 2A so a smaller regulator could have been chosen for the 3.3V net. Because 5.0V is always above the battery voltage, a boost regulator could have been chosen instead of the buck/boost regulator.

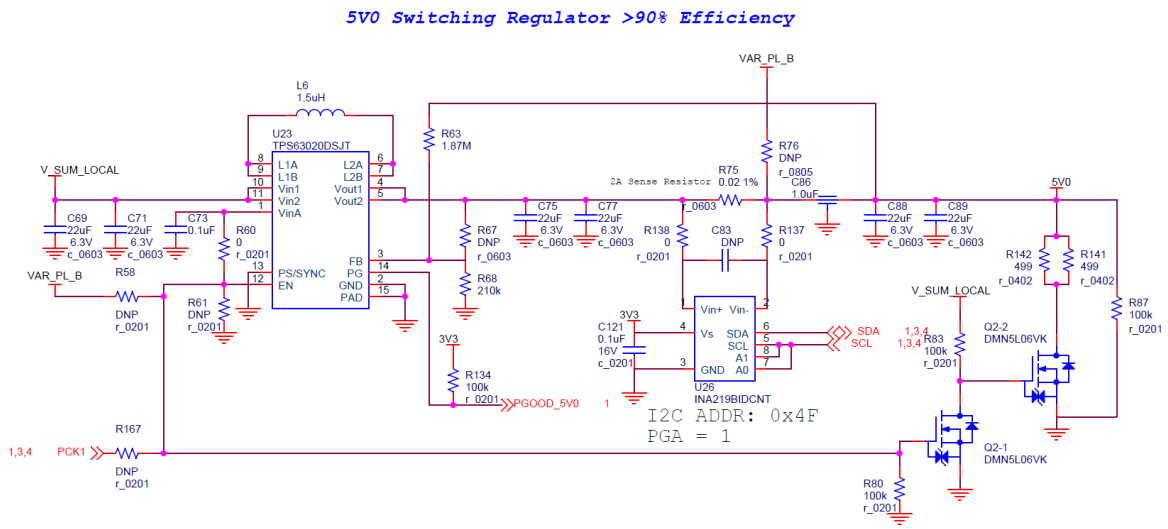

Figure 91: 5.0V Switching Regulator Provides Power for RF Switches, RF Detector, and Power Amplifier

The TPS63020 was chosen based on its efficiency, low external component count, output current and physical size. The efficiency of the TPS63020 is around 90% at the typical battery voltage of 3.7V. High efficiency regulators are required for CubeSats due to the limited solar input power and limited thermal dissipation. The average solar input power estimated for the 1U IPEX mission was 1.2W with 2 solar cells on each face of the satellite.

Heat sinks and fans are not applicable for space applications, so thermal energy is primarily dissipated through radiation. The heat from the radio needs to be conducted from the PCBA through heat straps or the satellite structure to an external surface on the satellite where it is radiated from the system. Thermal dissipation through radiation is much less than provided by convection, heat sinks, and fans in terrestrial applications. An example of a CubeSat thermal radiator is shown in Figure 92, which is taken from a presentation for the CPOD mission designed by Tyvak Nano-Satellite Systems. [23]

CPOD's thermal radiator is nearby the UHF antenna, which suggests that the radiator is designed to primarily dissipate heat from UHF radio internal to the satellite.

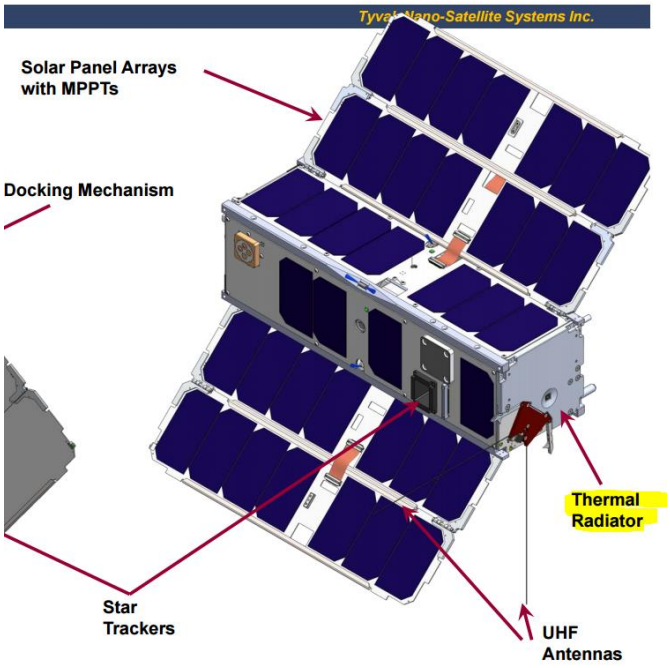

Figure 92: Example of UHF Radio Thermal Radiator, Tyvak CPOD Mission [23]

Switching regulators are typically not used for sensitive RF and analog circuitry due to high switching noise conducted into the power net. At a switching frequency of 2.4MHz and an RF frequency range of 2.4GHz to 2.5GHz, the 1000th to 2084th harmonic of the switching frequency would be of concern for the RF band components, which would already be at very low power. The most sensitive circuitry would be the base band RF detector circuits internal to the transceiver. Typically low-noise, low-dropout (LDO) linear DC regulators are utilized for sensitive analog circuits. However, LDOs regulate their output voltage by dissipating power across a transistor proportional to the voltage drop across the device. The higher the voltage difference between the input and output of an LDO, the lower the efficiency as calculated with the simple equation: $= \frac{V_{out}}{V_{in}}$. In

addition, LDOs can only output a voltage lower than the battery input voltage, so a switching regulator would need to be interfaced between the battery and input to an LDO.

The LDO would also require a large power supply rejection ratio (PSRR) at the switching regulators frequency. Expensive LDOs can be purchased with significant PSRR up to about 10MHz, however this would only block up to the 4^{th} harmonic of the TPS63020's 2.4MHz switching frequency. Additionally, PSRR decreases with smaller voltage headroom and higher current draw, therefore efficiency is traded for higher PSRR. Therefore a custom low pass power filter would provide a better solution to mitigating switching noise affecting the RF circuitry.

Not enough information is provided in the device datasheets to determine the center frequency and attenuation requirements of this power supply low pass filter. The decision was made to take the risk of using only switching regulators on the board with a feedthrough capacitor and additional bulk capacitors to reduce noise. If the switching regulators were still found to inject too much noise into the circuitry during testing, additional noise filtering would be designed into the second revision of the board with the solution determined empirically by physically modifying the first revision of the PCBA and measuring performance.

Component values for the input/output capacitors, switching inductor, and feedback resistors were chosen based on the TPS63020 datasheet. [47] After the regulator, a TI INA219 I2C power monitor provides current and output voltage measurements for the satellite's telemetry database. The power monitor's current sense resistor was sized for the maximum current expected from the regulator and the sense voltage range of the power monitor. The simplified schematic from the INA219's datasheet is shown in Figure 93. The power monitor was chosen because of past design heritage and low power consumption when commanded into a one-shot measurement

low power mode. The INA219 integrates an amplifier, analog to digital converter (ADC), and an I2C interface into a single package.

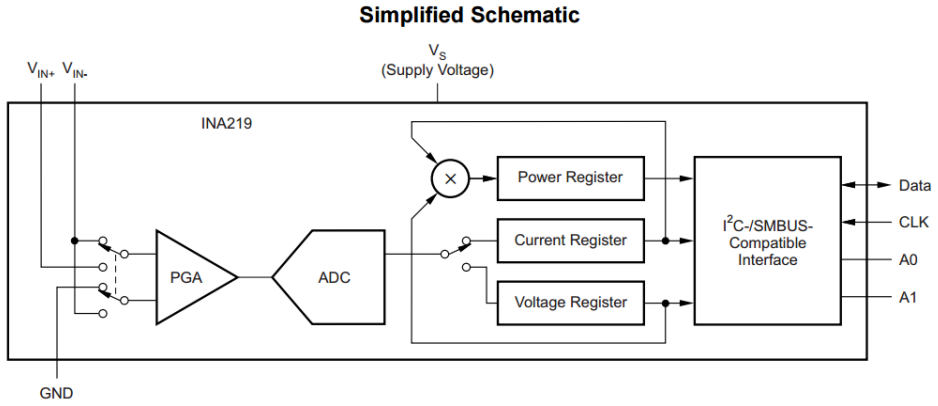

Figure 93: Texas Instruments INA219 Power Monitor Simplified Schematic [48]

A feedthrough capacitor and additional bulk capacitors are placed after the power monitor to reduce switching noise on the power net and reduce droop introduced by the sense resistor's impedance. The 499Ω resistors and NMOS transistors pull the voltage rail to ground when the regulator is disabled by discharging the power stored in the bulk capacitors and preventing a "floating" state. This discharge functionality is provided in some regulators, but not the TPS63020. Voltage rail discharge ensures that the circuitry is truly de-energized when the enable signal is de-asserted and not floating at an indeterminate voltage. In past experience, floating power rails have caused circuitry to be in an undefined state and exhibit unwanted behavior.

The regulators were designed with standalone testing of the ISIR on the evaluation microprocessor board in mind. The regulators are enabled simply when power is supplied to the board, but DNP and 0Ω resistors allow the board to be hardware configured allowing the System Board to enable/disable the regulators and bypass the 5.0V regulator entirely through its on-board regulator "VAR_PL_B."

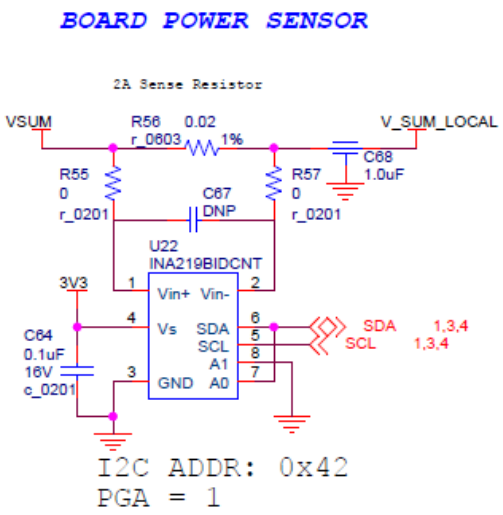

Figure 94: Board Input Power Sensor

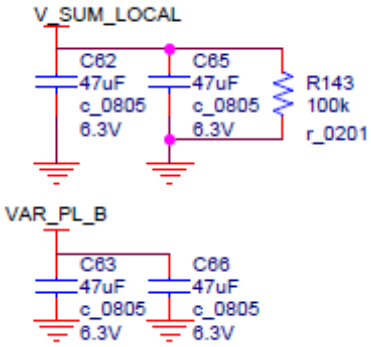

Figure 95: Additional Input Bulk Capacitors

Figure 94 shows the power sensor for the entire board, U22. The board derives all of its power from the satellite battery voltage “VSUM,” therefore all power consumed by the board will be measured by U22. By measuring the power at the battery voltage, the actual power draw of the board can be characterized without assuming efficiencies for the regulators. Figure 95 shows additional bulk capacitors for the System Board voltages. R143 simply discharges the battery voltage net when the battery is disconnected.

5.4 Transceiver Frequency Source

The AT86RF233 transceiver allows use of a crystal or oscillator as its 16MHz frequency source. According the evaluation board hardware user manual, the REB233SMAD transceiver evaluation board interfaces a Siward SX4025 crystal with two load capacitors of 10pF each to the AT86RF233 which is calibrated with the radio transceiver trim capacitors using the register XOSC_CTRL. The evaluation board user manual guarantees a tolerance within +20ppm and -5ppm. [25] However, the recommended operating range with the crystal is between -20 and 70C. The AT86RF233 also permits the usage of a temperature compensated crystal oscillator (TCXO) for its frequency source. A TCXO provides a more accurate frequency source across a larger temperature range, but will consume more power than using the crystal.

Both a crystal and TCXO source are designed into the schematic as shown in Figure 96. The board is resistor configurable to select one of the two frequency sources. During testing of the first board revision, the performance of the radio can be compared between using either frequency reference source; however only the TCXO is expected to be required in future revisions. All of the internal frequencies of the AT86RF233 are derived from this frequency reference source; therefore the overall system performance is determined by the reference frequency accuracy. The AT86RF233 datasheet specifies a required reference frequency accuracy of +/-30ppm for correct functionality at 2000kbps, as shown in Figure 97. [28] However, it is assumed a more accurate source is required due to tolerate additional Doppler shift between the transmitter and receiver.

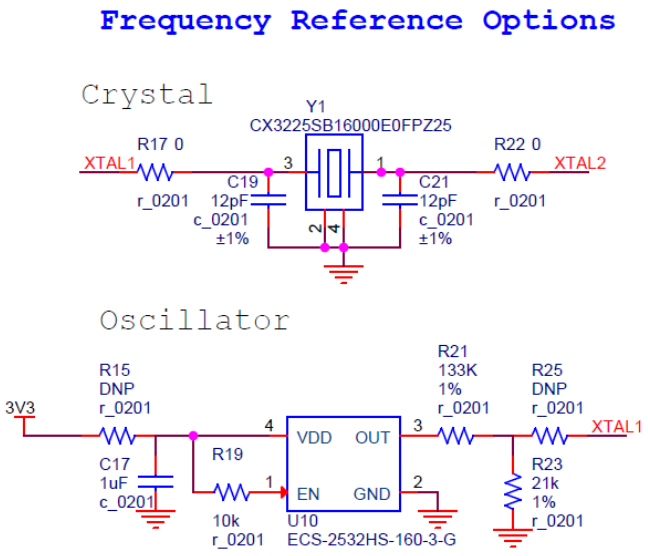

Figure 96: Transceiver Frequency Reference Options

f_{SRD}	Symbol rate deviation Reference frequency accuracy for correct functionality	PSDU bit rate				
		250kb/s	-60(1)		+60	ppm
		500kb/s	-40		+40	ppm
		1000kb/s	-40		+40	ppm
		2000kb/s	-30		+30	ppm

Figure 97: AT86RF233 Required Frequency Accuracy [28]

The AVX CX3225SB16000E0FPZ25, 16MHz crystal was chosen because it had the tightest frequency stability compared to other crystals at +/-10ppm. The crystal will operate within the -40 to 85C temperature range, but its frequency will vary an additional +/-16ppm. Similarly, the ECS Inc., ECS-2532HS-160-3-G TCXO was chosen due to its -40 to 85C operating range and +/-10ppm frequency stability. The output of the TCXO is reduced from 3.3V to between 400mV and 500mV as required by the AT86RF233 using a resistive divider.

The 12pF trim capacitors across the crystal were chosen carefully after consulting literature on the subject and referencing Atmel application notes; these capacitors can affect the frequency stability significantly and the AT86RF233 provides additional

internal trim capacitors to allow calibration of the reference frequency to correct for component tolerances as shown in Figure 98. [28] The 12pF value was calculated from a Microchip application note AN826, *"Crystal Oscillator Basics and Crystal Selection…".* [49] The capacitor value is calculated using the oscillator's effective load capacitance and crystal specification.

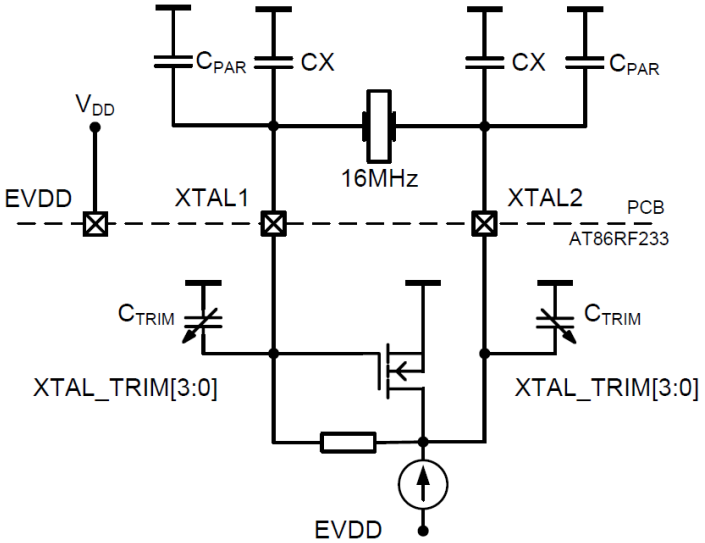

Figure 98: AT86RF233 Datasheet Simplified XOSC Schematic with External Components [28]

Kemet CBR02C120F3GAC 1% NPO capacitors were chosen for the 12pF capacitors to minimize frequency variations and drift due to the capacitor tolerance and temperature drift; these capacitors have a temperature stability of 30ppm which results in a total tolerance of 1.3% or 0.156pF across the -40C to 85C temperature range. Looking at the capacitor trim graph from the Atmel application note *"Crystal Characterization for AVR RF,"* shows that this 0.156pF tolerance results in approximately 1ppm variation. [50]

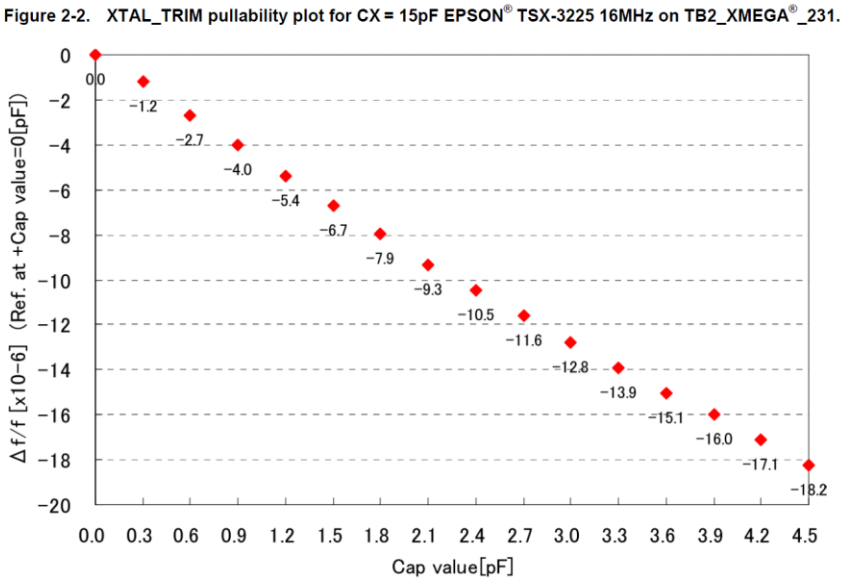

Figure 99: Trim Capacitor Graph from Atmel Application Note [50]

5.5 Amplifier Protection and RF Power Measurement

During development of several CubeSat missions in the PolySat lab, a common incident repetitively occurred: permanent damage to the UHF power amplifier due to transmitting without an antenna or load on the output of the UHF radio. During testing and troubleshooting, development satellites and “flatsats” are torn down, modified, and re-built; this happens hundreds of times during development of hardware for any given mission. Typically, the satellite software automatically transmits beacons when powered. If the person rebuilding the hardware forgets to place either a load or antenna on the output of the UHF radio, the power amplifier will overheat and become damaged from excessive reflected power into its output. This surface mount power amplifier then needs to be replaced with a new amplifier using a microscope and hot air gun soldering techniques.

The power amplifier could also become damaged if transmitting while the antenna was stowed or an object shorting the antenna due to excessive load mismatch. Similarly, LNAs were becoming damaged from excessive input power into the radio during receive

testing from inadequate attenuation at the radio's input. Needless to say, these common occurrences became irritating, time consuming, expensive, and provided motivation to design a protection circuit for radio amplifiers.

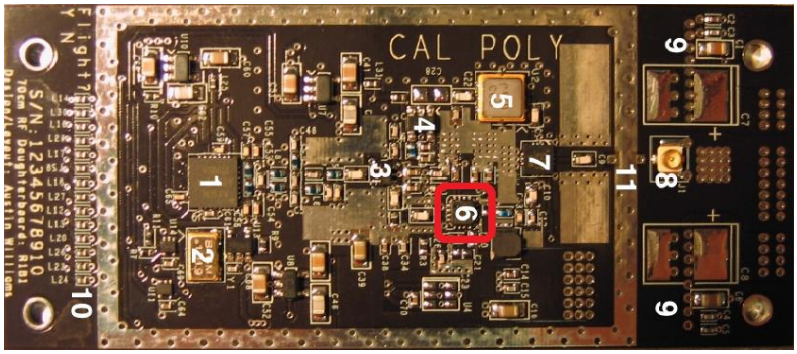

Figure 100: UHF Radio PCBA, Commonly Damaged Power Amplifier Circled in Red [2]

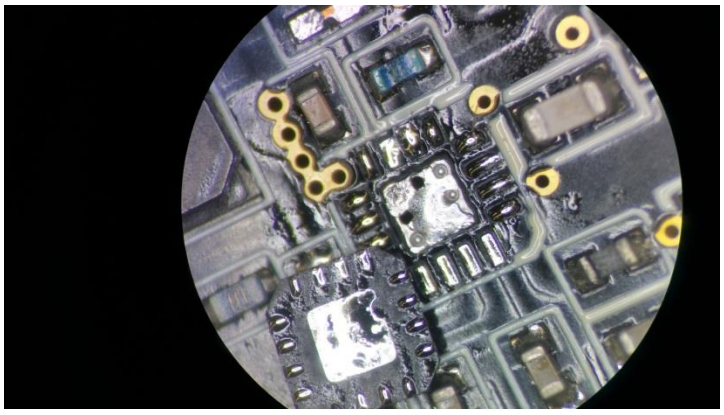

Figure 101: Removal of the UHF Power Amplifier (Microscope)

Power amplifiers have maximum voltage standing wave ratio (VSWR) ratings. VSWR is a measure of the magnitude of power reflected from the load and back to the power amplifier's input. A VSWR of 1:1 indicates a perfect match with no power reflecting and all output power dissipated in the load. A VSWR of 2.0:1 indicates minor mismatch with 33% of the signal reflected back to the amplifier. VSWR equal to 5.0:1 is 67% reflection, 10.0:1 is 82% reflection, and infinity:1 is 100% reflection. A voltage

reflection increases the instantaneous voltage on the amplifier output and increases current draw in the amplifier. High power dissipation caused by high collector current draw increases the amplifier temperature past its absolute maximum ratings causing permanent damage. [51] Similarly, LNAs have an absolute maximum input power before permanent damage occurs.

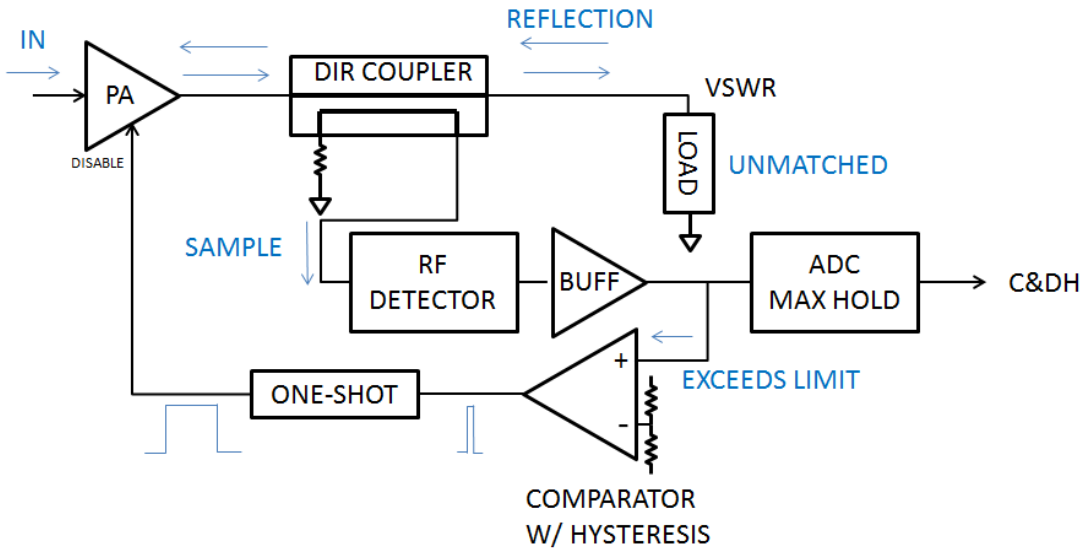

Figure 102: Power Amplifier Protection Circuit Block Diagram

The block diagram for the power amplifier protection circuit is shown in Figure 102. The protection circuit consists of a directional coupler, RF detector, and digital logic to disable the amplifier before the reflected power exceeds the amplifier's VSWR limit. The protection circuit is an active circuit that samples the reflected power, through a directional coupler and RF detector, and disables the power amplifier when the power reaches a resistor configurable limit. A comparator with hysteresis is utilized to detect when the sample exceeds the limit and a one-shot (mono-stable multi-vibrator) converts the comparator's alert signal into signal that disables the amplifier for a defined duration.

When the load exceeds the VSWR limit of the power amplifier and the amplifier transmits, then the protection circuit will disable the amplifier for a set amount of time,

allowing the component to cool down. When the disable time elapses, the amplifier will transmit again which will trigger the protection circuitry and disable the amplifier once again. The circuit will oscillate with the power amplifier transmitting for a short pulse and then becoming disabled for the long duration until the VSWR of the load changes to below the permissible limit or transmission halts. An analog to digital converter (ADC) is also added to the circuit to provide a measurement of the reflected power to the C&DH. The ADC has a register that stores the maximum value measured, which can be read and cleared by the C&DH for maximum VSWR measurements. The C&DH could act on this telemetry by alerting the user with the value or by reducing the power into the power amplifier.

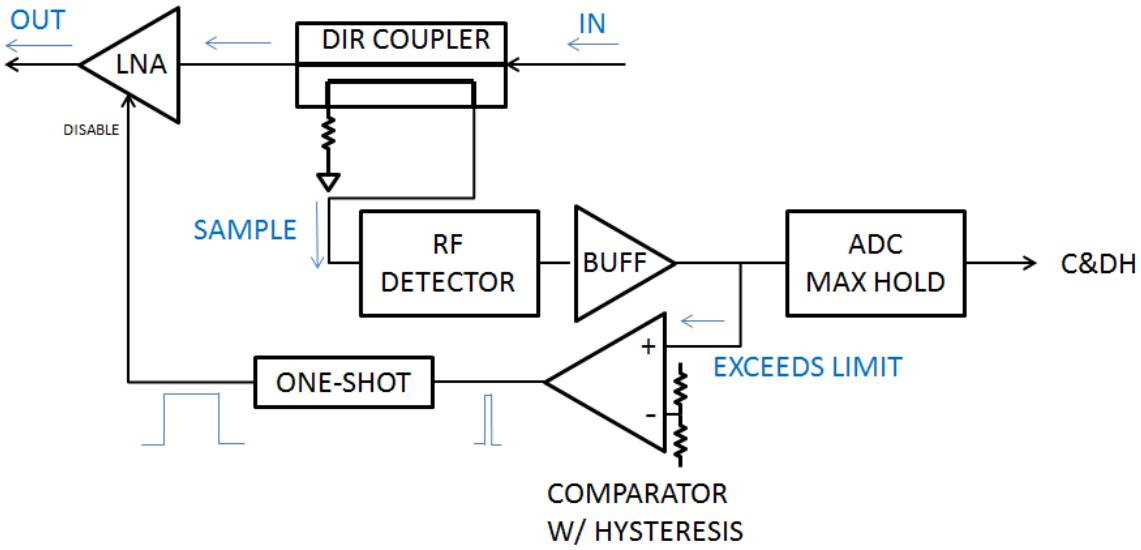

Figure 103: Low Noise Amplifier Protection Circuit Block Diagram

The block diagram for the LNA protection circuit is shown in Figure 103. The protection circuit is identical to the power amplifier circuit, with the difference being that the circuit samples the input signal power level instead of a reflected signal power level.

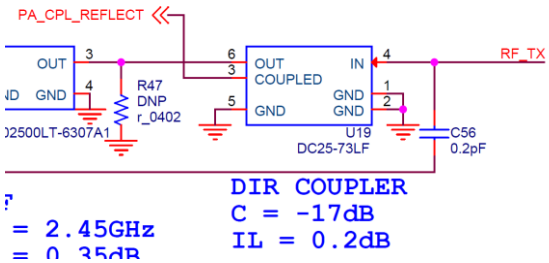

Figure 104: RF Directional Coupler, DC25-73LF

Figure 104 is the schematic snippet of the directional coupler used for both the power amplifier and LNA protection circuits. The coupler introduces an insertion loss of 0.2dB to the RF chain and has a coupling factor of C = -17dB indicating the RF sample from the “COUPLED” output will be 17dB less than the RF signal incident on the “IN” input.

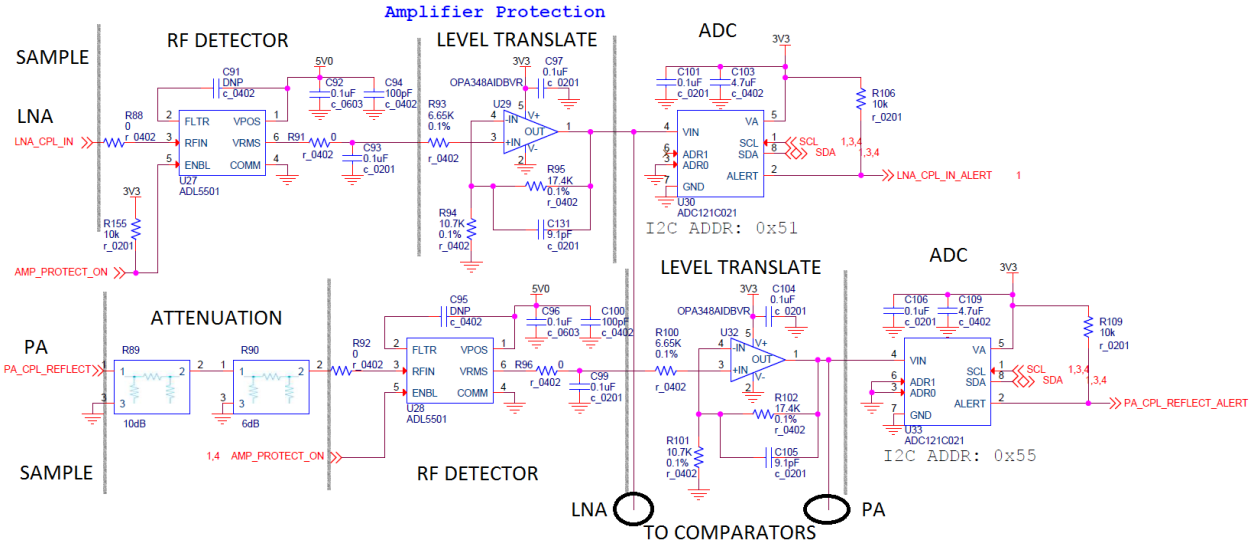

Figure 105: Amplifier Protection Schematic: Detector, Level Translator, and ADC

Figure 105 shows the first half of the amplifier protection schematic containing the RF detector, level translator, and ADC. The ADL5501 RMS 50MHz to 6GHz “TruPwr” detector manufactured by Analog Devices was chosen as the RF detector. In the pursuit

of simplicity, a design decision was made to use the same RF detector model for the PA and LNA power protection circuitry. The ADL5501 was chosen because of its low power draw, high input range allowing measurement of LNA input and PA output, high accuracy, and sufficient datasheet information and graphs. The Linear Technologies part LTC5505 was initially chosen due to its lower power consumption and higher input range, but the datasheet contained insufficient information regarding its accuracy and error variation with input voltage and temperature. The functional block diagram from the ADL5501 datasheet is shown in Figure 106. [52]

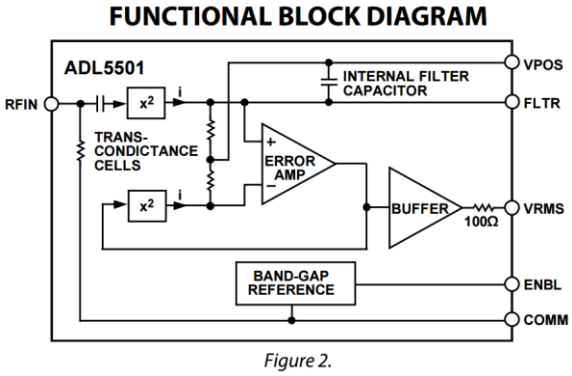

Figure 106: Analog Devices ADL5501 Datasheet Functional Block Diagram [52]

Absolute Maximum Ratings

Parameter	Rating	Unit
Supply Voltage (V_{CC}, V_{BIAS}, V_{EN})	6.0	V
Amp1 DC Current (I_{CC1})	100	mA
Amp2 DC Current (I_{CC2})	250	mA
Amp3 DC Current (I_{CC3})	1500	mA
CW Input Power, 50Ω, 2-Stage Operation	18	dBm
CW Input Power, 50Ω, 3-Stage Operation	18	dBm
Modulated (WCDMA) Input Power, 6:1 Output VSWR, 2-Stage Operation	10	dBm
Modulated (WCDMA) Input Power, 6:1 Output VSWR, 3-Stage Operation	18	dBm
Operating Junction Temperature	160	°C
Operating Temperature Range (T_L)	-40 to +85	°C
Storage Temperature	-40 to +150	°C
ESD Rating – Human Body Model (HBM)	Class 1A	
Moisture Sensitivity Level	MSL 3	

Figure 107: RFPA2026 Datasheet Absolute Maximum Ratings [42]

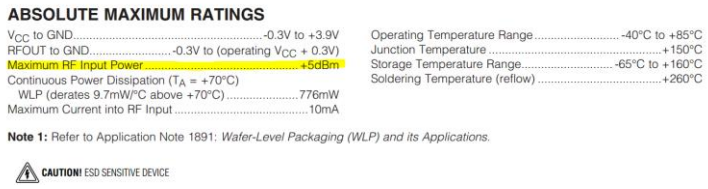

ABSOLUTE MAXIMUM RATINGS

V_{CC} to GND ..... -0.3V to +3.9V
RFOUT to GND ..... -0.3V to (operating V_{CC} + 0.3V)
Maximum RF Input Power ..... +5dBm
Continuous Power Dissipation (T_A = +70°C)
WLP (derates 9.7mW/°C above +70°C) 776mW
Maximum Current into RF Input 10mA

Operating Temperature Range ..... -40°C to +85°C
Junction Temperature ..... +150°C
Storage Temperature Range ..... -65°C to +160°C
Soldering Temperature (reflow) ..... +260°C

Note 1: Refer to Application Note 1891: *Wafer-Level Packaging (WLP) and its Applications.*

CAUTION! ESD SENSITIVE DEVICE

Figure 108: MAX2692 Datasheet Absolute Maximum Ratings [46]

The trigger values for the circuit were decided based off the maximum ratings within the RFPA2026 PA and MAX2692 LNA datasheets shown in Figure 107 and Figure 108. [34, 39] Although not explicitly stated, the RFPA2026 maximum output VSWR was inferred to be 6:1; an engineering margin of 50% was added for a design limit VSWR of 3:1. The LNA maximum input was stated to be +5dBm, which was translated to a design limit of 3dBm with 2dB of engineering margin.

Hysteresis is designed into the circuit to prevent oscillation during conditions near the limit of the circuit. The PA VSWR falling limit was chosen to be 1.8:1 and the LNA input power falling limit was chosen to be 0dBm. Therefore, the PA circuit will trigger when the load presents a 3:1 VSWR or higher and release when the load presents a 1.8:1 VSWR or lower. Similarly, the LNA protection circuit will trigger at an input of 3dBm and release at 0dBm. The protection circuit design hysteresis plots are shown in Figure 109 and Figure 110.

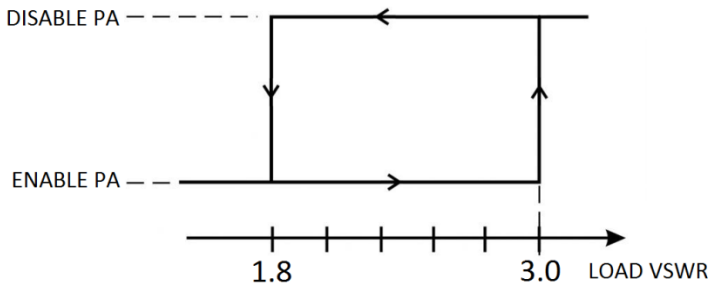

Figure 109: PA Protection Circuit Design Hysteresis

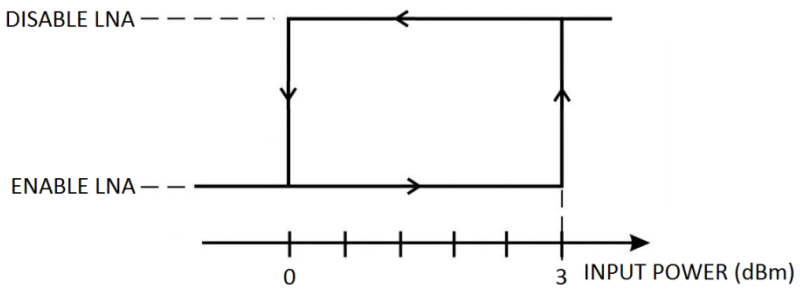

Figure 110: LNA Protection Circuit Design Hysteresis

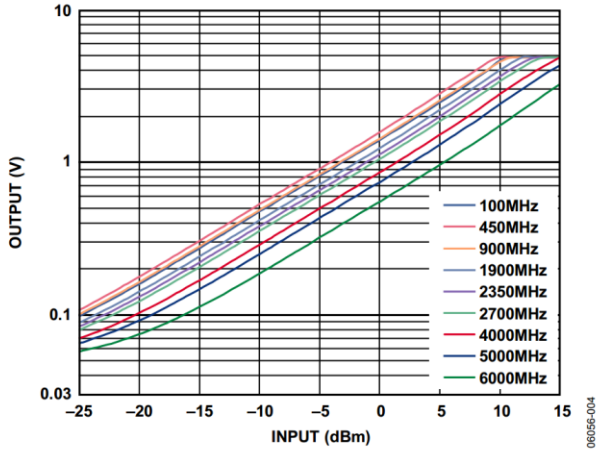

Figure 4. Output vs. Input Level; Frequencies = 100 MHz, 450 MHz, 900 MHz, 1900 MHz, 2350 MHz, 2700 MHz, 4000 MHz, 5000 MHz, and 6000 MHz; Supply = 5.0 V

Figure 111: ADL5501 Datasheet Output vs. Input Level [52]

The RF detector was operated at a supply of 5V because the datasheet characteristics and graphs were measured with the component powered from a 5V supply. The RF detector datasheet input power versus output voltage plot is shown in Figure 111. [52] Figure 112 shows the linearity versus input level for the RF detector, which illustrates the usable input range of the device. An accuracy of 1dB was desired for the amplifier protection circuitry; therefore the RF detector must be accurate within 1dB. The plot shows that inputs below -15dBm and above 7dBm produce excessive error therefore the usable range for the RF detector is between -15dBm and 7dBm. Additionally, the circuit should operate correctly over the PCBAs operating temperature

range of -40C to 85C (industrial). Figure 113 shows the error due to temperature drift; this plot indicates the detector will exhibit an error up to +/- 0.3dB at extreme temperatures compared to room temperature. The optimum point of operation is at the center of the input vs. output graph at -5dBm with the minimum error and highest linearity. Therefore, the power amplifier protection circuit was designed to operate near the -5dBm point.

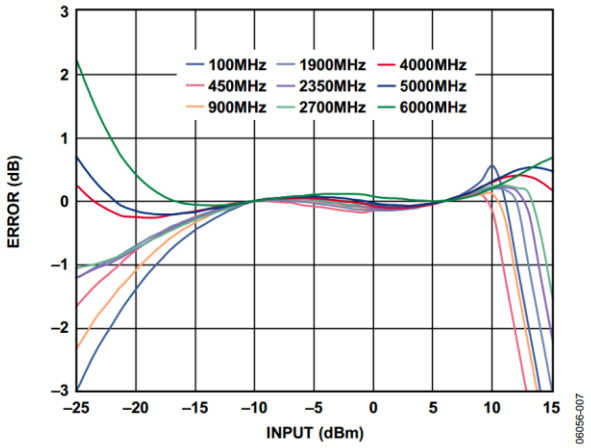

Figure 7. Linearity Error vs. Input Level; Frequencies = 100 MHz, 450 MHz, 900 MHz, 1900 MHz, 2350 MHz, 2700 MHz, 4000 MHz, 5000 MHz, and 6000 MHz; Supply = 5.0 V

Figure 112: ADL5501 Datasheet Linearity Error [52]

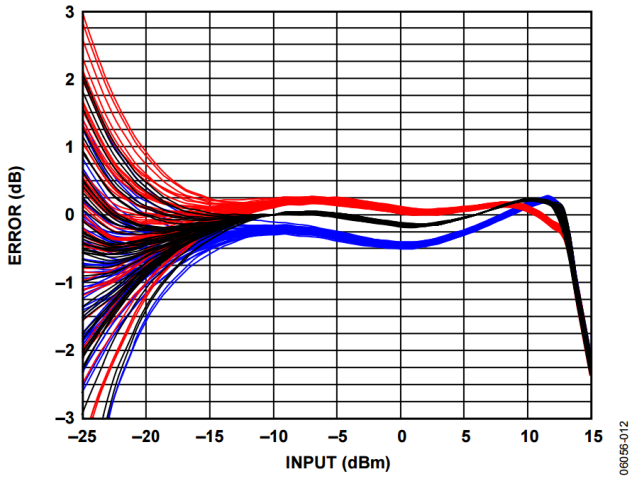

Figure 12. Temperature Drift Distributions for 50 Devices at −40°C, +25°C, and +85°C vs. +25°C Linear Reference; Frequency = 2350 MHz; Supply = 5.0 V

Figure 113: ADL5501 Datasheet Temperature Drift [52]

Considering the PA has a maximum output power of 34.5dBm, the insertion loss of the low pass filter, insertion and coupling factor of the coupler and the insertion loss of the RF switch, the maximum output of the coupler is 15.35dBm. Two attenuators with a combined attenuation of 16dB are added to the input of the PA protection RF detector to reduce the maximum input level to -0.65dBm. At the PA protection design limits of VSWR of 3:1 and 1.8:1 the input to the RF detector is approximately -3dBm and -8.2dBm respectively; these inputs are centered around -5dBm where there is minimal error. The LNA RF detector does not require additional attenuation and an LNA input at 3dBm and 0dBm corresponds to an RF detector input of -14dBm an -17dBm respectively; the -17dBm value is slightly out of the linear range for the detector, but not enough to warrant concern.

To reduce error from visually interpreting the datasheet plots within the RF detector datasheet, an online plot digitizer tool “WebPlotDigitizer” created by Ankit Rohatgi was utilized to convert the input versus output plot at 2350MHz into a csv data

file which was imported into excel. [53] The WebPlotDigitizer online application is shown in Figure 114.

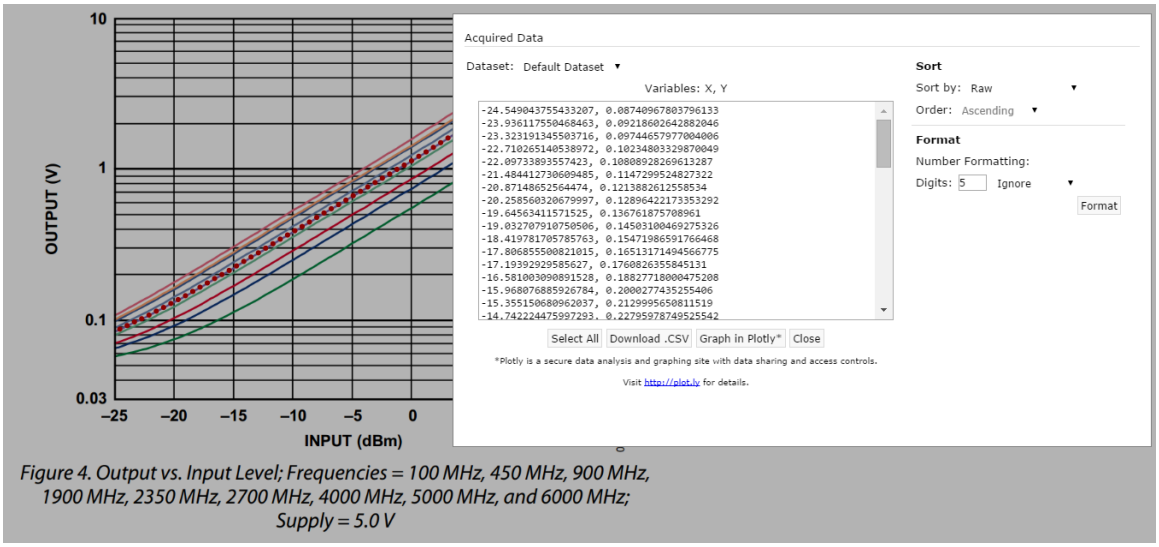

Figure 4. Output vs. Input Level; Frequencies = 100 MHz, 450 MHz, 900 MHz, 1900 MHz, 2350 MHz, 2700 MHz, 4000 MHz, 5000 MHz, and 6000 MHz; Supply = 5.0 V

Figure 114: Digitizing the ADL5501 Input vs Output Plot with WebPlotDigitizer [53]

The input versus output plot shows a trace for 2350MHz; however the center design frequency for the protection circuitry is at 2450MHz. Digitizing the conversion gain plot from the datasheet provided the difference in gain between 2350MHz and 2450MHz; the difference in gain is 2% as shown in Figure 115 which isn't too significant, but the factor of 0.98 to convert the 2350MHz plot to 2450MHz was used to reduce error.

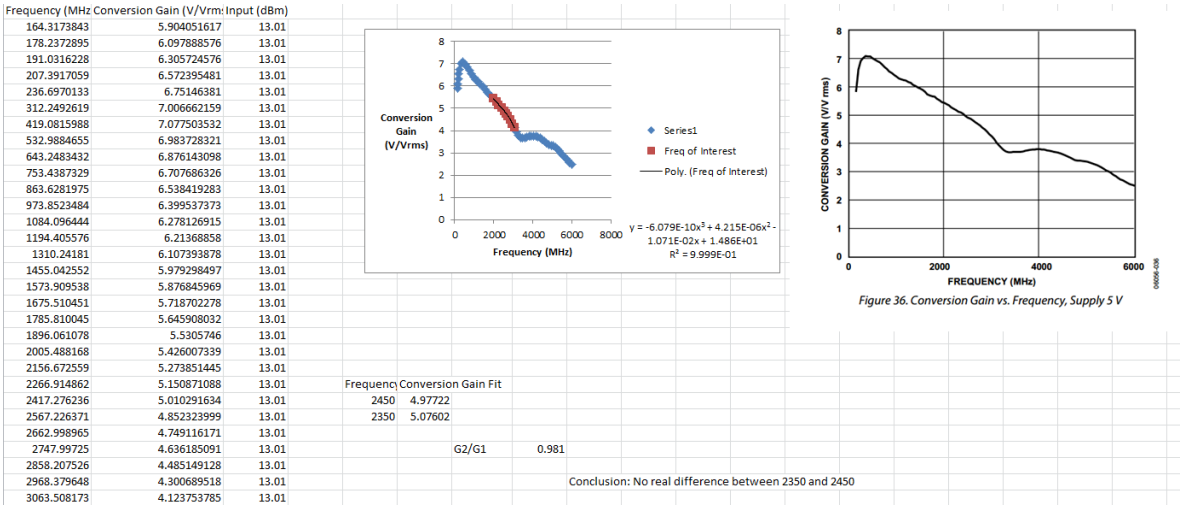

Frequency (MHz	Conversion Gain (V/Vrms	Input (dBm)
164.3173843	5.904051617	13.01
178.2372895	6.097888576	13.01
191.0316228	6.305724576	13.01
207.3917059	6.572395481	13.01
236.6970133	6.75146381	13.01
312.2492619	7.006662159	13.01
419.0815988	7.077503532	13.01
532.9884655	6.983728321	13.01
643.2483432	6.876143098	13.01
753.4387329	6.707686326	13.01
863.6281975	6.538419283	13.01
973.8523484	6.399537373	13.01
1084.096444	6.278126915	13.01
1194.405576	6.21368858	13.01
1310.24181	6.107393878	13.01
1455.042552	5.979298497	13.01
1573.909538	5.876845969	13.01
1675.510451	5.718702278	13.01
1785.810045	5.645908032	13.01
1896.061078	5.5305746	13.01
2005.488168	5.426007339	13.01
2156.672559	5.273851445	13.01
2266.914862	5.150871088	13.01
2417.276236	5.010291634	13.01
2567.226371	4.852323999	13.01
2662.998965	4.749116171	13.01
2747.99725	4.636185091	13.01
2858.207526	4.485149128	13.01
2968.379648	4.300689518	13.01
3063.508173	4.123753785	13.01

Figure 36. Conversion Gain vs. Frequency, Supply 5 V

Frequency	Conversion Gain Fit
2450	4.97722
2350	5.07602

G2/G1 0.981

Conclusion: No real difference between 2350 and 2450

Figure 115: Digitized RF Detector Conversion Gain Plot

Figure 116 shows the digitized data from the input vs output plot at 2350MHz and the extrapolation calculation to 2450MHz. This data was used to plot the extrapolated input vs output plot in excel. A fourth-order polynomial trend line was fit to the data and equation displayed on the plot as shown in Figure 116. This equation was used within excel to calculate the expected output voltage of the RF detector at the five power levels of interest: maximum PA reflected power (1dBm) and the upper and lower hysteresis limits of the PA and LNA; these output voltages are shown in column “Fit Result 2 (V)”. The conversion gain was calculated at each power level to compare against using the flat linear gain of 4.98.

	A	B	C	D	E	F
1	Input (dBm)	Input (Vrms)	Output (V)	Extrapolate to 2450MHz	Calc Conversion Gain (V/Vrms)	Datasheet Conversion Gain
2	-24.58218553	0.013193977	0.087409678	0.085748894	6.624968155	4.97722
3	-23.97091921	0.014155951	0.092186026	0.090434492	6.512174869	4.97722
4	-23.35972444	0.015187937	0.09744658	0.095595095	6.416051189	4.97722
5	-22.74832933	0.016295532	0.102348033	0.100403421	6.280742177	4.97722
6	-22.13710594	0.017483553	0.108089283	0.106035586	6.182340624	4.97722
7	-21.52603995	0.018757848	0.114729952	0.112550083	6.116370835	4.97722
8	-20.91487379	0.020125251	0.121388261	0.119081884	6.031639518	4.97722
9	-20.30383642	0.021592015	0.128964222	0.126513902	5.9727737	4.97722
10	-19.69274181	0.023165832	0.136761876	0.1341634	5.903602891	4.97722
11	-19.0816472	0.024854363	0.145031005	0.142275416	5.83523315	4.97722
12	-18.47073861	0.026665398	0.154719866	0.151780188	5.802270995	4.97722
13	-17.85984433	0.028608348	0.165131715	0.161994212	5.77215129	4.97722
14	-17.24892143	0.030692971	0.176082636	0.172737066	5.736904224	4.97722
15	-16.63808439	0.03292917	0.18827718	0.184699914	5.717641249	4.97722
16	-16.02704702	0.035329106	0.200027744	0.196227216	5.661839899	4.97722
17	-15.41608119	0.037903642	0.212999565	0.208952573	5.619501276	4.97722
18	-14.80527277	0.040665055	0.227959787	0.223628552	5.605790714	4.97722
19	-14.19449297	0.043627503	0.244194649	0.23955495	5.597263962	4.97722
20	-13.58364162	0.04680615	0.260986541	0.256027796	5.575902738	4.97722
21	-12.97270441	0.050216886	0.278166588	0.272881423	5.539303771	4.97722
22	-12.36196753	0.053874918	0.298387359	0.292717999	5.538520851	4.97722
23	-11.7511448	0.05779999	0.319198441	0.313133671	5.522465345	4.97722

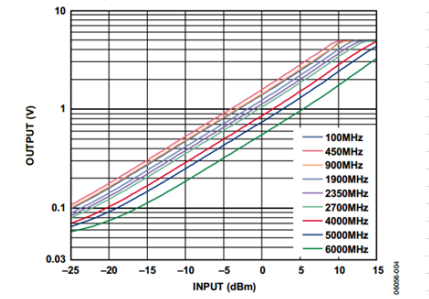

Figure 4. Output vs. Input Level; Frequencies = 100 MHz, 450 MHz, 900 MHz, 1900 MHz, 2350 MHz, 2700 MHz, 4000 MHz, 5000 MHz, and 6000 MHz; Supply = 5.0 V

Figure 116: Resulting Data within Excel with Additional Calculations

	O	P	Q	R	S	V
	Description	**Input Power (dBm)**	**Input Power (Vrms)**	**Fit Result 2 (V)**	**Calc Conv**	**After Op Amp1 (V)**
	Highest Meas	1	0.250890954	1.255	5.003	3.3014444
	PA UPPER	-3	0.15830149	0.810	5.114	2.1290897
	PA LOWER	-8.2	0.086993139	0.461	5.302	1.2129838
	LNA UPPER	-14	0.044615422	0.246	5.522	0.6479733
	LNA LOWER	-17	0.0315853	0.179	5.652	0.4694677

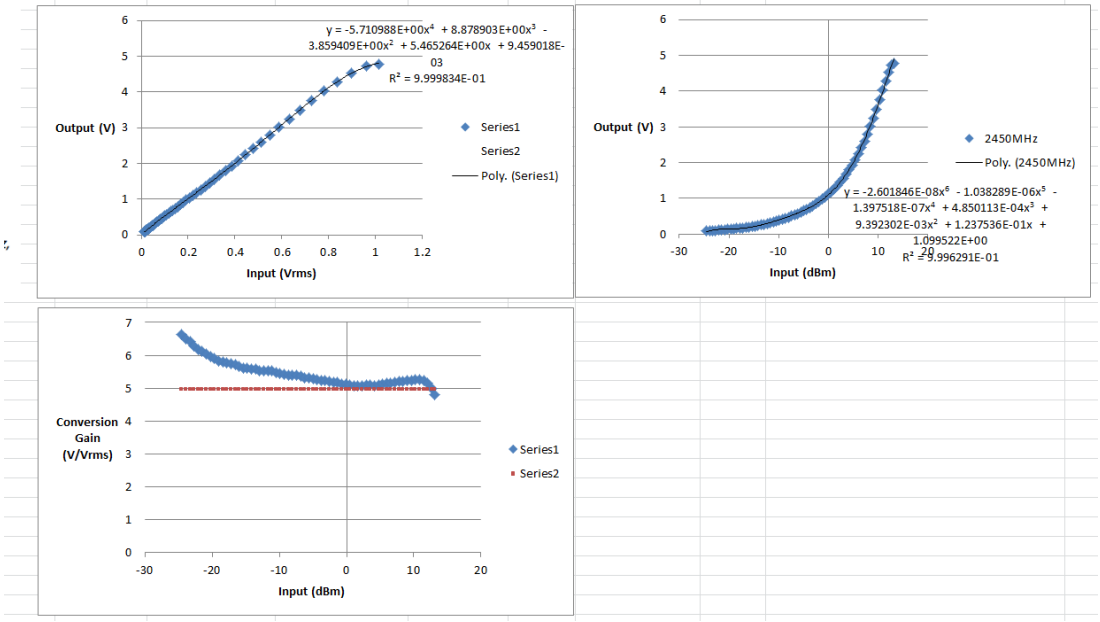

Figure 117: Excel Calculations for RF Detector Output at Amplifier Protection Limits

Now that the voltages from the RF detector at the limits have been found, the optimum gain for the level-converting, operational amplifier (op-amp) can be found to

maximize the accuracy of the ADC measurements by utilizing its input range up to 3.3V. Also, the higher voltage levels are required for the comparator input used later in the circuit to keep the signal above the comparators internal 400mV reference. The maximum voltage level expected to be read by the ADC was calculated by assuming a full reflection at max power from the power amplifier with additional margin resulting in 1dBm incident on the RF detector. 1dBm input results in 1.255V output which can be scaled up to 3.3V with a gain of 2.63 V/V.

As shown previously in Figure 105, an op-amp circuit in a non-inverting configuration is used to level convert the RF detector output voltage to higher voltage levels. The op-amp resistor values were calculated using the non-inverting gain equation: $G = 1 + \frac{R_2}{R_1}$. The input resistor balances the op-amp to reduce error as described in the article *"Design Balanced Op-Amp Circuits for Performance and Simplicity."* [54] The feedback capacitor attenuates high frequency noise above 1MHz by creating a low pass response which is described in Texas Instruments Amplifier WEBENCH webpage shown in Figure 118. [55]

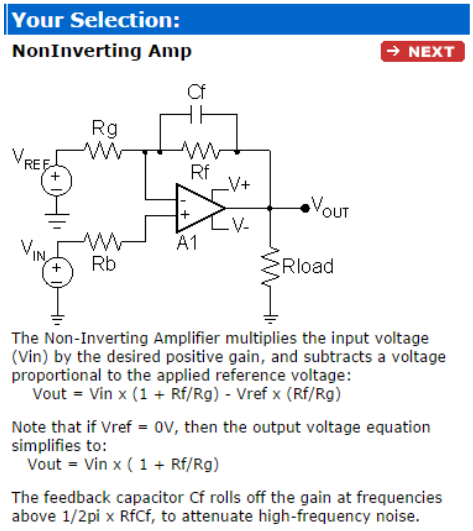

Figure 118: Texas Instruments WEBENCH Non-Inverting Amp Description [55]

The Texas Instruments ADC121C021 analog to digital converter (ADC) was selected to allow the C&DH microprocessor to read the power amplifier reflected power and LNA input power as well as the power amplifier transmitted power described later. The datasheet block diagram for the ADC121C021 is shown in Figure 119 [56] The ADC has a highest conversion and lowest conversion register which will store the maximum and minimum readings input to the ADC. The microprocessor can read and clear these registers and report the reflected power level to the user or act upon the level by either reducing input power to the power amplifier or disabling the protection circuitry. The alert pin from the ADC is also fed to the GPIO expander for read access by the microprocessor.

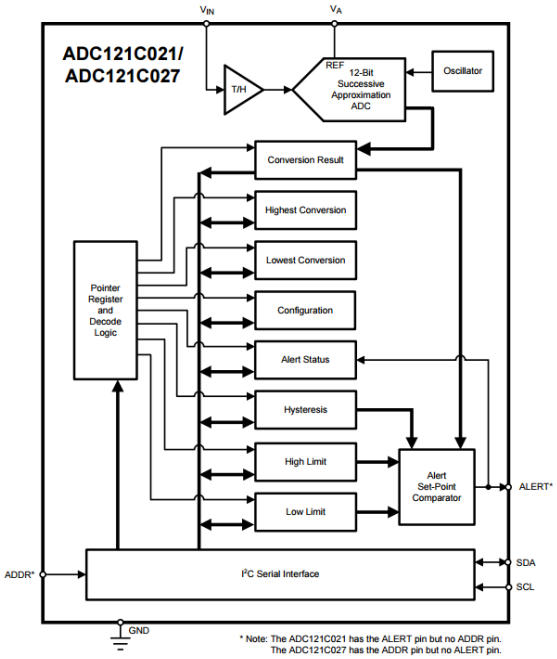

Figure 119: Texas Instruments ADC121C021 ADC Block Diagram [56]

Figure 120 shows the schematic for the remainder of the protection circuit. The amplified output of the RF detector is routed to the input of the Analog Devices ADCMP343 comparator. The comparator has an internal 400mV reference with

programmable hysteresis; the datasheet block diagram for the ADCMP343 is shown in Figure 121. [57]

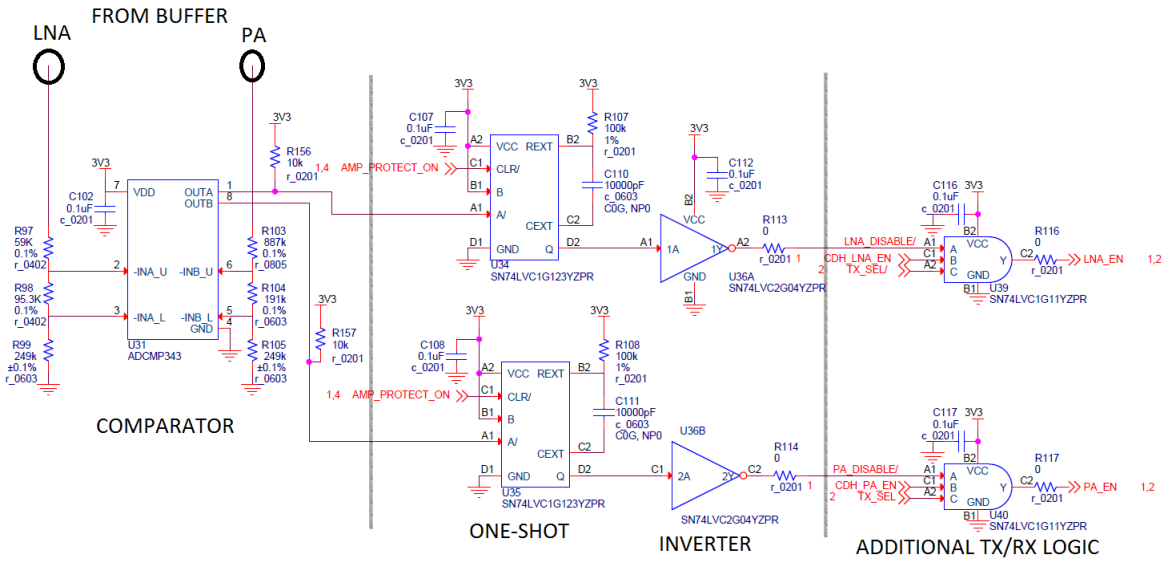

Figure 120: Amplifier Protection Schematic: Comparator, One-Shot, and Additional Logic

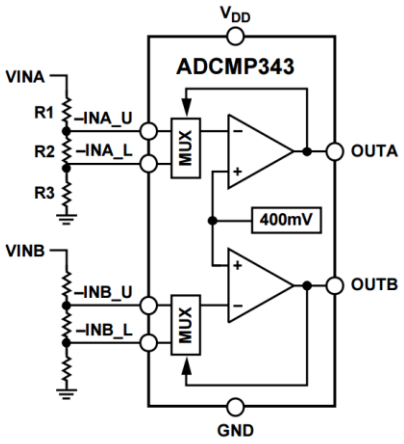

Figure 2. ADCMP343

Figure 121: Analog Devices ADCMP343 Datasheet Block Diagram [57]

The resistor values for the comparator were chosen following the equations within the datasheet and the desired hysteresis values chosen previously. The result is that the

comparator will output a low signal (0V) when the upper limit is reached and a high signal (3.3V) when the input is lower than the lower limit.

The output of the comparator is then routed to the input of a one-shot circuit designed using the SN74LVC1G123 mono-stable multi-vibrator. The external capacitor and resistor was chosen following the graph within the devices datasheet to output a high pulse for 1ms as shown in Figure 122. [58] After the one-shot is an inverter to convert the disable pulse from active high to active low. The active low disable signal is then fed to a 3-input logic AND gate with the transceivers TX/RX signal and GPIO signals allowing the C&DH to override and disable the PA or LNA independently. The transceiver TX/RX signal into the AND gate disables the LNA during transmit and disables the PA during receive.

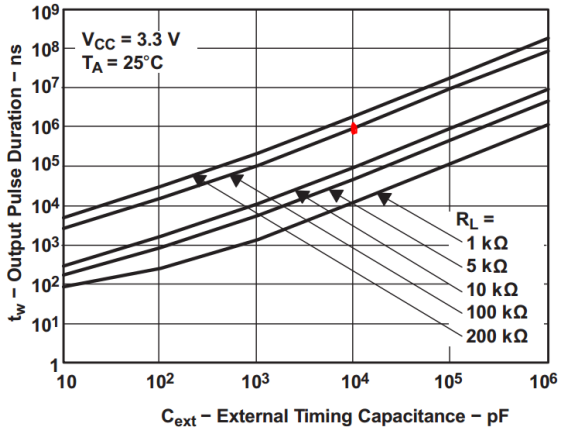

Figure 4. Output Pulse Duration
vs External Timing Capacitance

Figure 122: Texas Instruments SN74LVC1G123, One-Short Duration Graph [58]

In addition to the reflected power from the power amplifier, the output power of the amplifier is also recorded by an additional ADC shown in Figure 123. The circuit uses the same ADC as the amplifier protection circuitry. The input to the ADC is supplied by an RF detector circuit internal to the RFPA2026. Measuring the power transmitted by the amplifier allows calculation of the VSWR of the antenna as well as allowing the C&DH to

monitor and control the output power of the power amplifier in a closed-loop fashion by varying the output power from the transceiver input to the power amplifier. The C&DH could compensate for gain drift of the amplifier due to temperature.

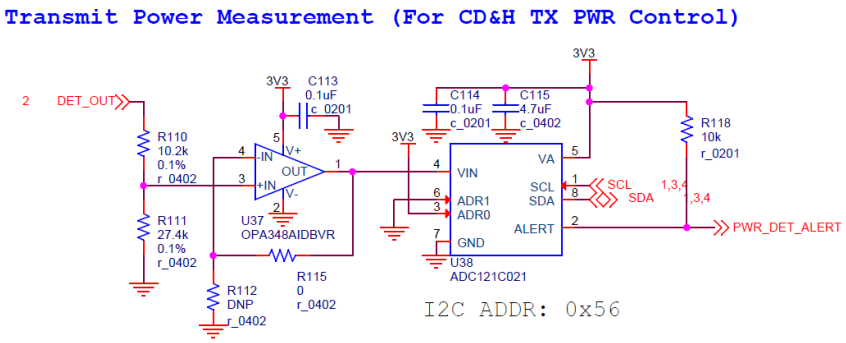

Figure 123: Transmit Power Measurement ADC

The RFPA2026 datasheet plot of “Detector Output versus Output Power” was digitized to find the output voltage at the maximum value of 36dBm. The ADC operates with a range to 3.3V, so the detector output was reduced with a resistive divider and buffered with a unity gain op-amp to the input of the ADC.

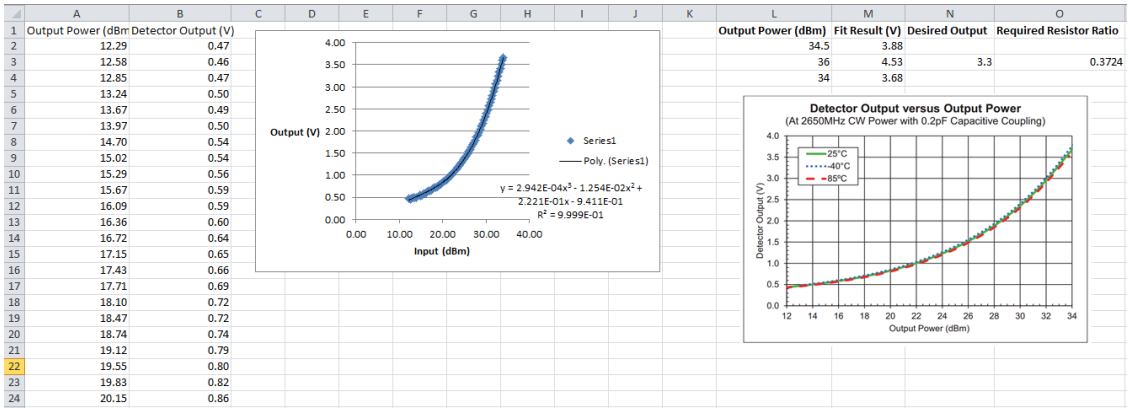

Output Power (dBm)	Detector Output (V)
12.29	0.47
12.58	0.46
12.85	0.47
13.24	0.50
13.67	0.49
13.97	0.50
14.70	0.54
15.02	0.54
15.29	0.56
15.67	0.59
16.09	0.59
16.36	0.60
16.72	0.64
17.15	0.65
17.43	0.66
17.71	0.69
18.10	0.72
18.47	0.72
18.74	0.74
19.12	0.79
19.55	0.80
19.83	0.82
20.15	0.86

Output Power (dBm)	Fit Result (V)	Desired Output	Required Resistor Ratio
34.5	3.88		
36	4.53	3.3	0.3724
34	3.68		

Figure 124: Digitized RFPA2026 Detector Output vs Output Power Plot

The protection circuitry and measurements of reflected, input, and output power would be useful during development, but may not be necessary or desired during flight. Therefore, the board has the provision to disable the protection circuitry through the

“AMP_PROTECT_ON” signal and command the ADCs into a shut-down state through I2C; disabling this circuitry would reduce the power consumption of the board. Therefore, the only down-side to the protection circuity and ADCs is the occupied area on the PCBA.

5.6 Development Interface

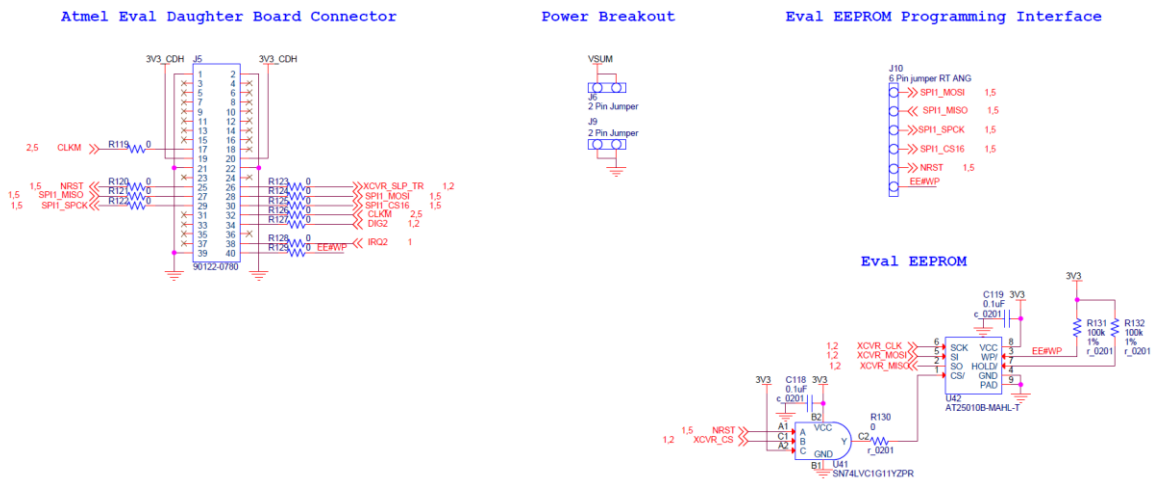

Figure 125: Evaluation Board Development Interface

Figure 125 shows the schematic for the development headers and EEPROM on the board. These components are not used in flight and are only for development purposes. The Atmel evaluation daughter board connector permits the board to be installed into the Atmel microprocessor PCB shown in Figure 34. While installed into the Atmel microprocessor PCBA, the microprocessor evaluation software can be utilized to perform receive sensitivity and transmit power testing exactly as performed for the transceiver evaluation board. The EEPROM is necessary to store information about the board, such as MAC address and external amplifier information, used by the Atmel evaluation software. These interfaces allow standalone testing of the ISIR independent of the satellite System Board without additional embedded software development.

5.7 Receive and Transmit Power Draw Estimation

The power draw of the radio during receive and transmit modes is estimated by consulting datasheets and totaling the current draw for each component at its expected operating state. Table 15 is a count of all the active components on the PCB and the expected power draw during receive mode. In receive mode, the power amplifier and power amplifier protection circuitry is disabled and the transceiver is commanded into high sensitivity listening mode. The temperature and power sensors are commanded into shutdown mode when not in use. The system processor will only probe the sensors every few minutes, which corresponds to an insignificant duty cycle and power draw.

The most significant loads during receive are the transceiver (43mW), low noise amplifier (15mW), and temperature compensated crystal oscillator (37mW). The total power draw in receive mode is calculated to be 97mW assuming a regulator efficiency of 90%. The design target was a receive power draw less than 200mW.

Table 16 shows the power draw estimation during transmission. In transmit mode the power amplifier is powered and amplifying, the transceiver is transmitting, the LNA is disabled, and the power amplifier protection circuitry is powered. The transmit power draw is 6.9W which is below the design target of 8W. The power amplifier dominates the transmit power drawing 6.8W during 2W saturated transmit with a 30% efficiency. 0.68W of heat is dissipated in the 90% efficient switching regulator. The power amplifier current draw was taken from a graph provided by RFMD for an evaluation board modified for 2.4GHz operation.

Table 15: Receive Power Draw Estimation

Device	Description	Number of Devices	Voltage (V)	Current (mA)	Power (mW)	Notes
AD7414	Temp Sensor	1	3.3	0.000003	0.0	Software commanded power down mode
AT24C128C-MAHM-T	EEPROM	1	3.3	0.006	0.0	Normal Idle draw
TCA9539RTW	GPIO Expander	1	3.3	0.03	0.1	Operating draw
ECS-2532HS-160-3-G	TCXO	1	3.3	10	36.7	
AT86RF233	Zigbee XCVR	1	3.3	11.8	43.3	RX Mode (Listen), High sensitivity
RFPA2026	Transmit PA	1	5	0	0.0	Not Transmitting
MAX2692	Receive LNA	1	3.3	4	14.7	
INA219AIDCNR	Power Monitor	1	3.3	0.015	0.1	Software commanded idle mode
ADC121C021	ADC	3	3.3	0.000002	0.0	Software commanded idle mode
ADL5501	RF detector	2	3.3	0.001	0.0	Detector Disabled during receive
HMC595E	RF Switches	3	5	0.05	0.8	
OPA348AIDBVR	Op Amp	3	3.3	0.065	0.7	
ADCMP343	Comparator	1	3.3	0.007	0.0	
SN74LVC1G123YZPR	One-Shots	2	3.3	0.00002	0.0	
AT25010B-MAHL-T	Eval EEPROM	1	3.3	0	0.0	Remove from board for Intrepid use
FXMA2102L8X	I2C Level Trans	1	3.3	0.005	0.0	
SN74LVC2T45YZPR	2-Bit Level Trans	3	3.3	0.004	0.0	
NLSV1T244MUTBG	1-Bit Level Trans	2	3.3	0.002	0.0	
SN74LVC2G04YZPR	Not Gate	2	3.3	0.01	0.1	
SN74LVC1G11YZPR	And Gate	2	3.3	0.01	0.1	
Regulator Efficiency:	0.9			**Total (mW):**	**97**	

Table 16: Transmit Power Draw Estimation

Device	Description	Number of Devices	Voltage (V)	Current (mA)	Power (mW)	Notes
AD7414	Temp Sensor	1	3.3	0.000003	0.0	Software commanded power down mode
AT24C128C-MAHM-T	EEPROM	1	3.3	0.006	0.0	Normal Idle draw
TCA9539RTW	GPIO Expander	1	3.3	0.03	0.1	Operating draw
ECS-2532HS-160-3-G	TCXO	1	3.3	10	36.7	
AT86RF233	Zigbee XCVR	1	3.3	13.8	50.6	TX at max power
RFPA2026	Transmit PA	1	5	1225	6805.6	Transmitting at 34.5dBm
MAX2692	Receive LNA	1	3.3	0.01	0.0	Off during transmit
INA219AIDCNR	Power Monitor	1	3.3	0.015	0.1	Software commanded idle mode
ADC121C021	ADC	3	3.3	0.000002	0.0	Software commanded idle mode
ADL5501	RF detector	2	3.3	1.5	11.0	Detector with -6dBm input
HMC595E	RF Switches	3	5	0.05	0.8	
OPA348AIDBVR	Op Amp	3	3.3	0.065	0.7	
ADCMP343	Comparator	1	3.3	0.007	0.0	
SN74LVC1G123YZPR	One-Shots	2	3.3	0.00002	0.0	
AT25010B-MAHL-T	Eval EEPROM	1	3.3	0	0.0	Remove from board for Intrepid use
FXMA2102L8X	I2C Level Trans	1	3.3	0.005	0.0	
SN74LVC2T45YZPR	2-Bit Level Trans	3	3.3	0.004	0.0	
NLSV1T244MUTBG	1-Bit Level Trans	2	3.3	0.002	0.0	
SN74LVC2G04YZPR	Not Gate	2	3.3	0.01	0.1	
SN74LVC1G11YZPR	And Gate	2	3.3	0.01	0.1	
Regulator Efficiency:	0.9			**Total (mW):**	**6906**	

6 Layout

After creating a netlist from the schematic, layout of the ISIR was performed over several weeks utilizing OrCAD PCB Editor. In order to fit the design within the small, single-sided 1.4” x 3.3” area specified by the System Board requirements, SMT lead-less and BGA components were required. During the layout, many components that were initially SOT or leadless packages had to be replaced with BGA equivalents to fit all the components on the board. The small form factor and complexity of BGA components requires automated assembly of the board by a PCBA assembly house and therefore additional cost. The board was a self-funded student project, so cost was a primary concern.

In order to reduce PCB fabrication cost, the board was designed with constraints adhering to PCB manufacturer Advanced Circuits’ 4-Layer PCB “$66 each” deal. The constraints of the $66 deal are outlined on the website and reproduced in Figure 126. The PCB stackup is also defined by the $66 deal as shown in Figure 127. Following the large drill and line/space requirements of the $66 deal design rules resulted in decreased component density and therefore less optimized PCB area. The board was fabricated at Advanced Circuits, but was shipped to a cheaper assembly house for pick and place assembly. To reduce cost, the boards were assembled with a long lead time; the assembled boards arrived about one month after the layout was completed.

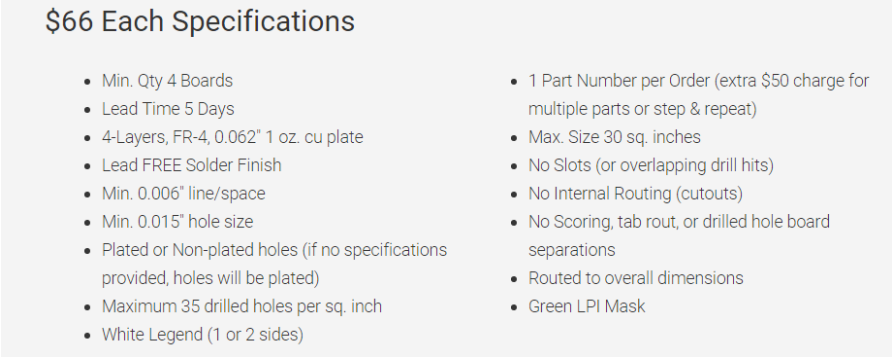

Figure 126: Advanced Circuits 4-Layer $66 Each PCB Deal [59]

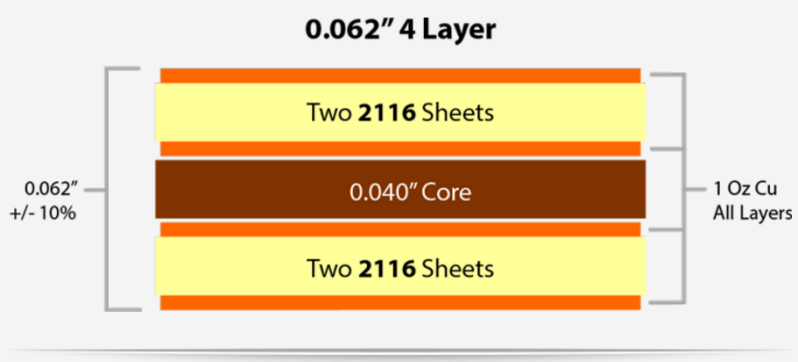

Figure 127: Advanced Circuits Standard 4-Layer Stackup [59]

A picture of the final, assembled PCBA without lid is shown in Figure 128. The final layout of the PCB and four layers are shown in Figure 129 through Figure 132. Due to minimal clearance with the Intrepid System Board, all of the components are mounted on the top side of the board; the single-sided assembly also reduced cost. The PCBA consists of 330 individual components, 841 connections, and 826 drilled holes for vias and mounting. A metal shield surrounds the RF components to reduce electromagnetic coupling into the sensitive RF circuitry. The switching regulator circuits for the board are placed outside this shield to minimize any coupling that might occur.

The top layer consists of component footprints, digital signal, and RF routing. The second layer is a solid, uninterrupted ground plane to provide consistent impedance for

RF and digital signals as well as minimize EMI from the PCBA. The third layer is primarily power floods routing the battery, 3.3V, and 5.0V power nets using wide copper shapes to minimize power net impedance, reducing inductance and therefore reducing noise coupling and rail collapse. The power layer is placed next to the ground plane to reduce EMI and provide minor decoupling capacitance. The bottom layer simply consists of low frequency digital signal routing with no practical characteristic impedance requirements.

Figure 128: Intrepid S-Band ISM Radio PCBA, Revision 1 (Shield Lid Removed)

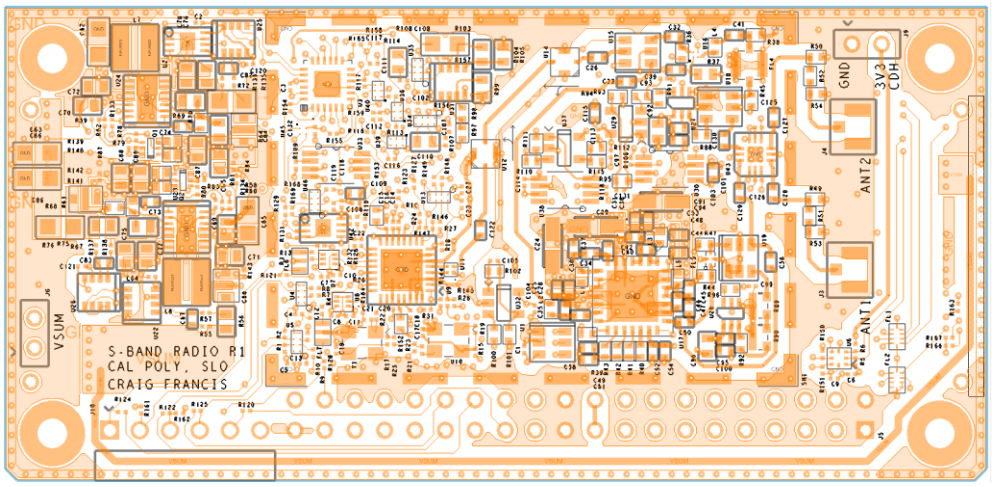

Figure 129: ISIR PCBA Layout Top, Signal and RF

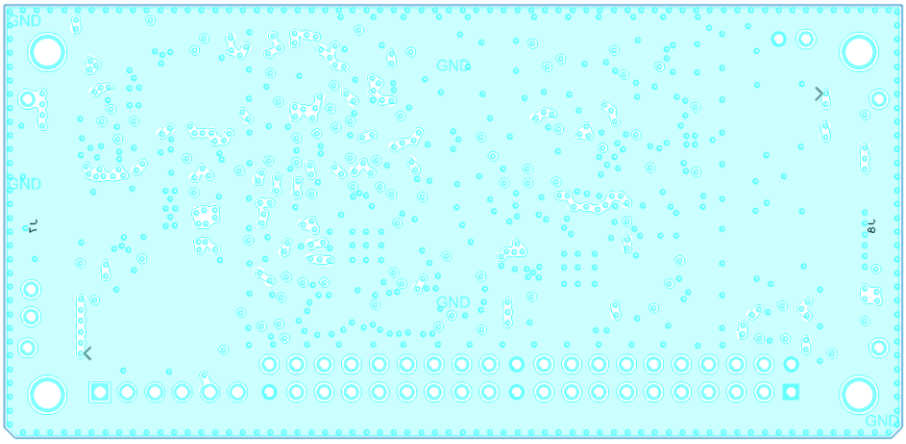

Figure 130: ISIR PCBA Layout Layer2, Ground

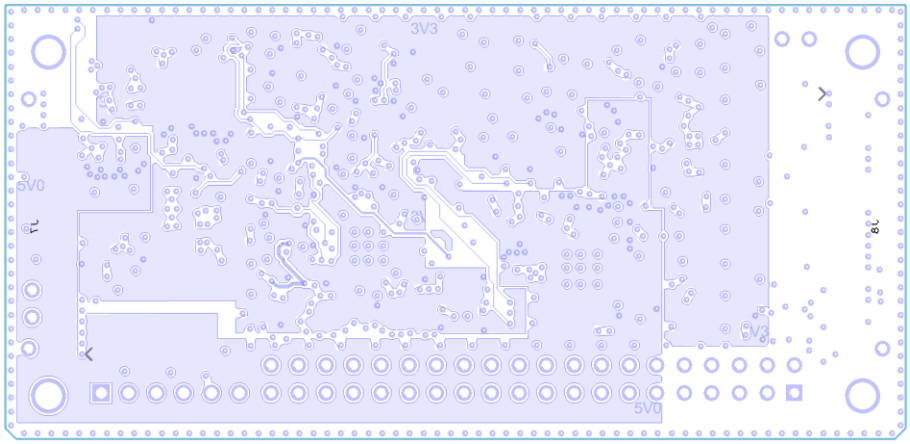

Figure 131: ISIR PCBA Layout Layer3, Power and Signal

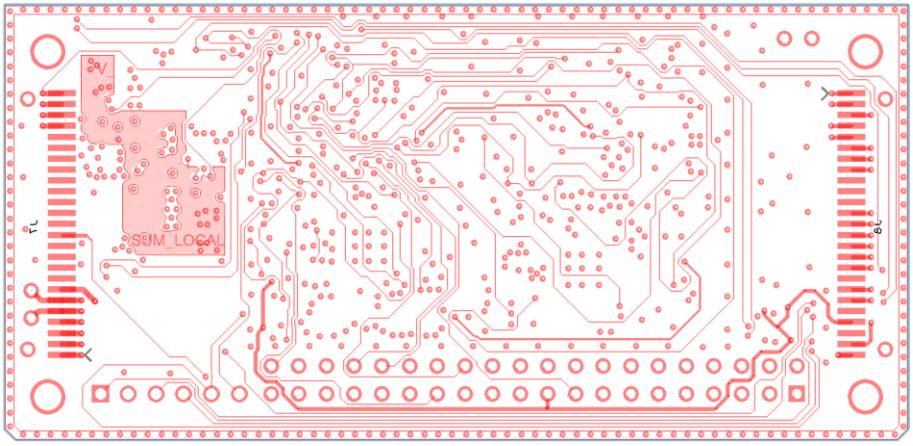

Figure 132: ISIR PCBA Layout Bottom, Power and Signal

Figure 133 shows the top layer with annotations calling out the location of the six important circuitry groups on the PCBA: power regulators, transceiver, low noise amplifier, power amplifier, antenna connectors, and development headers / test points.

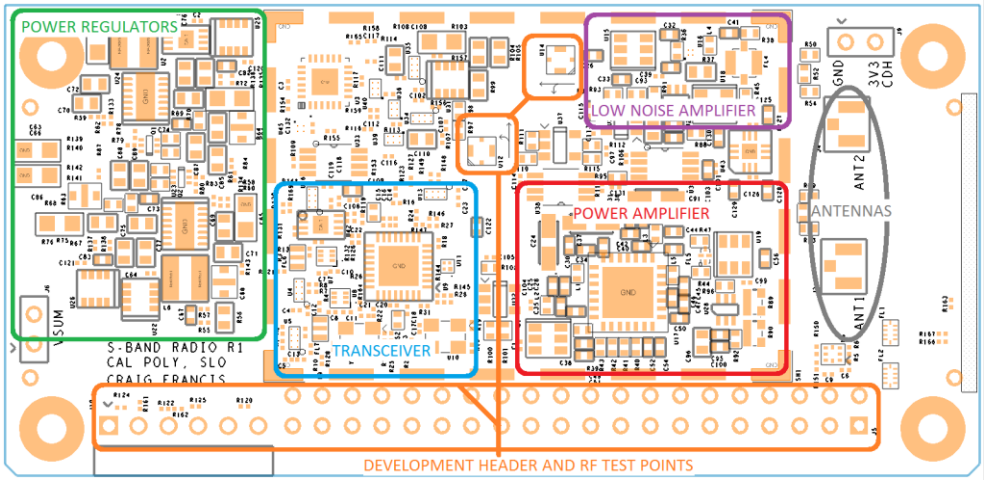

Figure 133: ISIR Annotated Top Layer

The layout of a mixed-signal and RF PCBA is absolutely critical to its final performance; many routing guidelines must be properly executed to ensure functionality. The following is a list of considerations that were taken into account during layout of the PCB:

- Power Distribution and IC Decoupling
- Switching Regulator Layout
- RF Layout and Characteristic Impedance
- Oscillator Layout
- PCB Layer Stack-Up
- EMI Reduction

Figure 134 shows the final layout for the TPS63020 switching regulator configured for 3.3V output. The layout recommendations from the datasheet were referenced, but the layout example reproduced in Figure 135 could not be implemented due to space

constraints. The inductor, capacitors, and feedback resistors are located as closely as possible to the regulator IC as possible to conserve space and minimize noise. The feedback resistor return path was carefully routed through the IC ground pin and into the thermal belly pad of the IC where it is connected to ground at a single point. It is important that the feedback return path is clean of any switching return current from the IC, inductor, and filtering capacitors. The thermal belly pad of the IC has as many vias that the design would permit to provide a low thermal impedance path to the ground plane. The 5.0V switching regulator circuitry layout is similar to the 3.3V regulator with minor component placement differences.

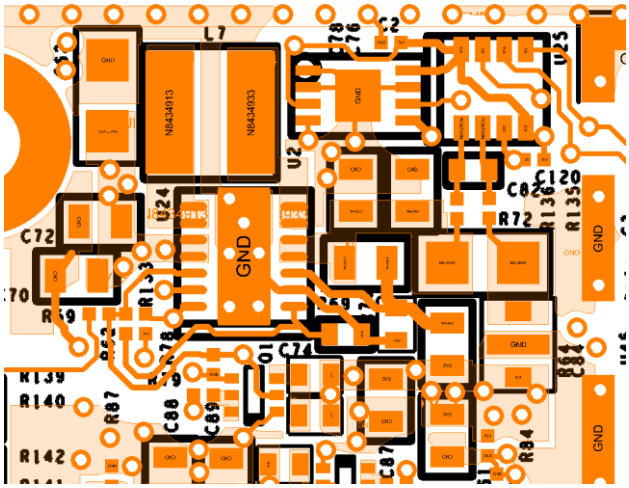

Figure 134: 3.3V Switching Regulator Layout

10.2 Layout Example

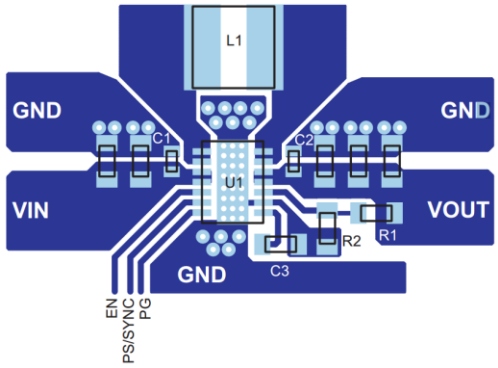

Figure 135: Switching Regulator Datasheet Layout Example [47]

Figure 136 shows the layout of the transceiver, crystal, oscillator, level translators, balun, and additional circuitry. The PCB layout description from the AT86RF233 evaluation board hardware user manual was referenced for digital and analog grounding of the transceiver, RF connection, and oscillator layout; snapshots from the application note are shown in Figure 137 and Figure 138. [60]

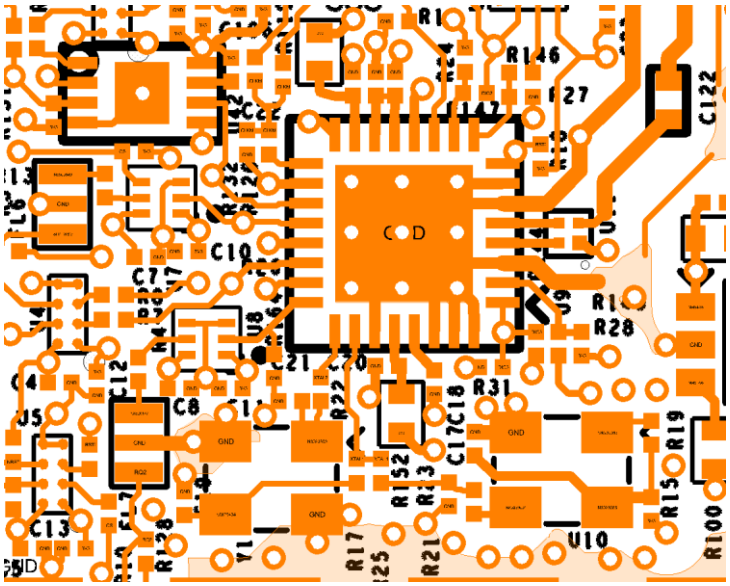

Figure 136: Transceiver Layout

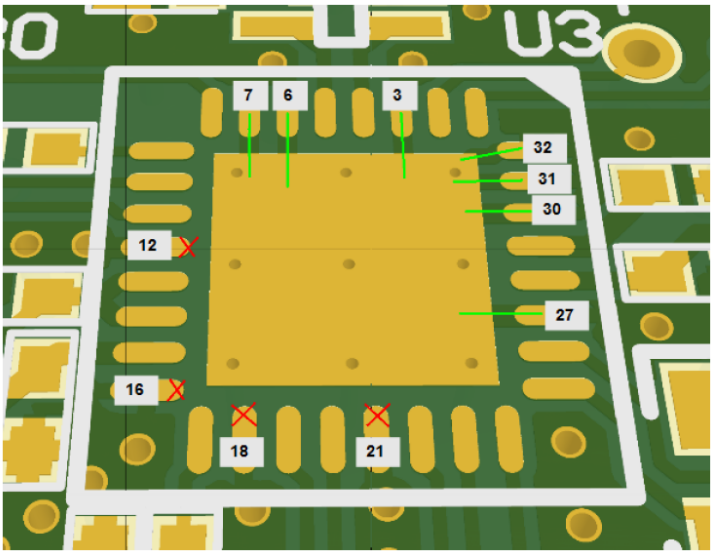

Figure 137: Atmel AT86RF233 Ground Connection Layout Recommendation [60]

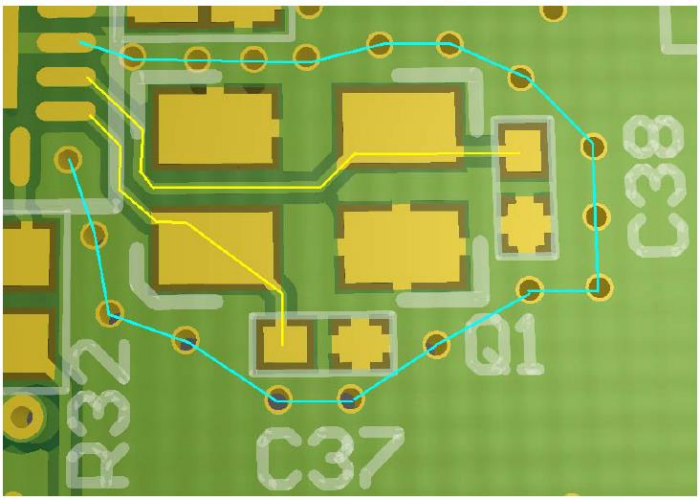

Figure 138: Atmel AT86RF233 Crystal Layout Recommendation [60]

Figure 139, Figure 140, and Figure 141 show the layout for the LNA, power amplifier, RF switches, and RF connectors. The datasheets, application notes, and evaluation board layout for each device was referenced during the layout and recommendations were implemented as practical within the board's space constraints. The components are extremely crowded and packed as closely as possible.

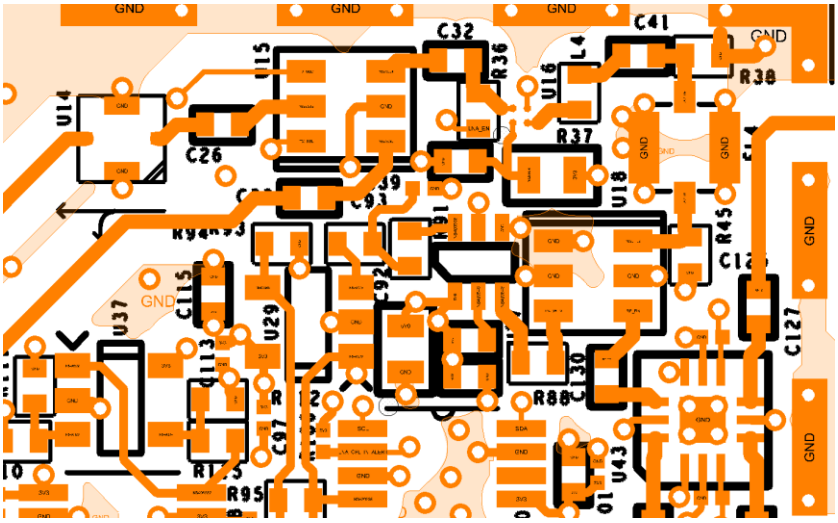

Figure 139: LNA Layout

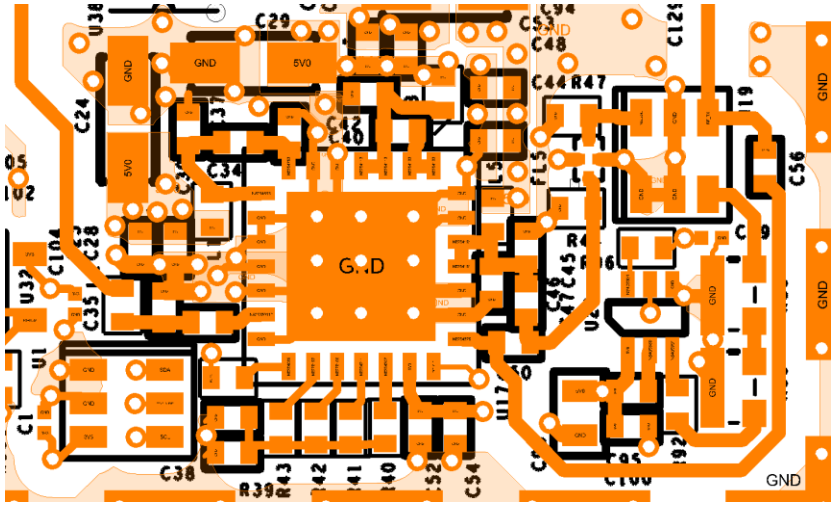

Figure 140: Power Amplifier Layout

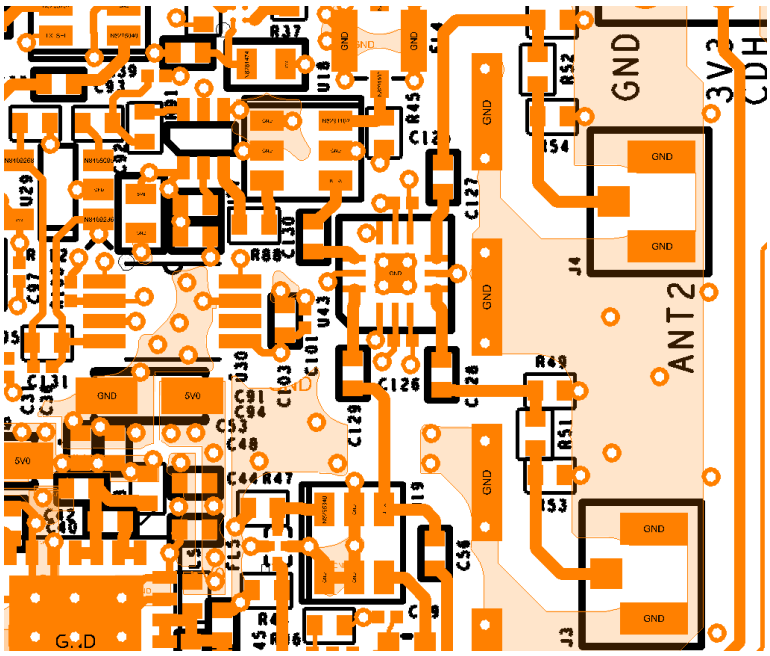

Figure 141: RF Switch and RF Connector Layout

Figure 142 shows the top layout of the board with RF traces colored red, ground connections colored gray, the 3.3V power net colored pink, and 5.0V colored purple.

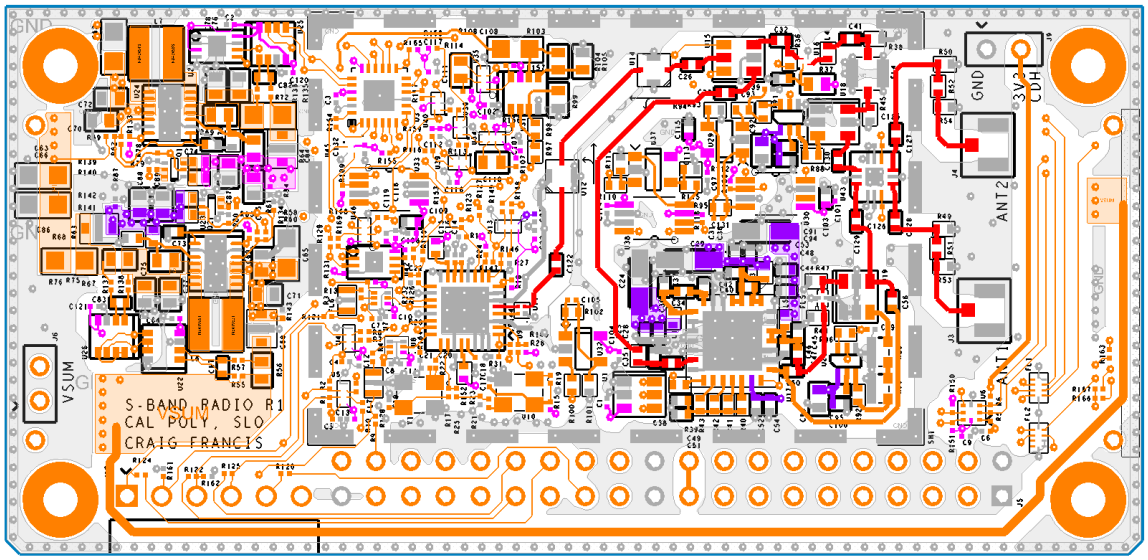

Figure 142: PCB with Highlighted Traces: RF = Red, GND = Gray, 3.3V = Pink, 5.0V = Purple

Stackup information from the PCB fabricator's website was utilized to calculate the appropriate RF trace width to achieve 50 Ohm impedance. The information from the website is reproduced in Figure 143, which shows the four layer stackup utilizes two sheets of 2216 pre-preg between the top copper foil and 2nd layer. The thickness of the pre-preg varies depending on the amount of copper material remaining on the two layers being bonded. The table shows the approximate pre-preg thickness for 30% and 70% copper utilization, these numbers were used to estimate the height between the top layer and the ground plane.

The resulting estimated PCB stackup is shown in Table 17. The stackup information was then inputted into the free Saturn PCB Design tool program to calculate the required width for 50Ω microstrip impedance as shown in Figure 144. The resulting trace width of 16.1 mils was used for the RF traces on the PCB.

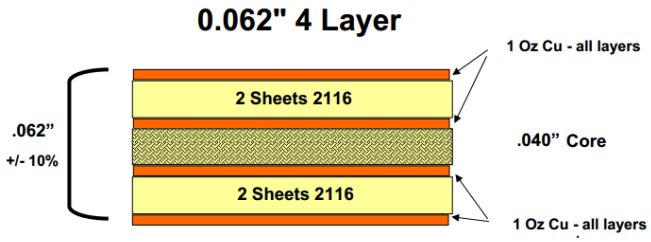

	A	B	C	D	E	F	G	H
Pre-Preg Styles	Against core with .5 oz copper and signal traces utilizing 30% of the board area	Against core with .5 oz copper and plane utilizing 70% of the board area	Against core with 1 oz copper and signal traces utilizing 30% of the board area	Against core with 1 oz copper and plane utilizing 70% of the board area	Against core with 2 oz copper and signal traces utilizing 30% of the board area	Against core with 2 oz copper and plane utilizing 70% of the board area	Against the top and bottom copper layers (foil).	Additional plies that are not directly against conductor layers
106	1.9	2.2	1.5	2.0	0.5	1.5	2.3	2.1
1080	2.6	2.8	2.1	2.6	1.1	2.2	3.0	2.7
2113	3.5	3.7	3.0	3.5	2.0	3.1	3.9	3.5
2116	4.7	4.9	4.2	4.7	3.2	4.3	5.1	4.6
7628	6.5	6.8	6.0	6.5	5.0	6.1	6.9	6.2

Figure 143: Advanced Circuits 4 Layer PCB Stackup and Prepreg Thicknesses

Table 17: PCB 4 Layer Stackup

LAYER	THICKNESS (mils)
COPPER 1: SIG/RF	1.4
PREPREG SHEET1	5.1
PREPREG SHEET2	4.7
COPPER 2: GND	1.4
CORE	39
COPPER 3: PWR	1.4
PREPREG SHEET3	4.7
PREPREG SHEET4	5.1
COPPER 4: SIG	1.4

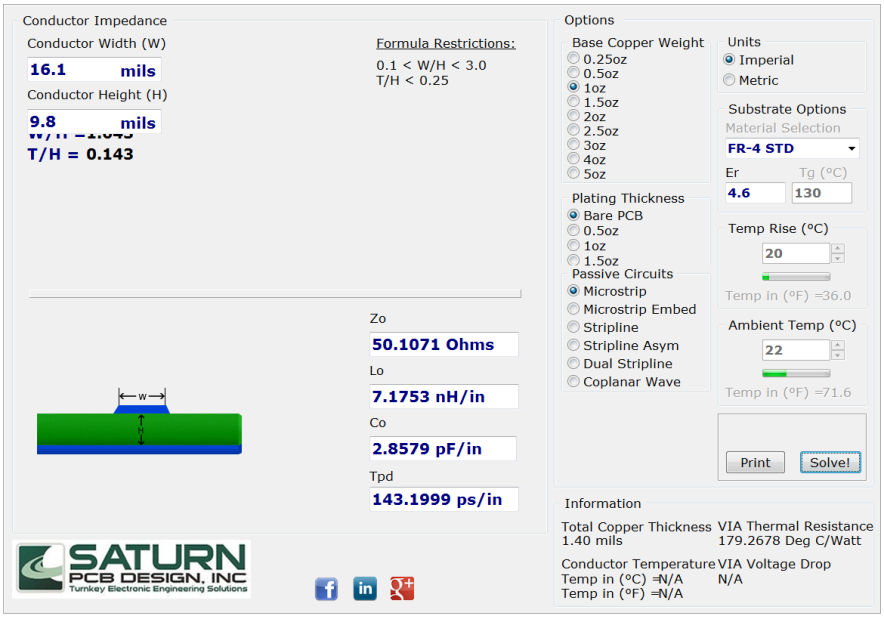

Figure 144: 50 Ohm Microstrip Trace Impedance Calculation by Saturn PCB Design Tool

To prevent the top layer ground plane flood from affecting the trace impedance, the ground flood was kept 40mils away when possible. The rule of thumb is to keep the copper pour four dielectric thicknesses away to reduce parasitic effects.

Component dimension information was also inputted during the layout which is shown in Figure 145 and Figure 146. This model allowed confirmation of adequate

clearance between the components and the RF shield case as well as clearance between components.

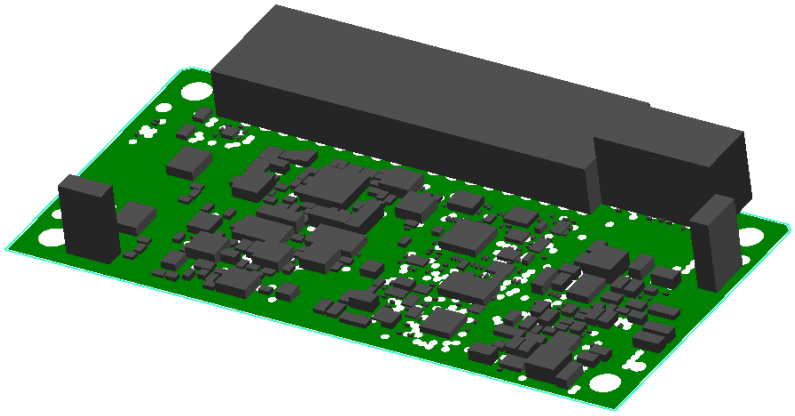

Figure 145: PCBA 3D Model with Component Height Information

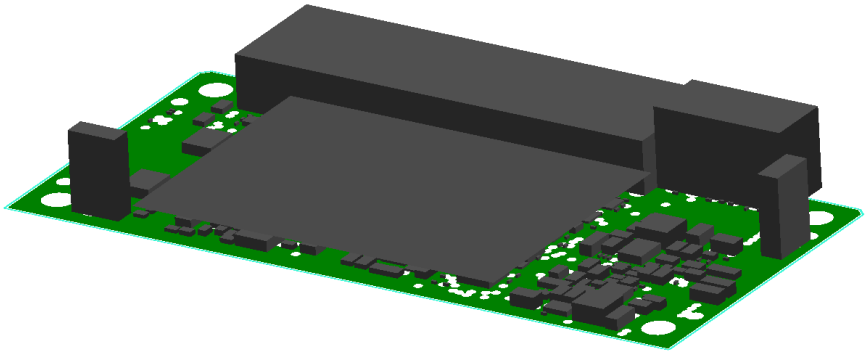

Figure 146: PCBA 3D Model with Shield Installed, Confirming no Mechanical Clearance Issues

Several days were dedicated to double checking the schematic, footprints, pinouts, connector orientations, and layout which resulted in several mistakes being caught and corrected prior to the board being ordered. It is important to double check all the details within a design before it is fabricated, because physically troubleshooting and correcting the mistakes on the finished board consumes much more time than performing the

proper due diligence. The PCB was also fit checked and inspected prior to assembly as shown in Figure 147.

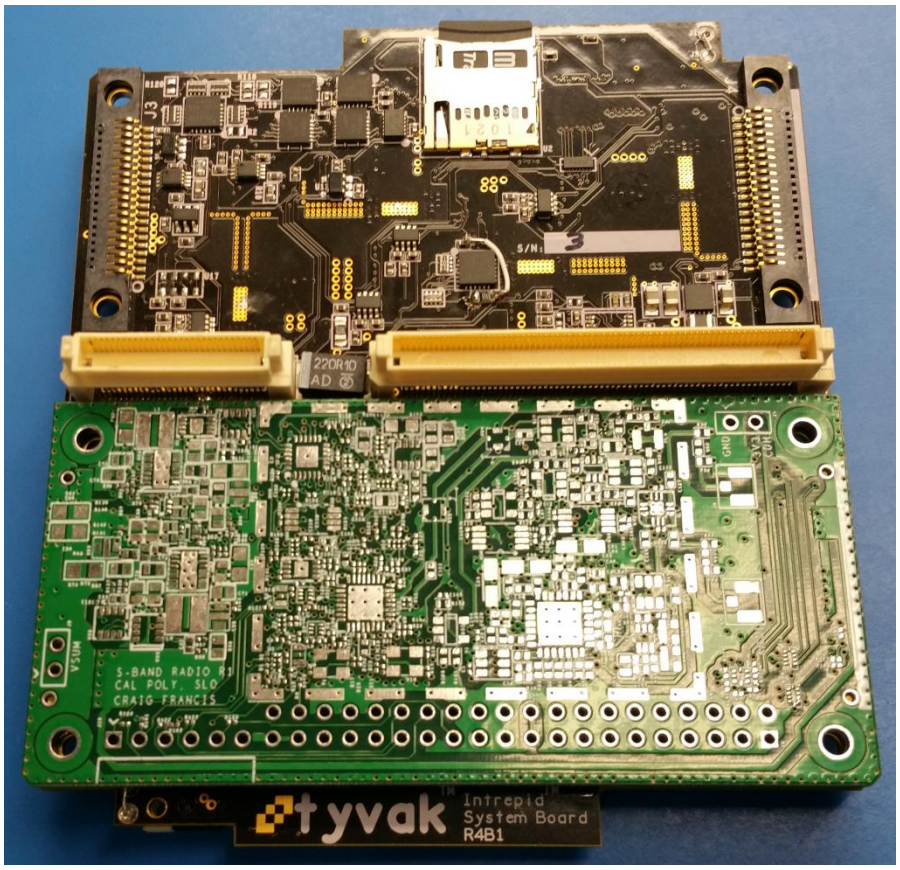

Figure 147: PCB Fit Check Prior to Assembly

7 PCBA Bring Up and Testing

7.1 Initial Bring Up and Troubleshooting

The PCBAs were visually inspected under a microscope for assembly issues upon reception. The four PCBAs passed visual inspection with no visible issues. A multimeter configured in continuity measurement mode was used to confirm no shorts present across the power nets and ground and no shorts across a random selection of capacitors. Next was the smoke test; the board was powered from a benchtop power supply configured at 4.0V with a 100mA current limit. The board drew 6mA indicating no major short present on the board. The power nets were then measured with a voltmeter to confirm the 3V3 and 5V0 regulators were operating nominally. The crystal was probed with an oscilloscope to confirm oscillator activity at the AT86RF233 transceiver.

The evaluation processor board reads the SPI EEPROM for configuration settings prior to communication with the transceiver. The EEPROM data from the evaluation board was extracted using the Aardvark USB to I2C/SPI hardware developed by TotalPhase. The Aardvark Flash Center software was utilized to extract the EEPROM data and to program a modified version to the ISIR. Figure 148 shows the ISIR EEPROM being programmed by the Aardvark and Figure 149 shows a screen capture of the Flash Center software reading the EEPROM data from the evaluation board.

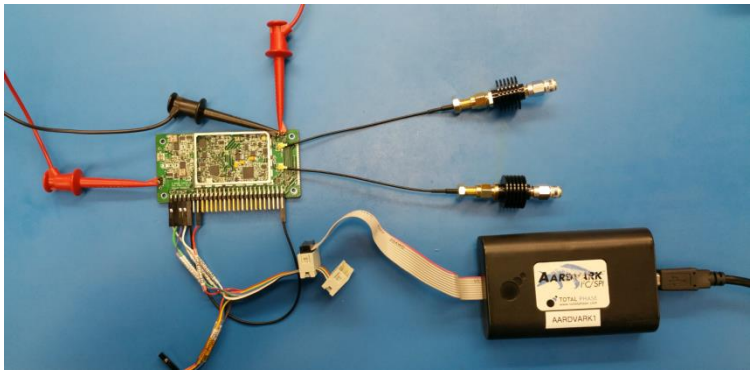

Figure 148: Flashing the ISIR EEPROM with Modified Configuration File

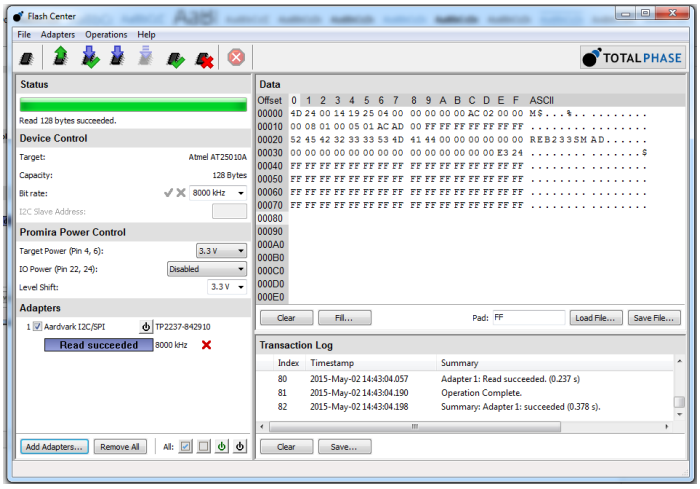

Figure 149: Aardvark Flash Center EEPROM Programming Software

After programming the ISIR EEPROM, the ISIR and evaluation processor board were connected and interfaced to a laptop. A partner evaluation board was also set up and a packet error rate test between the ISIR and the evaluation board was successful utilizing the evaluation software. Figure 150 shows the initial communication test between the evaluation board and the ISIR. This test confirmed that the transceiver, buffers, and regulators were functional. The test also confirmed the evaluation connector pinout was correct and that the software present on the evaluation processor board worked with the ISIR.

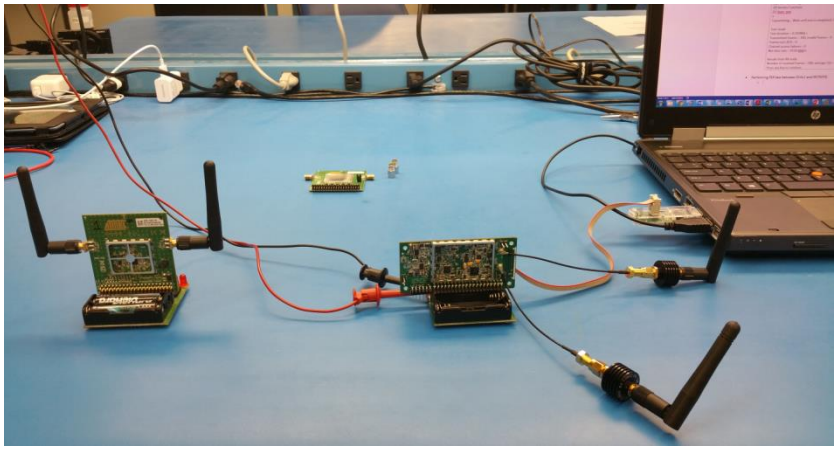

Figure 150: ISIR and Evaluation Board Initial Communication Test

7.2 Balun AC Coupling Issue

After initial bring up of the board, the transmit power from the AT86RF233 transceiver was measured utilizing the coaxial switch test point placed after the transceiver. The transceiver was configured for an output of 4dBm, but the output power measured -1.7dBm after accounting for cable loss; the transceiver was transmitting 6dB less than expected. The only device between the transceiver and test point was the balun and AC coupling capacitor. The AC coupling capacitor was shorted out and the issue remained, therefore the issue was with the balun. After consulting the datasheet for the AT86RF233 and balun, it was discovered that the balun was not AC coupled between the bias and the balanced input pins. Therefore the DC bias at the transceiver output pins RFP and RFN was being shorted to ground through the balun bias pin. Figure 151 shows an annotated snippet of the schematic with the areas missing the AC coupling capacitors circled.

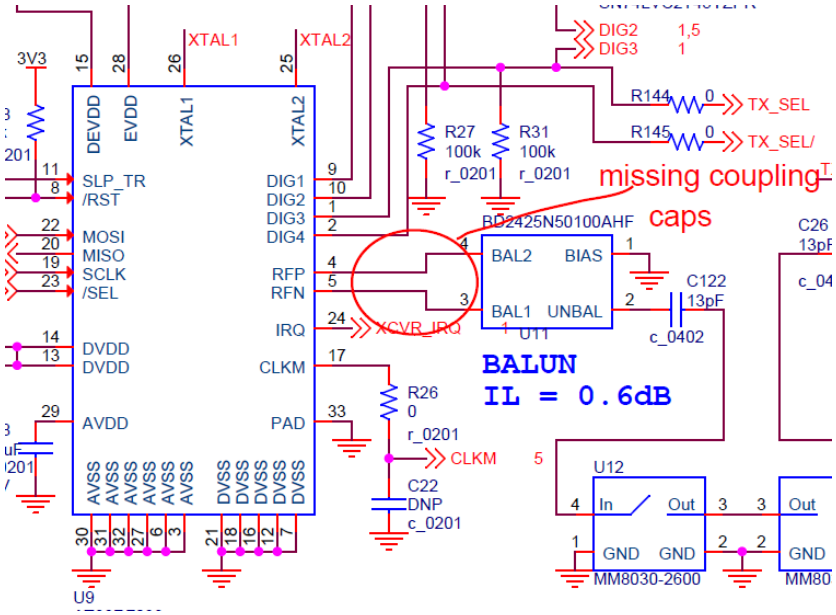

Figure 151: Balun Coupling Capacitors Missing, Annotated Schematic

The balun was then removed using a microscope and SMT hot-air gun rework station. The traces to the balun were cut using a Xacto knife and two 22pF, 0201 capacitors were soldered across the two cut traces. Figure 152 shows the reworked transceiver to balun interface with the added capacitors.

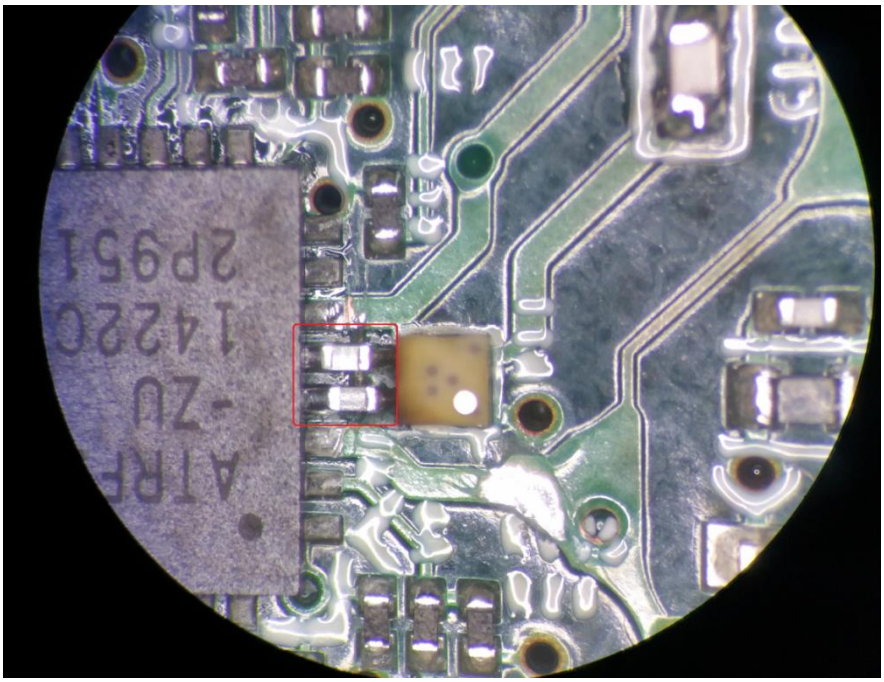

Figure 152: Reworked Board with Balun Coupling Caps Added

The balun and C122 decoupling capacitor were then replaced and the transceiver output power was re-measured as 3.5dBm which matched the configured output power of 4dBm minus the balun insertion loss of 0.6dB.

7.3 TCXO Voltage Divider Issue

During receive sensitivity testing, the crystal was swapped with the TCXO to evaluate whether the TCXO improved receive sensitivity. However, the receive sensitivity significantly degraded when the TCXO was connected. The TCXO output was then observed on an oscilloscope to be significantly smaller than expected. The TCXO had a resistive divider on its output to level convert the 3.3V oscillator output to 521mV

amplitude; however the measured amplitude was below 20mV. The AT86RF233 datasheet specifies a parasitic capacitance of 3pF at the XTAL1 oscillator input pin, and it turns out that the impedance of 3pF at 16MHz is 829Ω which is significantly smaller than the 21kOhm resistor in parallel from the divider. Therefore, a capacitive voltage divider was more appropriate for level translating the output of the TXCO. Figure 153 shows the annotated schematic snippet of the TCXO voltage divider.

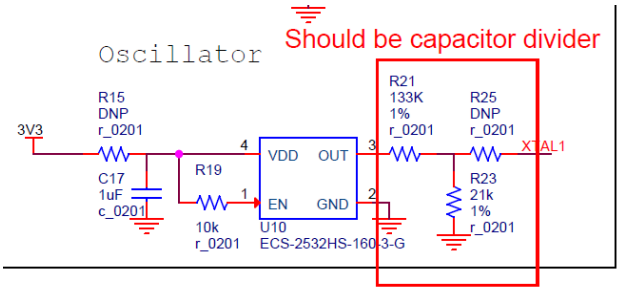

Figure 153: Oscillator Voltage Divider Issue, Annotated Schematic

R21, R23, and R25 were iteratively changed while observing the output of the TCXO on an oscilloscope and performing a packet error rate test with an evaluation board. The values that gave the best receive sensitivity and reduced ringing were R21 = 1.2pF, R23 = 10pF, and R25 = 270 Ohms. After resolving this issue, the TXCO and crystal produced identical receive sensitivity measurements.

7.4 Antenna Selection Switch Issue

The final RF switch did not perform transmit and receive switching as intended, which was immediately apparent after looking that the schematic. Figure 154 shows the switch which does allow selection of an antenna, but it does not perform the required transmit and receive switching between the LNA and PA during communication. Therefore, one RF connector was configured as always transmit and the other always receive. This issue could not easily be resolved through physical modification of the

board and must be corrected in a second board revision. However, testing could continue by merely using one RF port for receive and the other for transmit.

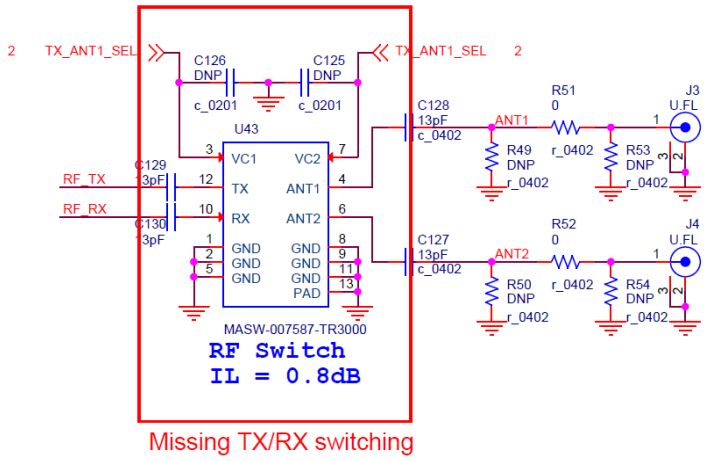

Figure 154: Antenna Selection Switch Issue, Annotated Schematic

7.5 Receiver Desensitization Issue

During initial receive sensitivity testing, the ISIR was found to perform 15dB worse than the evaluation board. 15dB is a significant difference, so mismatch loss from an un-tuned LNA was ruled out and a noise issue was suspected. The 3.3V and 5.0V switching regulators were bypassed with a benchtop supply to see if the switching noise was the cause of the issue. Surprisingly, the receive sensitivity degraded by an additional 10dB when powered by the benchtop supply.

Next, the LNA was bypassed and the transceiver's receive sensitivity was directly measured using the coaxial switch test point in front of the transceiver. The issue still occurred when connected directly to the transceiver; therefore the noise was interfering with the transceiver. The analog voltage rail 0Ω series resistor was replaced with a large ferrite, manufacturer part number MPZ 2012 S601A, and the issue was resolved. With the ferrite in series with the transceiver's analog voltage rail, the receive sensitivity matched the evaluation board. Another ferrite was placed in series with the LNA voltage

rail as well, but the receive sensitivity did not improve; therefore the LNA did not require a ferrite in series with its power supply. The baseband circuitry internal to the transceiver was probably jammed with noise on the 3.3V power net emitted by activity from nearby digital circuits and the ferrite filtered out the noise. Figure 155 shows the schematic and where R152 is replaced by a ferrite bead. R152 was intentionally placed in the schematic for the possibility of this issue.

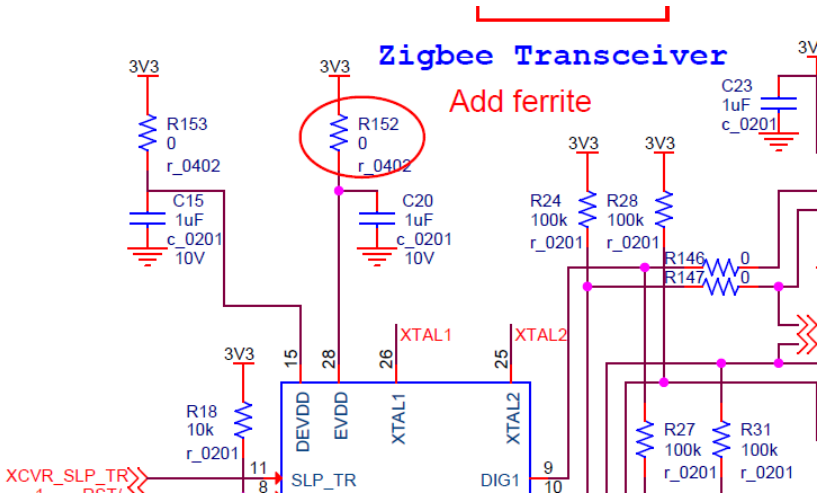

Figure 155: Ferrite Required on Transceiver Analog Power Net, Annotated Schematic

7.6 RF Leakage Issue

It was extremely difficult to isolate the transmitter and receiver during receive sensitivity testing. The problem of RF leakage was first encountered during receive sensitivity testing of the evaluation board and was discussed in: "*4.5.1 Evaluation Board Receive Sensitivity Measurements*." Due to RF leakage between the two boards, the receiver will receive the transmitted signal regardless if the receiver has an antenna or is terminated with a 50Ω load. The ISIR transmits at a power 30dB greater than the evaluation board; therefore the leakage issue was more difficult to overcome. Several

weekends were spent attempting to adequately shield the receiver and transmitter so that receive sensitivity testing could be performed.

Figure 156 shows a faraday cage constructed from a cardboard box and copper mesh. This faraday cage was adequate for receive sensitivity testing the UHF board at 400MHz, however it provided very little shielding at the ISIR frequency of 2.4GHz. The copper mesh box has poor gasketing between the lid and the walls which probably created large enough gaps in the faraday cage to allow 2.4GHz signals to pass right through.

Figure 156: Faraday Cage Constructed from Box and Copper Mesh Material, Inadequate Shielding

A second box shown in Figure 157 was constructed out of aluminum foil. Measurements showed that this box provided no shielding at all and was worse than the copper mesh Farday cage. The receiver was placed in the aluminum foil box and then the copper mesh box, but the RF leakage issue still persisted. The transmitter was also put in the shields with the receiver outside, but that also provided inadequate isolation. Different value attenuators were placed in series with the coaxial cable inside and

outside the box, but no configuration of the boxes or attenuators provided adequate isolation between the transmitter and receiver. The transmitter and receiver were moved as far apart as possible but the issue persisted, even with the transmitter and receiver in different rooms or different floor levels.

Figure 157: Faraday Cage Constructed from Box and Aluminum Foil, Inadequate Shielding

A third faraday cage was then implemented using metal paint cans as shown in Figure 158. Both the transmitter and receiver were shielded within the metal paint cans with fixed attenuators between the radio and the lid pass-through. The paint can lids were drilled and USB, power, and SMA pass-throughs were soldered through the lid while keeping openings as small as possible. Figure 159 shows the ISIR, USB adapter, power, and coaxial cable passed through the paint can lid.

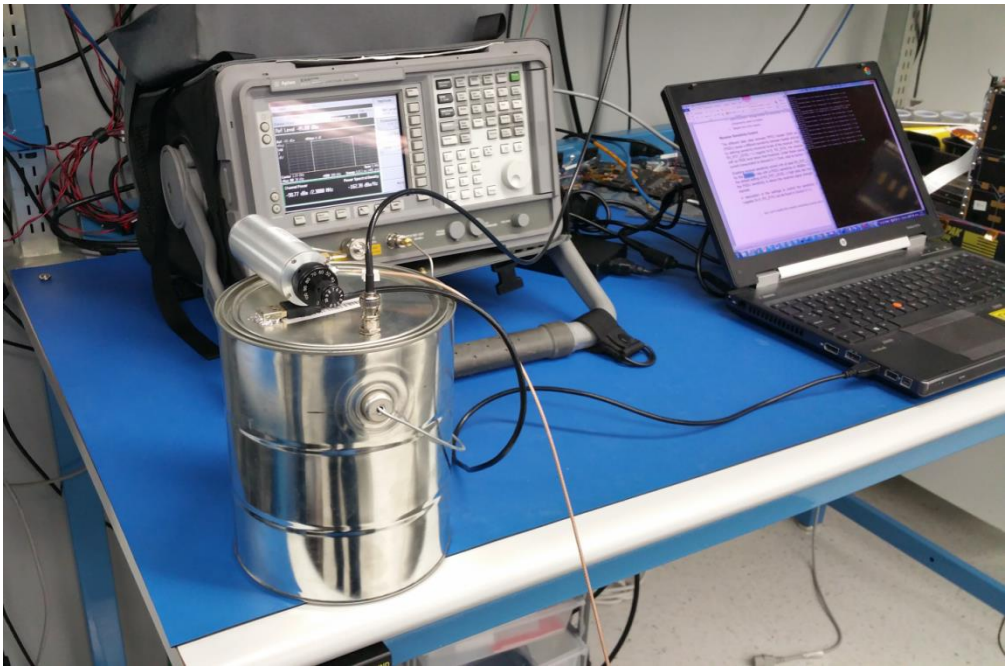

Figure 158: Paint Can Faraday Cage

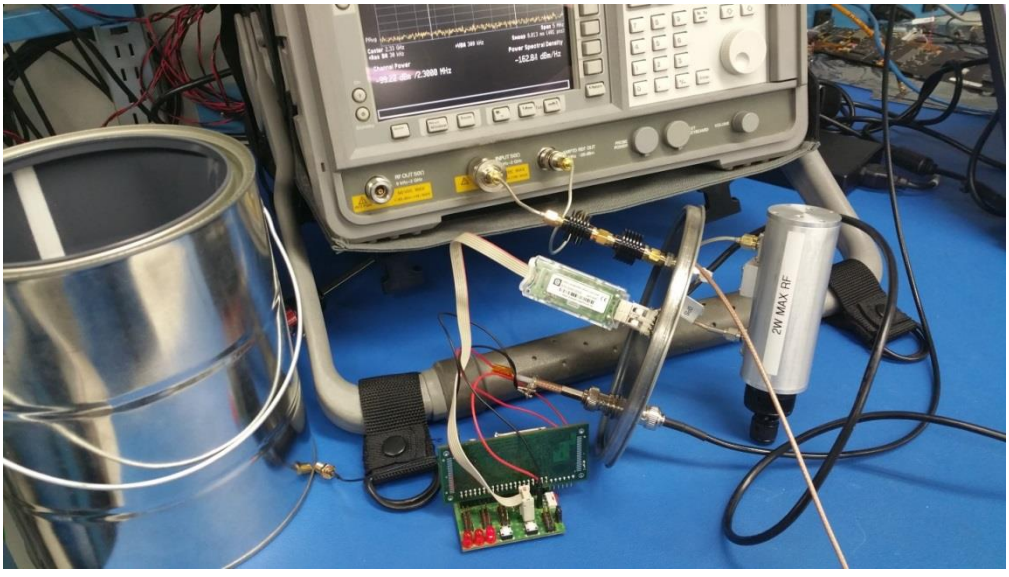

Figure 159: Paint Can Faraday Cage Lid with Pass Throughs

Initially, the paint can faraday cages did not provide adequate attenuation. A coating on the rim of the lid had to be sanded away to provide electrical continuity between the can and lid. The lid had to be aggressively formed against the can with a

screw driver handle each time the lid was replaced to provide adequate contact between the lid rim and the can; simply hammering the lid into the can resulted in too large of gaps and RF leakage. Ultimately, after a few weekends of frustration, the RF leakage issue was resolved with the paint can faraday cages and receive sensitivity testing could be performed.

7.7 2000kbps Packet Drop Issue

During receive sensitivity testing the packet error rate at 2000kbps was non-zero regardless of the attenuation between the transmitter and receiver. The evaluation boards also experienced the same issue, which indicated the issue was not from the ISIR design. This issue was accidently overlooked during the original evaluation board testing and it is unknown how a -87dBm measurement was obtained at 2000kbps. Around 5% of packets are dropped during the 2000kbps receive sensitivity test regardless of attenuation. After consulting the AT86RF233 datasheet, it was discovered that the receiver sensitivity control RX_PDT_LEVEL register value should be set to a value of 1 to achieve the -88dBm receive sensitivity at 2000kbps as shown in Figure 160. However, the evaluation software only allows modification of the transmitter's register settings. The receiver's register settings cannot be modified during the packet error rate test. Therefore, the 2000kbps packet drop issue was not resolved and needs to be investigated further once software is written for the ISIR.

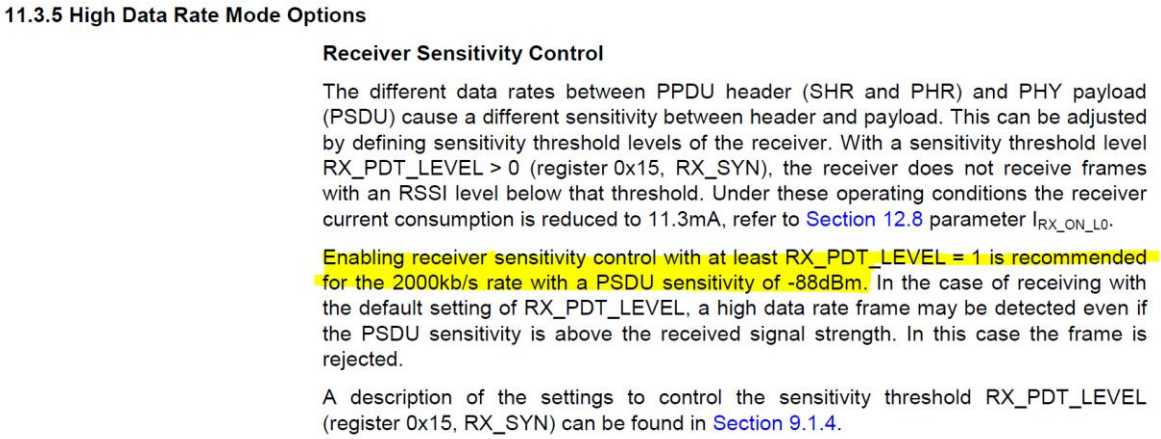

11.3.5 High Data Rate Mode Options

Receiver Sensitivity Control

The different data rates between PPDU header (SHR and PHR) and PHY payload (PSDU) cause a different sensitivity between header and payload. This can be adjusted by defining sensitivity threshold levels of the receiver. With a sensitivity threshold level RX_PDT_LEVEL > 0 (register 0x15, RX_SYN), the receiver does not receive frames with an RSSI level below that threshold. Under these operating conditions the receiver current consumption is reduced to 11.3mA, refer to Section 12.8 parameter $I_{RX\_ON\_L0}$.

Enabling receiver sensitivity control with at least RX_PDT_LEVEL = 1 is recommended for the 2000kb/s rate with a PSDU sensitivity of -88dBm. In the case of receiving with the default setting of RX_PDT_LEVEL, a high data rate frame may be detected even if the PSDU sensitivity is above the received signal strength. In this case the frame is rejected.

A description of the settings to control the sensitivity threshold RX_PDT_LEVEL (register 0x15, RX_SYN) can be found in Section 9.1.4.

Figure 160: Receive Sensitivity Control Register for 2000kbps, AT86RF233 Datasheet Excerpt [28]

7.8 ISIR PA Tuning and Transmit Power Measurements

Without any modifications to the board, the transmit power outputted by the ISIR measured around 30dBm, which is 3dB less than the 33dBm design target. However, this was expected due to the layout differences compared to the power amplifier evaluation board. It was expected that the passive component values of the tuning networks needed to be slightly modified to obtain maximum transmit power. However, the power amplifier tuning resulted in much more labor than anticipated, consuming about 4 weekend's worth of time. 2.4GHz is within the transition frequency range where lumped components are typically replaced with transmission line equivalents.

Capacitors and inductors are no longer well behaved in matching networks at high frequency due to the required low values and parasitic effects. Capacitance changes on the order of 0.1pF and a capacitor's effective series inductance on the order of 1nH considerably affects the match. The transmission line length between components also introduces non-negligible phase shift of the signal and must be accounted for when calculating the passive component values.

At first, a Smith chart approach was attempted, but this approach was later deemed ineffective due to component parasitic effects at 2.4GHz. Figure 161 shows the power amplifier S11 measurement with the original input matching circuit; the power amplifier input is well matched at 2.75GHz instead of the desired 2.4GHz.

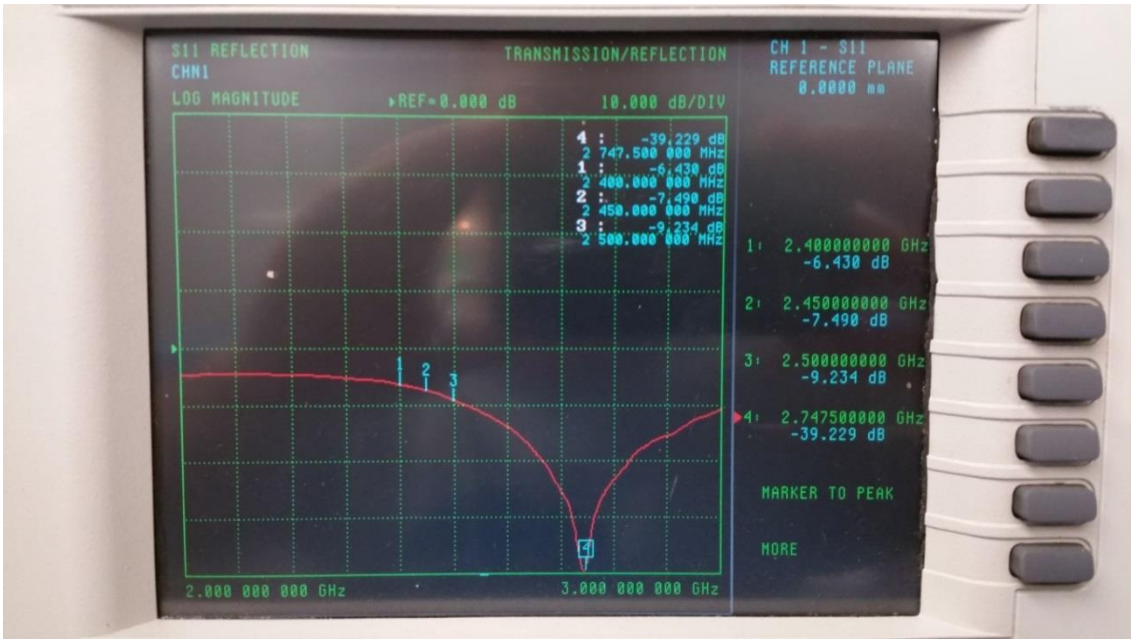

Figure 161: Power Amplifier Input S11

The input matching network values were slightly tweaked, but the S11 null could not be improved toward 2.4GHz. The input matching network was then completely removed and series components replaced with solder shorts. Figure 162 shows the Smith Chart measurement with the input matching network removed.

Figure 162: Power Amplifier S11 Smith Chart, Matching Network Removed

Figure 163 shows using Smith Chart freeware to calculate component values to match the input of the power amplifier using the VNA measurements. However, using the calculated component values did not provided the calculated match as shown in Figure 164. The transmission line lengths and approximate component parasitics were also accounted for in consecutive calculation attempts using the Smith chart software with no success. After a few weekends of researching and re-attempting matching the power amplifier input, no improvement could be achieved. The effect of simply placing one series component such as a coupling capacitor could not be predicted using the Smith chart software due to the uncertainty of the capacitor and the layout's parasitics. The parasitics could be modeled in advanced EM analysis microwave software by importing the layout into the software and obtaining passive component models from the vendors, however time did not permit this approach. Eventually, the Smith chart approach was dismissed in favor of an iterative approach.

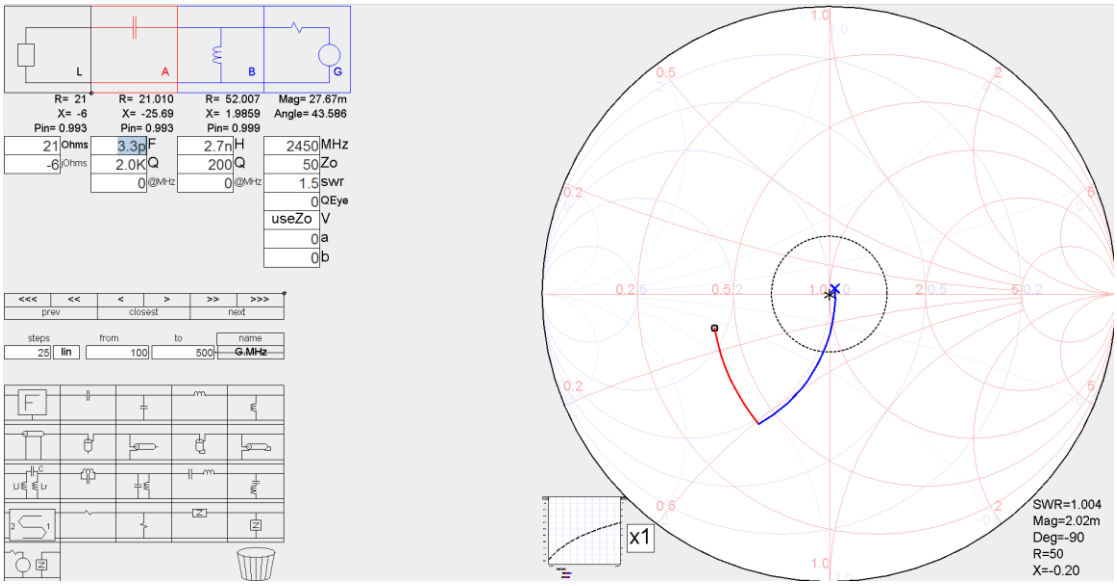

Figure 163: Smith Chart Software Used for Matching Power Amplifier Input

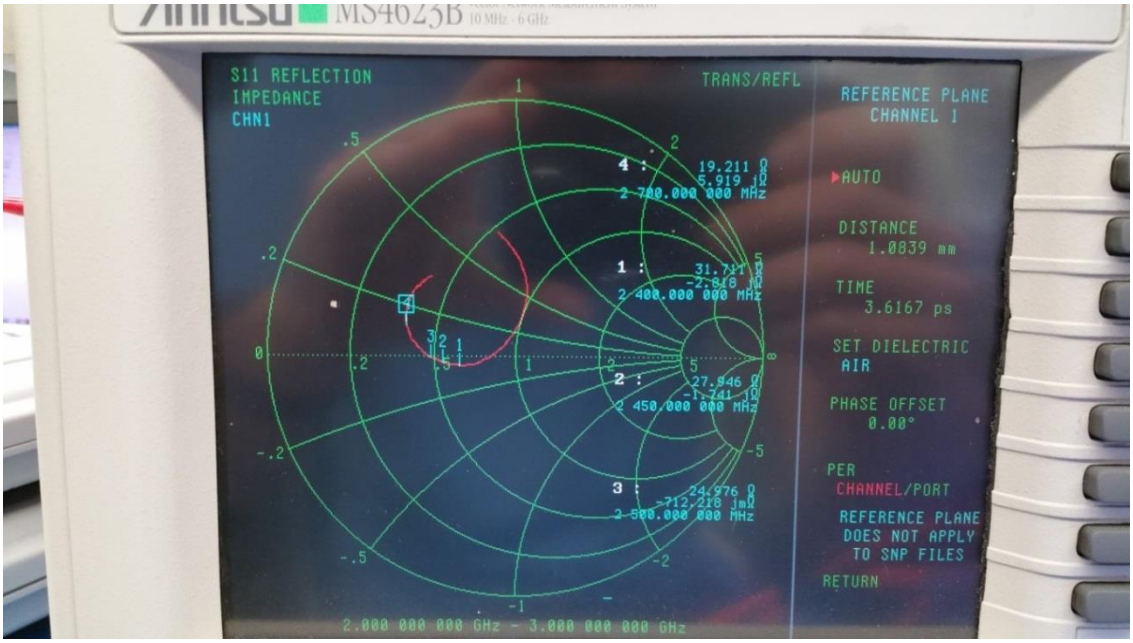

Figure 164: Resulting Power Amplifier S11 using Smith Chart Software Values, Not Matched

Figure 165 shows the power amplifier circuitry prior to tuning for maximum transmit power. The three-stage amplifier has four matching networks: input, stage 1 output,

stage 2 output, and stage 3 output these are shown as different colored boxes in the figure.

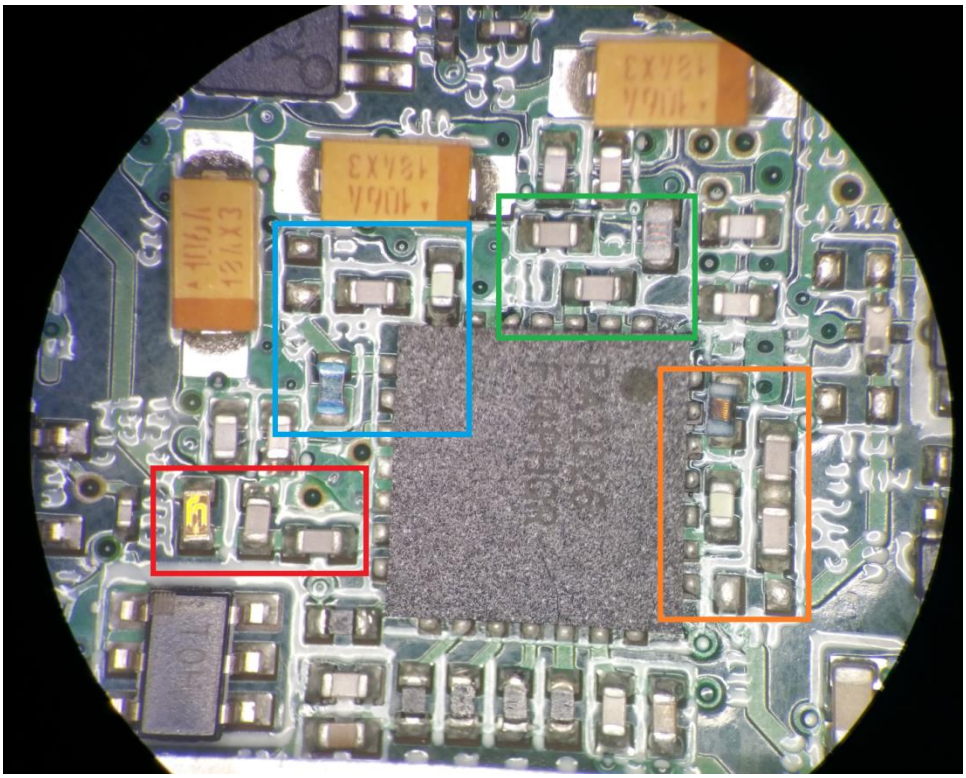

Figure 165: Power Amplifier Circuitry before Tuning, Matching Networks Indicated

The values of these components were iteratively varied while monitoring the resulting output power of the amplifier, usually starting with the last component in the network and moving toward the source. A Smith chart was referenced during the matching to gain insight into how the component was affecting the match and how the next component completed the match, but the Smith chart ultimately could not predict the final value.

Over the course of 3 weekends, 368 iterations were performed to achieve maximum transmit power. Each iteration took approximately 5 to 10 minutes to change a component value, energize the board, command transmission, and measure the result. Figure 166 shows a snapshot of the excel sheet utilized to track iterations and resulting S21 measurements; the figure shows 35 of the 368 iterations. Table 18 shows the final

matching network component values to obtain 33.4dBm output from the amplifier after accounting for cable loss and output series component loss. Figure 167 shows the final output power measurement with 10.46dB cable attenuation. Accounting for the theoretical 1.65dB component insertion loss after the amplifier, approximately 33.4dBm is output from the amplifier.

However, the amplifier should be capable of outputting 34.5dBm. This 1dB difference in output power is most likely due to non-optimal tuning or some unaccounted loss. The characteristic impedance of the traces was not well controlled and was calculated based off of unverified stack-up best guess assumptions from the manufacturer's website. The layout is also highly compressed compared to the evaluation board due to space constraints which may have introduced non-negligible leakage paths. The dielectric is FR4 which is somewhat lossy at 2.4GHz, but not lossy enough to fully account for the 1dB difference.

	A	B	C	D	E	F	G	H	I	J	K	L	M	N	O	P	Q	R	S	T
1		Input Stage			1st Stage				2nd Stage			Output Stage					S21 PA IN to U.FL		Increase	
2		L2	C35	C38	L1	C30	C37	C34	L3	C42	C40	L5	C45	C46	C47	C50				
3	Type	Serial	Shunt	Serial	Biasing	Shunt	Shunt	Serial	Biasing	Shunt	Serial	Biasing	Shunt	Shunt	Serial	Shunt	dB			
4	Value	1.8nH	.3pF	8.2pF	22nH	DNP	1.8pF	12pF	3.3nH	1.5pF	2pF	24nH	0.9pF	1.5pF	2pF	DNP	30.7			
206		4.1nH	DNP	1pF	22nH	DNP	3.3pF	15pF	22nH	1pF	2.2pF	24nH	2.7pF	DNP	2.7pF	DNP	31.8			
207		4.1nH	DNP	1pF	22nH	DNP	3.3pF	15pF	22nH	1pF	2.2pF	24nH	2.7pF	DNP	2.7pF	DNP	31.8			
208		8nH	DNP	1pF	22nH	DNP	3.3pF	15pF	22nH	1pF	2.2pF	24nH	2.7pF	DNP	2.7pF	DNP	30.3			
209		8nH	DNP	0.6pF	22nH	DNP	3.3pF	15pF	22nH	1pF	2.2pF	24nH	2.7pF	DNP	2.7pF	DNP	29.9			
210		3.9nH	DNP	0.6pF	22nH	DNP	3.3pF	15pF	22nH	1pF	2.2pF	24nH	2.7pF	DNP	2.7pF	DNP	31.1			
211		3.9nH	DNP	0.6pF	22nH	DNP	3.3pF	15pF	22nH	1pF	2.2pF	24nH	2.7pF	DNP	2.7pF	DNP	31.1			
212		3.9nH	DNP	0.8pF	22nH	DNP	3.3pF	15pF	22nH	1pF	2.2pF	24nH	2.7pF	DNP	2.7pF	DNP	31.5			
213		3.9nH	DNP	0.8pF	22nH	DNP	3.3pF	15pF	22nH	1pF	2.2pF	24nH	2.7pF	DNP	2.7pF	DNP	31.5			
214		3.9nH	DNP	1.8pF	22nH	DNP	3.3pF	15pF	22nH	1pF	2.2pF	24nH	2.7pF	DNP	2.7pF	DNP	32			
215		3.9nH	DNP	2.2pF	22nH	DNP	3.3pF	15pF	22nH	1pF	2.2pF	24nH	2.7pF	DNP	2.7pF	DNP	32.2		-0.8 INPUT	
216		SHORT	DNP	SHORT	22nH	0.5pF	3.3pF	15pF	22nH	0.5pF	2.2pF	24nH	2.2pF	DNP	3.3pF	DNP	33.5		Reverting back to	
217		SHORT	DNP	SHORT	22nH	0.5pF	3.3pF	15pF	22nH	0.5pF	2.2pF	24nH	2.2pF	DNP	3.3pF	DNP	33.6			
218		SHORT	DNP	SHORT	22nH	0.5pF	3.3pF	15pF	22nH	3.3pF	2.2pF	24nH	2.2pF	DNP	3.3pF	DNP	30.4			
219		SHORT	DNP	SHORT	22nH	0.5pF	3.3pF	15pF	22nH	3.3pF	1.8pF	24nH	2.2pF	DNP	3.3pF	DNP	29.3			
220		SHORT	DNP	SHORT	22nH	0.5pF	3.3pF	15pF	22nH	1pF	1.8pF	24nH	2.2pF	DNP	3.3pF	DNP	32.9			
221		SHORT	DNP	SHORT	22nH	0.5pF	3.3pF	15pF	22nH	1pF	2.2pF	24nH	2.2pF	DNP	3.3pF	DNP	33.4			
222		SHORT	DNP	SHORT	22nH	0.5pF	3.3pF	15pF	22nH	1pF	2.2pF	24nH	3pF	DNP	3.3pF	DNP	33.6			
223		SHORT	DNP	SHORT	22nH	0.5pF	3.3pF	15pF	22nH	1pF	2.2pF	24nH	3pF	DNP	3pF	DNP	33.5			
224		SHORT	DNP	SHORT	22nH	0.5pF	3.3pF	15pF	22nH	1pF	2.2pF	24nH	3pF	DNP	3pF || 0.1uF	DNP	33.8	34?		
225		SHORT	DNP	SHORT	22nH	0.5pF	3.3pF	15pF	22nH	1pF	2.2pF	24nH	3pF	DNP	3pF || 0.22uF	DNP	33.9	34?		
226		SHORT	DNP	SHORT	22nH	0.5pF	3.3pF	15pF	22nH	1pF	2.2pF	24nH	3pF	DNP	3pF || 0.33uF	DNP	33.8	34?		
227		SHORT	DNP	SHORT	22nH	0.5pF	3.3pF	15pF	22nH	1pF	2.2pF	24nH	3pF	DNP	3pF || 0.22uF	DNP	33.8			
228		SHORT	DNP	SHORT	22nH	0.5pF	3.3pF	22pF	22nH	1pF	2.2pF	24nH	3pF	DNP	3pF || 0.22uF	DNP	33.9			
229		SHORT	DNP	SHORT	22nH	0.5pF	3pF	22pF	22nH	1pF	2.2pF	24nH	3pF	DNP	3pF || 0.22uF	DNP	34			
230		SHORT	DNP	SHORT	22nH	0.5pF	2.5pF	22pF	22nH	1pF	2.2pF	24nH	3pF	DNP	3pF || 0.22uF	DNP	34.2			
231		SHORT	DNP	SHORT	22nH	0.5pF	2.2pF	22pF	22nH	1pF	2.2pF	24nH	3pF	DNP	3pF || 0.22uF	DNP	34.1		34.3	
232		SHORT	DNP	SHORT	22nH	0.5pF	2.2pF || 0.1pF	22pF	22nH	1pF	2.2pF	24nH	3pF	DNP	3pF || 0.22uF	DNP	34.1		34.4	
233		SHORT	DNP	SHORT	22nH	0.5pF	2.5pF || 0.1pF	22pF	22nH	1pF	2.2pF	24nH	3pF	DNP	3pF || 0.22uF	DNP	34.3		34	
234		SHORT	DNP	SHORT	22nH	0.5pF	2.5pF || 0.22pF	22pF	22nH	1pF	2.2pF	24nH	3pF	DNP	3pF || 0.22uF	DNP	24		34.2	
235		SHORT	DNP	SHORT	22nH	0.5pF	2.5pF	22pF	22nH	1pF	2.2pF	24nH	3pF	DNP	3pF || 0.22uF	DNP	34.2		34.2	
236		SHORT	DNP	SHORT	22nH	0.5pF	2.5pF || 0.1pF	22pF	22nH	1pF	2.2pF	24nH	3pF	DNP	3pF || 0.22uF	DNP	34.2		34.5	
237		SHORT	DNP	SHORT	22nH	0.6pF	2.5pF || 0.1pF	22pF	22nH	1pF	2.2pF	24nH	3pF	DNP	3pF || 0.22uF	DNP	34.2		34.266667	
238		SHORT	DNP	SHORT	22nH	0.7pF	2.5pF || 0.1pF	22pF	22nH	1pF	2.2pF	24nH	3pF	DNP	3pF || 0.22uF	DNP	34.2			
239		SHORT	DNP	SHORT	22nH	1pF	2.5pF || 0.1pF	22pF	22nH	1pF	2.2pF	24nH	3pF	DNP	3pF || 0.22uF	DNP	34.1			
240		SHORT	DNP	SHORT	22nH	0.5pF	2.5pF || 0.1pF	22pF	22nH	1pF	2.2pF	24nH	3pF	DNP	3pF || 0.22uF	DNP	34.1			
241		SHORT	DNP	SHORT	22nH	0.8pF	2.5pF || 0.1pF	22pF	22nH	1pF	2.2pF	24nH	3pF	DNP	3pF || 0.22uF	DNP	34.3			

Figure 166: Iterative/Empirical Power Amplifier Tuning Excel Sheet Snapshot (Iterations 206 through 241 of 368)

Table 18: Final Power Amplifier Tuning Values

	Input Stage			1st Stage				2nd Stage			Output Stage				
	L2	C35	C38	L1	C30	C37	C34	L3	C42	C40	L5	C45	C46	C47	C50
Type	Serial	Shunt	Serial	Biasing	Shunt	Shunt	Serial	Biasing	Shunt	Serial	Biasing	Shunt	Shunt	Serial	Shunt
Value	2.4nH	0.6pF	SHORT	22nH	0.8pF	2.5pF	22pF	3.3nH	0.3pF	2.2pF	24nH	3pF	DNP	SHORT	DNP

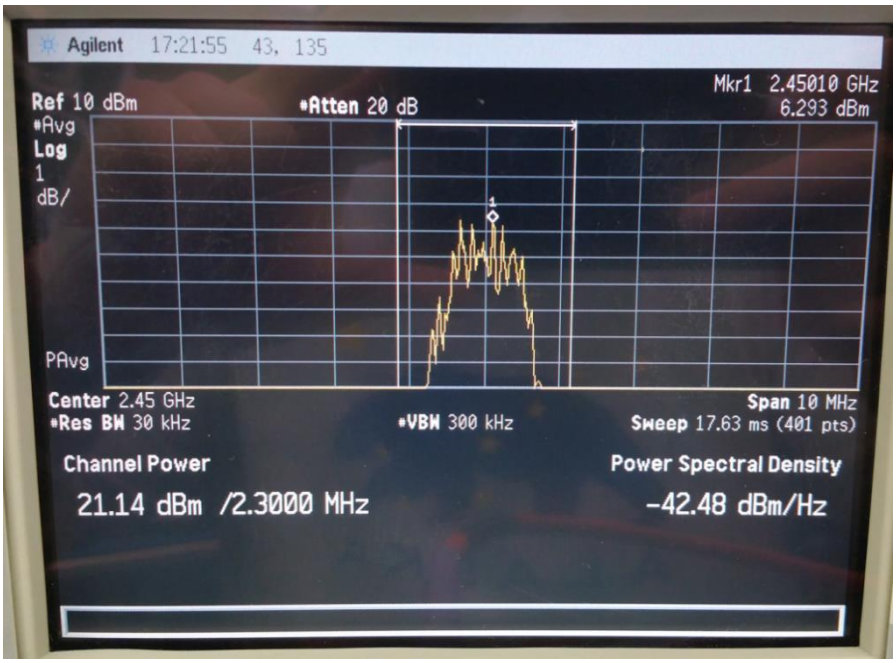

Figure 167: Final Output 31.8dBm Power Measurement (10.64dB Series Attenuation)

Figure 168 shows the measured board output power after subtracting measured cable loss from the measurement. The transceiver output power setting is varied from -17 to 4dBm to demonstrate the gain of the amplifier and compression above -5dBm.

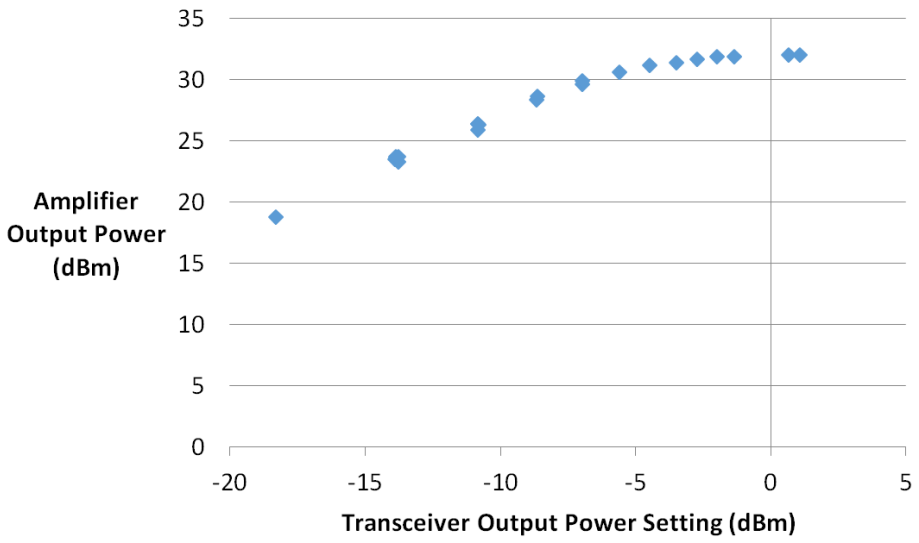

Figure 168: ISIR Transmit Power versus Input Power Register Setting

7.9 ISIR Receive Sensitivity Measurements

The ISIR receive sensitivity was measured using the same method of measuring the evaluation board receive sensitivity described in "*4.5.1: Evaluation Board Receive Sensitivity Measurements.*" However, at the time of this receive sensitivity testing, the same lab and hardware used in the evaluation testing was not available, so the evaluation board receive sensitivity was re-measured for a direct comparison without concern about measurement equipment differences.

The ISIR receive sensitivity testing was performed after tuning the amplifier to maximum transmit power. The receiver and transmitter were placed in paint can Faraday cages and connected with coaxial cable with a variable attenuator placed in-between. A packet error rate test was continuously performed between the radios while increasing the attenuation. Once the packet error rate reached around 5%, the input to the receiver was disconnected and connected to a spectrum analyzer for power measurement. Figure 169, Figure 170, and Figure 171 show the transmitter and receiver within the

Faraday cages connected across the lab with coaxial cable and variable attenuator in between.

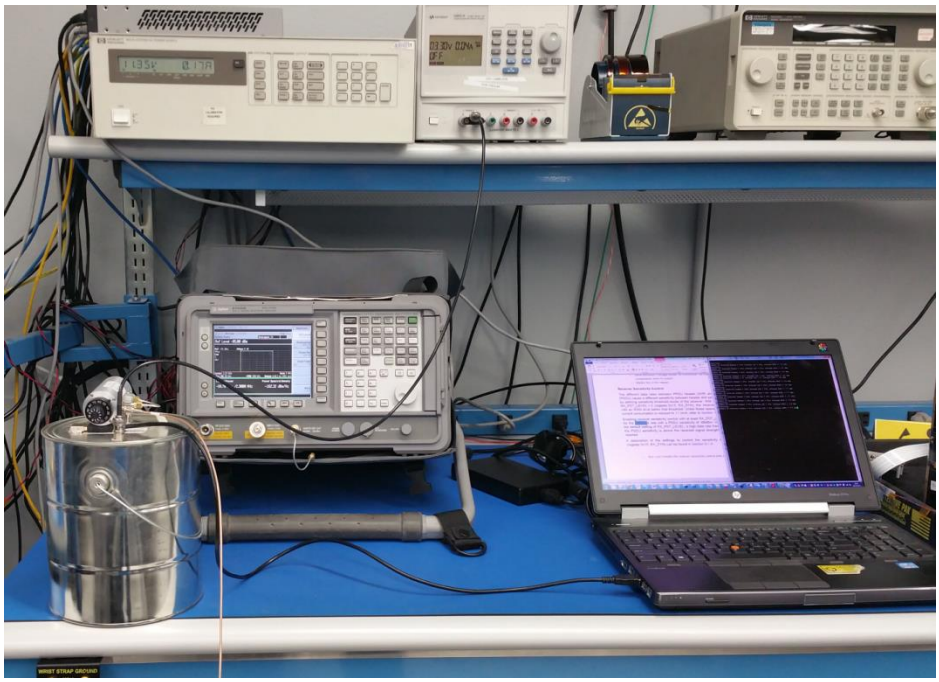

Figure 169: Receive Sensitivity Test Setup: Receive Radio

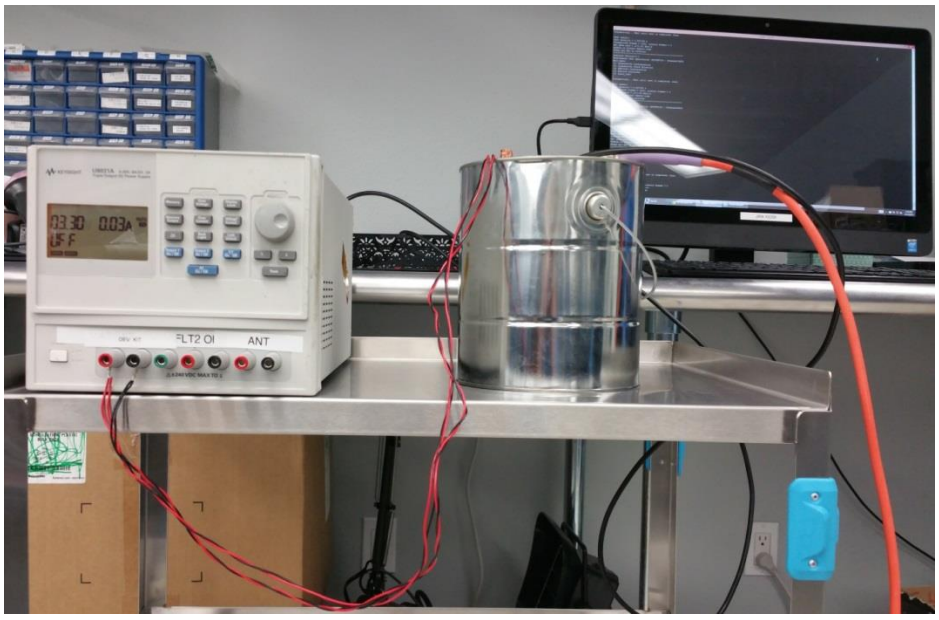

Figure 170: Receive Sensitivity Test Setup: Transmit Radio

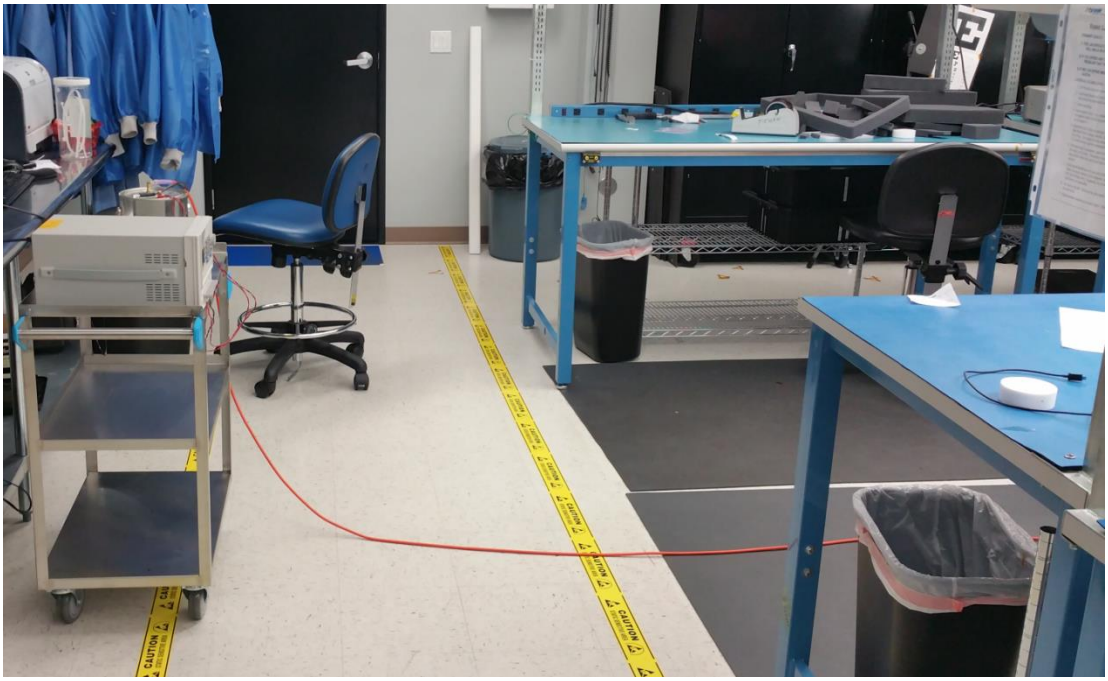

Figure 171: Receive Sensitivity Test Setup, Coax Cable Run

Figure 172 shows the noise measurement of the spectrum analyzer with no signal at its input. The spectrum analyzer is configured in a channel power measurement mode for measuring the power within the 2.3MHz signal bandwidth. The resolution bandwidth was reduced to 10kHz and pre-amplifier was enabled to provide the most sensitive measurement possible. However, the noise introduced by the spectrum analyzer into the measurement was still non-negligible and had to be subtracted from the receive sensitivity measurements.

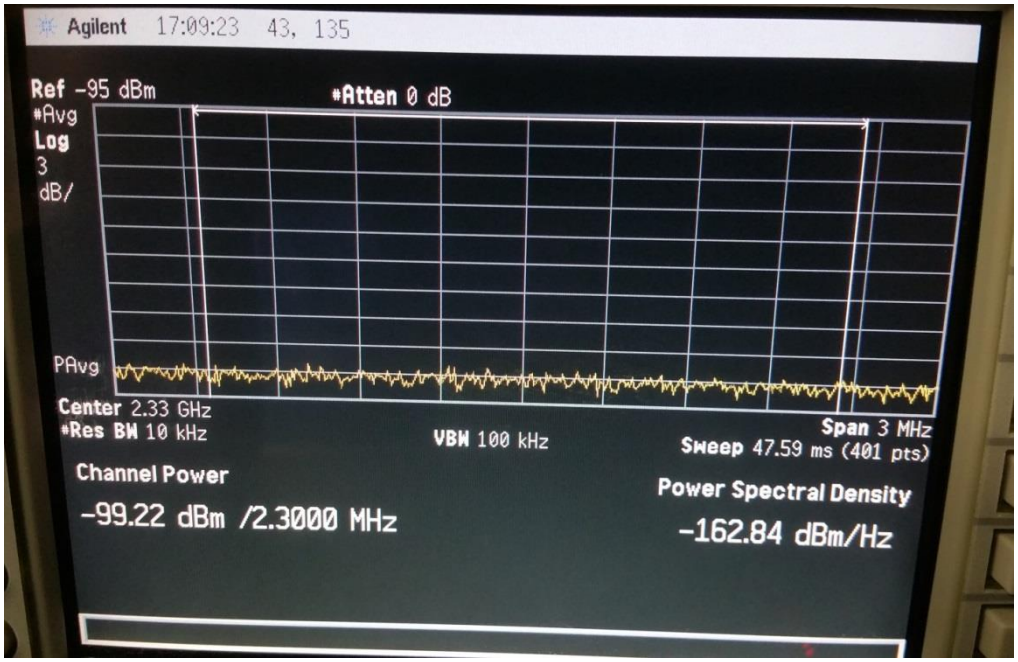

Figure 172: Spectrum Analyzer Noise Measurement (No Signal)

Figure 173 shows the signal measurement for the receive sensitivity at 500kHz as -93dBm. At this power level, the receiver decoded packets at an error rate of 6%. Subtracting the previously measured noise introduced by the spectrum analyzer results in a calculated receive sensitivity of -94dBm.

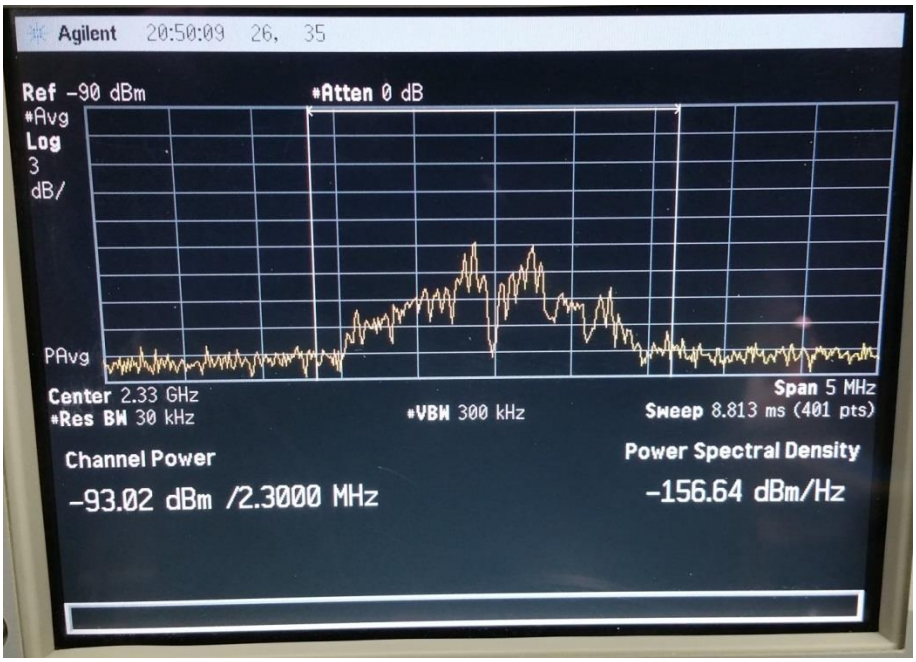

Figure 173: 500kbps Receive Sensitivity Measurement

The receiver sensitivity test was performed between two Intrepid S-Band ISM Radios and the sensitivity was recorded at the four data rates: 250kbps, 500kbps, 1000kbps, and 2000kbps. The same test with identical setup and hardware was performed with two evaluation boards for direct comparison. The results are shown in Table 19. The 2000kbps receive sensitivity measurement should be ignored due to the packet drop issue described in "*7.7* 2000kbps Packet Drop Issue." The evaluation board performed worse in this test setup than the initial evaluation board testing; it is hypothesized that RF leakage was not as adequately shielded as hoped during the previous testing.

The ISIR outperformed the evaluation board receive sensitivity by 2.8dB, 0.9dB, and 1.5dB at data rates 250kbps, 500kbps, and 1000kbps respectively. However, the sensitivity measured 2 dB worse than stated in the datasheet. The LNA should have theoretically provided a 2.36dB improvement over the evaluation board, and this is approximately true.

Table 19: Receive Sensitivity Test Results: ISIR compared to Evaluation Board

***Poor 2000kbps sensitivity due to software configuration issue, see 7.7**

Data Rate (kbps)	PER (%)	Meas. Signal Power (dBm)	Meas. SA Noise(dBm)	Calc. ISIR RX Sens. (dBm)	Eval. RX Sens. (dBm)	Datasheet (dBm)
250	1%	-96.2	-99.22	-99.1	-96.3	-101
500	6%	-93.0	-99.22	-94.2	-93.3	-96
1000	4%	-91.3	-99.22	-92.1	-90.6	-94
2000*	5%	-81.5	-99.22	-81.6	-83.4	-88

8 Future Work

A second revision of the Intrepid S-Band ISM Radio is warranted to correct the issues discovered in the first revision. Further development of this radio depends on the funding available and upcoming CubeSat missions. With appropriate funding, the designer can afford to control the stackup and dielectric of the board for improved characteristic impedance and less loss. The protection circuitry should also be fully tested prior to development of the second revision. After embedded software development for the ISIR has matured, the evaluation connectors can be removed from the second revision. The profile of the board can be reduced with the loss of the large evaluation headers. The board's interface can be modified to match the needs of the mission. The second revision should also incorporate an improved thermal path between the amplifier and satellite structure and thermal radiator.

Prior to additional development, a noise survey at Cal Poly should be conducted to confirm the presence of a frequency within the ISM band with minimal interference, such as the survey performed in Irvine in "4.2 *ISM Noise Floor*." Development of an S-Band CubeSat antenna must be completed. The antenna could either be a simple patch antenna or a deployable dish depending on the desired mission data rate. A 4.5 meter or larger dish with a 2.4GHz circular feed horn must be added to the PolySat Earth Station for adequate gain to complete the satellite link. The same dish with different feed horns could be used in the future for higher frequencies as more complex, higher data rate radios are developed. The future work outlined above could easily provide work for four or more student theses or senior projects; the future work is re-stated below as a bulleted list:

S-Band Future Work:

- 1st revision remaining testing
    - Amplifier protection circuitry
    - Compare power consumption measurements to estimates
- Embedded software development for System Board microprocessor
- 2nd Revision ISIR PCBA Design
    - Correct issues discovered during 1st revision testing
    - Remove evaluation board development headers and EEPROM
    - Tailor radio dimensions for specific mission and current bus architecture
    - Incorporate thermal path between amplifier and regulator to satellite thermal sink
- High-gain satellite antenna design
    - Deployable high gain antenna recommended
- Ground Station upgrades
    - ISM S-Band Noise survey
    - Add 4.5 meter dish with circular 2.4GHz feed horn to Cal Poly ground station
    - Transceiver selection, power amplifier, mast-mounted low noise amplifier

9 Summary and Conclusion

The Intrepid ISM S-Band Radio (ISIR) for the PolySat System Board was successfully designed, fabricated, tuned, and tested. The final specifications for the Intrepid S-Band ISM Radio (ISIR) are as follows:

Table 20: Intrepid ISM S-Band Radio Final Specifications

ISIR Final Specifications	
Frequency Range	2.322 to 2.527 GHz, 500kHz channel spacing
Channel Bandwidth	2.3MHz Spread Spectrum
Modulation	O-QPSK
Protocol	ZigBee
Data Rates and Receive Sensitivity (within 2.3MHz bandwidth)	• 250kbps: -99.1dBm • 500kbps: -94.2dBm • 1000kbps: -92.1dBm • 2000kbps: TBD
Maximum Transmit Power	31.8dBm (1.5W)
Receive Mode Power Consumption	90mW (Estimated)
Transmit Mode Power Consumption	6.9W (Estimated)
Digital Interface	SPI
Doppler Tolerance or Correction Capability	+/- 100kHz
Physical Dimensions	Intrepid Daughter Board B, 1.4” x 3.3”
Temperature Range	-40 to 85 C (Industrial)
Additional Features	• Amplifier Protection • Transmit and Reflected Power Measurement • DC Power and Temperature Measurement • Dual Antenna Diversity Support • EEPROM for Unique Board Info

FCC frequency restrictions will require missions with this radio to operate within 2400-2483.5 MHz ISM band with high terrestrial interference, however measurements demonstrate that surveying the ground station location and carefully selecting quiet nulls within the ISM band can eliminate interference to thermal noise levels. With further student future work and appropriate funding, a high-data rate CubeSat ISM S-Band communication can be implemented by the Cal Poly PolySat lab to support future higher data throughput missions.

REFERENCES

[1] PolySat, "CP8 (IPEX)," [Online]. Available: http://polysat.calpoly.edu/launched-missions/cp8-ipex/. [Accessed 29 March 2016].

[2] B. Klofas, "Klofas.com," [Online]. Available: http://www.klofas.com/. [Accessed 02 April 2016].

[3] B. Klofas, "CubeSat Communication Systems," 10 March 2015. [Online]. Available: http://www.klofas.com/comm-table/table.pdf. [Accessed 04 April 2016].

[4] B. Klofas, "CubeSat Radios: From kilobits to Megabits," 2014 February 2014. [Online]. Available: http://www.klofas.com/papers/kilobits_to_Megabits.pdf. [Accessed 04 April 2016].

[5] A. Williams, "A Compact, Reconfigurable UHF Communication System Design For Use With Polysat's Embedded Linux Platform," California Polytechnic State University, San Luis Obispo, 2013.

[6] "Earth Station," PolySat, 2016. [Online]. Available: http://polysat.calpoly.edu/ground-station/. [Accessed 6 March 2016].

[7] M2 Antenna Systems, "436CP42UG, 420-440 MHZ," 2016. [Online]. Available: http://www.m2inc.com/amateur/436cp42ug-420-440-mhz/. [Accessed 6 March 2016].

[8] G. McDonald, "STACKING, PHASING and MATCHING YAGIS," [Online]. Available: http://www.grantronics.com.au/docs/StkYagis.pdf. [Accessed 6 March 2016].

[9] D. Adamy, EW101: A First Course in Electronic Warfare, Norwood, MA: Artech House, Inc., 2001.

[10] D. L. Adamy, EW103: Tactical Battlefield Communications Electronic Warfare, Norwood, MA: Artech House, 2009.

[11] AMSAT-UK, "Spreadsheet Calculators," January 2013. [Online]. Available: http://www.amsatuk.me.uk/iaru/spreadsheet.htm. [Accessed 6 March 2016].

[12] ON Semiconductor, "AX5042 Datasheet," [Online]. Available: http://www.onsemi.com/pub_link/Collateral/AX5042-D.PDF. [Accessed 6 March 2016].

[13] eoPortal Directory, "Aeneas nanosatellite of USC/SERC," [Online]. Available: https://directory.eoportal.org/web/eoportal/satellite-missions/a/aeneas. [Accessed 6

March 2016].

[14] RF HAMDesign, "4.5 Meter MESH DISH KIT (F/D=0.45)," [Online]. Available: http://www.rfhamdesign.com/products/parabolicdishkit/45meterdishkit/index.php. [Accessed 30 April 2016].

[15] "CFR 47: Telecommunication," *Office of the Federal Register National Archives and Records Administration ,* 2007.

[16] M. Lazarus, "ISM vs. Spread Spectrum -- Avoiding the FCC," Microwave Journal, 1 October 2000. [Online]. Available: http://www.microwavejournal.com/articles/3061-ism-vs-spread-spectrum-avoiding-the-fcc. [Accessed 6 March 2016].

[17] NASA, "CR-2004-213551, Measurements of Man-Made Spectrum," National Technical Information Service, Washington, DC, 2004.

[18] Atmel Corporation, "Atmel AT02845: Coexistence between ZigBee and Other 2.4GHz Products," September 2013. [Online]. [Accessed 2015].

[19] FCC, "Guidance On Obtaining Licenses For Small Satellites," 15 March 2013. [Online]. Available: https://www.fcc.gov/document/guidance-obtaining-licenses-small-satellites. [Accessed 13 March 2016].

[20] FCC, "Experimental Licensing System Generic Search," [Online]. Available: https://apps.fcc.gov/oetcf/els/reports/GenericSearch.cfm. [Accessed 13 March 2016].

[21] FCC, "Texas A&M University AggieSat Lab, United States of America FEDERAL COMMUNICATIONS COMMISSION EXPERIMENTAL RADIO STATION CONSTRUCTION PERMIT AND LICENSE," 16 October 2012. [Online]. Available: https://apps.fcc.gov/els/GetAtt.html?id=130334&x=.. [Accessed 13 March 2016].

[22] D. L. Adamy, EW102: A Second Course in Electronic Warfare, Horizon House Publications, Inc., 2004.

[23] A. Williams, "CubeSat Proximity Operations Demonstration (CPOD) Mission Update, Cal Poly CubeSat Workshop," Tyvak Nano-Satellite Systems Inc., 22 April 2015. [Online]. Available: http://mstl.atl.calpoly.edu/~bklofas/Presentations/DevelopersWorkshop2015/Williams_CPOD.pdf. [Accessed 6 March 2016].

[24] C. MacGillivray, "Miniature Deployable High Gain Antenna for CubeSats, 2011 CubeSat Developers Workshop," Boeing Phantom Works, 22 April 2011. [Online]. Available: http://mstl.atl.calpoly.edu/~bklofas/Presentations/DevelopersWorkshop2011/47_Ma

cGillivray_Miniature_Antennas.pdf. [Accessed 6 March 2016].

[25] Atmel Corporation, "Atmel AT03911: REB233CBB Module – User Manual," July 2013. [Online]. Available: http://www.atmel.com/Images/Atmel-42156-WIRELESS-AT03911-REB233CBB-Module-User-Manual_Application-Note.pdf. [Accessed 6 March 2016].

[26] I. Bland, "Receive Sensitivity Characterization of the PolySat Satellite Communication System," California Polytechnic State University, San Luis Obispo, 2010.

[27] J.-F. Levesque, K. Doerksen and I. Mas , "Design, Modeling and Evaluation of a 2.4GHz FHSS Communications System for NarcisSat," in *17th AIAA/USU Conference on Small Satellites*, Utah, 2003.

[28] Atmel Corporation, "AT86RF233 PRELIMINARY DATASHEET," July 2014. [Online]. Available: http://www.atmel.com/Images/Atmel-8351-MCU_Wireless-AT86RF233_Datasheet.pdf. [Accessed 6 March 2016].

[29] Mini-Circuits, "Mini-Circuits Home Page," [Online]. Available: http://www.minicircuits.com/.

[30] Tyvak Nano-Satellite Systems LLC, *Intrepid Pico-Class CubeSat System Board User Guide - Rev F,* 2014.

[31] Samtec, Inc., "SEI, SIBF SERIES ONE PIECE INTERFACE," [Online]. Available: http://suddendocs.samtec.com/catalog_english/sei.pdf. [Accessed 6 March 2016].

[32] R. Curtis, "SCLA008: Using High-Speed CMOS and Advanced CMOS Logic in Systems With Multiple VCC Supplies or Partial Power Down," Texas Instruments, April 1996. [Online]. Available: http://www.ti.com.cn/cn/lit/an/scla008/scla008.pdf. [Accessed 6 March 2016].

[33] Texas Instruments Incorporated, "SN74LVC2T45 Dual-Bit Dual-Supply Bus Transceiver With Configurable Voltage, Datasheet," December 2014. [Online]. Available: http://www.ti.com/lit/ds/symlink/sn74lvc2t45.pdf. [Accessed 6 March 2016].

[34] E. Bogatin, Signal and Power Integrity - Simplified (2nd Edition), Ann Arbor, Michigan: Edwards Brothers, 2013.

[35] Atmel Corporation, "Atmel AT02865: RF Layout with Microstrip," May 2013. [Online]. Available: http://www.atmel.com/images/atmel-42131-rf-layout-with-microstrip_application-note_at02865.pdf. [Accessed 6 March 2016].

[36] Anaren , "Model BD2425N50100AHF Ultra Low Profile 0404 Balun, Datasheet," [Online]. Available: http://www.anaren.com/sites/default/files/BD2425N50100AHF%20Data%20Sheet%20Rev%20A.pdf. [Accessed 6 March 2016].

[37] Hittite Microwave Corporation, "HMC595 / 595E GaAs MMIC 3 WATT T/R SWITCH, DC - 3 GHz, Datasheet," [Online]. Available: http://www.analog.com/media/en/technical-documentation/data-sheets/hmc595.pdf. [Accessed 6 March 2016].

[38] muRata, "Preliminary Specification of COAXIAL CONNECTOR, MM8030-2600B/RJ3/RK0," August 2008. [Online]. Available: http://media.digikey.com/pdf/Data%20Sheets/Murata%20PDFs/MM8030-2600.pdf. [Accessed 6 March 2016].

[39] muRata, "Microwave Coaxial Connectors," [Online]. Available: http://www.mouser.com/ds/2/281/o33e-4435.pdf. [Accessed 6 March 2016].

[40] muRata, "Application Manual for Power Supply Noise Supression and Decoupling for Digital ICs," 20 July 2010. [Online]. Available: http://www.murata.com/~/media/webrenewal/support/library/catalog/products/emc/emifil/c39e.ashx. [Accessed 6 March 2016].

[41] muRata, "Sim Surfing, Characteristics Viewer," [Online]. Available: http://ds.murata.co.jp/software/simsurfing/en-us/index.html. [Accessed 6 March 2016].

[42] RF Micro Devices Inc., "RFPA2026, 3-Stage Power Amplifier Module, 2W, 700MHz to 2700MHz, Datasheet," 2013. [Online]. Available: http://www.rfmd.com/store/downloads/dl/file/id/28401/rfpa2026_data_sheet.pdf. [Accessed 6 March 2016].

[43] RFMD, *RFPA2026 2300MHz-2700mhz tuning power point presentation,* 2014.

[44] TDK, "Multilayer Chip Low Pass Filters For Bluetooth & 2.4GHz W-LAN DEA Series DEA102500LT-6307A1, Datasheet," [Online]. Available: https://product.tdk.com/info/en/documents/data_sheet/rf_lpf_dea102500lt-6307a1_en.pdf. [Accessed 6 March 2016].

[45] TDK, "Multilayer Band Pass Filter For 2400-2500MHz DEA252450BT-2027A1, Datasheet," June 2015. [Online]. Available: https://product.tdk.com/info/en/documents/data_sheet/rf_bpf_dea252450bt-2027a1_en.pdf. [Accessed 6 March 2016].

[46] Maxim Integrated Products, "MAX2692/MAX2695 WLAN/WiMAX Low-Noise Amplifiers, Datasheet," September 2011. [Online]. Available: https://datasheets.maximintegrated.com/en/ds/MAX2692-MAX2695.pdf. [Accessed 3 March 2016].

[47] Texas Instruments, "TPS6302x High Efficiency Single Inductor Buck-Boost Converter With 4-A Switches, Datasheet," October 2015. [Online]. Available: http://www.ti.com/lit/ds/slvs916d/slvs916d.pdf. [Accessed 6 March 2016].

[48] Texas Instruments, "INA219 Zerø-Drift, Bidirectional Current/Power Monitor With I, Datasheet," December 2015. [Online]. Available: http://www.ti.com/lit/ds/slvs916d/slvs916d.pdf. [Accessed 6 March 2016].

[49] Microchip Technology Inc., "AN826 Crystal Oscillator Basics and Crystal Selection for rfPICTM and PICmicro® Devices," 2002. [Online]. Available: http://ww1.microchip.com/downloads/en/AppNotes/00826a.pdf. [Accessed 6 March 2016].

[50] Atmel Corporation, "Atmel AVR2067: Crystal Characterization for AVR RF," 2013. [Online]. Available: http://www.atmel.com/images/atmel-42068-crystal-characterization-for-avr-rf_application-note_avr2067.pdf. [Accessed 6 March 2016].

[51] W. Karoui, "A protection circuit for HBT RF power amplifier under load mismatch conditions," Freescale Semiconductors , [Online]. Available: http://homepages.laas.fr/parra/NEWCAS-TAISA08_PROCEEDINGS/PAPERS/61.pdf. [Accessed 6 March 2016].

[52] Analog Devices, "ADL5501, 50 MHz to 6 GHz TruPwr Detector, Datasheet," 2009. [Online]. Available: http://www.analog.com/media/en/technical-documentation/evaluation-documentation/ADL5501.pdf. [Accessed 6 March 2016].

[53] A. Rohatgi, "WebPlotDigitizer: Web based tool to extract data from plots, images, and maps," [Online]. Available: http://arohatgi.info/WebPlotDigitizer/. [Accessed 6 March 2016].

[54] D. Knollman, "Design Balanced Op-Amp Circuits For Performance And Simplicity," Electronic Design, 10 March 2014. [Online]. Available: http://electronicdesign.com/analog/design-balanced-op-amp-circuits-performance-and-simplicity. [Accessed 6 March 2016].

[55] National Semiconductor, "WEBENCH Amplifier Design Tools," [Online]. Available: http://webench.ti.com/appinfo/webench/amplifiers/select_topology.cgi?Topology=NonInverting+Amp. [Accessed 6 March 2016].

[56] Texas Instruments, "ADC121C021/ADC121C021Q/ADC121C027 I2C-Compatible, 12-Bit Analog-to-Digital Converter with Alert Function, Datasheet," March 2013. [Online]. Available: http://www.ti.com.cn/cn/lit/ds/symlink/adc121c021.pdf. [Accessed 6 March 2016].

[57] Analog Devices, "Datasheet ADCMP341/ADCMP343, Dual 0.275% Comparators and Reference with Programmable Hysteresis," 2013. [Online]. Available: http://www.analog.com/media/en/technical-documentation/data-sheets/ADCMP341_343.pdf. [Accessed 6 March 2016].

[58] Texas Instruments, "SN74LVC1G123 Single Retriggerable Monostable Multivibrator With Schmitt-Trigger Inputs, Datasheet," July 2004. [Online]. Available: http://www.mouser.com/ds/2/405/sn74lvc1g123-405826.pdf. [Accessed 6 March 2016].

[59] Advanced Circuits, "Home Page," [Online]. Available: http://www.4pcb.com/. [Accessed 6 March 2016].

[60] Atmel Corporation, "Atmel AVR2162: REB233SMAD – Hardware User Manual," July 2012. [Online]. Available: http://www.atmel.com/Images/doc42006.pdf. [Accessed 6 March 2016].

[61] N. Ayat and M. Mehdipour, "Accurate Doppler Prediction Scheme for Satellite Orbits," 2006. [Online]. Available: http://www.wseas.us/e-library/conferences/2006madrid/papers/502-497.pdf. [Accessed 6 March 2016].

[62] Atmel Corporation, "Atmel AVR2162: REB233SMAD – Hardware User Manual," July 2012. [Online]. Available: http://www.atmel.com/Images/doc42006.pdf. [Accessed 6 March 2016].

Appendix A: Intrepid S-Band ISM Radio R1 Schematic

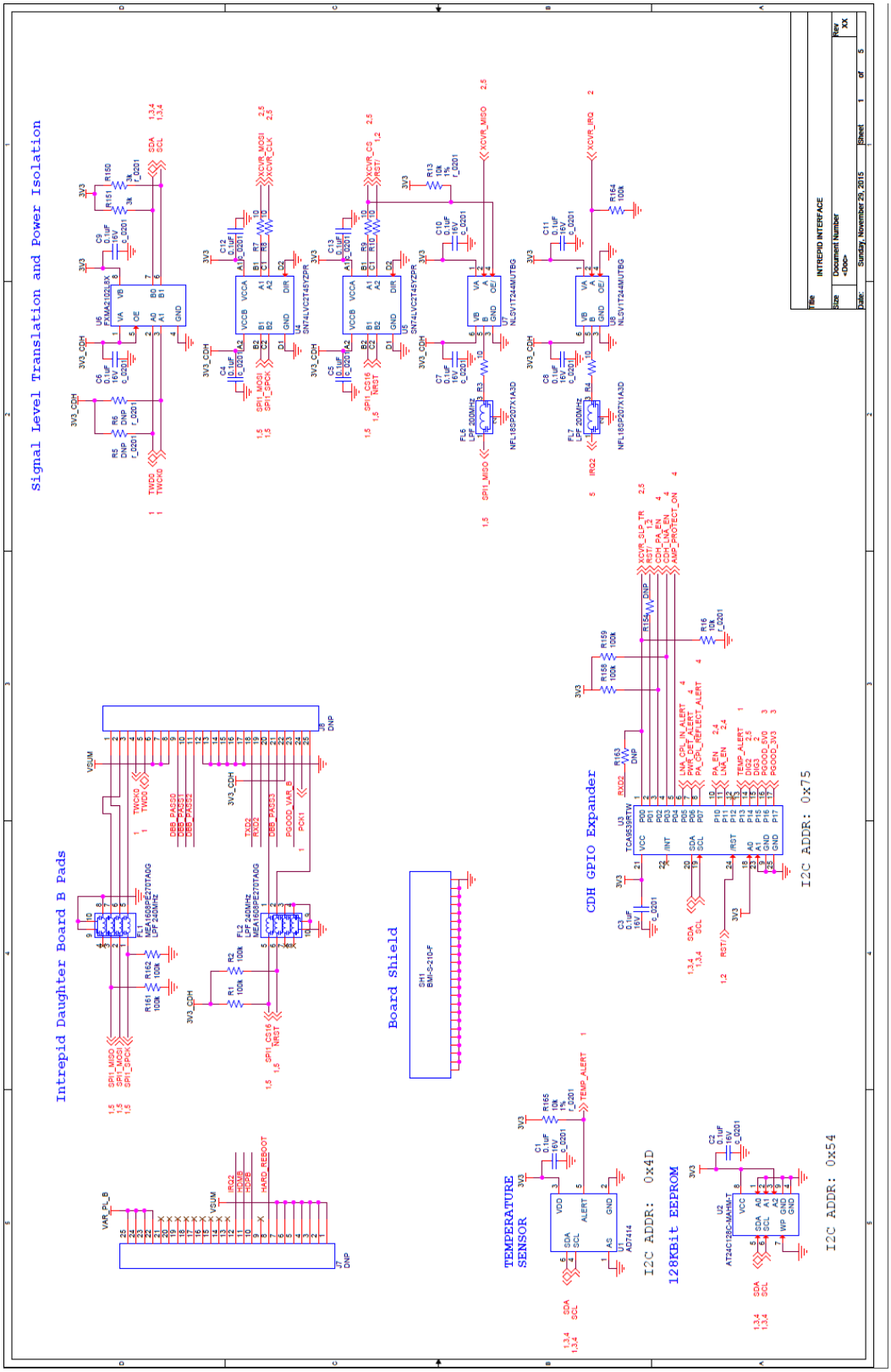

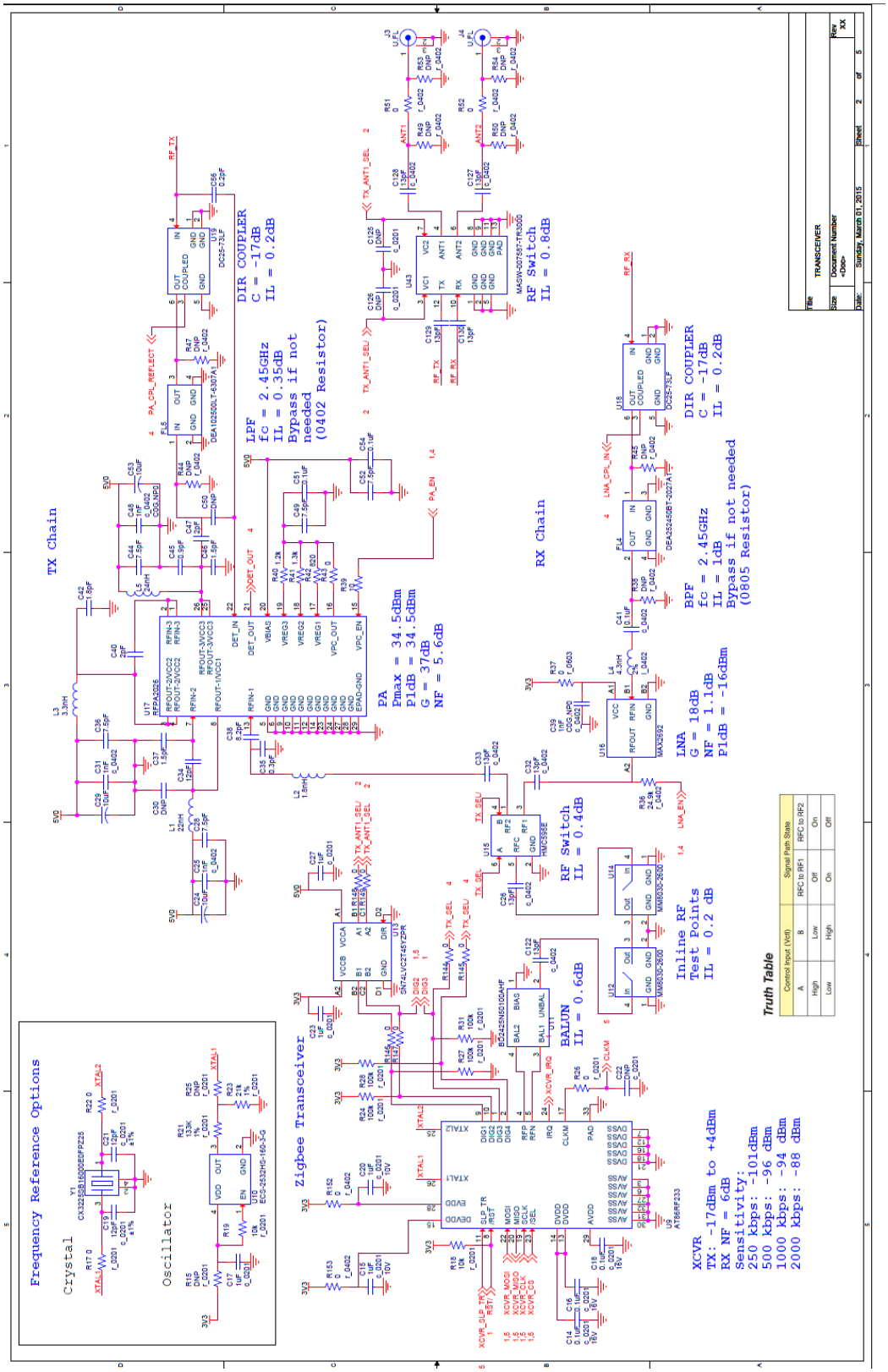
TX Chain
RX Chain
Frequency Reference Options
Crystal
Oscillator
Zigbee Transceiver
PA
Pmax = 34.5dBm
P1dB = 34.5dBm
G = 37dB
NF = 5.6dB
LPF
fc = 2.45GHz
IL = 0.35dB
Bypass if not needed
(0402 Resistor)
DIR COUPLER
C = -17dB
IL = 0.2dB
RF Switch
IL = 0.8dB
LNA
G = 18dB
NF = 1.1dB
P1dB = -16dBm
BPF
fc = 2.45GHz
IL = 1dB
Bypass if not needed
(0805 Resistor)
RF Switch
IL = 0.4dB
BALUN
IL = 0.6dB
Inline RF
Test Points
IL = 0.2 dB
XCVR
TX: -17dBm to +4dBm
RX NF = 6dB
Sensitivity:
250 kbps: -101dBm
500 kbps: -96 dBm
1000 kbps: -94 dBm
2000 kbps: -88 dBm
Truth Table
Control Input (Vctl)
Signal Path State
A
B
RFC to RF1
RFC to RF2
High
Low
Off
On
Low
High
On
Off
Title: TRANSCEIVER
Size:
Document Number
<Doc>
Rev
XX
Date: Sunday, March 01, 2015
Sheet 2 of 5

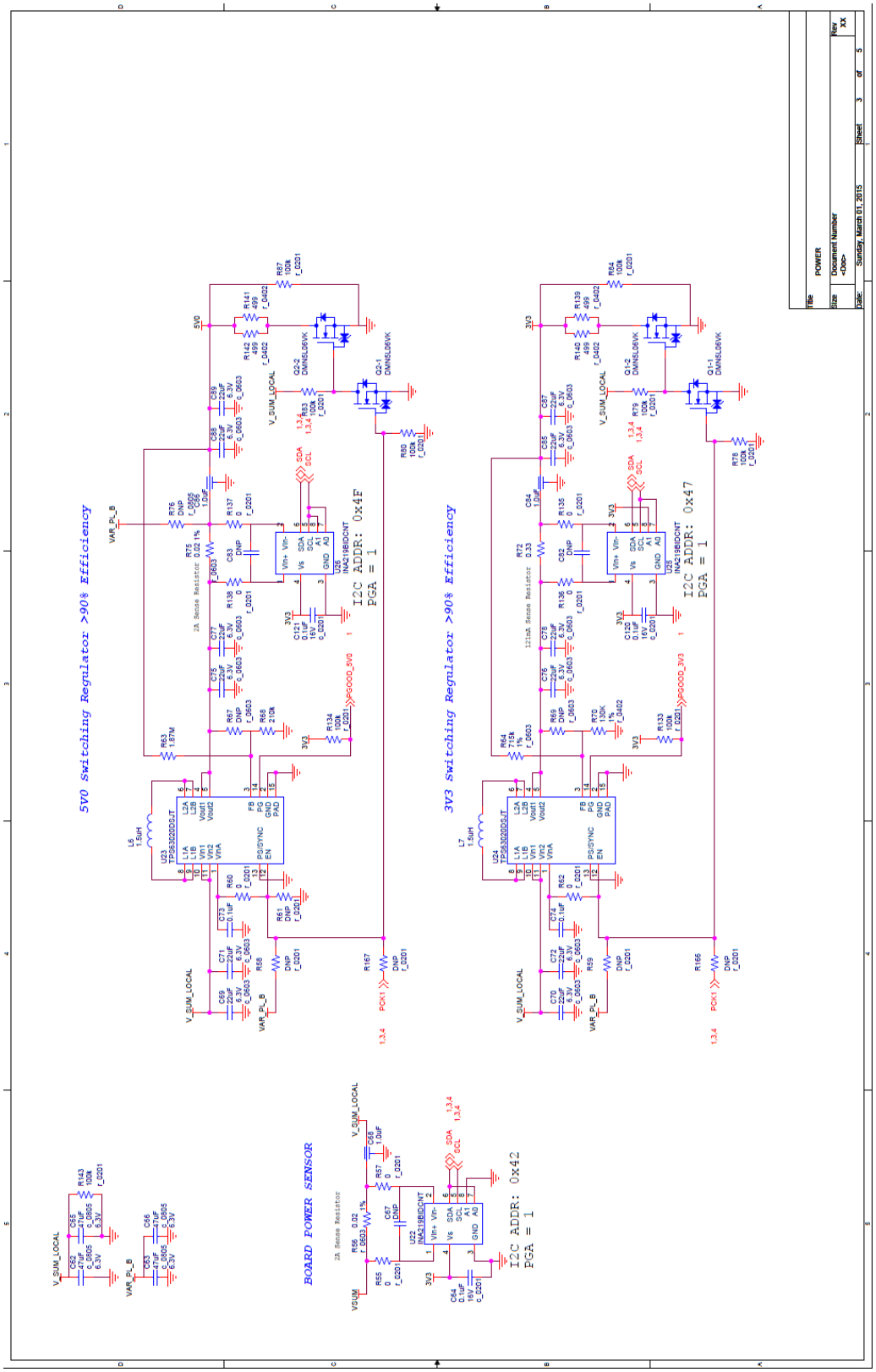
5V0 Switching Regulator >90% Efficiency
3V3 Switching Regulator >90% Efficiency
BOARD POWER SENSOR
I2C ADDR: 0x4F
PGA = 1
I2C ADDR: 0x47
PGA = 1
I2C ADDR: 0x42
PGA = 1
POWER
Sunday, March 01, 2015
Sheet 3 of 5

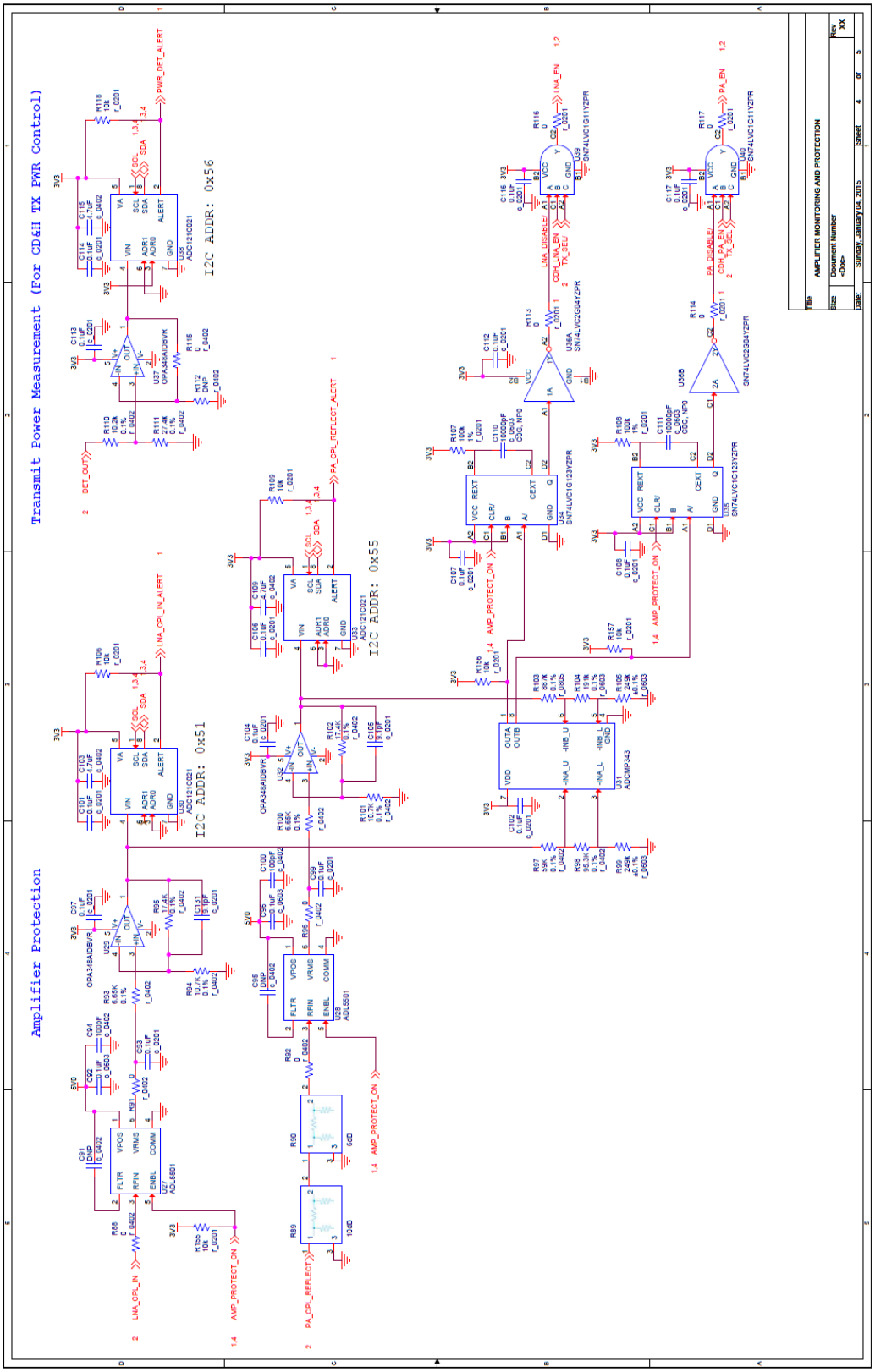
Transmit Power Measurement (For CD&H TX PWR Control)
Amplifier Protection
I2C ADDR: 0x51
I2C ADDR: 0x55
I2C ADDR: 0x56
AMPLIFIER MONITORING AND PROTECTION
Sunday, January 04, 2015

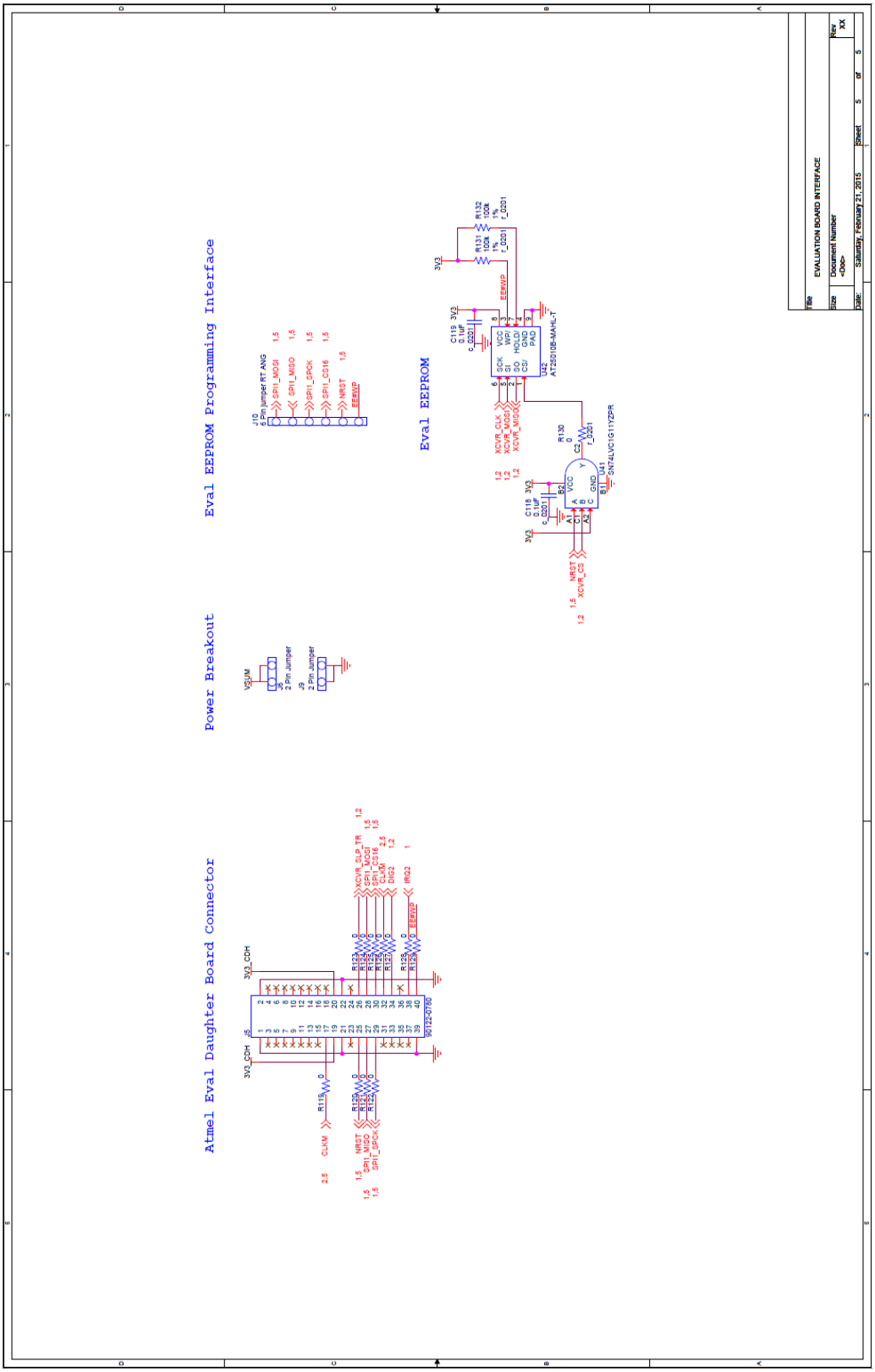
Atmel Eval Daughter Board Connector
Power Breakout
Eval EEPROM Programming Interface
Eval EEPROM
Title
EVALUATION BOARD INTERFACE
Size
Document Number
<Doc>
Rev
XX
Date:
Saturday, February 21, 2015
Sheet
5
of
5